IMPACT OF CLIMATE CHANGE ON FUTURE FLOW OF BRAHMAPUTRA RIVER BASIN USING SWAT MODEL

M. Sc. Engineering Thesis

by

Sarfaraz Alam

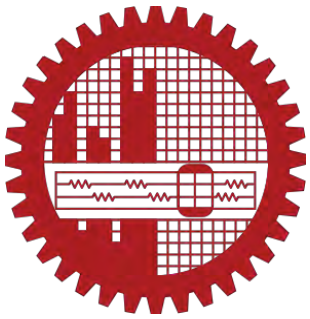

Department of Water Resources Engineering,
Bangladesh University of Engineering and Technology (BUET)
Dhaka

April 2015

IMPACT OF CLIMATE CHANGE ON FUTURE FLOW OF BRAHMAPUTRA RIVER BASIN USING SWAT MODEL

M. Sc. Engineering Thesis

by

Sarfaraz Alam

Roll no: 0413162032 P

Submitted to

Department of Water Resources Engineering,
Bangladesh University of Engineering and Technology, Dhaka
in partial fulfillment of the requirement for the degree of
Master of Science in Water Resources Engineering

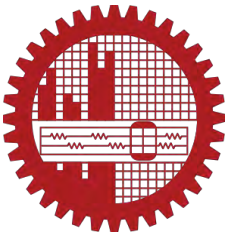

Department of Water Resources Engineering,
Bangladesh University of Engineering and Technology (BUET)
Dhaka

April 2015

IMPACT OF CLIMATE CHANGE ON FUTURE FLOW OF BRAHMAPUTRA RIVER BASIN USING SWAT MODEL

M. Sc. Engineering Thesis

by

Sarfaraz Alam

Roll no: 0413162032 P

Submitted to

Department of Water Resources Engineering,
Bangladesh University of Engineering and Technology, Dhaka
in partial fulfillment of the requirement for the degree of
Master of Science in Water Resources Engineering

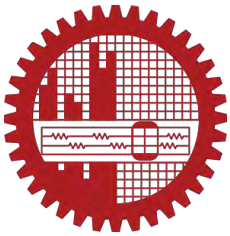

Department of Water Resources Engineering,
Bangladesh University of Engineering and Technology (BUET)
Dhaka

April 2015

Bangladesh University of Engineering and Technology, Dhaka
Department of Water Resources Engineering

Certificate of Thesis

The thesis titled **"Impact of Climate Change on Future Flow of Brahmaputra River Basin Using Swat Model"**, submitted by Sarfaraz Alam, Roll no. 0413162032 P, Session April 2013, to the Department of Water Resources Engineering, Bangladesh University of Engineering and Technology, has been accepted as satisfactory in partial fulfillment of the requirements for the degree of Master of Science in Water Resources Engineering and approved as to its style and content. Examination held on April 13, 2015.

_____
Dr. Md. Mostafa Ali — Chairman (Supervisor)
Associate Professor
Department of Water Resources Engineering,
Bangladesh University of Engineering and Technology, Dhaka.

_____
Dr. Md. Sabbir Mostafa Khan — Member (Ex-Officio)
Professor and Head
Department of Water Resources Engineering,
Bangladesh University of Engineering and Technology, Dhaka.

_____
Dr. Md. Ataur Rahman — Member
Professor
Department of Water Resources Engineering,
Bangladesh University of Engineering and Technology, Dhaka.

_____
Mrs. Sara Ferdousi — Member
Assistant Professor
Department of Water Resources Engineering,
Bangladesh University of Engineering and Technology, Dhaka.

_____
Dr. Md. Mizanur Rahman — Member (External)
Executive Engineer
Surface Water Hydrology Division, BWDB,
72 Green Road, Dhaka-1205.

Candidate's Declaration

It is hereby declared that this thesis or any part of it has not been submitted elsewhere for the award of any degree or deploma

Supervisor

_____

Dr. Md. Mostafa Ali
Associate Professor
Department of Water Resources Engineering,
Bangladesh University of Engineering and
Technology, Dhaka.

Candidate

_____

Sarfaraz Alam

Roll No: 0413162032P

ACKNOWLEDGEMENT

I would like to express my gratitude and thanks to my supervisor Dr. Md. Mostafa Ali for his excellent supervision, motivation and productive criticism throughout the research. My sincere appreciation is due to Dr. Sabbir Mostafa Khan, Professor and Head, Department of Water Resources Engineering, BUET, for his timely cooperation and guidance.

I also intend to express my gratitude to Dr. Ataur Rahman, Professor, Dept. of Water Resources Engineering, BUET, and Mrs. Sara Ferdousi, Assistant Professor,Dept. of Water Resources Engineering, BUET, for their careful review and suggestions. I am also grateful to Dr. Md. Mizanur Rahman, Executive Engineer, Surface Water Hydrology Division, Bangladesh Water Development Board (BWDB), for his kind consent to be a member of examination board. His precious comments, constructive criticism and suggestions in this study are duly appreciated. I am very much thankful to Dr. Md. Zahidul Islam of Alberta Environment and Sustainable Resource Development for his valuable suggestions, comments, inspiration and guidance throughout the research. I would like to express my heartfelt thanks to Tanvir Ahmed and Ahmmed Zulfiqar Rahaman of Center for Environmental and Geographic Information Services (CEGIS) for their valuable suggestions.

I would also like to convey my gratefulness to my parents (Sharif Alam and Nasrin Sharif) and sisters for their encouragements and assistance during my work.

Above all, I am thankful to Allah, the most Gracious, and most Merciful for giving me this excellent opportunity.

Sarfaraz Alam

ABSTRACT

Brahmaputra River Basin(BRB) is one of the largest basins among Ganges-Brahmaputra-Meghna (GBM) river system carrying enormous volume of water through Bangladesh. The response of this basin due to climate changes is one of the key issues to be investigated due to its socio-economic and environmental vulnerability. A semi-distributed hydrological model of the BRB has been developed using the Soil Water Assessment Tool (SWAT). It has been calibrated and validated for the streamflow measured at the Bahadurabad station for the climate normal period (1981 to 2010).

Synthetic approach of climate change modeling has been applied to assess the changes in water availability due to future potential changes in temperature and precipitation in BRB. Twenty hypothetical climate change scenarios (perturbed temperatures and precipitation: precipitationfrom -20% of climate normal period to +40% at 10% interval and temperature change of 0°C to 6°C at 2°C interval) were applied to the calibrated and validated model in order to investigate the sensitivity of BRB mean annual and mean seasonal streamflow under the impact of climate change in the 21st century. The results revealed that the changes in annual streamflow due to changes in precipitation and temperature are linear. It appears that with respect to the climate normal (1981-2010), the changes in average annual streamflow (keeping temperature unchanged) are ± 12.83% per ±10% change in precipitation. In contrast, streamflow response to the increase in temperature (keeping precipitation unchanged) is -2.49% per °C.

The calibrated hydrological model of BRB then has been used to assess the impact of climate change on water availability of BRB by applying different climate change scenarios of selected General Circulation Models (GCM). The selection of GCM was based on the Representative Concentration Pathways (RCPs) scenarios of eight Intergovernmental Panel on Climate Change (IPCC) GCMs for the 21st century. Six climate change scenarios, viz. as warmest, coolest, driest, wettest, moderate warm and moderate wet were selected based on the projected precipitation and temperature of the 21st century obtained from four RCPs (RCP 2.6, RCP 4.5, RCP 6.0 and RCP 8.5) of eight GCMs (BCC-CSM1.1, BCC-CSM1.1(m), GISS-E2-H, GISS-E2-R, Had-

GEM2-ES, MIROC-ESM, MIROC-ESM-CHEM, MRI-CGCM3). From the analysis of temperature and precipitation data BCC-CSM1.1 RCP 8.5, HadGEM2-ES RCP 8.5, MIROC-ESM-CHEM RCP 8.5, GISS-E2-R RCP 2.6, MRI-CGCM3 RCP 6.0 and GISS-E2-H RCP 4.5 were selected as the wettest, driest, warmest, coolest, moderate wet and moderate warm scenario, respectively. The high resolution spatial distribution of temperature and precipitation of these GCMs were obtained using the pattern scaling technique and were further applied to the SWAT hydrological model.

SWAT simulated mean annual, mean dry period (December to May), and mean wet period (June to November) seasonal streamflow of BRB for the 2010-2039 (2020s), 2040-2069 (2050s), and 2070-2099 (2080s) of the 21st centurywere compared with the corresponding climate normal (1981-2010) streamflow. In general, BRB projected an increase in the mean annual streamflow for 21st century under the climate projections for almost all the six scenarios considered in this study. However, GISS-E2-R RCP2.6 (coolest) and HadGem2-ES RCP8.5 (driest) projected decrease in annual average flow at Bahadurabad station during 2080s and 2020s respectively. The maximum projected increase in mean annual streamflow found are 15.019%, 32.457% and 47.436% for MIROC-ESM-CHEM RCP8.5 (warmest), GISS-E2-H RCP4.5 (moderate warm) and BCC-CSM1.1 RCP8.5 (wettest) in 2020s, 2050s and 2080s respectively. The minimum projected change in streamflow found are -3.290%, 1.800% and -0.908% for HadGEM2-ES RCP8.5 (driest), GISS-E2-R RCP2.6 (coolest) and GISS-E2-R RCP2.6 (coolest) in 2020s, 2050s and 2080s respectively. On average, at the end of 21st century (2080s), the mean dry and wet period streamflow of BRB is projected to increase by about 177.93% and 11% of their mean dry and wet period discharge in climate normal period, respectively. In 2080s, maximum increases in dry and wet period flow were found for GISS-E2-H RCP 4.5 (moderate warming) and BCC-CSM1.1 RCP8.5 (wettest), respectively. Lowest dry and wet period flows were found for MRI-CGCM3 RCP6.0 (moderate wet) and GISS-E2-R RCP2.6 (coolest) scenarios, respectively.

Table of Contents

ACKNOWLEDGEMENT i

ABSTRACT ii

Table of Contents iv

List of Tables vii

List of Figures x

List of Abbreviation xiv

Chapter 1 Introduction 1

1.1 Climate Change Impact Assessment 1

1.2 Background of The Study 2

1.3 Description of the Study Area 2

1.4 Research Objective 4

1.5 Organization of the thesis 5

Chapter 2 Theory and Literature Review 6

2.1 Review of Climate Change Modeling for Hydrological Impact Assessment 6

2.1.1 Approaches of Climate Change Scenario Generation: 7

2.1.2 Climate Change Scenarios 11

2.1.3 Downscaling Climate Parameters 15

2.1.4 Pattern Scaling 21

2.1.5 Marksim Tool 26

2.2 Review of Physically Based Hydrological Modeling 28

2.2.1 Modeling Concepts of Hydrologic Processes 30

2.2.2 Advantages and Limitations of Physically Based Hydrologic Modelling 30

2.3 Review of Climate Change Impact on Water Availability of BRB 32

2.4 SWAT Model 35

2.4.1 Conceptual Basis 35

2.4.2 Water Balance 35

2.4.3 Hydrology 43

2.4.4 SWAT Advanages 47
Chapter 3 Methodology 48
3.1 Introduction 48
3.2 Data Collection 49
3.2.1 Digital Elevation Model, Land use and Soil Data 49
3.2.2 Weather and Discharge data 51
3.3 Bias Correction 52
3.4 Steps of Model Setup 53
3.5 Synthetic Approach of Climate Change Scenario Generation 53
3.6 Selection of Climate Models and Scenarios 54
3.7 Pattern Scaling 55
3.8 Future Scenario Generation 55
3.8.1 Correction of flow for future scenarios 56
Chapter 4 Model Development 57
4.1 Introduction 57
4.2 Steps of Model Setup 57
4.2.1 Biases in NASA POWER Precipitation 57
4.2.2 Watershed Delineation 64
4.2.3 Weather Data Definition 65
4.2.4 Simulation Method Selection 66
4.2.5 Sensitive Parameter Selection 66
4.3 Calibration and validation 68
4.3.1 Calibration using SWAT-CUP tool 68
4.3.2 Model Performance Evaluation 70
Chapter 5 Results and Discussions 72
5.1 Introduction 72
5.2 Water Balance of the BRB 72
5.3 Selection of Climate Change Scenarios 74
5.3.1 Selection of Points for Analysis: 75

5.3.2 Selection of Scenarios: 83
5.4 Sensitivity Analysis 84
5.4.1 Sensitivity to Precipitation Change: 85
5.4.2 Sensitivity to Temperature Change: 87
5.4.3 Sensitivity to the Combined Effect of Temperature and Precipitation 89
5.5 Spatial Distribution of High Resolution Climate Data 90
5.6 Climate Change Impact on Flow of BRB 91
5.6.1 Mean Annual Stream Flow Analysis 93
5.6.2 Maximum Annual Stream Flow Analysis 104
5.6.3 Minimum Annual Stream Flow Analysis 114
5.6.4 Climate Change Impact at Kurigram Station 121
Chapter 6 Conclusions and Recommendations 123
6.1 Conclusions 123
6.2 Recommendations for Future Studies 124
Reference 126
Appendix A 143
Appendix B 152
AppendixC 155
AppendixD 181
AppendixE 196

List of Tables

Table No. **Title** **Page No.**

Table 1.1: Mean annualprecipitation in Ganges, Brahmaputra and Meghna basin (Mirza, 2003).....4

Table 2.1: Examples of Hydrological Impact Studies Based on Synthetic Climate Change Scenarios.....9

Table 2.2: Spatial Resolution of selected GCMs in IPCC TAR and AR5.....10

Table 2.3: Median temperature anomaly over pre-industrial levels and SRES comparisons based on nearest temperature anomaly (Moss et.al., 2010).....13

Table 2.4: List of recent studies on effect of climate change on water resources based on statistical downscaling approach of GCMs output.....19

Table 2.5: List of recent studies n effect of climate change on water resources based on dynamic downscaling downscaling 20

Table 2.6: Selected physically based hydrologic model, spatial description and discretization type 29

Table 2.7: Advantages and limitations of physically based distributed hydrologic models over lumped conceptual models 31

T C C strandardized precipitation 33

Table 2.9:Changes in mean annual and mean peak discharge of GBM basin for CSIRO9, UKTR, GFDL and LLNL.....34

Table 2.10:Changes in 10 year return period flood for A1B and A2 scnerio in 2080-2099.....34

Table 3.1:Land use distribution in Brahmaputra River Basin.....49

Table 3.2: Basic input data used in this study.....52

Table 4.1: All the calculations done in this step to correct the bias in NASA POWER data. 60

Table 4.2: Monthly ratios obtained for bias correction.....61

Table 4.3: Most sensitive SWAT parameters and their fitted values for Brahmaputra river basin 67

Table 4.4: Model performance statistics for calibration (1981-1995) and validation period (1996-2010) of the Brahmaputra river basin.....70

Table 4.5: General Reported ratings for Nash-Sutcliffe efficiency (NSE), Mean relative bias (PBIAS), Root mean square error-standard deviation

ratio (RSR) and Coefficient of determination (R2) for calibration and validation process (Rossi et al, 2008). 70
Table 5.1: Annual average water balance of Brahmaputra River Basin.(1981-1995)....72
Table 5.2: Average monthly water availability of Brahmaaputra river basin (all in mm) 74
Table 5.3: Precipitation change (%) for RCP 2.6 76
T T C RCP 77
Table 5.5: Precipitation change (%) for RCP 4.5 78
Table 5.7: Precipitation change (%) for RCP 6.0 80
T T C RCP 81
Table 5.9: Precipitation change (%) for RCP 8.5 81
T T C RCP 82
Table 5.11: Selected scenarios from the analysis of precipitation and temperature change of all the scenarios....83
Table 5.12: Mean annual discharge (m^3/s) due to the changes in temperature and precipitation....84
Table 5.13: Changes in mean annual discharge (%) due to the changes in temperature and precipitation....84
Table 5.14: Mean dry season (Jan-May) discharge (m^3/s) due to the changes in temperature and precipitation....84
Table 5.15: Changes in mean dry season (Jan-May) discharge (%) due to the changes in temperature and precipitation....85
Table 5.16: Mean wet season (June-December) discharge (m^3/s) due to the changes in temperature and precipitation....85
Table 5.17: Changes in mean wet season (June-December) discharge (%) due to the changes in temperature and precipitation....85
Table 5.18: Change in Discharge (%) for all the six scenarios in 2020s 96
Table 5.19: Change in Discharge (%) for all the six scenarios in 2050s 98
Table 5.20: Changes in Discharge (%) for all the six scenarios in 2080s....99
Table 5.21: Change in Maximum Discharge (%) for all the six scenarios in 2020s 107
Table 5.22: Change in Maximum Discharge (%) for all the six scenarios in 2050s 108
Table 5.23: Change in Maximum Discharge (%) for all the six scenarios in 2080s 109

Table 5.24: Change in Minimum adjusted discharge (%) for all the six scenarios in 2020s 115
Table 5.25: Change in Minimum adjusted discharge (%) for all the six scenarios in 2050s 116
Table 5.26: Change in Minimum adjusted discharge (%) for all the six scenarios in 2080s 117

List of Figures

Figure No. **Title** **Page No.**

Figure 1.1: Brahmaputra River Basin 3

Figure 2.1: Different approaches of climate change modeling for water resources impact assessment (Islam, 2011a). 7

Figure 2.2: Changes in radiative forcing relative to pre-industrial conditions. 14

Figure 2.3: Trends in concentrations of greenhouse gases (van Vuuren, 2011). 14

Figure 2.4: Emissions of main greenhouse gases across the RCPs..... 15

Figure 2.5: Hydrologic process in SWAT 36

Figure 2.6: HRU/Subbasin in command loop (Neitsch, S.L.et. al., 2005)..... 37

Figure 2.7: In-stream processes modeled by SWAT 41

Figure 3.1: Digital Elevation Model of Brahmaputra River Basin 50

Figure 3.2:Land use map of Brahmaputra River Basin 50

Figure 3.3:Soil use map of Brahmaputra River Basin 51

Figure 4.1: Location of NASA Power stations, BMD stations and NCDC stations 58

Figure 4.2: Bias correction at Rangpur and Sayedpur station (Two stations average as both are near to one NASA Power station) 62

Figure 4.3: Bias correction at Ishurdi station 62

Figure 4.4: Bias correction at Tangail station 63

Figure 4.5: Bias correction at Nagqu station..... 63

Figure 4.6: Bias correction at Shilguri station 64

Figure 4.7: Bias correction at Lhasa station..... 64

Figure 4.8: Sub basins and delineated stream network of Brahmaputra River Basin 65

Figure 4.9: Global sensitivity analysis of calibration parameters 67

Figure 4.10: Monthly observed and simulated flows for the calibration and validation period 1981 to 2010..... 69

Figure 4.11: Scatter plot of observed vs simulated flow at Bahadurabad station for 1981-2010……7

Figure 5.1: Schematic figure of water balance of Brahmaputra River Basin. 73

Figure 5.2: Average (1981-1995) monthly water availability of Brahmaaputra River Basin (all in mm)..... 73

Figure 5.3: Selected locations in Brahmaputra river basin for GCM data extraction and analysis 75

Figure 5.4: ΔT C ΔP(%) plot of all the models for RCP2.6 77

Figure 5.5: ΔT C ΔP(%) plot of all the models for RCP 4.5 79

Figure 5.6: ΔT C ΔP(%) plot of all the models for RCP 6.0 80

Figure 5.7: ΔT C ΔP(%) plot of all the models for RCP 8.5 83
Figure 5.8: Changes in annual mean streamflow (%) at Bahadurabad station dueto changing ΔP (%). 86
Figure 5.9: Mean monthly streamflow at Bahadurabad station due to ΔT C ΔP=-10% to +40% (10% increment)..... 86
Figure 5.10: Changes in mean monthly streamflow (%) at Bahadurabad station due to ΔT C ΔP=-10% to +40% (10% increment)..... 87
Figure 5.11: Changes in ΔQ (%) at Bahadurabad station due to changing ΔT C 88
Figure 5.12: Mean monthly streamflow (m3/s) at Bahadurabad station due to ΔP=0% and ΔT C 88
Figure 5.13: Changes in mean monthly streamflow (%) at Bahadurabad station due to ΔP=0% and ΔT C 89
Figure 5.14: Changes in ΔQ vs ΔP at Bahadurabad station due to changing ΔP and ΔT 89
Figure 5.15: Changes in ΔQ vs ΔT at Bahadurabad station due to changing ΔT C)..... 90
Figure 5.16: Spatial distribution of precipitation for base period 90
Figure 5.17: Spatial distribution of maximum temperature for base period 91
Figure 5.18: Spatial distribution of minimum temperature for base period..... 91
Figure 5.19: Mean monthly discharge (m^3/s) for 2020s at Bahadurabad station for Brahmaputra river basin 92
Figure 5.20: Mean monthly discharge (m^3/s) for 2050s at Bahadurabad station for Brahmaputra river basin 93
Figure 5.21: Mean monthly discharge (m^3/s) for 2080s at Bahadurabad station for Brahmaputra river basin 93
Figure 5.22: Box-plot of mean annual discharge (m^3/s) of all the scenarios for 2020s, 2050s and 2080s 94
Figure 5.23: Box-plot of mean dry period discharge (m^3/s) of all the scenarios for 2020s, 2050sand 2080s..... 95
Figure 5.24: Box-plot of mean wet period discharge (m^3/s) of all the six scenarios for 2020s, 2050sand 2080s..... 95
Figure 5.25: ΔT C 2020s, 2050s and 2080s..... 99
F ΔT C 2020s, 2050s and 2080s..... 100
F 7 ΔT C 2020s, 2050s and 2080s..... 100

F ΔP (%) vs changes in mean annual discharge (%) of six scenarios for2020s, 2050s and 2080s 101
F 9 ΔP (%) vs changes in mean dry period discharge (%) of six scenarios for2020s, 2050s and 2080s 101
F 3 ΔP for2020s, 2050s and 2080s 102
Figure 5.31: Modeled vs Estimated Qmean (m^3/s) plot of all the scenarios for 2020s, 2050s and 2080s 104
Figure 5.32: Box-plot of max annual discharge (m^3/s) of all the six scenariosfor 2020s, 2050s and 2080s 105
Figure 5.33: Box-plot of max dry period discharge (m^3/s) of all the six scenariosfor 2020s, 2050s and 2080s 105
Figure 5.34: Box-plot of max wet period discharge (m^3/s) of all the six scenariosfor 2020s, 2050s and 2080s 106
F 3 ΔT C for2020s, 2050s and 2080s 110
F 3 ΔT C for2020s, 2050s and 2080s 110
F 37 ΔT C scenarios for 2020s, 2050s and 2080s 111
F 3 ΔP (%) vs changes in maximum annual discharge (%) of six scenarios for2020s, 2050s and 2080s 111
F 39 ΔP (%) vs changes in maximum dry period discharge (%) of six scenarios for 2020s, 2050s and 2080s 112
F ΔP (%) vs changes in maximum wet period discharge (%) of six scenarios for 2020s, 2050s and 2080s 112
Figure 5.41: Modeled vs Estimated Qmax (m^3/s) plot of all the scenarios for 2020s, 2050s and 2080s 114
F ΔT C 2020s, 2050s and 2080s 118
F 3 ΔT C for 2020s, 2050s and 2080s 118
F ΔT C for 2020s, 2050s and 2080s 119
F ΔP (%) vs changes in minimum annual discharge (%) of six scenarios for 2020s, 2050s and 2080s 119

F ΔP (%) vs changes in minimum dry period discharge (%) of six scenarios for 2020s, 2050s and 2080s 120
F 7 ΔP (%) vs changes in minimum wet period discharge (%) of six scenarios for 2020s, 2050s and 2080. 120
Figure 5.48: Mean monthly streamflow at Kurigram station in 2020s 121
Figure 5.49: Mean monthly streamflow at Kurigram station in 2050s 122
Figure 5.50: Mean monthly streamflow at Kurigram station in 2080s 122

List of Abbreviation

Acronym	Definition
2020s	2010-2039
2050s	2040-2069
2080s	2070-2099
BMD	Bangladesh Meteorological Department
BRB	Brahmaputra River Basin
BWDB	Bangladesh Water Development Board
DEM	Digital Elevation Model
ET	Evapotranspiration
FAO	Food and Agriculture Organization
GBM	Ganges Brahmaputra Meghna
GCM	General Circulation Model
HWSD	Harmonized World Soil Database
NASA	National Aeronautics and Space Administration
NASA POWER	NASA Prediction Of Power Worldwide Energy Resources
NCDC	National Climatic Data Center
NOAA	National Oceanic and Atmospheric Administration
PET	Potential Evapotranspiration
RCM	Regional Climate Model
RCP	Representative Concentration Pathways
SWAT	Soil Water Assessment Tool
USGS	U.S. Geological Survey

Chapter 1

Introduction

1.1 Climate Change Impact Assessment

Bangladesh is widely recognized as one of the most vulnerable countries to climate change. Due to the geographic location, too much flow during monsoon and scarcity during dry period has become highly sensitive to the contribution of flow from the major basins. The flow also greatly affects the socio-economic conditions, such as the population growth, inequity, poverty, regional development, food production etc. Climate change will alter the flow pattern and seasonal variation which will have significant impact on total development of the country (Climate change cell, 2006).

High flow during monsoon period causes flood all over the country which depends on the flow contribution of the major river basins, namely Ganges-Brahmaputra-Meghna (GBM)river system. According to IPCC fourth assessment report (IPCC-WGII, 2007) - (a) Annual mean rainfall exhibits increasing trends in Bangladesh (b) Decadal rain anomalies are above long term averages since 1960s (c) Recurring floods have taken place during 2002, 2003, and 2004 (d) Cyclones originating from the Bay of Bengal have been noted to decrease since 1970 but the intensity has increased and (e) Frequency of monsoon depression and cyclone is also increasing with the change of climate.

Different parts of the country are frequently facing water scarcity during post monsoon and pre-monsoon period when the rainfall diminishes and temperature increases (Climate change cell, 2006). Average temperature has registered an increasing trend of about 1°C in May and 0.5°C in November during the 14 year period from 1985 to 1998 (IPCC AR4 WG2, 2007). Water shortages greatly affecting rapid urbanization and industrialization, population growth and inefficient water use, which are worsened by the adverse impacts on demand, supply, water quality and climate change (Climate change cell, 2006). Increased temperature and reduced rainfall causes increased evapotranspiration and reduced crop yield. So, it stands that the assessment of the impact of climate change to the future availability of water in the major river basins is a national priority.

1.2 Background of The Study

The Ganges-Brahmaputra-Meghna (GBM) river basin is one of the most vulnerable areas in the world under the potential impact of climate change (Gain, 2011). Gain(2011) mentioned three major reasons for such susceptibility to climate change which are snow melt, flood and sea level rise. First, strong influence of snow and ice melt in the upstream as 60 percent of the area has elevation greater than 2000m where cryospheric process is important. Increased temperature would lead to an increase in summer flow followed by a reduction of flow when glacier disappears and snowfall reduces (Immerzeel, 2008). Secondly, extreme flooding and monsoon rainfall greatly influence the basin hydrology of Ganges and Brahmaputra river basin (Warrick et. al, 1996). If climate change influence the intensity of monsoon rain which may cause variability of available water in other seasons. Such as too much water may flow during monsoon which will cause reduction of dry season flow unless water is stored in any reservoir (Oki and Kanae, 2006). Thirdly, climate change will cause sea level rise which will lead to backwater effect in Ganges Brahmaputra basin (Agrawala et. al., 2005). So in order to face the future disaster or scarcity, better understanding of the basin response to future climate change is crucial.

In this research an attempt has been made to get a comprehensive understanding of the comprehensive basin characteristics of Brahmaputra River Basin (BRB). The basin response to different climate change scenarios has been analyzed in detail.

1.3 Description of the Study Area

Brahmaputra River Basin (BRB) is one of the major basins in the world draining an area of about 530,000 km^2 through China (50.5%), India (33.6%), Bangladesh (8.1%) and Bhutan (7.8%) (Immerzeel, 2008). After originating from Kailash range in Tibet (China), it flows 2,900 km and meets Ganges in Bangladesh. Flow of this basin experiences various environments. After Himalayan slopes it enters India at elevation of 660m and then flows southward for about 220 km to reach Pasighat (Ghosh, 2012). It is known as Brahmaputra river after the confluence of two major tributaries, Dibang and Lohit at Pasighat. After flowing 710 km through Assam valley it enters Bangladesh. Almost hundred tributaries contribute runoff to the Brahmaputra river among which 15 in the north bank and 10 in the south are pretty large (Sarma, 2004). The river has gentle bed slope in the lower reaches falling at a rate of 0.079 m per km,

whereas in the Himalayan region the channel is narrow and gradient is about 16.8 m per km (Sarma, 2005). Figure 1.1 shows the extent of Brahmaputra river basin over different countries.

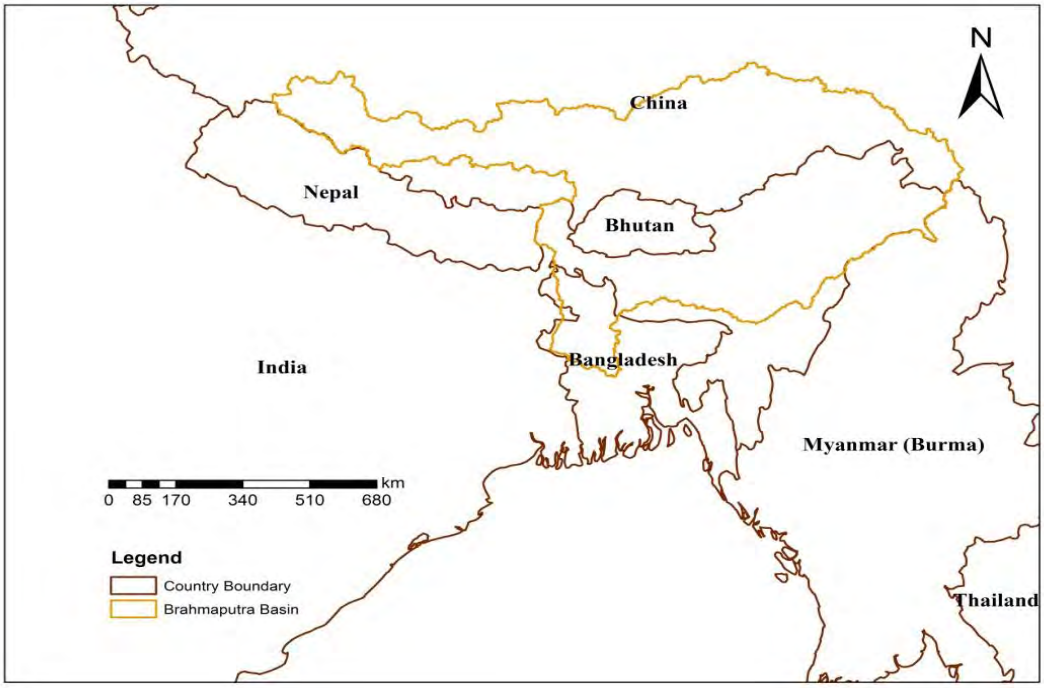

Figure 1.1: Brahmaputra River Basin

Brahmaputra river is known as Jamuna river in Bangladesh which is highly braided in nature having a width of 6 to 18 km.The average annual discharge is about 20,000 m^3/s (Immerzeel, 2008). Immerzeel (2008) classified the basin into three different physiographic zones: Tibetal Plateau (TP), Himalayan belt (HB) and the floodplain (FP). Each zone responds differently to climate change. The area coverage of TP, HB and FP are 44.4%, 28.6% and 27% with an elevation of greater than 3500, 100-3500 and less than 100 m (Immerzeel, 2008). Average temperature in lower BRB varies from17°C in winter and 27°C high in summer and the total annual precipitation in monsoon months (JJAS) is 2354 mm (Gain, 2011). Bahadurabad station is the major discharge measurement station having high quality long period data. For any hydrological assessment of this basin it is the most important source of reliable data. So in this study long term discharge data of Bahadurabad station will be used for calibration and validation of the model.

Table 1.1: Mean annualprecipitation in Ganges, Brahmaputra and Meghna basin (Mirza, 2003).

Basin	Country	Mean annual precipitation (mm)
Ganges	Nepal	1860
	India	450-2000
	Bangladesh	1570
Brahmaputra	Tibet (China)	400-500
	Bhutan	500-5000
	India	2500
	Bangladesh	2400
Meghna/ Barak	India	2640
	Bangladesh	3575

Mean annual precipitation for the GBM is shown in Table 1.1. The general circulation over the basin area undergoes abrupt seasonal changes during late spring and early summer due to tropospheric warming over the Asian landmass, and causes early summer rains over the basin (Heet et.al., 1987). The mean annual value of such pre-monsoonal heavy rains shows a rainfall above 100 mm/day for 7.7 days and above 300 mm/day for 1.6 days for the observation period of 1993–2001 (Soja and Starkel, 2007). The river basin receives high-intensity storm events frequently during the four monsoon months from June to September (Ghosh, 2012). Rainfall is very much high in Cherapunji region where rainfall remains above 100 mm/day for around 28.3 days and 5 days are found with rainfall greater than 300 mm/day based on the observed rainfall during 1993-2001 (Soja and Starkel, 2007). About 66-85% of annual rainfall occurs during monsoon and 20-30% occurs during pre-monsoon season, whereas small percentage of rainfall occurs in winter (Sarma, 2005).

1.4 Research Objective

The specific objectives of this study are:

a. To develop and calibrate a hydrological model of Brahmaputra river basin using Soil Water Assessment Tool (SWAT).
b. To identify the future extreme and moderate climate scenarios and corresponding GCMs for Brahmaputra river basin.
c. To generate high resolution climatic data for selected GCMs using Pattern Scaling.

d. To study the impacts of climate change on future flow of Brahmaputra river basin for selected stations.

1.5 Organization of the thesis

Chapter 1 is an introduction to the thesis. Here, the background of the study has been discussed, study area has been introduced and objective of the thesis is described.

Chapter 2 is literature review. This chapter contains review of literature of several topics which include- review of climate change modeling, hydrological model types and its properties, climate change study on water availability in Brahmaputra river basin, SWAT model concept and capacities to simulate several hydrologic processes.

Chapter 3 discusses the steps followed in the present thesis to setup, calibrate/validate the model, analyze sensitivity of climate parameters to simulate dischargeand assess the impact of climate change on flow in Brahmaputra river basin.

Chapter 4 describes the detail procedure followed to setup hydrological model of Brahmaputra river basin. This chapter describes the bias correction done on climate data, parameters used to calibrate the model and evaluate the performance of calibration/validation.

Chapter 5 is results and discussions which contains discussion on water balance, sensitivity analysis, selection of climate change scenarios to be used for simulation and impact of climate change on water availability.

Chapter 6 is conclusions and recommendations. This chapter gives a summary of the results obtained in this study and also includes recommendations for further study relevant to this topic.

Chapter 2
Theory and Literature Review

2.1 Review of Climate Change Modeling for Hydrological Impact Assessment

Warming of the climate system in recent decades is unequivocal because of the observational evidences which confirm the increases in global average air and ocean temperatures (Bates et.al., 2008). These changes in global climate can affect a number of components of the hydrological cycle and hydrological systems (e.g. precipitation, snowmelt, evaporation, soil moisture, runoff etc). Such changes in hydrologic system will affect nearly every aspect of human well-being, from agricultural productivity and energy use to flood control, municipal and industrial water supply, fishery and wildlife management. So it is obvious to understand how a change in global climate could affect regional water supplies. Literature review of current studies indicates that climate change modeling for hydrological impact studies generally done in three steps (Islam, 2011a):

Step 1: Runoff simulation under present climatic conditions for climate normal period (a 30 years period, usually 1961-1990 or 1971-2000 or 1981-2010) using a hydrologic model calibrated and validated with historical data;

Step 2: Generation of climate change scenarios for different future periods (usually three 30 years period of 21st century, namely, 2010-2039, 2040-2069, and 2070-2099);

Step 3: Runoff simulation under changed climatic conditions for future periods based on the generated climate change scenarios.

The effect of climate change on surface water resources in future is usually demonstrated by comparing the runoff generated from step 3 and step 1. Runoff simulation under present and changed climate (Step 1 and 3) is usually conducted by hydrologic models. Scientific literatures on hydrological impacts of climate change contain a large number of reports detailing the application of various hydrologic models in global, regional, or basin scale.

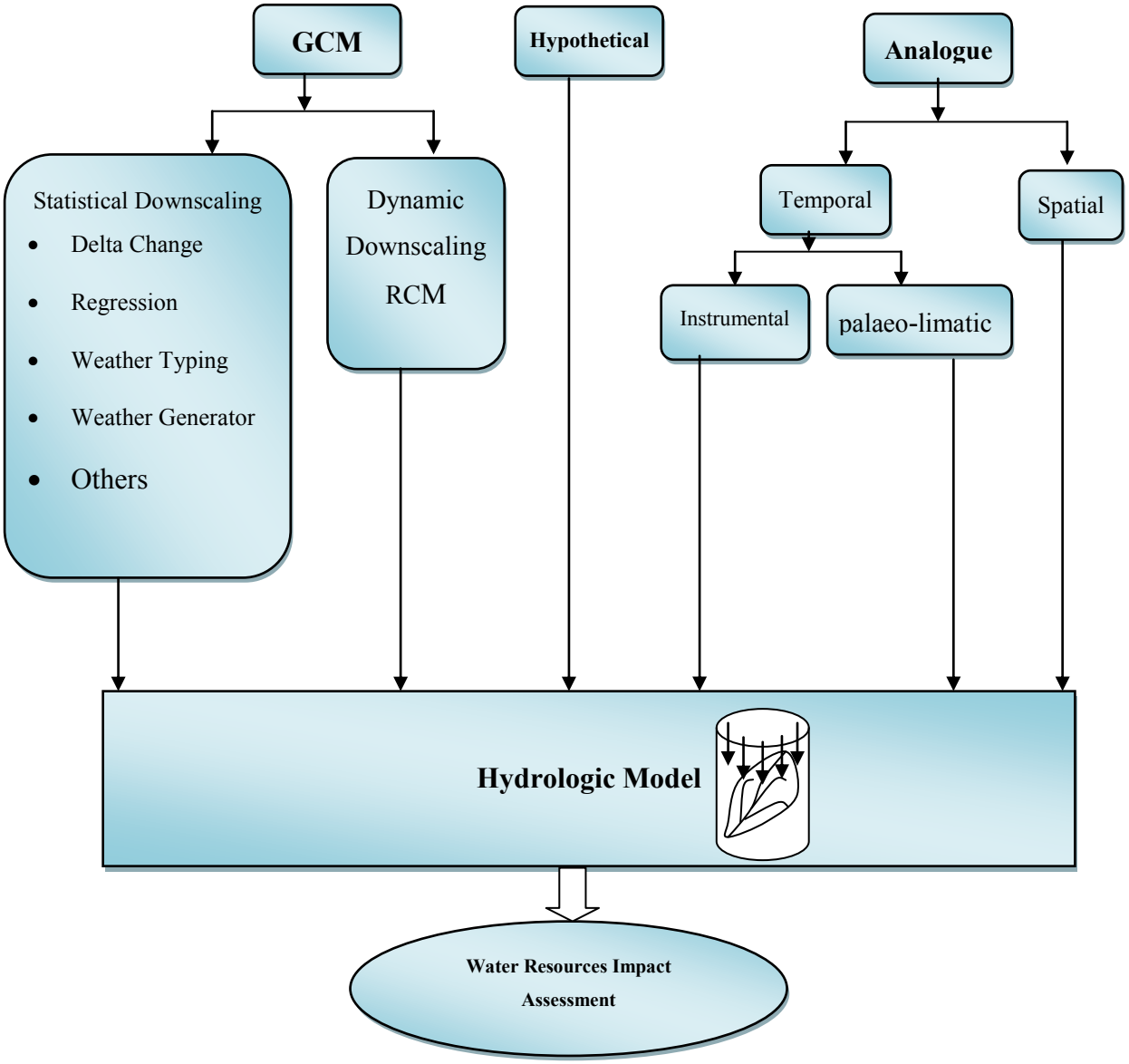

Figure 2.1: Different approaches of climate change modeling for water resources impact assessment (Islam, 2011a).

2.1.1 Approaches of Climate Change Scenario Generation:

There are different approaches to generate climate change scenarios for hydrological impact studies. They can be broadly classified as synthetic approach, analogue approach and climate model based approach (Figure2.1) and will be discussed in the following paragraphs:

2.1.1.1 Synthetic Approach

In the synthetic approach the future climatic variables (mostly precipitation and temperature) are changed incrementally by arbitrary amounts. These changes can be made in annual, seasonal or monthly scales. Climate change scenario generation in this method consists of three steps:

Step 1: Estimation of average annual or monthly changes in climate data. Typically temperature and precipitation changes are estimated by,

$$\Delta T = +1°, +2°, \text{ and } +4°$$
$$\Delta P = 0, \pm 10\%, \pm 20\%$$

Step 2: Perturbation of historical time series of climatic data. Typically temperature and precipitation for climate change scenario are perturbed as,

$$T2 = T1 + \Delta T \quad (2.1)$$
$$P2 = P1 + \Delta P \quad (2.2)$$

where T1, T2 and P1, P2 are the historic and future temperature and precipitation respectively.

Step 3: Drive a calibrated hydrological model based on perturbed precipitation and temperature to simulate hydrological characteristics (runoff, soil moisture, evapotranspiration etc.).

Many climate change studies on water resources impact assessment are based on this approach (e.g. Nemec and Schaake, 1982; Gleick, 1986, 1987; McCabe and Ayers, 1989; Schaake and Liu, 1989; Nash and Gleick, 1990; Vehviläinen and Lohvansuu, 1991; Panagoulia, 1991; Arnell, 1992; Ng and Marsalek, 1992; Whetton et.al., 1993; Avila et.al., 1996; ; Singh and Kumar, 1997; Xu and Halldin, 1997; Xu, 2000; Guo et.al., 2002; Davies, 2004; Jiang et.al., 2007). A summary of those studies is shown is Table 2.1.

Table 2.1: Examples of Hydrological Impact Studies Based on Synthetic Climate Change Scenarios.

Authors	Location	Predictand	Perturbation
Nemec and Schaake(1982)	Leaf River Basin, USA Pease River Basin, USA Nzoia River Basin, western Kenya.	T P	±1, +3 °C ± 10%, ± 25%
Schaake and Liu (1989)	Southeast, USA	ET P	+10% +10%
Nash and Gleick (1990)	Colorado River Basin	T P	+2, +4 °C 0, ± 10%, ± 20%
Whetton et.al.(1993)*	Perth, Australia	ET P	+20% to 40% -20% to 40%
Chiew et. al. (1995)	Australia	T P	0, +2, +4 °C 0, ± 10%, ± 20%, ± 30%, ± 40%
Xu and Halldin (1997)	NOPEX Area ,Europe	T P	+2, +4 °C ± 10%, ± 20%
Fowler (1999)*	Auckland, New Zealand	ET P	-20% to 40% -20% to 40%
Xu (2000)	Central Sweden	T P	+1, +2, +4 °C 0,± 10%, ± 20%
Davies (2004)*	North-Central Sweden	T P	-5 to +15 °C -10% to 40%
Jiang et.al. (2007)	Dongjiang Basin, South China	T P	+1, +2, +4 °C 0, ±10%, ± 20%
Guo et.al. (2002)	China	T P	±1, ±2, ±3 ° C 0%, ±25%, 50%, 100%

* Response surfaces plotting; Abbreviations: T–Temperature, P– Precipitation, ET– Potential Evapotranspiration (Islam, 2011a).

2.1.1.2 Analogue Approach of Climate Change Modeling

In analogue approach, climate change scenarios are constructed by identifying recorded climate regimes which may resemble the future climate in a given region (IPCC, 2001). In this approach the fundamental assumption is that, climate will respond in the same way to a unit change in forcing despite its source or the boundary conditions in place at the time. Analogue approach can be spatial or temporal. In spatial analogue approach attempts are made to identify regions which have a climate that is similar to that projected for the study region in the future. In temporal analogues for a given location a past climate is analyzed to resemble the projected future climate for that location (Islam, 2011a).

Table 2.2: Spatial Resolution of selected GCMs in IPCC TAR and AR5

	Model	Institution	Resolution Lat x Long	Reference
1	BCC-CSM 1.1	Beijing Climate Center, China Meteorological Administration	2.8125 x 2.8125	Wu, T., 2012
2	BCC-CSM 1.1(m)	Beijing Climate Center, China Meteorological Administration	2.8125 x 2.8125	Wu, T., 2012
3	CSIRO-Mk3.6.0	Commonwealth Scientific and Industrial Research Organisation and the Queensland Climate Change Centre of Excellence	1.875 x 1.875	Collier, M.A.et.al., 2011
4	FIO-ESM	The First Institute of Oceanography	2.812 x 2.812	Song, Z., Qiao, F., Song, Y.
5	GFDL-CM3	Geophysical Fluid Dynamics Laboratory	2.0 x 2.5	Donner, L.J.et.al., 2011
6	GFDL-ESM2G	Geophysical Fluid Dynamics Laboratory	2.0 x 2.5	Dunne, J.P.et.al., 2012
7	GFDL-ESM2M	Geophysical Fluid Dynamics Laboratory	2.0 x 2.5	Dunne, J.P.et.al., 2012
8	GISS-E2-H	NASA Goddard Institute for Space Studies	2.0 x 2.5	Schmidt, G.A.et.al., 2006.
9	GISS-E2-R	NASA Goddard Institute for Space Studies	2.0 x 2.5	Schmidt, G.A.et.al., 2006
10	HadGEM2-ES	Met Office Hadley Centre	1.2414 x 1.875	Collins, W.J.et.al.2011)
11	IPSL-CM5A-LR	Institut Pierre-Simon Laplace	1.875 x 3.75	Dufresne, J.L.et.al., 2013
12	IPSL-CM5A-MR	Institut Pierre-Simon Laplace	1.2587 x 2.5	Dufresne, J.L.et.al., 2013
13	MIROC-ESM	Atmosphere and Ocean Research Institute (The University of Tokyo), National Institute for Environmental Studies, and Japan Agency for Marine-Earth Science and Technology	2.8125 x 2.8125	Watanabe, S.et.al., 2011
14	MIROC-ESM-CHEM	Atmosphere and Ocean Research Institute (The University of Tokyo), National Institute for Environmental Studies, and Japan Agency for Marine-Earth Science and Technology	2.8125 x 2.8125	Watanabe, S.et.al.,2011
15	MIROC5	Japan Agency for Marine-Earth Science and Technology, Atmosphere and Ocean Research Institute (The University of Tokyo) and National Institute for Environmental Studies	1.4063 x 1.4063	Watanabe, S.et.al.,2010
16	MRI-CGCM3	Meteorological Research Institute	1.125 x 1.125	Yukimoto, S., 2012
17	NorESM1-M	Norwegian Climate Centre	1.875 x 2.5	Kirkevag, A., Iversen, T., Seland, O., debernard,J.B., Storelvmo, T., Kristjansson, J.E.,2008

Many climate change studies on water resources are found in literature were based on analogue approach (e.g. Palutikof, 1987; Krasovskaia and Gottschalk, 1992;

Knox,1993; Zorita and Storch, 1999; Cohen and Kulkarni, 2001; Bouraoui et.al., 2004; Yao et.al., 2009; Orlowsky et.al., 2010). Most of them used temporal analogue approach based on historical measurement of precipitation, temperature and river flows.

2.1.1.3 Climate change modeling based on general circulation models

Development of General Circulation Models (GCMs) is one of the most prominent climate change research advancements starting from the early 1990s onwards, and they are the most advanced tools currently available for simulating the response of the global climate system to changing atmospheric composition (e.g. increase in atmospheric CO_2 on the mean global climate) (IPCC, 2001; Shackley et.al., 1998). GCMs are numerical atmospheric model coupled with three dimensional dynamic ocean models, together with complex land surface schemes and sea ice models, and can provide considerable potential for the study of climate change and variability (Fowler et.al., 2007; Shackley et.al., 1998). GCMs used to solve equations describing the movement of energy and momentum, along with the conservation of mass at discrete points on the entire surface of the Earth, at a fixed time interval, and for separate layers in the atmosphere defined by a regular grid (Wilby, 2009).

Initially atmospheric General Circulation Models (GCMs) were run to equilibrium under current ($1xCO_2$) and doubled ($2xCO_2$) emissions forcing to estimate their potential effect on global climate. After being coupled with Oceanic Circulation Models, these GCMs are forced with transient greenhouse emissions to allow for the estimation of the rate at which climate changes might occur. Table 2.2 shows different GCMs available, their institution and resolutions.

2.1.2 Climate Change Scenarios

The new scenarios are called Representative Concentration Pathways (RCPs). There are four pathways: RCP8.5, RCP6, RCP4.5 and RCP2.6. According to van Vuuren (2011a)-

"Two important characteristics of RCPs are reflected in their names. The word "representative" signifies that each of the RCPs represents a larger set of scenarios in the literature. In fact, as a set, the RCPs should be compatible with the full range of

emissions scenarios available in the current scientific literature, with and without climate policy. The words "concentration pathway" are meant to emphasize that these RCPs are not the final new, fully integrated scenarios (i.e. they are not a complete package of socio-economic, emission and climate projections), but instead are internally consistent sets of projections of the components of radiative forcing that are used in subsequent phases. The use of the word "concentration" instead of "emissions" also emphasizes that concentrations are used as the primary product of the RCPs, designed as input to climate models. Coupled carbon-cycle climate models can then as well calculate associated emission levels (which can be compared to the original emissions of the IAMs) (see Hibbard et.al., 2007). In total, a set of four pathways were produced that lead to radiative forcing levels of 8.5, 6, 4.5 and 2.6 W/m^2,bythe end of the century. Each of the RCPs covers the 1850–2100 period, and extensions have been formulated for the period thereafter (up to 2300)."

2.1.2.1 RCP Primary Characteristics

RCP 8.5 was developed using the MESSAGE model and the IIASA Integrated Assessment Framework by the International Institute for Applied Systems Analysis (IIASA), Austria. This RCP is characterized by increasing greenhouse gas emissions over time, representative of scenarios in the literature that lead to high greenhouse gas concentration levels (Riahi et.al., 2007).

RCP6.0 was developed by the AIM modeling team at the National Institute for Environmental Studies (NIES) in Japan. It is a stabilization scenario in which total radiative forcing is stabilized shortly after 2100, without overshoot, by the application of a range of technologies and strategies for reducing greenhouse gas emissions (Fujino et.al., 2006; Hijioka et.al., 2008).

RCP 4.5 was developed by the GCAM modeling team at the Pacific Northwest N L ‘ J G C R I JGCRI U States. It is a stabilization scenario in which total radiative forcing is stabilized shortly after 2100, without overshooting the long-run radiative forcing target level (Clarke et.al., 2007; Smith and Wigley, 2006; Wise et.al., 2009).

RCP2.6 was developed by the IMAGE modeling team of the PBL Netherlands Environmental Assessment Agency. The emission pathway is representative of scenarios in the literature that lead to very low greenhouse gas concentration levels. It

— -and- ” ;

around 3.1 W/m^2 by mid-century, and returns to 2.6 W/m^2 by 2100. In order to reach such radiative forcing levels, greenhouse gas emissions (and indirectly emissions of air pollutants) are reduced substantially, over time (Van Vuuren et.al., 2007). (Characteristics quoted from van Vuuren et.al,. 2011a)

Emissions and concentrations, forcings and temperature anomalies Each Representative Concentration Pathway (RCP) defines a specific emissions trajectory and subsequent radiative forcing (a radiative forcing is a measure of the influence a factor has in altering the balance of incoming and outgoing energy in the Earth-atmosphere system, measured in watts per square metre).

Table 2.3: Median temperature anomaly over pre-industrial levels and SRES comparisons based on nearest temperature anomaly (Moss et.al., 2010).

Name	**Radiative forcing**	**CO_2 equiv (p.p.m.)**	**Temp anomaly (°C)**	**Pathway**	**SRES temp anomaly equivalent**
RCP8.5	8.5 W/m^2 in 2100	1370	4.9	Rising	SRES A1F1
RCP6.0	6 W/m^2 post 2100	850	3.0	Stabilization without overshoot	SRES B2
RCP4.5	4.5 W/m^2 post 2100	650	2.4	Stabilization without overshoot	SRES B1
RCP2.6 (RCP3PD)	3 W/m^2 before 2100, declining to 2.6 Wm^2 by 2100	490	1.5	Peak and decline	None

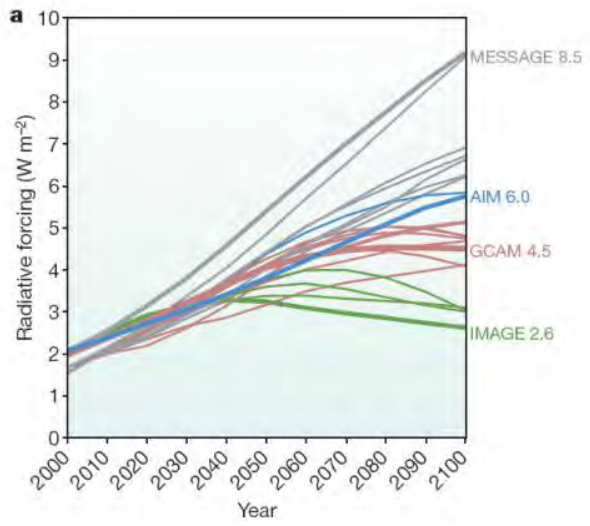

Figure 2.2: Changes in radiative forcing relative to pre-industrial conditions. Bold coloured lines show the four RCPs; thin lines show individual scenarios from approximately 30 candidate RCP scenarios that provide information on all key factors affecting radiative forcing (Moss et. al., 2010)

The forcing trajectories are consistent with socio-economic projections unique to each RCP. For example, RCP2.6 (RCP3PD) assumes that through drastic policy intervention, greenhouse gas emissions are reduced almost immediately, leading to a

‘ T - RCP8.5 - assumes more or less unabated emissions.

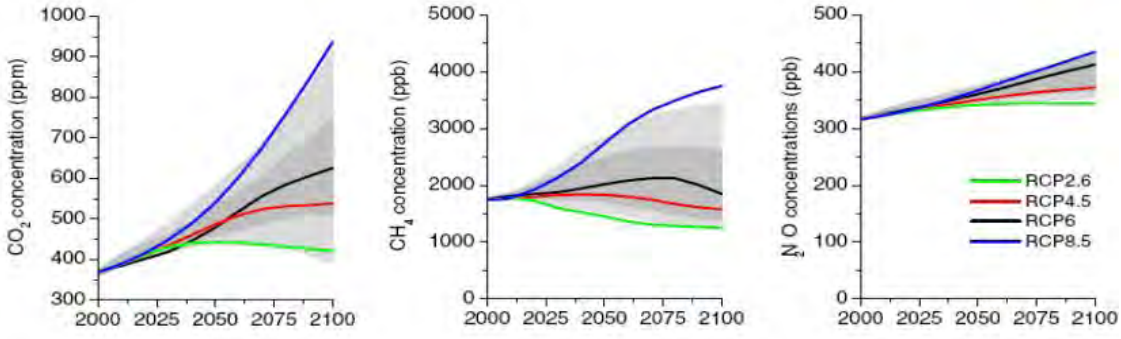

Figure 2.3: Trends in concentrations of greenhouse gases (van Vuuren, 2011). Grey area indicates the 98th, 90th percentile (light/dark grey) of the recent EMF-22 study (Clarke et.al., 2010)

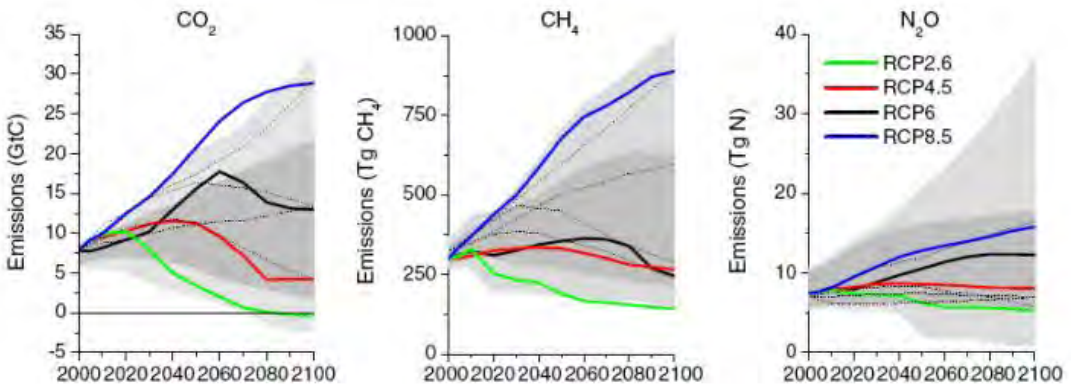

Figure 2.4: Emissions of main greenhouse gases across the RCPs. Grey area indicates the 98th and 90th percentiles (light/dark grey) of the literature. The dotted lines indicate four of the SRES marker scenarios. Note that the literature values are not harmonized (van Vuuren et.al., 2011a).

2.1.3 Downscaling Climate Parameters

Climate scenarios based on GCMs simulations have been using increasingly to predict future climatic change impact studies. However, they are not designed to assess the hydrological impact and to do so we need to resolve some of their limitations: GCMs remain coarse in spatial resolution and are unable to resolve various subgrid scale features required for impact studies (Fowler et.al., 2007); Techniques of resolving these gaps between GCMs and hydrological models are usually known as

_ ‘ T GCM

wide numbers of downscaling techniques are found in literature. These techniques can broadly be classified into two categories: statistical downscaling and dynamic downscaling and will be discussed in the following paragraphs.

2.1.3.1 Statistical Downscaling of GCMs Outputs to Local Scale

In statistical downscaling, empirical relationships are established between the GCM-scale climate variables (predictors) and local-scale meteorological variables (predictands) using various statistical methods (Fowler et.al., 2007; Boe et.al., 2007). In general, the empirical relationship can be expressed as,

$$Y = f(X) \qquad \textbf{(2.3)}$$

Where, Y is the local climate variable not adequately described in GCMs and need to be downscaled for hydrologic impact studies, X is the set of large-scale climate variables and f is the function relating them.

Statistical downscaling techniques may be such as delta change method (or perturbation method) or more sophisticated methods as regression models, weather typing schemes and weather generators (Fowler et.al., 2007).

2.1.3.1.1 Delta Change Approach

Given that GCMs can simulate the relative changes more accurately than the actual values (Smith and Pitts, 1997; Fowler et al,. 2007), in this approach the changes between the control and future GCM simulations are applied to the baseline observations, usually known as climate normal, by adding or multiplying the mean climatic change factors. For example, the temperatures and precipitations are downscaled as,

$$T_2 = T_1 + (T_2' - T_1') \quad \textbf{(2.4)}$$

$$P_2 = P_1 \times \frac{P_2'}{P_1'} \quad \textbf{(2.5)}$$

Where,T_1 (P_1) is the baseline observed temperature (precipitation), T_2 (P_2) is the future temperature (precipitation), T_1' (P_1') is the GCM simulated mean temperature (precipitation) for control run, and T_2' (P_2')is the GCM simulated mean temperature (precipitation) for future climate scenario.

Delta change approach has been used in a wide number of climate change studies on water resources. Early studies are based on GCMs simulations for equilibrium 2 x CO2 condition (e.g. Lettenmaier and Gan, 1990; Chiew et.al., 1995; Arnell and Reynard, 1996; Middelkoop et.al., 2001) and later studies are based on IPCC SRES emission scenarios (e.g. Miller et al, 2003; Kerkhoven and Gan, 2008; Githui et.al., 2009; Boyer et.al., 2010; Kerkhoven and Gan, 2010).

2.1.3.1.2 Regression Model Approach

Regression models techniques includes multiple regression model (MLR), artificial neural networks (ANNs), canonical correlation analysis (CCA), singular value

decomposition (SVD), logistic regression model, multi-way partial least squares regression model (N-PLS) etc (Islam, Z., 2011a). In many studies the regression approach started with principal component analysis (PCA) of both the large and local scale variables, which eventually resulted in a significant reduction in data while retaining the signal in the time series.

Multiple linear regressions (MLR) are the least computationally demanding downscaling techniques. In this method predictands (e.g. temperature, precipitation) are downscaled from a set of predictors using least squares. MLR may be based either directly on GCMs grid point data or on principal components (PCs) of predictor fields (Huth, 2002).

2.1.3.1.3 Weather Typing Approach

Weather types are defined as aggregate representation of meteorological variables characterizing regional weather patterns (Hay et.al., 1992). In this downscaling approach empirical relationships are developed between the weather classes and local and regional climate variations. General steps are:

- Defining the weather types,
- Conditioning local surface variables,
- Modeling the circulation-surface climate relationship,
- Estimating climate change by applying GCMs simulated outputs into the model.

There are different approaches to define a weather type or large scale atmospheric patterns. They may be based on exiting circulation-type catalogues (synoptically), by statistical groupings, and by fuzzy rules. Synoptic method (e.g. Lamb Weather Types) typically defines weather types based on empirical orthogonal functions (EOFs) from pressure data or by indices from sea level pressure (SLP) data. Statistical methods include principal components analysis, canonical correlation analysis, and cluster analysis. Recent development is fuzzy rules method. Local surface variables (e.g. precipitation) are conditioned on daily weather patterns by deriving conditional probability distributions for observed statistics, associated with a given atmospheric circulation pattern. General approaches to model the circulation-surface climate

relationship are using Markov Chain models, linear regression, canonical correlation analysis, sampling from present-day instrumental analogue data (Islam, 2011a).

2.1.3.1.4 Weather Generator Approach

Weather generators (WGs) are statistical models that produce time series of meteorological data that have similar statistical properties as that of observed data (Chen et al, 2010). In other words, WGs replicate statistical attributes (e.g. mean and variance) of meteorological observation, but do not reproduce actual sequences of observed events (Wilks and Wilby, 1999). WGs simulating precipitation have two components: precipitation occurrence model and precipitation amount model. In Simple WGs, precipitation occurrence are modeled stochastically by first-order Markov Chain model that emulates transitions between wet and dry spells or dry-days. The probability of precipitation on a given day is based on the wet or dry status of the previous day and can be defined in terms of the two transition probabilities,

$$P00 = 1 - P01 \quad (2.6)$$

$$P10 = 1 - P11 \quad (2.7)$$

where, P01 is the probability of a wet day following a dry day (i.e. probability of {precipitation on day t and no precipitation on day t-1}) and P11= the probability of a wet day following a wet day (i.e. probability of {precipitation on day t and precipitation on day t-1})

More sophisticated WGs includes second-order and third-order Markov chain models for precipitation occurrence and exponential or fourth root methodfor quantifying precipitation amount and are better able to reproduce precipitation occurrence or persistence (Fowler et.al., 2007).

In order to adapt a WG for climate change assessment the model parameters need to be adjusted. There are two approaches (Wilby et.al., 2009):

First, relationships between key parameters (e.g. wet day probabilities) and slowly varying indices of atmospheric circulation that are well simulated by GCMs are developed. Then, the changes in the frequency of those atmospheric patterns as

projected by GCMs are translated into revised weather generator parameters, and daily weather sequences under future forcing are generated.

Second, delta change approach is applied to generate daily weather series for climate change period and the WG is recalibrated. Then, recalibrated WG is driven to synthesize infinitely long daily sequences with the same statistical properties as climate change period.

Table 2.4: List of recent studies on effect of climate change on water resources based on statistical downscaling approach of GCMs output.

Authors	**Study Area**	**Techniques**	**Predictand**
Kerkhoven and Gan (2008; 2010)	Athabasca River Basin, Fraser River Basin, Canada	Delta Change	P,T
Githui et.al. (2009)	Nzoia river catchment in western Kenya	Delta Change	P, T
Boyer et.al. (2010)	Hydrological regimes of the St. Lawrence tributaries, Quebec, Canada.	Delta Change	P, Tmax, Tmin
Huth (2002)	Central Europe.	MLR, SVD	T
Tolika et.al. (2007)	Greece	ANN	P
Matulla (2005)	Austria	CCA	P, T
Penlap (2004)	Cameron	CCA	P
Windman et.al. (2003)	Oregon and Washington Area, USA	SVD	P
Abaurrea and Asín (2005)	Ebro valley, Spain	LRM	P
Bergant and Kajfez-Bogataj (2005)	Slovenia	N-PLS	P,T
Bárdossy et.al. (2005)	Ruhr catchment, Germany	WT	P
Vrac et.al. (2007)	Illinois, USA.	WT	P
Cheng et.al. (2010)	Ontario, Canada	WT	P
Qian et.al. (2010)	Agricultural Regions of Canada	WG	P
Eum et al (2010)	Nakdong River Basin in Korea	WG	P
Wilby et al (2006)	Kennet catchment, UK	SDSM (Hybrid)	P
Souvignet et.al. (2010).	Upper-Elqui watershed, Chile	SDSM (Hybrid)	P

Abbreviations for techniques: MLR – Multiple Linear Regression methods, ANN –Artificial Neural Networks, CCA – Canonical Correlation Analysis, SVD – Singular Value Decomposition, LRM – Logistic Regression Model, N-PLS – Multi way Partial Least Square Method, WG – Weather Generators, WT – Weather Typing, SDSM – Statistical Down Scaling Model (hybrid); Abbreviations for predictands: T – temperature, P – precipitation (Islam, 2011b)

2.1.3.1.5 Other Statistical Downscaling Approaches

Wilby et.al. (2002) developed a hybrid of stochastic weather Generator and regression model, namely, SDSM (Statistical Downscaling Model). The regression component of SDSM uses daily atmospheric circulation patterns and moisture variables to condition local weather generator parameters at application sites and the stochastic component enables the generation of multiple simulations by slightly differing time series attributes while maintaining the same overall statistical properties (Wilby, 2006; Fowler, 2007). Table 2.4 shows a list of recent studies conducted on the effect of climate change on water resources based on statistical downscaling.

2.1.3.2 Dynamic Downscaling of GCMs Outputs to Local Scale

In dynamic downscaling, a higher resolution climate model, usually Regional Climate Model (RCM) is used to produce higher resolution outputs. RCM can be nested within a GCM or large-scale and lateral boundary conditions from GCMs may be used to run RCMs in offline mode to produce downscaled meteorological variables required to drive hydrological models. Typically atmospheric fields simulated by a GCM (e.g. surface pressure, wind, temperature and vapor) are fed into the boundary of the RCM at different vertical and horizontal levels (Wilby et al, 2009).

Table 2.5: List of recent studies n effect of climate change on water resources based on dynamic downscaling downscaling (Islam, 2011b)

Authors	**Area**	**RCMs**	**GCMs**
Sushama et.al. (2006)	UK	CRCM	CGCM2
Fowler and Ekström (2009)	UK	ARPEGE, HadRM3P, HIRHAM, RCAO, CHRM, CLM, REMO, PROMES, RegCM, RACMO2, METNO	HadCM3, HadAM3P, HadAM3H, ECHAM4
López-Moreno et.al. (2008)	Pyrenees	HIRHAM, METNO, HadRM3, RCAO, UCM	HadAM3H
Kay and Jones (2010)	UK.	HadRM3	HadCM3
Chiew et.al. (2010)	South-east Australia	CCAM	CSIRO MK3.0
Qian et.al. (2010)	Western United States	WRF	CAM
Zhang et.al. (2011)	Assiniboia watershed, Canada	PRECIS, CRCM	HadCM3, CGCM3

Several studies are found in literature to assess the ability of RCMs to simulate climate variables relevant to hydrological impact studies and noticeable illustrations ‘ to the study of climate change and its potential impacts (Fowler et.al., 2007). Table 2.5 shows some of the recent studies.

2.1.4 Pattern Scaling

The conceptual framework of the scalability hypothesis is that the regional response of a climate variable is linearly related to the global mean temperature change. These ideas were first introduced by Santer et.al. (1990) and referred to as the pattern scaling technique. This technique relies on the assumption that the anthropogenic climate change signal at any region and/or any time horizon, referred to as the response pattern, is linearly related with the global temperature change at the corresponding scenario and period.

Justification of applying pattern-scaling techniques in climate scenario construction as summarized in the IPCC Third Assessment Report, there are five key sources of uncertainties associated with constructing climate scenarios for impact and adaptation assessments (Lu, X. and Hulme, M., 2002): (1) Uncertainties in future emissions of greenhouse gases (GHGs); (2) Uncertainties in converting emissions to GHG concentrations; (3) Uncertainties in converting concentrations to radiative forcing; (4) Uncertainties in modelling climate response to a given forcing; (5) Uncertainties in converting model response into inputs for impact studies. While the results of GCM simulations probably capture a large part of the uncertainty ranges in (4) and (5), they certainly do not encapsulate the range of uncertainties in (1), (2) and (3).

The application of pattern scaling has a rich literature behind it. Murphy et.al. (2007), Watterson (2008), Giorgi (2008), Harris et.al. (2006) and Harris et.al. (2010), May (2008), Ruosteenoja et.al. (2007), Raisanen and Ruokolainen (2006), Cabre et.al. (2010) and Watterson and Whetton (2011) use it to produce regional climate change projections, and Dessai et.al. (2005) and Fowler et.al. (2007) for impact studies. It has been recently used to describe the regional effects of global temperatures reaching high thresholds of change, e.g., 4°C(May, 2008; Sanderson et.al. 2011) and its performance has been tested using the RCPs (Ishizaki et.al.2012).

Mitchell et.al. (1999) and Huntingford and Cox (2000) used a linear least squares regression on a sequence of periods. More recently Hulme et.al. (2002) and Kjellström and Bärring (2006) applied this technique to construct regional climate change scenarios. They assessed the application of pattern-scaling technique to regional climate model experiments and evaluated the validity of the technique applied to for different surface variables. More recently Giorgi (2008) proposed a simple equation to express regional climatic changes for thetwenty first century in terms of the global temperature change without dependence on the emission pathways, using the latest multi-model ensemble of global change simulations.

Due to constraints of time and resources, only a limited number of GCM experiments can be conducted. However, if we are truly to assess the risk of climate change being dangerous, impact and adaptation studies need scenarios that span a very substantial part of the possible range of future climates (Pittock, 1993; Parry et.al., 1996; Risbey, 1998; Jones, 1999; Hulme and Carter, 2000). As a convenient solution to the scarcity of GCM experiments that have sampled the range of climate projection uncertainties, in particular uncertainties caused by different emissions scenarios, pattern-scaling techniques have been developed to provide a low cost alternative to expensive AOGCM and RCM experiments for creating a range of climate scenarios that embrace uncertainties relating to different emissions, concentration and forcing scenarios. This approach involves normalising GCM response patterns (usually) according to the respective GCM global mean temperature change. These normalised patterns are then rescaled using a scalar (global mean temperature change, DTg) derived from simple climate models (e.g. MAGICC) and representing the particular emissions scenario under consideration.

Pattern-scaling method was first suggested by Santer et.al. (1990) and was employed in the IPCC First Assessment Report to generate climate scenarios for the year 2030 (Mitchell et.al., 1990) using patterns from 2xCO2 GCM experiments. It has subsequently been widely adopted in climate scenario generators and have been used with results from coupled ocean-atmosphere global models (e.g., in ESCAPE (Rotmans et.al., 1994), IMAGE-2 (Alcamo et.al., 1994), SCENGEN (Hulme et.al., 1995a,b; 2000), SILMUSCEN (Carter et.al., 1995, 1996), COSMIC (Schlesinger

et.al., 1997) and CLIMPACTS (Kenny et.al., 2000)). More recently, Hulme et.al. (2002) applied pattern-scaling method to results from regional climate model simulations to construct nationwide climate scenarios.

Steps to scale GCM response patterns across emissions scenarios and time horizons. Four steps that illustrates process for scaling one GCM climate response pattern to generate climate change patterns corresponding to a range of emissions scenarios and time horizons.

Step 1: D — rn”
I z _ -to- ‘
_ ‘ f changes in one climate variable from the average of a good number of ensemble GCM experiments forced with the highest emissions scenarios (e.g. SRES A1FI) for the time period far into the future (e.g. 2080s)

Step 2: Normalizing — rn”
Clim — ” STEP
normalized by the global mean warming of that GCM experiment1 from which the
— rn”

Step 3: Obtaining scalars
This is to derive the magnitude of global warming by a specified time period in the future for a given emissions scenario simulated by the simple climate model (e.g. MAGICC). For the IPCC TAR, MAGICC was run to estimate the annual global mean temperature changes up to 2100 for SRES emissions scenarios. This model was tuned to reproduce the climate responses from much more complex GCMs. MAGICC simulated annual global mean temperature changes from 1990 to 2100 for seven SRES emissions scenarios and seven GCMs are available from the IPCC DDC website (http://ipcc-ddc.cru.uea.ac.uk/asres/sres_home.html).

Step 4: Scaling the normalized pattern
The pattern of changes in climate variables for a specified time period in the future and a given emissions scenario can be obtained by multiplying normalised pattern from STEP 2 by the respective scalar from STEP 3.

2.1.4.1 Uncertainties Introduced by Pattern-Scaling

All pattern-scaling applications rely on the following two fundamental assumptions: - the anthropogenic climate change signal can be adequately defined from GCM response patterns; - these response patterns are representative across a wide range of possible anthropogenic forcings; - regional climate response patterns are a function of global temperature change. This could be problematic. First, it can be difficult to establish whether the pattern of change represents a climatic response to radiative forcing or is simply (largely or partly) an artifact of natural climatic variability. It may

— l” q

— ” to year variability, especially for some variables (e.g. precipitaiton) rather than others (e.g. temperature). Second, regional climate may not respond coherently to increased radiative forcing, and hence the pattern of change may not be constant over time. This is particularly a potential problem for the application to cases of stabilisation forcing scenarios.

Whetton et.al. (1998) have shown that for parts of the Southern Hemisphere a highly non-linear regional rainfall response was demonstrated in an AOGCM forced with a stabilisation scenario, a response that could not easily be handled using a linear pattern-scaling technique. Third, similar global mean temperature change can be associated with quite different regional climate response patterns, depending on the magnitude and pattern of the aerosol forcing. Pattern – scaling using single global warming scalar is unlikely to work well to capture the regional variations in climate responses, especially in the case of heterogeneous aerosol forcing. There is some evidence, however, to suggest that separate greenhouse gas and aerosol response patterns can be assumed to be additive (Ramaswamy and Chen, 1997) and pattern-scaling methods have subsequently been adapted by Schlesinger et.al. (1997, 2000) for the case of heterogeneously forced scenarios.

Assessment of uncertainties introduced by pattern-scaling Mitchell et.al. (1999) have explored the assumptions underlying pattern-scaling techniques by examining the effect of scaling decadal, ensemble mean temperatureand precipitation patterns in the suite of HadCM2 experiments. Although their response patterns were defined using only 10-year means, using four-member ensemble means improved the performance

of the technique when applied to reconstructing climate response patterns in AOGCM experiments forced with alternative scenarios. This confirmed earlier work by Oglesby and Saltzman(1992), among others, who demonstrated that temperature response patterns derived from equilibrium GCMs were fairly uniform over a wide range of concentrations, scaling linearly with global mean temperature. The main exception occurred in the regions of enhanced response near sea ice and snow margins. Mitchell et.al. (1999) concluded that the uncertainties introduced by scaling ensemble decadal mean temperature patterns across different forcing scenarios are

may not hold for variables with high spatial variability such as precipitation. Hulme et.al. (2002) assessed the application of pattern-scaling technique to Hadley Centre regional climate model (HadRM3) experiments. They compared the seasonal average temperature and precipitation changes for the 2080s from the scaled SRES A2 scenario to represent SRES B2 scenario and a single HadRM3 B2 simulation. The differences between these two scenarios are generally small for temperature and in some seasons for precipitation. However, precipitation in winter is significantly different and in autumn the two scenarios contain a different sign of change in some parts of the UK. The differences could be attributed to a combination of the internal variability of the climate system and from errors introduced by pattern-scaling. To quantify the relative contribution of these two factors to the expressed differences, a larger set of model experiments would be needed.

Pattern-scaling techniques almost certainly perform best in the case of surface air temperature and in cases where the response pattern has been constructed so as to maximize the signal-to-noise ratio. Though pattern-scaling approach is problematic in cases of heterogeneous aerosol forcing, the SRES scenarios generally include only rather small aerosol forcing. In fact, for most parts of the world, particularly in Europe and North America, sulphate aerosol emissions are projected to decline over time, although South-east Asia may experience increased level of aerosol forcing. The SRES forced GCM experiments did not separate aerosol forcing from greenhouse gas forcing and so application of separate greenhouse gas and aerosol forced patterns (as was done in SCENGEN 2.4) is no longer possible. While pattern-scaling techniques are a convenient way of handling emissions uncertainty, they introduce an uncertainty of their own into climate scenarios that is difficult to quantify. In the absence of much

larger samples of climate model experiments to draw upon, pattern-scaled climate change scenarios are likely to continue to be widely used in impacts and integrated assessments. It is therefore important to consider, or to assess where possible, this aspect of uncertainty when applying pattern-scaling techniques to develop climate change scenarios. For instance, most GCM experiments reviewed by IPCC TAR (and will be available from the IPCC DDC website) are forced by more than one SRES emissions scenario, it would be beneficial to assess the uncertainty introduced by pattern-scaling via comparing pattern-scaled scenario against the scenario derived directly from the model simulation.

Much of the evaluation of pattern scaling in the literature has been conducted on just a single variable– surface temperature. In many ways this variable may represent the best opportunity for pattern scaling:

- temperature is the same variable as the scaler,
- temperature is spatially continuous,
- temperature is represented well by GCMs,
- temperature has a high signal-to-noise ratio under radiative forcing.

Precipitation offers a much sterner test for pattern scaling:

- precipitation is notthe same variable as the scaler,
- precipitation is spatially discontinuous,
- precipitation is notrepresented as well as temperature by GCMs,
- precipitation has a relatively lowsignal-to-noise ratio.

Mitchell et.al. (2001) confirmed the accuracy of pattern scaling for precipitation, since temperature pattern. If pattern scaling may be applied to precipitation, we might

2.1.5 Marksim Tool

MarkSim was developed in the 1980s and 1990s to simulate weather from known sources of monthly climate data from around the world (Jones & Thornton 1993, 1997, 1999, 2000). It divides the world into 720 clusters of climate that are distinct

from one another and fits a third order Markov model to the precipitation data. The temperature data simulation is derived from SIMMETEO (Geng et.al., 1988). The radiation data are based on the model of Donatelli and Campbell (1997).

For each of the about 9,200 stations with usable daily data, the third order Markov chain model of rainfall was developed. The results were grouped according to climate cluster, and regression equations for each of the Markov parameters were calculated using the monthly average rainfall and temperature figures for each station within the cluster. The model can now be fitted to any monthly climate data record by determining to which cluster it belongs, and using the relevant regression equations.

Markov models are excellent simulations of the rainfall process, but they do have limitations. It was found quite early in the analysis (Jones & Thornton, 1993) that a simple first or second order process, while adequate for temperate regions, would not fit well enough for the tropics. Hence we went with the third order model. Another deficiency we found was that Markov processes ordinarily underestimate the variance of rainfall. This is solved in MarkSim by resampling the Markov probability coefficients for each year of simulation. This is because the coefficients themselves are only estimates and have an error term. Once we reincorporate this error term by resampling, the rainfall variance agrees with the observed. The latest publication for MarkSimGCM and for this application is that for the 4th approximation models. (Jones and Thornton 2013)

Table 2.2 shows all the models used by MarkSim for pattern scaling. Yearly data interpolated by bilinear interpolation from the original GCM pixel sizes (Brown, O. 2013) _H ‘ e for the period ran from 1961 to 2005. Prediction data ran from 2006 to 2099. Means for rainfall, tmax and tmin were calculated from the _ ‘ ‘ GCM

The process used is the delta process in its simplest form, all variables were adjusted _ ‘

WorldClim.v1.3. The GCM data provided annual deviations for the years 2006 to 2099. 4th order polynomials were fitted to every pixel.

2.2 Review of Physically Based Hydrological Modeling

Hydrologic modeling involves formulating the mathematical models to represent the hydrologic processes such as, precipitation, snowmelt, interception, evapotranspiration, infiltration, sub-surface flow, and surface flow, as well as the interaction between them. Hydrologic modeling can be challenging because it involves highly nonlinear processes, complex interactions and high spatial variability at basin scale. Starting from the mid of the nineteenth century, the evolution of hydrologic modeling is continuing from lumped conceptual models to physically based distributed models with the development of understanding the physical processes, computational efforts and data retrieving facilities. Lumped conceptual hydrologic models consider three basic processes within a river basin: the loss of water from storage to atmosphere; storage of water in soil, vegetation, aquifer, and in rivers; routing of flow over the surface (Gosain et.al., 2009). Physically based hydrologic models are based on known scientific principles of energy and water fluxes whereas, conceptual models are based on conceptual storages and model parameters that require calibration. In physically based hydrologic modeling the hydrologic process of water movement are modeled either by the finite difference approximation of the partial differential equation representing the mass, momentum and energy balance or by empirical equations (Abbott et.al., 1986b). Typically the primary components of hydrologic cycle related to the land phase are taken into consideration. These are: interception, snowmelt, evapotranspiration, sub-surface runoff, groundwater flow, surface runoff and channel routing.

Hydrologic models can be classified according to the physical processes involved in modeling as conceptual and physically based (Refsgaard, 1996). In conceptual models each of the hydrologic processes, that we r ead into our observations of the catchment, are represented by simplified mathematical relationships, where as in physically based model the detail physical processes can be represented in a deterministic way by representations of mass, momentum and energy conservation (Refsgaard, 1996). According to the spatial description of the watershed process, hydrologic models can be classified as lump and distributed models. In a lumped model the spatial variability of watershed characteristics are ignored, while in a distributed model the spatial variability of vegetation, soil,

topography, etc are taken into account. The conceptual models are usually lumped while the physically based model in practice has to be distributed in manner (Refsgaard, 1996).

Table 2.6: Selected physically based hydrologic model, spatial description and discretization type (Islam, 2011b)

Model Acronym	Model Definition	Principle Reference(s)	Semi/Fully Distributed	Discretization type*
TOPMODEL	TOPography based hydrological MODEL	Beven and Kirby (1976,1979) Beven et.al. (1995)	Semi	HRU
WATBAL		Knusden et.al. (1986)	Semi	OG
SHE	European Hydrologic System	Abbot et.al. (1986a, 1986b)	Fully	OG
ISBA	Interaction Soil Biosphere Atmosphere	Nolihan and Planton (1989) Nolihan and Mahfouf (1995)	Fully	OG
IHDM	Institute of Hydrology Distributed Model	Beven et.al. (1987) Calver and Wood (1995)	Fully	HRU
THALES		Grayson et.al. (1992a; 1995)	Fully	IE
SLURP	Semi-distributed Land Use-based Runoff Processes	Kite (1995)	Semi	GRU
MIKE SHE	MIKE System Hydrologique European	Refsgaard and Storm (1995)	Fully	OG
SWAT	Soil and Water Assessment Tool	Arnold et.al. (1998a)	Semi	HRU
WATFLOOD/SPL9	Waterloo Flood Forecasting Model	Kouwen (1988) Kouwen (2000) Kouwen and Mousavi (2002)	Fully	OG
HRCDHM	Hydrologic Research Centre Distributed Hydrologic Model	Carpenter et.al. (2001)	Semi	HRU
DPHM-RS	Semi-distributed Physically based Hydrologic Model using Remote Sensing and GIS	Biftu and Gan (2001, 2004)	Semi	HRU
R.WATER.FEA		Vieux and Gaver (1994)	Fully	IE
tRIBS	TIN-based Real-time Integrated Basin Stimulator	Ivanov et.al., 2004	Flly	TIN
TOPNET		Bandaragoda et.al. (2004)	Semi	HRU
MISBA	Modified Interaction Soil Biosphere Atmosphere	Kerkhoven and Gan (2006)	Fully	OG
LISTFLOOD		Van der Knijff et.al. (2010) De Roo et.al. (2000)	Fully	OG
HydroGeoSphere		Therrien et.al. (2005; 2010)	Fully	OG
PAWS	Process-based Adaptive Watershed Simulator	Shen and Phanikumar (2010)	Fully	OG
CREST	The Coupled Routing and Excess Storage	Wang et.al. (2011)	Fully	OG

2.2.1 Modeling Concepts of Hydrologic Processes

In physically based hydrologic modeling the hydrologic process of water movement are modeled either by the finite difference approximation of the partial differential equation representing the mass, momentum and energy balance or by empirical equations (Abbott et.al., 1986b).

Typically the primary components of hydrologic cycle related to the land phase are taken into consideration. These are: interception, snowmelt, evapotranspiration, sub-surface runoff, groundwater flow, surface runoff and channel routing. A number of physically based hydrologic models have been reviewed and modeling concepts of these physical processes used by various hydrologic models will be discussed in the following sections. Selected model acronyms and principal reference(s) are listed in Table 2.6.

2.2.2 Advantages and Limitations of Physically Based Hydrologic Modelling

Lumped conceptual hydrologic models consider three basic processes within a river basin: the loss of water from storage to atmosphere; storage of water in soil, vegetation, aquifer, and in rivers; routing of flow over the surface (Gosain et.al., 2009). Focus on the physically based distributed hydrologic modeling started in order to minimize or overcome the deficiencies of the conceptual models. Conceptual models are controlled by various parameters to represent the hydrologic processes. Parameters of these models are estimated either by manual curve fitting or by optimizing the objective functions, thus making less or no physical interpretation of the fitted parameters. Therefore, unrealistic parameter values may be obtained through errors in measurements (Abbott et al., 1986a). In lumped conceptual models the mathematical representation of hydrologic processes are only an approximate representation of the real world. So the errors in parameter estimation also can be raised from model structure (Beven, 1989). The calibration of conceptual models requires long meteorological and hydrological records which are not always available, especially for the un-gauged catchments (Gosain et.al., 2009). Spatial heterogeneities of landuse, soil, and input variables are not considered in lumped conceptual models (Abbott et al., 1986a). The effects of landuse changes resulting from the ‘

be undertaken by altering the parameter values to reflect changes as the parameters

are not based on physical processes (Abbott et.al., 1986a). The calibration and validation of lumped conceptual models depends on the accuracy of both inputs and outputs. So, uncertainty is involved in estimating the input variables, especially the evapotranspiration may cause significant changes in calibration and validation processes (Beven, 1989). Different set of parameter values may result equal quality of good results in a lumped conceptual model (Beven, 1989). As discussed in the previous paragraph, the development of physically based hydrologic model was initiated to overcome the deficiencies associated with the lumped conceptual models, by using parameter values with physical interpretation and considering their spatial variability (Abbott et al., 1986a). However, the physics on which the equations of physically based hydrologic models are based is the small scale physics of homogeneous system and in application these models lump up the small scale physics to the model grid scale without considering any theoretical framework (Beven, 1989).

Table 2.7: Advantages and limitations of physically based distributed hydrologic models over lumped conceptual models (Islam, 2011b)

Advantages Over Lumped Conceptual Model
• Parameters in physically based models are based on physics • Physically based are developed from well established scientific laws at micro-scale to water behavior at the meso-scale or regional scale • Consider the spatial heterogeneities of landuse, soil, and input variables. • Can consider the effects of the landuse changes on the hydrologic cycle. • Less (or no) calibration is needed.
Limitations
• Lump up the small scale physics to the model grid scale without considering any theoretical framework. • Calibration by the comparison of the predicted and observed hydrograph cannot be considered a sufficient test of model that implies the internal response of catchment. • Context of original purpose of development is often lost when models applied beyond the scope of their capabilities. • Development of some physically based model is not dynamic nor it is in conjunction of a field program • Many models are developed from limited data sources. • Calibration testing on one or two catchments is also insufficient test of

Calibration of most physically based hydrologic models is usually performed by the comparison of predicted and observed hydrograph which is a necessary test but cannot be considered a sufficient test of model that implies the internal response of catchment (Beven, 1989). In application of physically based hydrologic models, the context of their original purpose of development is often lost when they are applied beyond the scope of their capabilities (Grayson et.al., 1992a). Development of some physically based model is not dynamic nor is it in conjunction of a field program (Dunne, 1983). Many models are developed from limited data sources. C ‘ universal applicability (Grayson et.al., 1992a). A summary of advantages and limitations of physically based distributed hydrologic models over lumped conceptual models discussed in the aforementioned paragraphs is listed in below.

2.3 Review of Climate Change Impact on Water Availability of BRB

Several climate change studies on water availability in Ganges-Brahmaputra-Meghna basin have been conducted (e.g. Mirza et al, 1997; Seidal et.al., 2000; Mirza, 2002; Mirza, 2003; Gain et.al., 2011; Jeulanda, 2013; Ghosh, 2012). However, only a few studies have been conducted to assess the water availability of Brahmaputra river basin (BRB). In most of the cases empirical or regression model were developed relating the climate parameters to the streamflow. Due to the nonlinearity of the hydrologic processes it is not sufficient to use conceptual, empirical or regression models to predict streamflow. Also, some calibrated model parameters of these models may not be valid when the hydrologic regime of the river basin changes because of anthropogenic impacts.

Mirza et.al.(1997) used an empirical model to test the sensitivity of runoff of Ganges-Brahmaputra-Meghna basin to the change in temperature and precipitation from -1°C to +5°C and -10% to +20% respectively. It was observed that Ganges basin is relatively sensitive to the changes in temperature and precipitation. For temperature and precipitation change of +2°C,+10% and +4°C, 20% runoff at Delhi station precipitation change was found +19% and 29% respectively. For temperature beyond 4°C runoff tend to decrease. Whereas at Gauhati station on Brahmaputra river runoff change for +2°C temperature and +10% precipitation changes was found +13% which is lower than Ganges. On the other hand runoff increase in Meghna basin at

Sylhet station for +2°C(P), +10%(P) was +11%. For +5°C(T), +20%(P) scenario runoff change at Gauhati, Delhi and Sylhet was found +22% , +35% and 21%.

Seidal et.al. (2000) used the Snowmelt Runoff Model (SRM) to determine the changes in flood for +1.5°C temperature change and 10% precipitation change (summer). It was found that in the new climate, the flood peaks will be increased by about 20% for Ganges and 30% for Brahmaputra as compared with the year 1995 (Seidal et.al., 2000).

T C C temperature and strandardized precipitation

Basin	CSIRO9(ΔP%)	HadCM2(ΔP%)	GFDL(ΔP%)	LLNL(ΔP%)
Ganges	25.94(25.5)	-30.12(-8.4)	28.14(13.8)	-11.94(1.5)
Brahmaputra	-3.24(-1.5)	25.25(21.6)	-10.43(21.6)	-8.67(4.2)
Meghna	24.13(13.5)	14.67(29.1)	12.47(33.9)	-11.99(23.1)

Note: Mean Annual Peak Discharge: Ganges=54000m^3/s, Brahmaputra= 67000m^3/s, Meghna=14000m^3/s (Mirza, 2002)

Mirza(2002) studied the sensitivity of 20 yr floods to the changes in temperature of 2, 4, 6C and standardized precipitation change on Ganges-Brahmaputra-Meghna basin. 4GCM model (CSIRO9, HadCM2, GFDL, LLNL) outputs were used in a simple empirical model to evaluate the sensitivity. Mirza (2002) stated that HadCM2, GFDL and LLNL models are in agreement about increases in precipitation whereas CSIRO9 model shows a very slight decrease in precipitation. GFDL was found to project highest increase in precipitation and LLNL with lowest. Percentage changes in mean C temperature and standardized precipitation are shown in Table 2.8.

Mirza (2003) z C temperature change and standardized precipitation change using sequence of empirical models. Similar to his previous study (Mirza, 2002) he used the results of CSIRO9, GFDL and LLNL GCMs to calculate the changes in mean annual discharge and mean peak discharge in Ganges-Brahmaputra-Meghna basin, HadCM2 was replaced by UKTR. The changes in mean annual and mean peak discharge for GBM are shown in Table 2.9.

Table 2.9:Changes in mean annual and mean peak discharge of GBM basin for CSIRO9, UKTR, GFDL and LLNL.

GCM	T(◦C)	Ganges		Brahmaputra		Meghna	
		Changes in mean annual discharge (%)	Changes in mean peak discharge (%)	Changes in mean annual discharge (%)	Changes in mean peak discharge (%)	Changes in mean annual discharge (%)	Changes in mean peak discharge (%)
CSIRO9	2	13.5	9.7	–0.03	–0.02	4.5	7.9
	4	27	19.4	–0.06	–0.04	9	15.7
	6	40.5	29.1	–0.09	–0.06	13.5	23.6
UKTR	2	21.1	15.2	6.3	5.6	11.4	19.9
	4	42.2	30.4	12.8	11.2	22.8	39.8
	6	63.3	45.6	19.2	17	34.2	59.7
GFDL	2	7.3	5.2	4.5	4.04	11.3	19.8
	4	14.6	10.4	9	8.09	22.6	39.5
	6	21.9	15.6	13.5	12.14	33.9	59.4
LLNL	2	0.8	0.6	0.9	0.8	7.7	13.5
	4	1.6	1.2	1.8	1.6	15.4	26.9
	6	2.4	1.8	2.7	2.4	23.1	40.4

Gain et.al. (2011) investigated the effect of climate change on both low and high flows of the lower Brahmaputra. Twelve GCMs (MICRO, GFDL, GISS, CCCMA, CGCM, BCCR, HADGEM, NCAR,ECHAM and three others) results for A1B and A2 scenarios were used through discharge-ensemble modeling. GCMs were prioritized through weighing based on their performance. The change in 10 year return period floods for projected scenarios are shown in Table 2.10. A peak flow that currently occurs every 10 yr will occur at least once every two years during the time slice 2080–2099 (Gain, 2011).

Table 2.10:Changes in 10 year return period flood for A1B and A2 scnerio in 2080-2099

	A1B_2080-99	A2_2080-99
Discharge(m^3/s)	130000	140000
Percent Change	58.54	70.73

Note: Current 1:10 year flood= 82000m^3/s

Ghosh(2012) used the downscaled data of A2 scenario from PRECIS to estimate the annual peak discharge and frequency of annual peak discharge in Brahmaputra basin using a distributed hydrological model RISE (Rice Irrigation System Evaluation). It was found that Tezpur gauging site might experience an increment of 11.7% in the

median value of pre-monsoonal peak discharge series. Whereas the increasing trend at Guwahati and Dhrubi station were expected to increase 27.8% and 27.7% respectively (Ghosh, 2012).

Jeulanda (2013) considered the results of 16 GCMs for A2 scenario to determine the flow in Ganges basin using semi-distributed hydrological model SWAT (Soil Water Assessment Tool) and hydrological routing model. Three of the 16 models show decreased flow at Farakka whereas six models show increase in flow more than 20%. Overall range of change in mean flow was found between -21% (CM4 (IPSL)) to +37%(CGCM2 (MRI)).

M. Masood et. al. (2014) assessed the impact of climate change on GBM basin in three time slices- present-day (1979–2003), near-future (2015–2039) and far-future (2075–2099) periods. He used MRI AGCM3.2S data as input in a macro scale hydrologic model H08. It was found that by the end of 21st century +14, +15, and +18 % changes in runoff will occur in the Brahmaputra, Ganges and Meghna basin due to the mean change in precipitation of +14.0, +10.4, and +15.2 % (entire GBM is projected to be warmed 3ºC).

2.4 SWAT Model

2.4.1 Conceptual Basis

SWAT divides a watershed into subwatersheds. Each subwatershed is connected through a stream channel and further divided into Hydrologic Response Unit (HRU). HRU is a unique combination of a soil and a vegetation type in a subwatershed, and SWAT simulates hydrology, vegetation growth, and management practices at the HRU level.

2.4.2 Water Balance

Water balance is the driving force behind everything that happens in the watershed. To accurately predict the movement of pesticides, sediments or nutrients, the hydrologic cycle as simulated by the model must conform to what is happening in the watershed. The simulation of hydrologic cycle can be separated into **land phase** and **water or routing phase**. Land phase controls the amount of water, sediment, nutrient and pesticide loading to the main channel in each subbasin whereas routing phase

defines the movement of water, sediments, etc through the channel network of the watershed to the outlet.Schematic of pathways available for water movement in SWAT is shown in the Figure 2.6. It involves various elements such as snow, canopy storage, infiltration, evapotranspiration, lateral subsurface flow, surface runoff, transmission losses, return flow etc.

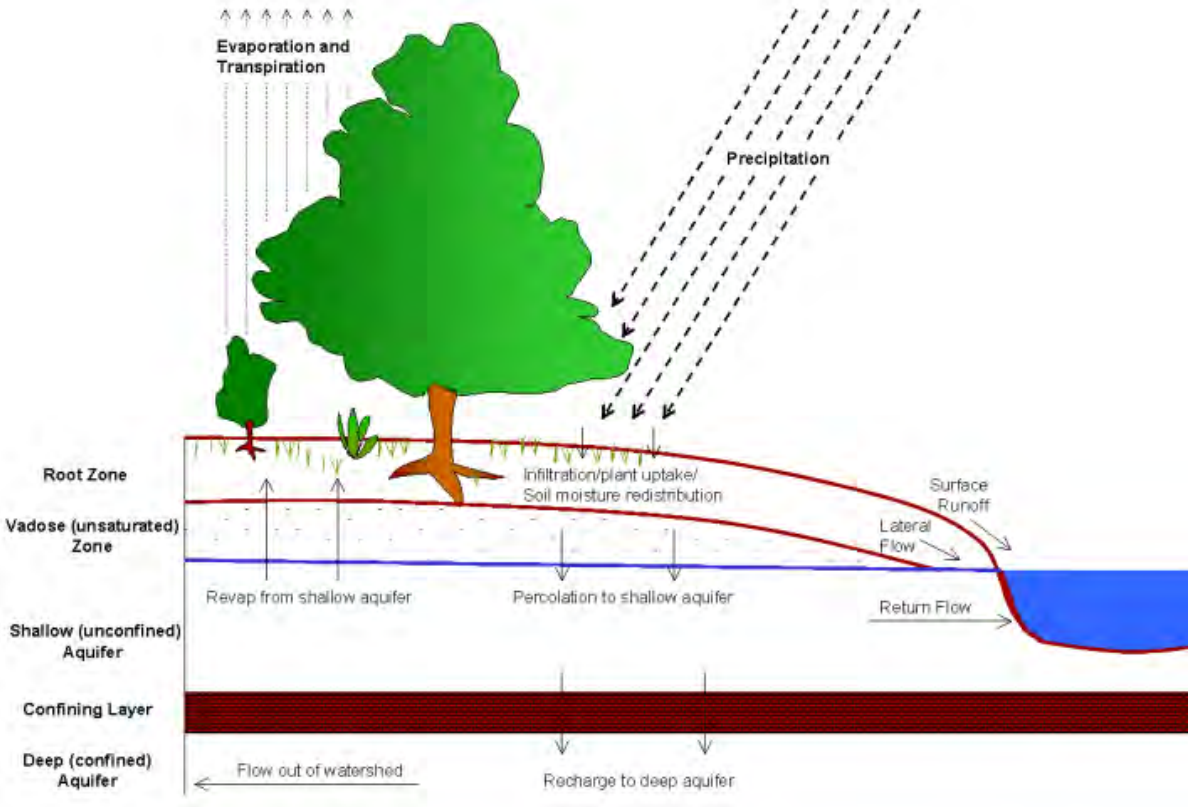

Figure 2.5: Hydrologic process in SWAT

2.4.2.1 Land phase of the hydrologic cycle:

Hydrologic cycle simulated by swat is based on the water balance equation

$$SW_t = SW + \sum_{i=1}^{t} (R_i - Q_i - ET_i - P_i - QR_i) \quad \textbf{(2.8)}$$

Where SW_t is the final soil water content (mm H_2O), SW0 is the initial soil water content on day i (mm H_2O), Q_{surf} is the amount of surface runoff on day i (mm H_2O), E_a is the amount of evapotranspiration on day i (mm H_2O), wseep is the amount of water entering the vadose zone from the soil profile on day i(mm H_2O), and Q_{gw} is the amount of return flow on day i(mm H_2O).

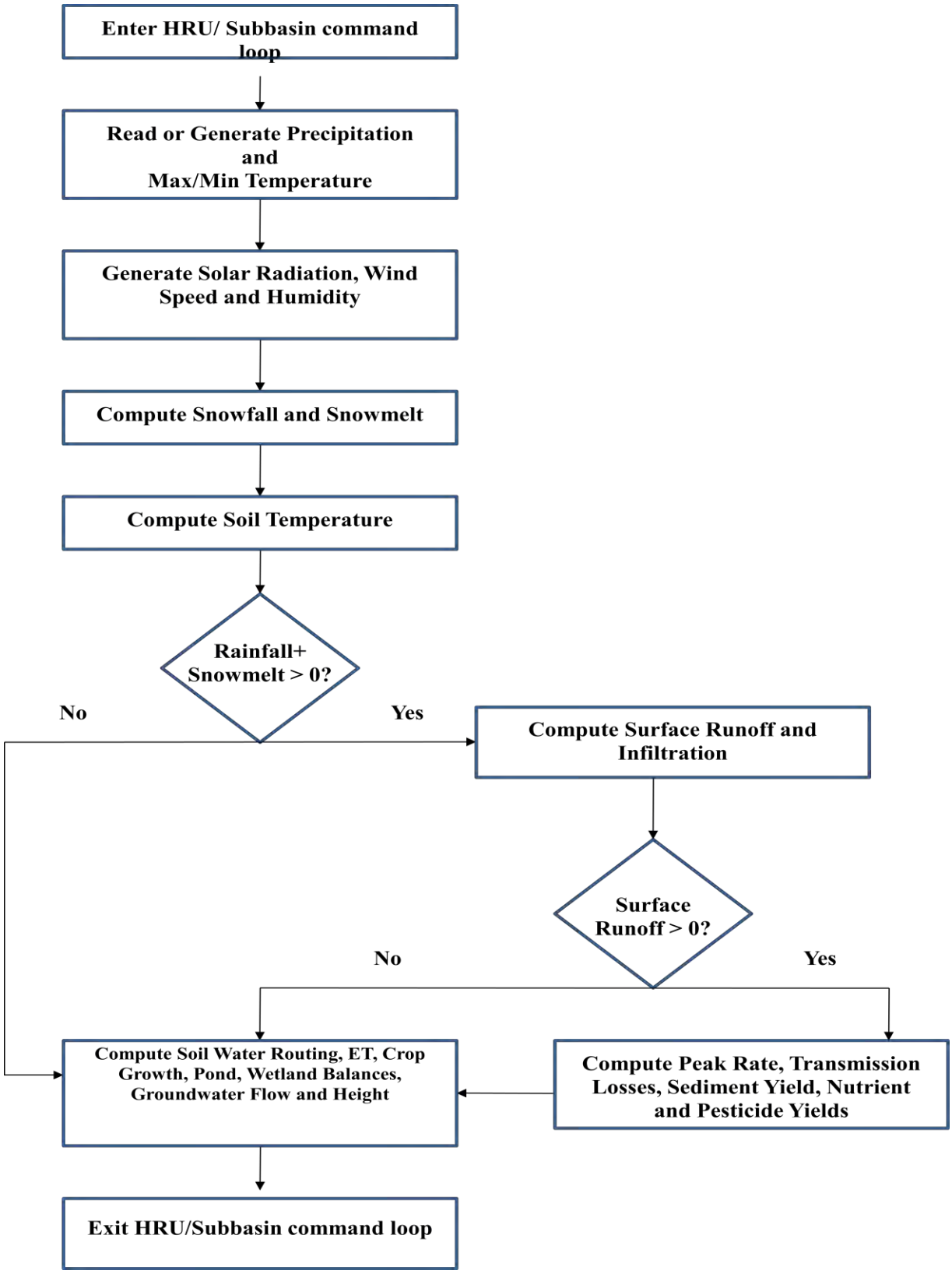

Figure 2.6: HRU/Subbasin in command loop (Neitsch, S.L.et. al., 2005)

2.4.2.1.1 Snow

Swat classifies precipitation as rain or freezing rain/snow using the average daily temperature.

Snow cover: This component of swat can handle simple uniform cover to complex non-uniform cover due to shading, drifting, topography and land cover. User defines a threshold snow depth above which snow coverage will always extend over 100% of the area.

Snow melt: snow melt is controlled by air and snow pack temperature, melting rate, and the areal coverage of snow. If snow is present, it is melted on days when the maximum temperature exceeds 0C using a linear function of the difference between the average snow pack-maximum air temperature and the base or threshold temperature for snow melt. Melted snow is treated the same as rainfall for estimating runoff and percolation.

2.4.2.1.2 Canopy Sorage

Canopy storage is the water intercepted by vegetative surfaces (the canopy) where it is held and made available for evaporation. When using the curve number method to compute surface runoff, canopy storage is taken into account in the term initial abstractions. However, if methods such as Green & Ampt are used to model infiltration and runoff, canopy storage must be modeled separately. SWAT allows the user to input the maximum amount of water that can be stored in the canopy at the maximum leaf area index for the land cover. This value and the leaf area index are used by the model to compute the maximum storage at any time in the growth cycle of the land cover/crop. When evaporation is computed, water is first removed from canopy storage.

2.4.2.1.3 Infiltration

Infiltration refers to the entry of water into a soil profile from the soil surface. As infiltration continues, the soil becomes increasingly wet, causing the rate of infiltration to decrease with time until it reaches a steady value. The initial rate of infiltration depends on the moisture content of the soil prior to the introduction of water at the soil surface. The final rate of infiltration is equivalent to the saturated

hydraulic conductivity of the soil. Because the curve number method used to calculate surface runoff operates on a daily time-step, it is unable to directly model infiltration. The amount of water entering the soil profile is calculated as the difference between the amount of rainfall and the amount of surface runoff. The Green & Ampt infiltration method does directly model infiltration, but it requires precipitation data in smaller time increments.

2.4.2.1.4 Evapotranspiration

Evapotranspiration is a collective term for all processes by which water in the liquid or solid phase at or near the earth's surface becomes atmospheric water vapor. Evapotranspiration includes evaporation from rivers and lakes, bare soil, and vegetative surfaces; evaporation from within the leaves of plants (transpiration); and sublimation from ice and snow surfaces. The model computes evaporation from soils and plants separately as described by Ritchie (1972). Potential soil water evaporation is estimated as a function of potential evapotranspiration and leaf area index (area of plant leaves relative to the area of the HRU). Actual soil water evaporation is estimated by using exponential functions of soil depth and water content. Plant transpiration is simulated as a linear function of potential evapotranspiration and leaf area index.

Potential evapotranspiration: Potential evapotranspiration is the rate at which evapotranspiration would occur from a large area completely and uniformly covered with growing vegetation which has access to an unlimited supply of soil water. This rate is assumed to be unaffected by micro-climatic processes such as advection or heat-storage effects. The model offers three options for estimating potential evapotranspiration: Hargreaves (Hargreaves et.al., 1985), Priestley-Taylor (Priestley and Taylor, 1972), and Penman-Monteith (Monteith, 1965). The three PET methods included in swat vary in the amount of required inputs. The Penman-Monteith method requires solar radiation, air temperature, relative humidity and wind speed. The Priestley-Taylor method requires solar radiation, air temperature and relative humidity. The Hargreaves method requires air temperature only.

2.4.2.1.5 Lateral Subsurface Flow

Lateral subsurface flow, or interflow, is streamflow contribution which originates below the surface but above the zone where rocks are saturated with water. Lateral subsurface flow in the soil profile (0-2m) is calculated simultaneously with redistribution. A kinematic storage model is used to predict lateral flow in each soil layer. The model accounts forvariation in conductivity, slope and soil water content.

2.4.2.1.6 Surface Runoff

Surface runoff, or overland flow, is flow that occurs along a sloping surface. Using daily or subdaily rainfall amounts, SWAT simulates surface runoff volumes and peak runoff rates for each HRU.

Surface Runoff Volume: It is computed using a modification of the SCS curve number method (USDA Soil Conservation Service, 1972) or the Green & Ampt infiltration method (Green and Ampt, 1911). In the curve number method, the curve number varies non-linearly with the moisture content of the soil. The curve number drops as the soil approaches the wilting point and increases to near 100 as the soil approaches saturation. The Green & Ampt method requires sub-daily precipitation data and calculates infiltration as a function of the wetting front matric potential and effective hydraulic conductivity. Water that does not infiltrate becomes surface runoff. SWAT includes a provision for estimating runoff from frozen soil where a soil is defined as frozen if the temperature in the first soil layer is less than 0°C. The model increases runoff for frozen soils but still allows significant infiltration when the frozen soils are dry.

Peak Runoff Rate: Peak runoff rate predictions are made with a modification of the rational method. In brief, the rational method is based on the idea that if a rainfall of intensity i begins instantaneously and continues indefinitely, the rate of runoff will increase until the time of concentration, t_c, when all of the subbasin is contributing to flow at the outlet. In the modified Rational Formula, the peak runoff rate is a function of the proportion of daily precipitation that falls during the subbasin t_c, the daily surface runoff volume, and the subbasin time of concentration. The proportion of rainfall occurring during the subbasin t_c is estimated as a function of total daily

rainfall using a stochastic technique. The subbasin time of concentration is estimated using Mannin ‘ F

2.4.2.1.7 Transmission Losses

Transmission losses are losses of surface flow via leaching through the streambed. This type of loss occurs in ephemeral or intermittent streams where groundwater contribution occu SWAT L ‘ method described to estimate transmission losses.

2.4.2.1.8 Return Flow

Return flow, or base flow, is the volume of streamflow originating from groundwater. SWAT partitions groundwater into two aquifer systems: a shallow, unconfined aquifer which contributes return flow to streams within the watershed and a deep, confined aquifer which contributes return flow to streams outside the watershed (Arnold et.al., 1993). Water percolating past the bottom of the root zone is partitioned into two fractions—each fraction becomes recharge for one of the aquifers. In addition to return flow, water stored in the shallow aquifer may replenish moisture in the soil profile in very dry conditions or be directly removed by plant. Water in the shallow or deep aquifer may be removed by pumping.

2.4.2.2 Routing Phase of Hydrologic Cycle

Once swat determines the loading of water, sediment, nutrients and pesticides to the main channel, the loading are routed through the stream network of the watershed using a command structure similar to that of HYMO (Williams and Hann, 1972). Additionally swat also models the transformation of chemicals in the stream and streambed.

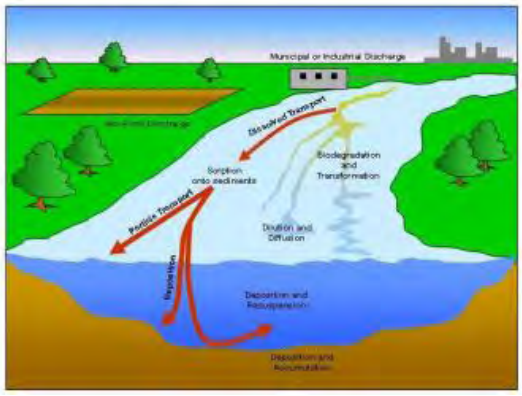

Figure 2.7: In-stream processes modeled by SWAT

2.4.2.2.1 Routing in the Main Channel or Reach

As water flows downstream, a portion may be lost due to evaporation and transmission through the bed of the channel. Another potential loss is removal of water for agricultural or human use. Flow may be supplemented by the fall of rainfall or addition of water from point source. In swat flow is routed using variable storage coefficient method developed by Williams (1969) or the Maskinghum routing method.

2.4.2.2.1.1 Variable Storage Routing

The variable storage routing method was developed by Williams (1969) and used in the HYMO (William and Hann, 1973) and ROTO (Arnold et.al., 1995) models.
For a given reach segment, storage routing is based on the continuity equation

$$V_{in} - V_{out} = \Delta V_{stored} \quad (2.9)$$

Where V_{in} is the volume of inflow during the time step (m3 H_2O), V_{out} is the volume of outflow during the time step (m3 H_2O ΔV_{stored} is the change in volume of storage during time step (m3 H_2O). After rearranging the equation it can be written as

$$Q_{out,2} = SC\ (q_{in,ave} + V_{stored,1} / \Delta t) \quad (2.10)$$

SC is the storage coefficient, $q_{in,ave}$ is the average of $q_{in,1}$ and $q_{in,2}$ where $q_{in,1}$ is the inflow rate at the beginning of the time (m^3/s), $q_{in,2}$ is the inflow rate at the end of the time step (m^3/s), $q_{out,2}$ Δ
time step (s).

2.4.2.2.1.2 Muskinghum Routing

The Muskingum method is a commonly used hydrologic routing method in situations requiring a variable storage-discharge relationship (Chow et.al., 1988). The Muskingum method models the storage volume of flooding in a river channel using a combination of wedge and prism storage (see schematic below). The key parameters in Muskingum routing are K (travel time) and X (weighting coefficient). The value of X depends on the shape of the wedge storage to be modeled, and the value of X ranges from 0 for reservoir type storage to 0.5 for a full wedge. In natural streams, X

is between 0 and 0.3 with a mean value near 0.2 (Chow et.al., 1988). K is the time required for an incremental flood wave to traverse its reach, and it may be estimated as the observed time of travel of peak flow through the reach (Chow et.al., 1988). If observed inflow and outflow hydrographs are available for a river reach the values of K and X can be determined to provide the best fit (or narrowest loop) relative to the observed flows.

It is necessary to enter a bankfull discharge, Manning's N parameter, slope, length, width, number of segments to represent the reach, an averaging weighting coefficient (X), and weighting coefficient for celerity. The weighting coefficient for celerity is the weight that should be given to the celerity calculated for the bankfull discharge. The weighting coefficient should be between 0 and 1. A weight of 1 uses the bankfull discharge celerity; a weight of zero uses only the celerity calculated for discharge at 10 percent of bankfull. In any case, the weighted estimate of celerity is used for all routing, regardless of changes in inflow. This differs from variable parameter Muskingum Cunge routing, where the celerity is calculated with each change in flow.

2.4.3 Hydrology

2.4.3.1 Rainfall Intensity

The rainfall intensity is the average rainfall rate during the time of concentration. Based on this definition, it can be calculated with the equation

$$\mathbf{I=R_{tc} / t_{conc}} \qquad \mathbf{(2.11)}$$

Where I is the rainfall intensity (mm/hr) , R_{tc} is the amount of rain falling during the time of concentration (mm H_2O), and t_{conc} is the time of concentration for the subbasin (hr).

2.4.3.2 Percolation

Percolation is calculated for each soil layer in the profile. Water is allowed to percolate if the water content exceeds the field capacity water content for that layer and the layer below is not saturated.

The volume of water available for percolation in the soil layer is calculated

$$SW_{ly,access} = SW_{ly} - FC_{ly} \quad \text{if} \quad SW_{ly} > FC_{ly} \quad (2.12)$$

$$SW_{ly,access} = 0 \quad \text{if} \quad SW_{ly} <= FC_{ly} \quad (2.13)$$

Where $SW_{ly,access}$ is the drainable volume of water on a given day (mm H_2O), SW_{ly} is the water content of the soil layer on a given day (mm H_2O). The amount of water that moves from one layer to the underlying layer is calculated using storage routing methodology.

2.4.3.3 Lateral Flow

Lateral flow will be significant in areas with soils having high hydraulic conductivities in surface layers and an impermeable semi permeable layer at a shallow depth. In such a system, rainfall will percolate vertically until it encounters the impermeable layer. The water then ponds above the impermeable layer forming a saturated zone of water, i.e. a perched water table. This saturated zone is the source of water for lateral subsurface flow.

Swat incorporates a kinematic storage model for subsurface flow developed by Sloan et al (1983) and summarized by Sloan and Moore (1984). This model simulates subsurface flow in a two dimensional cross-section along a flow path down a steep hillslope.

2.4.3.4 Groundwater System

An aquifer —

nt"(D 99 A q

aquifer whose upper boundary is the water table whereas a confined aquifer is bounded above and below by geologic formations whose hydraulic conductivity are significantly lower than that of the aquifer.

2.4.3.5 Shallow Aquifer

The water balance for the shallow aquifer is:

$$aq_{sh,i} = aq_{sh,i-1} + w_{rchrg,sh} - Q_{gw} - w_{revap} - w_{pump,sh} \quad (2.14)$$

where $aq_{sh,i}$ is the amount of water stored in the shallow aquifer on day i (mm H_2O), $aq_{sh,i-1}$ is the amount of water stored in the shallow aquifer on day i-1 (mm H_2O),

w_{rchrg},sh is the amount of recharge entering the shallow aquifer on day I (mm H_2O), Q_{gw} is the groundwater flow, or base flow, into the main channel on day i (mm H_2O), w_{revap} is the amount of water moving into the soil zone in response to water deficiencies on day (mm H_2O) and $w_{pump,sh}$ is the amount of water removed from the shallow aquifer by pumping on day i (mm H_2O).

2.4.3.6 Deep Aquifer

The water balance for the deep aquifer is:

$$\mathbf{aq_{dp,i} = aq_{dp,i-1} + w_{deep} - w_{pump,dp}} \qquad \mathbf{(2.15)}$$

where $aq_{dp,i}$ is the amount of water stored in the deep aquifer on day i (mm H_2O), $aq_{dp,i-1}$ is the amount of water stored in the deep aquifer on day i-1(mm H_2O), w_{deep} is the amount of water percolating from the shallow aquifer into the deep aquifer on day i (mm H_2O), and $w_{pump,dp}$ is the amount of water removed from the deep aquifer by pumping on day i (mm H_2O). If the deep aquifer is specified as the source of irrigation water or water removed for use outside the watershed, the model will allow an amount of water up to the total volume of the deep aquifer to be removed on any given day.

2.4.3.7 Transmission Loss

During periods when a stream receives no groundwater contributions, it is possible for water to be lost from the channel via transmission through the side and bottom of the channel. Transmission losses are estimated with the equation

$$\mathbf{tloss = K_{ch} \times TT \times P_{ch} \times L_{ch}} \qquad \mathbf{(2.16)}$$

Where tloss are the channel transmission losses (m2 H_2O), Kch is the effective hydraulic conductivity of the channel alluvium (mm/hr), TT is the flow travel time (hr), P_{ch} is the wetted perimeter (m), and L_{ch} is the channel length (km). Transmission losses from the main channel are assumed to enter bank storage or the deep aquifer.

2.4.3.8 Evaporation Loss

Evaporation losses from the reach are calculated:

$$\mathbf{E_{ch} = coef_{ev} \times E_o \times L_{ch} \times W \times fr_{\Delta t}} \qquad \mathbf{(2.17)}$$

Where E_{ch} is the evaporation from the reach for the day (m^3 H_2O), $coef_{ev}$ is an evaporation coefficient, E_o is the potential evaporation (mm H_2O), L_{ch} is the channel length (km), W is the channel width at water level (m), and fr_{Δ} is the fraction of the time step in which water is flowing in the channel.

The evaporation coefficient is a calibration parameter for the user and is allowed to vary between 0 and 1. The fraction of the time step in which water is flowing in the channel is calculated by dividing the travel time by the length of the time step.

2.4.3.9 Bank Storage

The amount of water entering bank storage on a given day is calculated

$$\mathbf{bnk_{in} = tloss\ x(1-fr_{trans})} \qquad \mathbf{(2.18)}$$

Where bnk_{in} is the amount of water entering bank storage (m^3H_2O), tloss are the channel transmission losses (m^3H_2O), and fr_{trans} is the fraction of transmission losses portioned to the deep aquifer.

Bank storage contributes flow to the main channel or reach within the subbasin. Bank flow is simulated with a recession curve similar to that used for groundwater. The volume entering the reach from bank storage is calculated

$$\mathbf{V_{bnk} = bnk\ x\ (1-exp[-\alpha_{bnk}])} \qquad \mathbf{(2.19)}$$

Where V_{bnk} is the volume of water added to the reach via return flow from bank storage (m3 H_2O), bnk is the total amount of water in bank storage (m3 H_2O), and α_{bnk} is the bank flow recession constant or constant of proportionality.

2.4.3.10 Channel Water Balance

Water storage in the reach at the end of the time step is calculated:

$$\mathbf{V_{stored,2} = V_{stored,1} + V_{in} - V_{out} - tloss - E_{ch} + div + V_{bnk}} \qquad \mathbf{(2.20)}$$

Where $V_{stored,2}$ is the volume of water in the reach at the end of the time step (m^3 H_2O), $V_{stored,1}$ is the volume of water in the reach at the beginning of the time step (m^3H_2O), V_{in} is the volume of water flowing into the reach during the time step(m^3 H_2O), V_{out} is the volume of water flowing out of the reach during the time step

(m^3H_2O), tloss is the volume of water lots from the reach via transmission through the bed(m^3 H_2O), E_{ch} is the evaporation from the reach for the day (m^3 H_2O), div is the volume of water added or removed from the reach for the day through diversions (m^3 H_2O), and Vbnk is the volume of water added to the reach via return low from bank storage (m^3 H_2O). As the transmissions losses, evaporation and other water losses for the reach segment are calculated, the amount of outflow to the next reach segment is reduced by the amount of the loss.

2.4.4 SWAT Advanages

- Physically based
- Requires generally available information as input
- Computationally efficient
- Capable of being used on ungauged watersheds
- Enables users to study long-term impacts.

Chapter 3

Methodology

3.1 Introduction

Assessment of climate change impact on the flow of any river basin using hydrological model involves several steps. Numerous amount of preprocessing and post-processing is one of the major difficulties faced by the researchers. In the present work initially several types of data such as, Digital Elevation Model, land use pattern, soil distribution, climate data and flow time series were collected to setup a semi-distributed model using SWAT. Steps followed in the present research can be described as following:

Step 1-Data Collection: This include DEM, land use pattern, soil distribution, climate data and flow time series

Step 2- Bias Correction: Correcting bias in the climate data (specifically precipitation)

Step 3-Model Setup: Model setup which includes watershed delineation, weather data setup, HRU definition and selection of calculation methods.

Step 4-Sensitivity Analysis: Sensitivity analysis of the calibration parameters, calibration using the selected parameters, validation of the model and evaluation of the performance

Step 5-Scenario Selection: Selection of scenarios for climate change impact assessment.

Step 6-PatternScaling: Obtaining high resolution projected climate data of selected scenarios

Step 7-Climate Change Impact Assessment: Run the model with high resolution projected data and analyzed the impact of climate change on the flow of Brahmaputra river Basin

3.2 Data Collection

3.2.1 Digital Elevation Model, Land use and Soil Data

Digital Elevation Model (DEM) of 3 arc second or 90 m grid resolution was downloaded from Shuttle Rudder Topography Mission (SRTM) website (http://srtm.csi.cgiar.org). Collected DEM was resampled to obtain relatively coarser resolution data in order to increase the computation efficiency. This was further used to delineate the watershed and the drainage pattern for the surface area analysis.

Soil map of the selected area was collected from Harmonized World Soil Database (HWSD). It has 1km grid resolution and provides soil properties of two layers (0-30 cm) and (30-100 cm) depth. It includes soil properties like particle-size distribution, bulk density, organic carbon content, available water capacity, soil texture, available water content, saturated hydraulic conductivity etc. There are 29 types of soil class data in the GBM basins.

Table 3.1:Land use distribution in Brahmaputra River Basin

Land use	**Area (%)**
Agricultural land	23
Deciduous forest	-
Evergreen forest	17
Mixed forest	6
Herbaceous land	36
Shrub Land	9
Pasture	-
Water bodies	-
Snow and ice	5
Bare land	2
Other type	2
Total	100

Land use is one of the most important factors that affect surface erosion, runoff, and evapotranspiration in a watershed. Parameters like infiltration, root depth and M ‘ L BRB been collected from USGS (United State Geological Survey) - Global Land Cover 2000 database. The required area is available from South Central Asia dataset. The data is available in geographic coordinate system - WGS84 datum. There are 11 types of land use data in GBM basins. Land use classes for Brahmaputra river basin is

shown in Table 3.1. Land use classes have been parameterized based on existing SWAT land use classes.

SWAT model stores the information required to simulate plant growth, in the plant growth database file for individual plant. The plant growth database distributed with SWAT includes parameters for most of the common plant species.

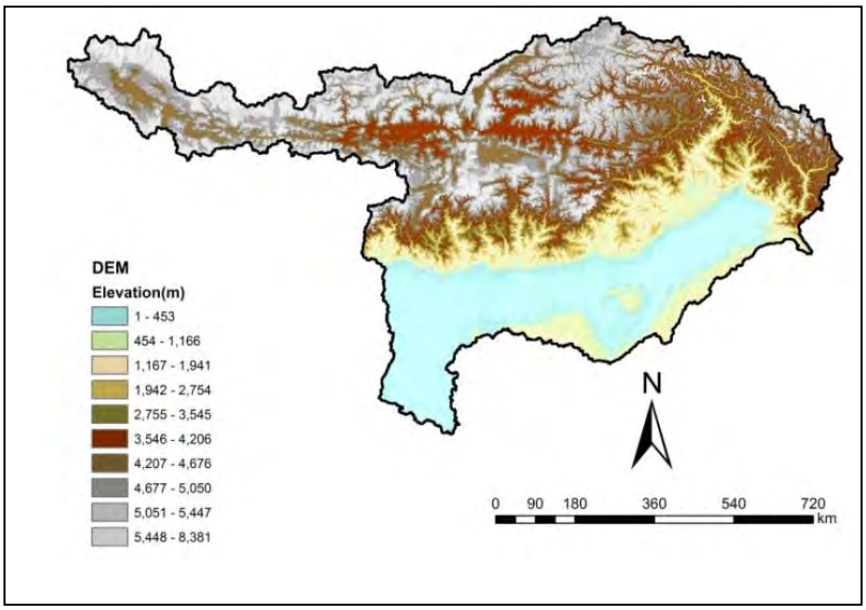

Figure 3.1: Digital Elevation Model of Brahmaputra River Basin

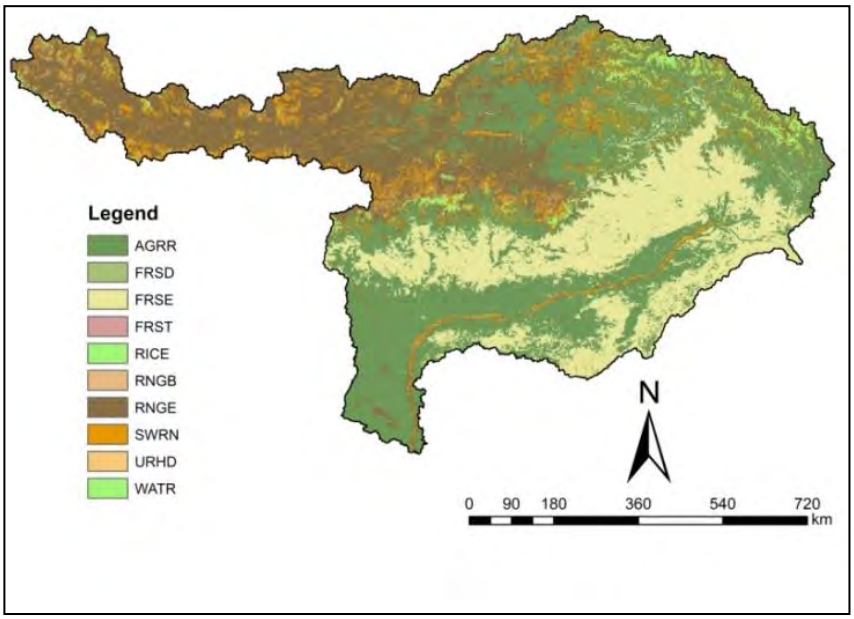

Figure 3.2:Land use map of Brahmaputra River Basin

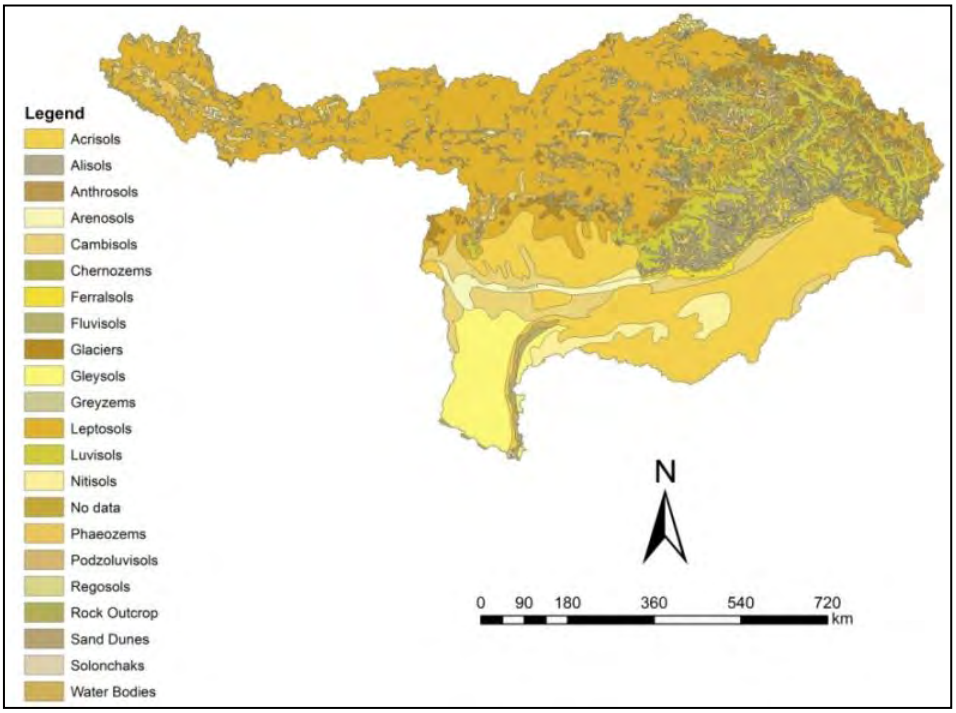

Figure 3.3:Soil use map of Brahmaputra River Basin

3.2.2 Weather and Discharge data

The SWAT model requires different types of meteorological data to simulate the hydrological processes. These include daily values of precipitation, maximum and minimum temperature, solar radiation, relative humidity and wind speed. For this study, meteorological data for the BRB have been collected from the National Aeronautics and Space Administration Prediction of Worldwide Energy (NASA POWER, link http://power.larc.nasa.gov). The data includes daily meteorological data (precipitation, minimum and maximum temperature) for the climate normal period (1981 to 2010). Table 3.2 shows basic data used in this study including their source, resolution and time period.

Table 3.2: Basic input data used in this study

Type	Description	Source/Reference	Original spatial resolution	Period	Remarks
Physical Data	Digital Elevation Map (DEM)	SRTM[a]	90 m x 90 m		DEM was resampled to get relatively coarser resolution raster file for faster computation
	Soil data	HWSD[b]	30 arc second		
	Land use data	USGS			
Meteorological Data	Precipitation, temperature	Bangladesh Meteorological Department (BMD)	Ishurdi, Tangail, Sayedpur station	1981-2010	NCDC and BMD data were used for the bias correction of NASA Power precipitation data. While using NCDC stations some data were missing. Data period for comparison were kept same for this source.
		NASA Power[c]		1981-2010	
		NCDC[d]	Nagqu (China) and Lhasa (China)	All available	
			Shilguri (India)		
Hydrological Data	Discharge	Bangladesh Water Development Board (BWDB)	Gauged	1981-2010	Discharge (monthly) data was collected at Bahadurabad station. Some data were missing for dry period flow.
GCM Data	Precipitation, maximum temperature, minimum temperature	BCC-CSM1.1 BCC-CSM1.1(m) GISS-E2-H GISS-E2-R HADGEM2-ES MRICGCM3 MIROC-ESM MIROC-ESM-CHEM	2.8125 x 2.8125 2.8125 x 2.8125 2.0 x 2.5 2.0 x 2.5 1.2414 x 1.875 1.125 x 1.125 2.8125 x 2.8125 2.8125 x 2.8125	2005-2100	All data are downloaded from ESGF Portal[e]. Precipitation and temperature data were extracted at four points in Brahmaputra river basin.

[a]Shuttle Rudder Topographic Mission.[b]Harmonized World Soil Database
[c]NASA Prediction of Power Worldwide Energy Resources (http://power.larc.nasa.gov/cgi-bin/cgiwrap/solar/hirestimeser.cgi?email=daily@larc.nasa.gov).
[d]National Climatic Data Center. [e]Earth System Grid Federation (http://pcmdi9.llnl.gov/esgf-web-fe/)

3.3 Bias Correction

NASA POWER precipitation data were corrected for bias after comparing with the measured precipitation data at six stations in BRB. The correction was made based on the monthly averaged data of both observed and nearest NASA Power station data. This bias corrected precipitation along with the temperature data were further used as

input in the SWAT model. Steps followed for bias correction of precipitation can be described as following:

Step 1: Monthly average precipitation(mm) were calculated for each of the six observed stations and nearest NASA POWER stations.

Step 2: Ratio of monthly precipitation for observed station and corresponding nearest NASA POWER station were determined (For each month separately, that is for one station 12 ratios for 12 months).

Step3: Ratios of each month for six stations were averaged. So, finally 12 ratios for 12 months obtained.

Step 4: Averaged ratios for each month was multiplied to all the NASA POWER stations (different averaged value for different month).

3.4 Steps of Model Setup

Five sequential steps have been followed to set up the SWAT model, which are (1) watershed delineation, (2) weather data definition, (3) editing SWAT inputs and simulation, (4) model calibration and validation and (5) Finally, streamflow simulation (both for present condition as well as in future) at different crucial points in some major rivers which are basically outflow of different sub-catchments. Detail description of model development is given in chapter 4.

3.5 Synthetic Approach of Climate Change Scenario Generation

In this study sensitivity of SWAT simulated streamflow has been investigated by changing precipitation and temperature by arbitrary amounts. The changes can be made in annual, seasonal or monthly scale. In this study the perturbation in precipitation and temperature were made in monthly scale. Climate change scenario generation in this method consists of two steps. First, estimation of average annual or monthly changes in climate data. Temperature and precipitation changes are estimated

ΔT ° ° ° ΔP= 0, ±10%, ±20%, 30% and 40%. Second, perturbation of historical time series of climatic data. The perturbation of temperature

T T ΔT P P ΔP T T P P

are the historic and future temperature and precipitation, respectively.

3.6 Selection of Climate Models and Scenarios

There are lots of GCMs available at different resolution for projecting future climate scenarios. There exist great variations in outputs values from one GCM to another. Some tend to give high changes in temperature and precipitation, whereas some give moderate changes. Moreover it is very much difficult to work with all the GCMs at a time. So selecting a model for assessing the hydrological impact of climate change is one of the most important tasks. Four points are selected all over the basin at which GCM results are extracted and used for further analysis. An assessment on different GCMs for four scenarios (RCP 2.6, RCP 4.5, RCP 6.0 and RCP 8.5) according to IPCC AR5 (IPCC 5thAssessment Report) has been conducted to justify the use of specific GCM outputs. Projected temperature and precipitation over the three periods of the 21st century O GCM‘ RCP is analyzed for Brahmaputra river basin to identify the warmest, coolest, driest, wettest, moderate warm and moderate wet scenarios. Precipitation and mean temperature obtained from different GCMs were average for three periods, viz. 2010-2039 (2020s), 2040-2069 (2050s) and 2070-2099 (2080s). Changes of precipitations and temperature from the base period were analyzed separately for all the periods. Finally, selection of scenarios were done based on the changes at the end of 21st century which is represented by 2080s. Steps followed can be summarized as following:

Step 1: Precipitation, maximum and minimum temperature data are extracted at four points in Brahmaputra river basin for each of the eight GCMs and four RCP scenarios for the period 2010-2100.

Step 2: Monthly average precipitation and maximum/minimum temperature were determined for three time periods, viz. 2020s (2010-2039), 2050s (2040-2069) and 2080s (2070-2099). Monthly average precipitation and temperature (max/min) were also calculated for base period (GCM base period data is available up to 2005. So thirty year period was selected as base, viz. 1970-2000) for each GCM.

Step 3: C C
period were calculated for each GCM and RCPs.

Step 4: For selecting scenarios for further study, changes at the end of 21st century (2080s) were considered. Scenario giving highest temperature and precipitation change were selected as the warmest and wettest. Driest and coolest scenario gave minimum positive or highest negative value of precipitation and temperature consecutively. Scenarios gave nearest changes in temperature and precipitation to median value were selected as moderate warm and moderate wet scenario respectively.

3.7 Pattern Scaling

In this study, Pattern scaling has been used to obtain future climate change scenarios. An open source tool namely MarkSim has been used for projecting climate change and obtaining high resolution precipitation and temperature data of selected six scena R M S
(Latitude x Longitude). Marksim uses WorldClim climate data as the base period data source (most of the data cover period 1960-1990, It uses historical weather data from a number of databases.) (Jones, P.G. and Thornton P.K., 2013). For base period we get precipitation, maximum and minimum temperature data for 365 days (1961-2005 averaged). For future projection of different scenarios we get data from 2013-2099. As described in section 3.6,we used 2010-2039 as 2020s, but as Marksim gives output from 2013 for projected scenarios. So, for the analysis of projected flow of different scenarios, we used 2013-2039 as 2020s (Other periods 2050s and 2080s are same as described earlier). Climate parameters derived from MarkSim have further been used as an input in SWAT model to generate future projected streamflow of BRB for the 21st century.

3.8 Future Scenario Generation

Temperature and precipitation data of 6 climate change scenarios obtained from pattern scaling, viz. warmest, coolest, wettest, driest, moderate warm and moderate wet were used to characterize the range of potential impact of climate changes on flow of Brahmaputra river basin.

3.8.1 Correction of flow for future scenarios

The hydrological model of BRB was run wit

precipitation and maximum, minimum temperature data for base condition (Marksim uses 1961-2005 averaged data as base data, data source is WorldClim database) and six scenarios. Flow obtained using MarkSim base period data was lower than the observed data (Monthly average flow was compared, observed data period was 1981-2010). So, it was necessary to adjust the flow obtained using high resolution data obtained after pattern scaling. For this following steps were followed:

Step 1: Ratio of flow for projected scenario and base period (using Marksim base period data) was determined.

$$\text{Ratio} = \frac{\text{Flow obtained for projected scenario}}{\text{Flow obtained for based period (MarkSim base period data)}} \quad \textbf{(3.1)}$$

Step 2: The Ratio obtained for each of the six scenarios (monthly average/ mean annual/ maximum annual/ minimum annual) were multiplied by the observed data (1981-2010 averaged) to obtain the adjusted flow for each of the scenarios

$$\text{Adjusted flow} = \text{Ratio} \times \text{Observed flow} \quad \textbf{(3.2)}$$

Chapter 4

Model Development

4.1 Introduction

The physically based hydrological model SWAT of Arnold and Allen (1996) selected for this study operates on daily time step and uses physiographical data such as elevation, soil use, land use, meteorological data and river discharge. As described earlier, the effects of spatial variations in topography, land use, soil and other characteristics of watershed hydrology are incorporated by dividing a basin into several sub-basins based on drainage areas of tributaries and then the sub-basins are further divided into a number of Hydrological Response Units (HRUs) based on land cover and soils. Each HRU is assumed to be spatially uniform in terms of land use, soil, topography and climate.

4.2 Steps of Model Setup

Initially the climate data which would be used as input in the SWAT model should be checked for bias. Due to high level of variability and uncertainty only precipitation data is checked for bias comparing with the observed data. After bias correction five sequential steps have been followed to set up the SWAT model, which are watershed delineation, weather data definition, editing SWAT inputs and simulation. Finally, flow has been generated (both for present condition as well as in future) at different crucial points in some major rivers which are basically outflow of different sub-catchments. The descriptions of these steps are given in the following sections:

4.2.1 Biases in NASA POWER Precipitation

Precipitation is the most important and sometimes an uncertain variable in hydrological modeling (Islam and Gan 2015). Mismatch between observed and NASA POWER precipitation may lead to greater uncertainty and less reliable outputs from the hydrologic assessment. It is possible the adjust some model parameters to suppress over-simulated and increase under-simulated runoff, but that would not address the real problem and make more sense to question the validity of NASA POWER Precipitation data. So, comparison of mean monthly precipitation between few observed stations and nearby NASA POWER grid points for the same period

have been made to identify the extent of deviation. Six points have been selected within BRB based on the availability of data as shown in Figure 4.1.

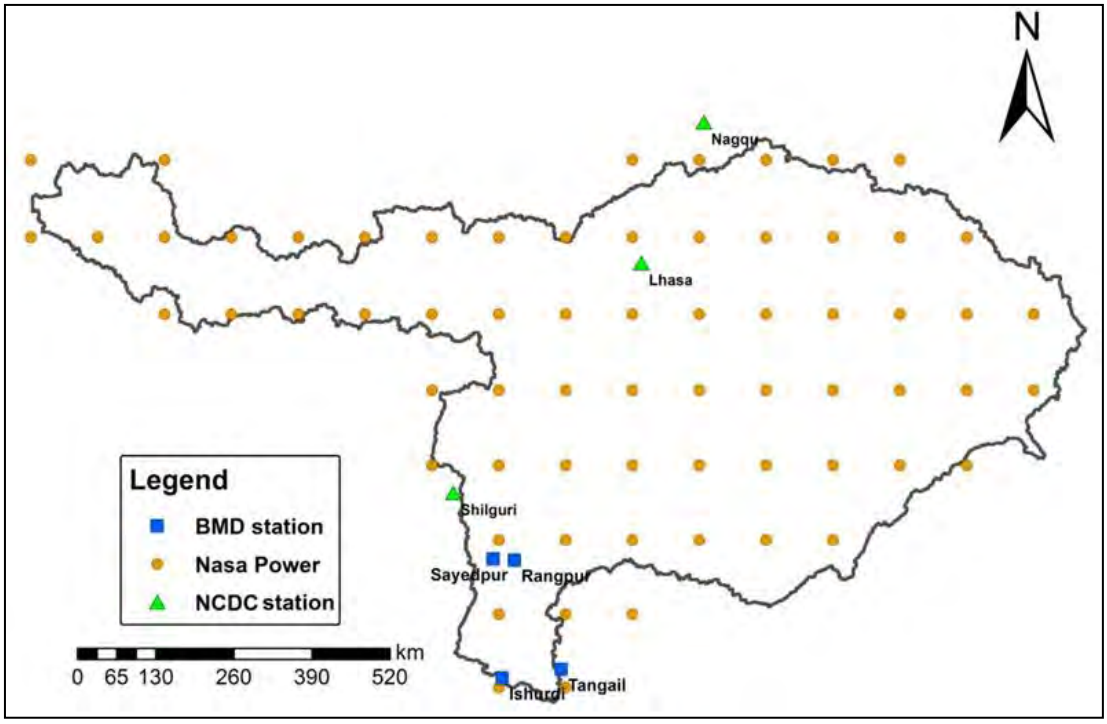

Figure 4.1: Location of NASA Power stations, BMD stations and NCDC stations

Figure 4.2-4.7 show monthly comparison of average precipitation between NASA POWER and observed station. Precipitation data of Rangpur, Sayedpur, Ishurdi and Tangail have been collected from BMD whereas data of Shilguri, Lhasa and Nagqu were collected from NCDC website. It is evident there exist no similar pattern of variability, that is for some station observed value is higher where as at some stations NASA POWER is overestimating. This variability also exists between the months.

In order to remove biases in NASA POWER data, a methodology applied in Islam and Gan (2015) has been adapted and will be discussed below:

Step 1: Ratio of mean monthly observed precipitation and mean monthly precipitation from nearby NASA POWER grid has been determined for all the six stations.

Step 2: These month ratios of six stations were averaged for each month separately to estimate the average monthly precipitation bias ratio for the BRB

Step 3: Monthly ratio obtained from previous step was used to adjust all NASA POWER stations precipitation to remove the bias. This adjustment leads the bias corrected precipitation.

Table 4.1: All the calculations done in this step to correct the bias in NASA POWER data.

	Jan	Feb	Mar	Apr	May	Jun	Jul	Aug	Sep	Oct	Nov	Dec
NASA POWER (mm)	0.2135	0.2056	0.3539	1.0400	2.7204	6.8282	9.1383	7.1301	6.3744	2.4416	0.2919	0.1671
Sayedpur station(mm)	0.2860	0.4173	0.8679	3.7416	8.6842	15.8578	15.7559	11.6731	13.0189	6.0311	0.2622	0.2470
Sayedpur/ NASA POWER	1.3396	2.0299	2.4526	3.5977	3.1922	2.3224	1.7242	1.6372	2.0424	2.4702	0.8983	1.4785
NASA POWER(mm)	0.2006	0.2788	0.6391	1.6127	3.5963	9.2413	11.5009	9.2308	8.8261	4.2111	0.4831	0.2432
Ishurdi station(mm)	0.2148	0.5645	0.9631	2.2173	4.9263	8.0813	9.0436	6.8576	9.8604	4.0419	0.4841	0.2915
Ishurdi/ NASA POWER	1.0707	2.0244	1.5071	1.3749	1.3698	0.8745	0.7863	0.7429	1.1172	0.9598	1.0022	1.1982
NASA POWER(mm)	0.9011	0.8458	1.0222	3.2651	8.1501	13.4252	16.8461	13.3332	11.3976	4.9441	1.3570	0.5196
Shilguri station(mm)	0.3900	1.5974	1.2438	5.7342	13.5906	18.0324	27.4000	22.1774	19.4308	8.7802	0.8766	1.3460
Shilguri/ NASA POWER	0.4328	1.8886	1.2168	1.7562	1.6676	1.3432	1.6265	1.6633	1.7048	1.7759	0.6460	2.5904
NASA POWER(mm)	0.1264	0.1913	0.3468	0.7944	1.5998	3.1485	3.9579	4.4410	3.3290	0.9144	0.2075	0.0795
Lhasa(mm)	0.0277	0.0491	0.0999	0.2446	0.9357	2.3918	3.9746	4.0158	2.3143	0.2327	0.0243	0.0239
Lhasa/ NASA POWER	0.2194	0.2567	0.2880	0.3078	0.5849	0.7597	1.0042	0.9043	0.6952	0.2545	0.1173	0.3002
NASA POWER(mm)	0.1859	0.3113	0.5061	0.9033	1.7311	3.4681	3.6945	3.8796	3.2004	1.0596	0.3012	0.1490
Nagqu(mm)	0.4787	0.7063	1.1248	1.4567	1.7877	2.0082	2.2462	1.7800	1.4134	0.7918	0.4927	0.5359
Nagqu/ NASA POWER	2.5749	2.2689	2.2225	1.6127	1.0327	0.5790	0.6080	0.4588	0.4416	0.7472	1.6361	3.5973
NASA POWER(mm)	0.1505	0.2717	0.8090	2.2310	4.4656	9.8526	11.7031	9.0818	8.7149	4.5395	0.6364	0.1738
Tangail(mm)	0.1987	0.8654	1.4645	3.6333	8.3665	10.5666	10.6955	8.7587	9.4107	5.3742	0.8373	0.3703
Tangail/ NASA POWER	1.3208	3.1855	1.8102	1.6286	1.8735	1.0725	0.9139	0.9644	1.0798	1.1839	1.3157	2.1313

Table 4.2: Monthly ratios obtained for bias correction

Sl. No	Jan	Feb	Mar	Apr	May	Jun	Jul	Aug	Sep	Oct	Nov	Dec
Sayedpur	1.3396	2.0299	2.4526	3.5977	3.1922	2.3224	1.7242	1.6372	2.0424	2.4702	0.8983	1.4785
Ishurdi	1.0707	2.0244	1.5071	1.3749	1.3698	0.8745	0.7863	0.7429	1.1172	0.9598	1.0022	1.1982
Shilguri	0.4328	1.8886	1.2168	1.7562	1.6676	1.3432	1.6265	1.6633	1.7048	1.7759	0.6460	2.5904
Lhasa	0.2194	0.2567	0.2880	0.3078	0.5849	0.7597	1.0042	0.9043	0.6952	0.2545	0.1173	0.3002
Nagqu	2.5749	2.2689	2.2225	1.6127	1.0327	0.5790	0.6080	0.4588	0.4416	0.7472	1.6361	3.5973
Tangail	1.3208	3.1855	1.8102	1.6286	1.8735	1.0725	0.9139	0.9644	1.0798	1.1839	1.3157	2.1313
Average	1.1597	1.9423	1.5829	1.7130	1.6201	1.1585	1.1105	1.0618	1.1802	1.2319	0.9359	1.8827

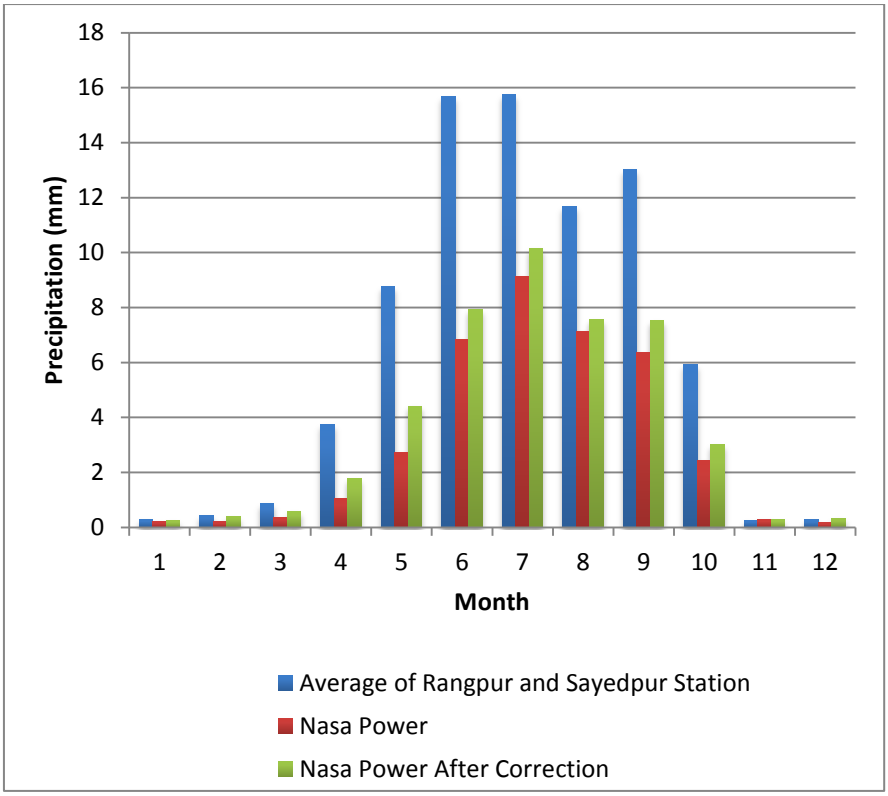

Figure 4.2: Bias correction at Rangpur and Sayedpur station (Two stations average as both are near to one NASA Power station)

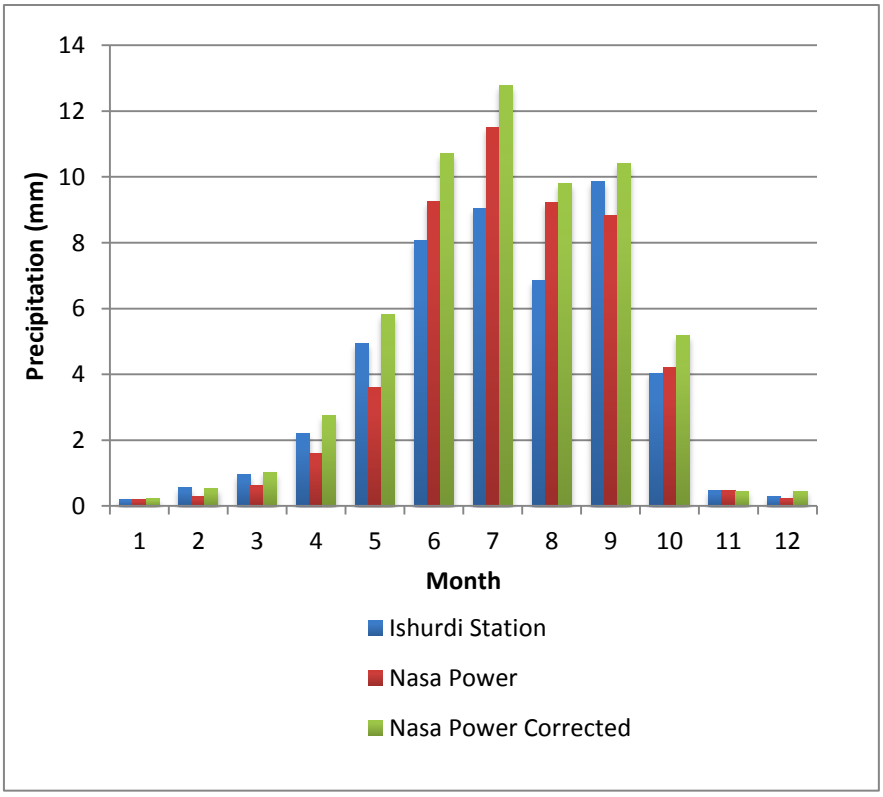

Figure 4.3: Bias correction at Ishurdi station

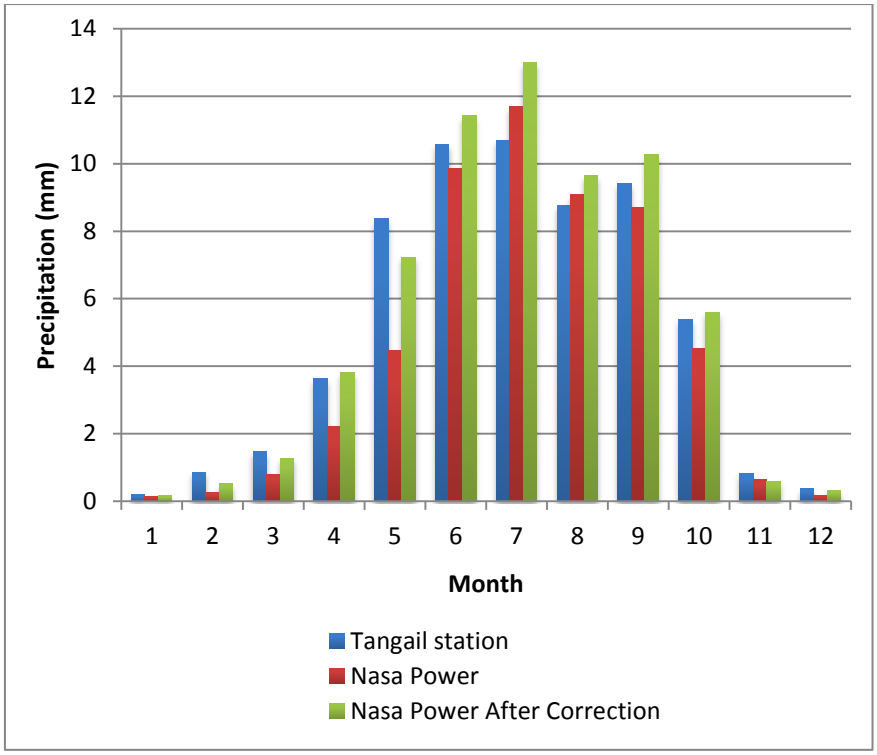

Figure 4.4: Bias correction at Tangail station

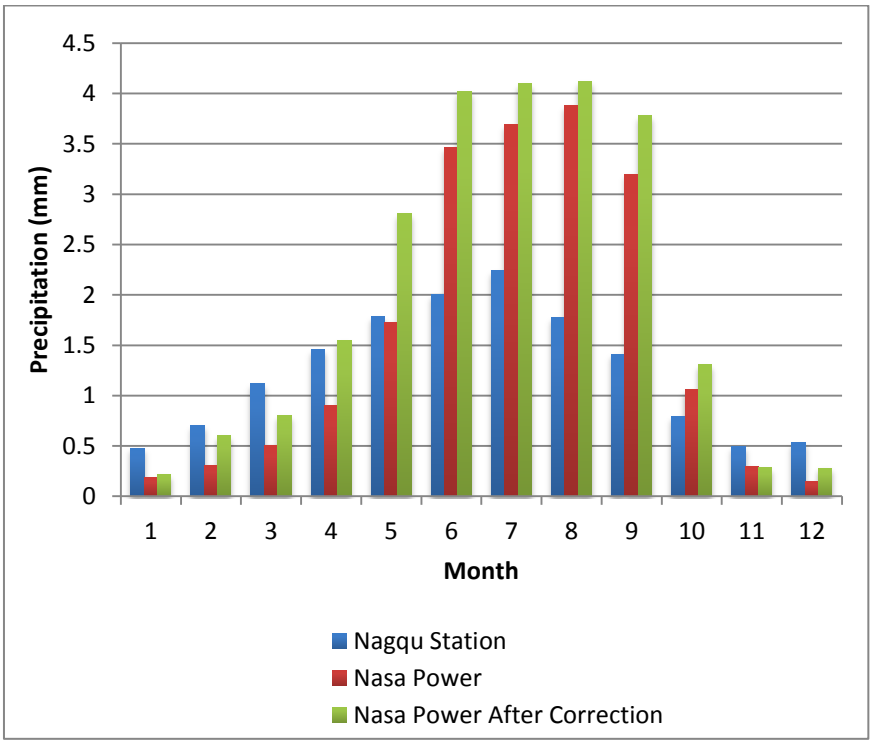

Figure 4.5: Bias correction at Nagqu station

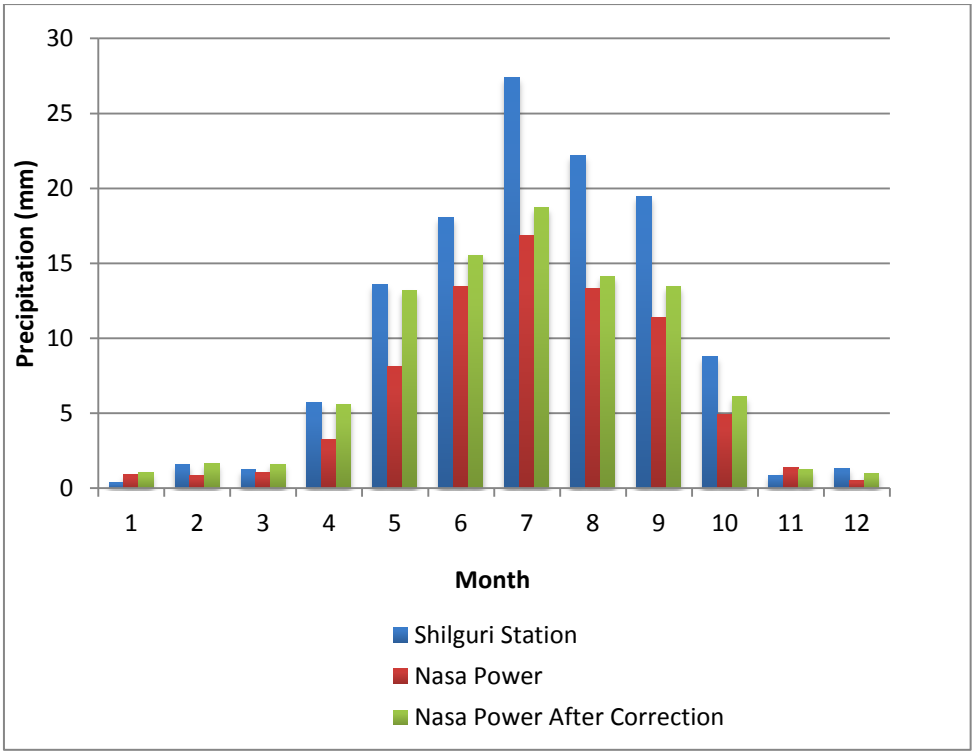

Figure 4.6: Bias correction at Shilguri station

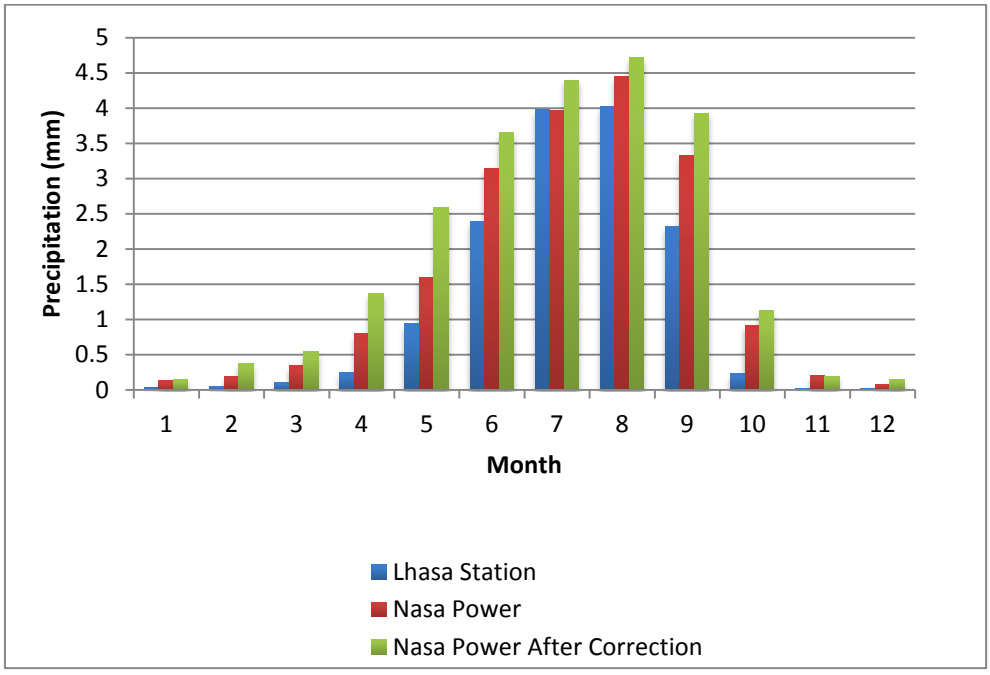

Figure 4.7: Bias correction at Lhasa station

4.2.2 Watershed Delineation

The first step in the model setup involves a delineation of the basin and sub-basin boundaries. This is accomplished using the automatic watershed delineation tool of

ArcSWAT 2012.10.2.16 employing a 900 m DEM (re-sampled from 90 m DEM) for GBM basins and 200 m DEM (re-sampled from 300 m DEM) for Bangladesh. The Universal Transverse Mercator (UTM) projection has been used for the DEM and all other GIS layers. All the watershed delineation steps such as filling sink, defining flow direction and accumulation have been done automatically through the user interface. After watershed delineation, BRB basins have been divided into 149 watersheds based on the threshold area of 200,000 ha. After delineation, the basin was divided into 149 sub-basins as shown in Figure 4.8. Soil and landuse maps were loaded into SWAT to extract the landuse and soil information of the BRB. The land use, soil layer and slope class were overlaid to define the HRUs of the BRB. A total of 1020 HRUs (Average area 687 km^2) were produced and included in the simulation. The discretization of basin into HRUs allows a detailed simulation of the hydrological processes.

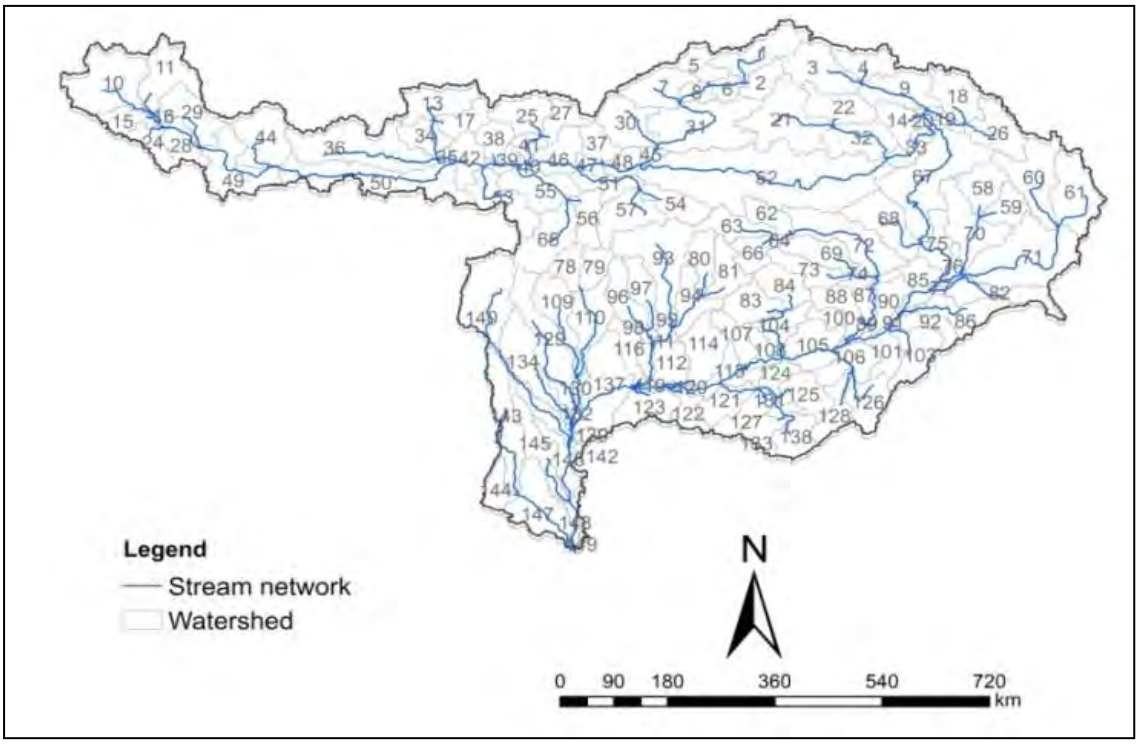

Figure 4.8: Sub basins and delineated stream network of Brahmaputra River Basin

4.2.3 Weather Data Definition

The climate of a watershed provides the moisture and energy inputs that control the water balance and determine the relative importance of the different components of the hydrologic cycle. The climatic variables required by SWAT consist of daily precipitation, maximum/minimum air temperature, solar radiation, wind speed and

relative humidity. The model allows values for daily precipitation, maximum/minimum air temperatures, solar radiation, wind speed and relative humidity to be input from records of observed or generated data using weather generator tools (WXGEN) (Arnold et.al., 2009b).

The weather data for the GBM basins have been used from NASA power. The data includes daily weather data (precipitation, minimum and maximum temperature) starting from 1981 to 2010 which is used for SWAT modeling calibration. Similar weather data for Bangladesh from the BMD has been collected for the same time frame.

4.2.4 Simulation Method Selection

The SWAT model has been simulated for the period of 1981 to 2010 based on the availability of data. To describe the distribution of rainfall, SWAT provides two options: a skewed normal distribution and a mixed exponential distribution. In the simulation for the present study, the skewed normal probability distribution function

SWAT M _

equation to define the rate and velocity of flow. Water is routed through the channel network using the variable storage routing method or the Muskingum River routing method. In this simulation the variable storage method has been used for channel routing. For estimating runoff, the SCS curve number method has been used . The Hargreaves method has been used to calculate potential evapotranspiration (PET) as it requires less weather parameter.The skewed normal distribution method has been used for rainfall distribution. Note that, the model was applied for 1978 to 2010 with a daily time step in order to facilitate the 3 years warm-up period where 1978-1980 was taken same as the year 1981.

4.2.5 Sensitive Parameter Selection

Model users are often faced with the different task of determining which parameters to calibrate so that the model response mimics the actual field, subsurface, and channel conditions as closely as possible. When the number of parameters in a model is substantial as a result of either a large number of sub-processes being considered or because of the model structure itself, the calibration process becomes complex and computationally extensive (Rosso, 1994; Sorooshian and Gupta, 1995). In such cases,

sensitivity analysis is helpful for identifying and ranking parameters that have a significant impact on specific model outputs of interests (Saltelli et.al., 2000).

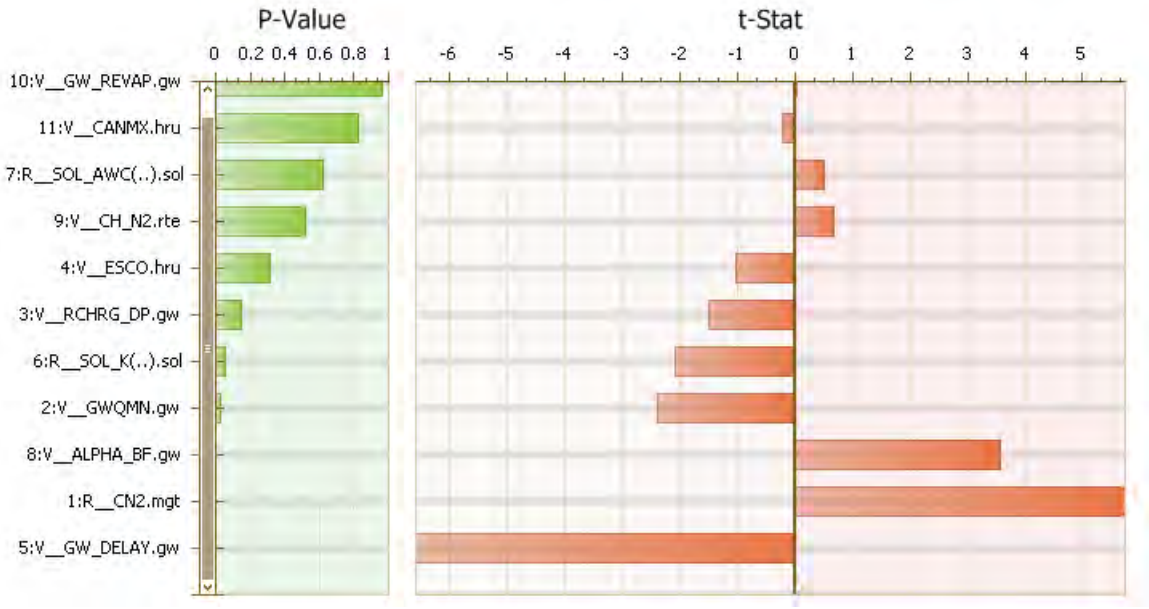

Figure 4.9: Global sensitivity analysis of calibration parameters

Table 4.3: Most sensitive SWAT parameters and their fitter values for Brahmaputra river basin

Rank	Parameter	Description	Range	Fitted value
1	v__GW_REVAP.gw	Ground water revap co-efficient	0.02 - 0.2	0.059
2	v__GWQMN.gw	Threshold water depth in the SA	0 - 3000	2416.667
3	v__ESCO.hru	Soil evaporation factor	0 - 1	0.78
4	r__SOL_AWC().sol	Soil available water capacity	± 0.25	0.0776
5	v__RCHRG_DP.gw	Deep aquifer percolation fraction	0 - 1	0.035
6	r__CN2.mgt	Curve number	± 0.25	-0.055
7	r__SOL_K().sol	Saturated hydraulic conductivity	± 0.25	0.0833
8	v__CH_N2.rte	M ‘	0.02-0.03	0.029167
9	v__GW_DELAY.gw	Groundwater delay time	20-100	21.333
10	v__ALPHA_BF.gw	Baseflow alpha factor	0.02 - 0.2	0.197
11	v__CANMX.hru	Maximum canopy storate	0-10	1.833

The qualifier (r_) refers that the value is multiplied by 1 plus a factor.
The qualifier (v_) refers to the substitution of a parameter by a value.
The qualifier (a_) refers to the addition of a parameter by a value.

For the present study, sensitivity analysis was performed using the Latin hypercube one-factor-at-a- time (LH-OAT) (Van Griensven et.al., 2002, 2005) method to rank

the simulation parameters of the model for each sub basin. Sensitivity analysis can be performed for many inputs such as for flow, sediment discharge, Organic Nitrogen, Phosphorus etc. In this study, sensitivity analysis is performed only for stream flow, as the study objective is to assess the availability of water. Figure 4.9 shows the results and sensitivity of various parameters used in SWAT model calibration, this analysis was done by using SWAT-Cup tool Total 11 parameters have been selected to find out their sensitivity on flow conditions. Most sensitive parameters and their fitted values are shown in Table 4.3.

4.3 Calibration and validation

There are numerous parameters in hydrological models which can be classified as physical parameters (i.e., parameters that can be physically measurable from the properties of watershed) and process parameters (i.e., parameters represents properties which are not directly measurable) (Sorooshian and Gupta, 1995). A sensitivity analysis of parameters was carried out by regressing Latin Hypercube generated parameters against objective function values (SWAT-cup, 2012). It was found that, out of 27 selected parameters, the Ground water revap co-efficient, threshold water depth in the shallow aquifer for flow, soil evaporation compensation factor, available water capacity, q ‘ for main channel, curve number, saturated hydraulic conductivity, maximum canopy storage, groundwater delay time fl parameters to which the flow has sensitivity. However the curve number (CN2) was found to be the main sensitivity parameter for all outlets. The model was calibrated from 1981 to 1995 and validated form 1996 to 2010 with monthly observed stream flow data at Bahadurabad station.

In calibration and validation stage, model performance is evaluated based on statistically and graphically.

4.3.1 Calibration using SWAT-CUP tool

Automated model calibration requires that the uncertain model parameters are systematically changed, the model is run, and the required outputs (corresponding to measured data) are extracted from the model output files. The main function of an

interface is to provide a link between the input/output of a calibration program and the model. The simplest way of handling the file exchange is through text file formats. SWAT-CUP is an interface that was developed for calibration of SWAT. Using this generic interface, any calibration/uncertainty or sensitivity program can easily be linked to SWAT. The program links Sequential Uncertainty Fitting (SUFI2) (Abbaspour et.al., 2004; 2007), Particle Swarm Optimization (PSO), Generalized Likelihood Uncertainty Estimation (GLUE) (Beven and Binley, 1992), Parameter Solution (ParaSol) (Van Griensven and Meixner, 2003), and Markov chain Monte Carlo (MCMC) (e.g., Kuczera and Parent, 1998; Vrugt et.al., 2003) algorithm to SWAT. It enables sensitivity analysis, calibration, validation, and uncertainty analysis of SWAT models and can help decrease modelling uncertainty by removing some probable sources of modeling and calibration errors. Based on previous studies it was found that SUFI2 has better performances in calibrating SWAT quickly in a computationally less expensive method and also with less no. of iterations. So, SUFI2 has been used to perform the calibration of SWAT at selected calibration points of the GBM basins.Figure 4.10 shows the graphical representation of monthly observed and simulated flow for both calibration and validation period. It was found that the simulated flow is in great compliance with the observed discharge for both monsoon and dry season.

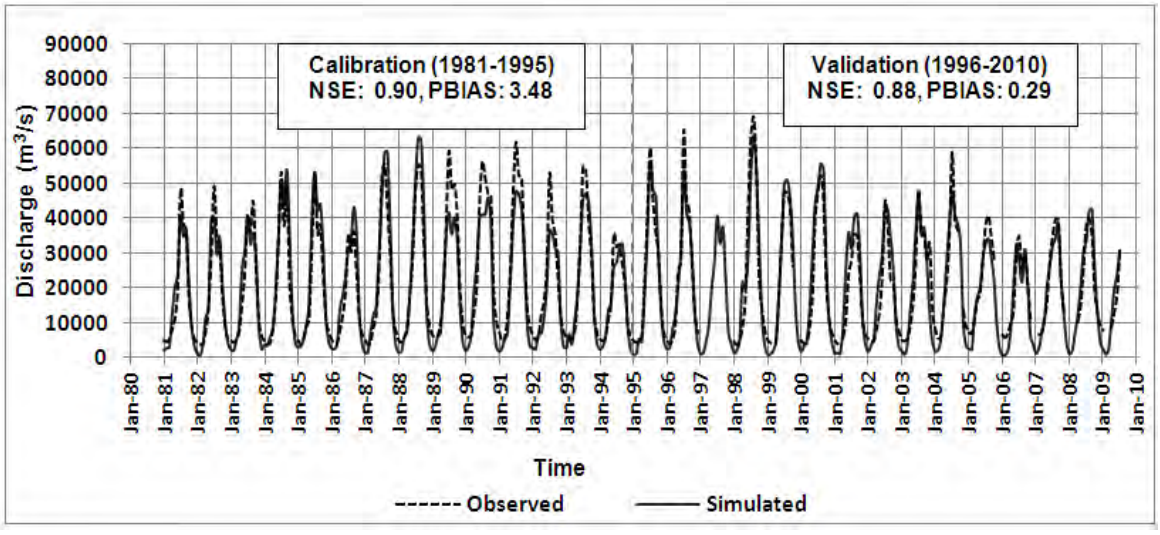

Figure 4.10: Monthly observed and simulated flows for the calibration and validation period 1981 to 2010

Table 4.4: Model performance statistics for calibration (1981-1995) and validation period (1996-2010) of the Brahmaputra river basin

Period	Observed Mean (m^3/s)	Simulated Mean (m^3/s)	Model performance			
			NSE	R^2	PBIAS	RSR
Calibration	21205.34037	20468.29833	0.90	0.90	3.48	0.32
Validation	21902.88773	19944.6344	0.89	0.89	0.29	0.34

Table 4.5: General Reported ratings for Nash-Sutcliffe efficiency (NSE), Mean relative bias (PBIAS), Root mean square error-standard deviation ratio (RSR) and Coefficient of determination (R^2) for calibration and validation process (Rossi et al, 2008).

Formula	Value	Rating
$NSE = 1 - \left[\frac{\sum_i^n (xobs(i) - ymod(i))2}{\sum_i^n (xobs(i) - \overline{xobs})2}\right]$	>0.65 0.54 to 0.65 >0.50	Very Good Adequate Satisfactory
$PBIAS = \left[\frac{\sum_i^n (xobs(i) - ymod(i))}{\sum_i^n xobs(i)}\right]$	< ± 20% ± 20% to ± 40% > ± 40%	Good Satisfactory Unsatisfactory
$RSR = \left[\frac{\sqrt{\sum_i^n (xobs(i) - ymod(i))^2}}{\sqrt{\sum_i^n (xobs(i) - \overline{xobs})^2}}\right]$	≤ RSR ≤ ≤ RSR ≤ ≤ RSR ≤ 7 RSR ≥ 7	Very Good Good Satisfactory Unsatisfactory
$R^2 = \left[\frac{\left[\sum_i^n (xobs(i) - \overline{xobs})(ymod(i) - \overline{ymod})\right]^2}{\left[\sum_i^n (xobs(i) - \overline{xobs})^2 \sum_i^n (ymod(i) - \overline{ymod})^2\right]}\right]$		Satisfactory

Note: xobs=observed flow, ymod= model/simulated flow

4.3.2 Model Performance Evaluation

Statistically the performance of the model has been evaluated using the Nash–Sutcliffe Efficiency value (NSE), the coefficient of determination (proportion of the variance in the observations explained by the model, R^2), percent bias (PBIAS) and the ratio of the root mean square error between the simulated and observed values to

the standard deviation of the observations (RSR). The statistical model performance is given in Table 4.4. General reported rating of NSE, R^2, PBIAS and RSR are given in Table 4.5. The NSE values are 0.90 and 0.86 for calibration and validation period respectively. The co-efficient of determination (R^2) values are 0.90 for calibration and 0.87 for validation period. The PBIAS and RSR values are found to be 3.48 and 0.32 in calibration stage and 3.27 and 0.56 in validation stage, respectively. These statistics demonstrate SWAT generally performed well in both calibration and validation stages based on historical measured data for BRB (Moriasi et.al., 2007), which establishes the basis for conducting climate change studies based on the simulations of SWAT, ‘ unchanged. Scatter plot of observed vs simulated flow at Bahadurabad station for 1981-2010 has been plotted in Figure 4.11. Simulated flow shows good compliance with the observed flow at this station.

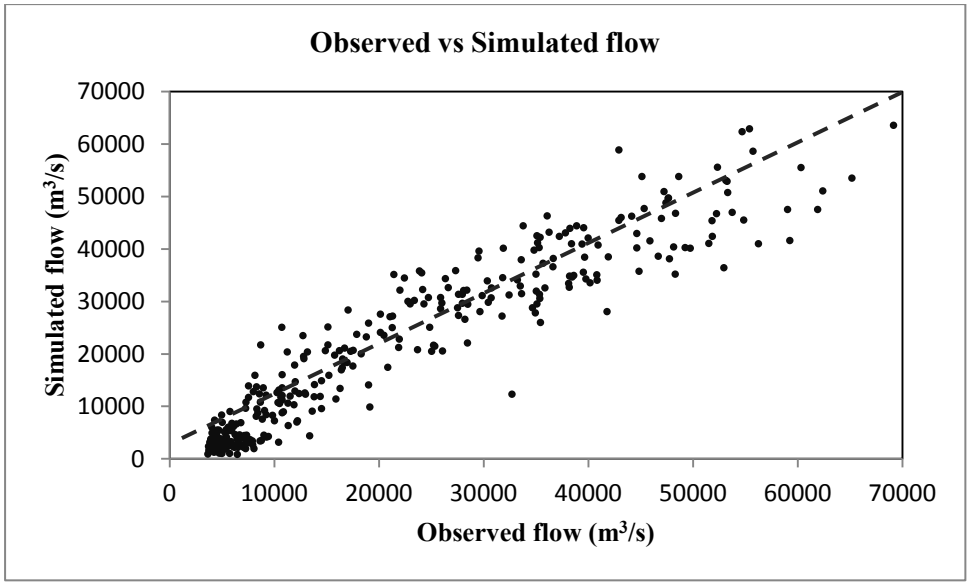

Figure 4.11: Scatter plot of observed vs simulated flow at Bahadurabad station for 1981-2010

Chapter 5

Results and Discussions

5.1 Introduction

After model setup and calibration/validation, several types of analysis were done in order to assess the water availability in BRB and impact of climate change on flow for different scenarios. In this chapter, initially the basin water balance was discussed which quantifies water distribution throughout the basin. After this, temperature and precipitation change obtained for several GCMs and RCPs were discussed based on which six climate scenarios were selected. Projected flow for high resolution precipitation and temperature of six selected scenarios were then analyzed to identify the impact of climate change on flow of Brahmaputra river basin.

Table 5.1: Annual average water balance of Brahmaputra River Basin.(1981-1995)

Water Balance Component	**Amount(mm)**
Precipitation (PR)	1342
Snowfall(SF)	153
Surface runoff (SR)	246.65
Lateral soil flow contribution(LatQ)	119.31
Ground water contribution to streamflow (GWQ)	555.52
Revap or shallow aquifer recharges(SAR)	33.61
Deep Aquifer Recharges (DAR)	21.74
Total water yield/ flow(WY)	925.98
Percolation out of soil(PER)	621.27
Actual evapotranspiration(ET)	328.1
Potential evapotranspiration(PET)	579.1
Change in soil water storage (SW)	37.07

Note: SW=PR+SF-SR-LatQ-GWQ-SAR-DAR-ET

5.2 Water Balance of the BRB

Water balance is the assessment of water resources and its use in the system. The computation includes all water receiving components (rainfall, snow fall etc.) within the system as well as water losses (evaporation, percolation, runoff etc) from the system. The main principle of water balance is the difference between total incoming water and total losses equal to storage in the system. For water balance analysis of the study area, the calibrated SWAT models have been simulated for the time period of 1981 to 2010 and the hydrological components have been analyzed to compute

average annual water balance. The simulation results of the annual water balance for the Brahmaputra River Basin (BRB) is given in Table 5.1.

The water balance in SWAT considers precipitation and snow fall as inflow to the sub-basin (the basic modeling unit in SWAT), evapotranspiration and deep percolation as loss and surface runoff and lateral flow as the outflow. The average annual basin precipitation and snowfall over the BRB are about 1342 mmand 153.29 mm respectively.

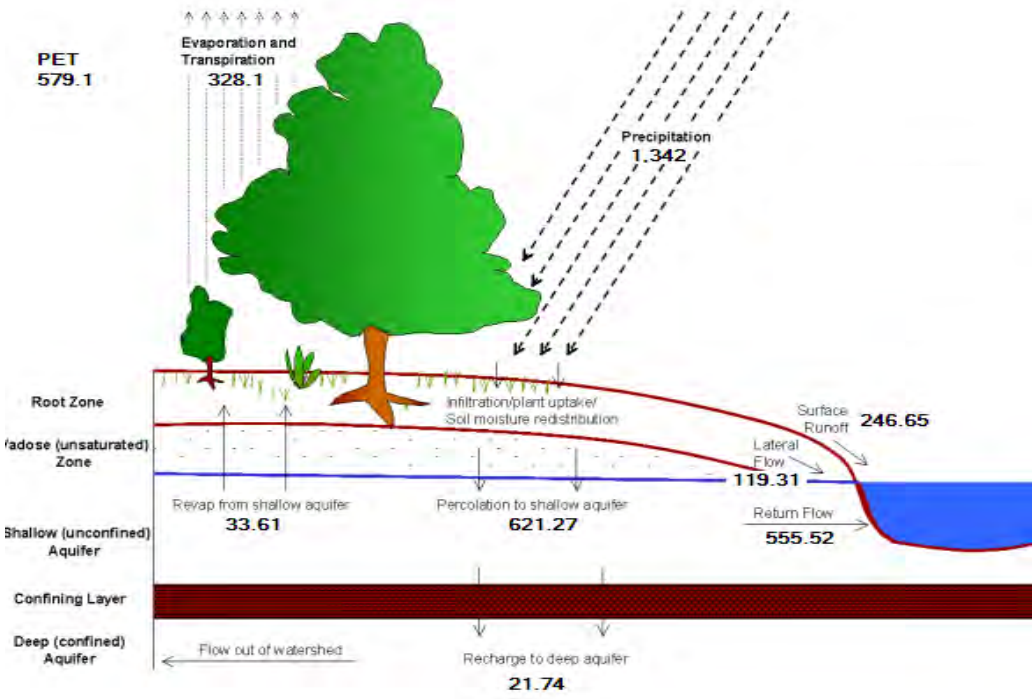

Figure 5.1: Schematic figure of water balance of Brahmaputra River Basin.

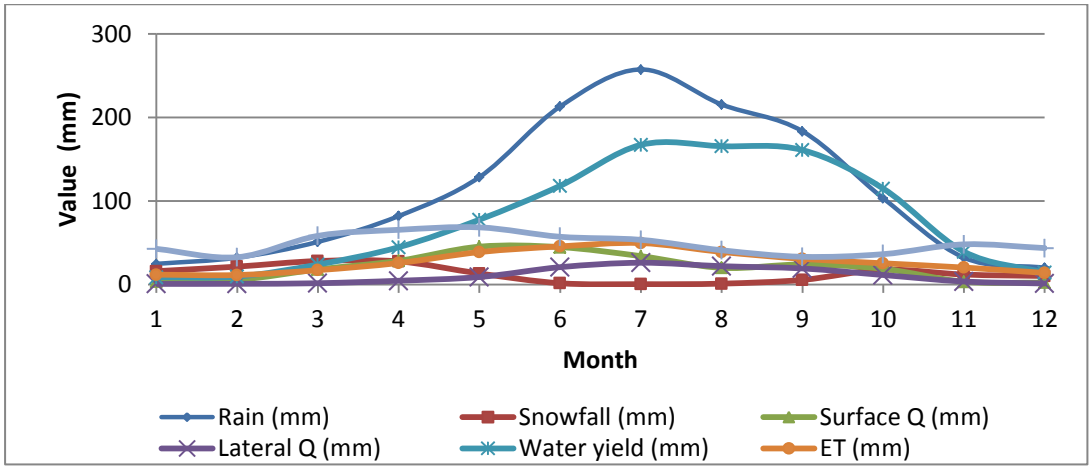

Figure 5.2: Average (1981-1995) monthly water availability of Brahmaaputra River Basin (all in mm)

Table 5.2: Average monthly water availability of Brahmaaputra river basin (all in mm)

Month	Rain (mm)	Snowfall (mm)	Surface Q (mm)	Lateral Q (mm)	Water yield (mm)	ET (mm)	PET (mm)
1	24.63	15.85	3.57	0.6	8.58	11.66	42.53
2	32.02	21.32	5.49	0.71	9.43	11.26	32.57
3	50.95	28	17.94	1.43	23.79	17.07	58.13
4	81.85	27.5	28.28	4.41	44.55	25.62	65.35
5	128.43	13.07	45.2	8.85	77.51	38.71	68.27
6	212.97	1.41	44.61	20.66	118.04	45.52	57.02
7	257.26	0.3	33.82	25.94	167.04	49.47	53.33
8	215.33	0.94	19.83	21.81	165.39	38.85	40.87
9	183.28	5.43	23.84	19.1	160.77	30.56	33.06
10	103.07	17.57	18.66	11.24	114.71	25.28	36.23
11	32.08	11.83	3.26	3.45	39.24	20.21	47.93
12	19.9	10.07	2.13	1.1	14.07	13.78	43.5

The annual evapotranspiration loss is 328.1 mm, which is 35% of annual inflow for Brahmaputra basins. Annual percolation in the Brahmaputra basin is 621.27 mm which is 67% of annual inflow. After the losses, the remaining water contributes to stream flow as surface runoff and lateral flow. A schematic figure of water availability in BRB is shown in Figure 5.1.

Monthly water availability of the base scenario has been analyzed and given in Table 5.2. Flows are mainly concentrated in the wet period (June to November). For Brahmaputra basin peak flow occurs during July.

5.3 Selection of Climate Change Scenarios

Numerous GCMs are available at different resolution for projecting future climate scenarios. There exist great variations in output values from one GCM to another. Some tend to give high changes in temperature and precipitation, whereas some give moderate changes. Moreover it is very much cumbersome to work with all the GCMs at the same time. So selecting a model for assessing the hydrological impact of climate change is one of the most important tasks. In the present study an attempt has been made to identify the warmest, coolest, wettest, driest, moderate warm and moderate wet scenarios for the BRB. Eight models have been selected for this

analysis based on the availability of data. So there were 32 scenarios (8 GCMs and 4 RCPs, viz RCP 2.6, RCP 4.5, RCP6.0, RCP 8.5) for selecting the required scenarios.

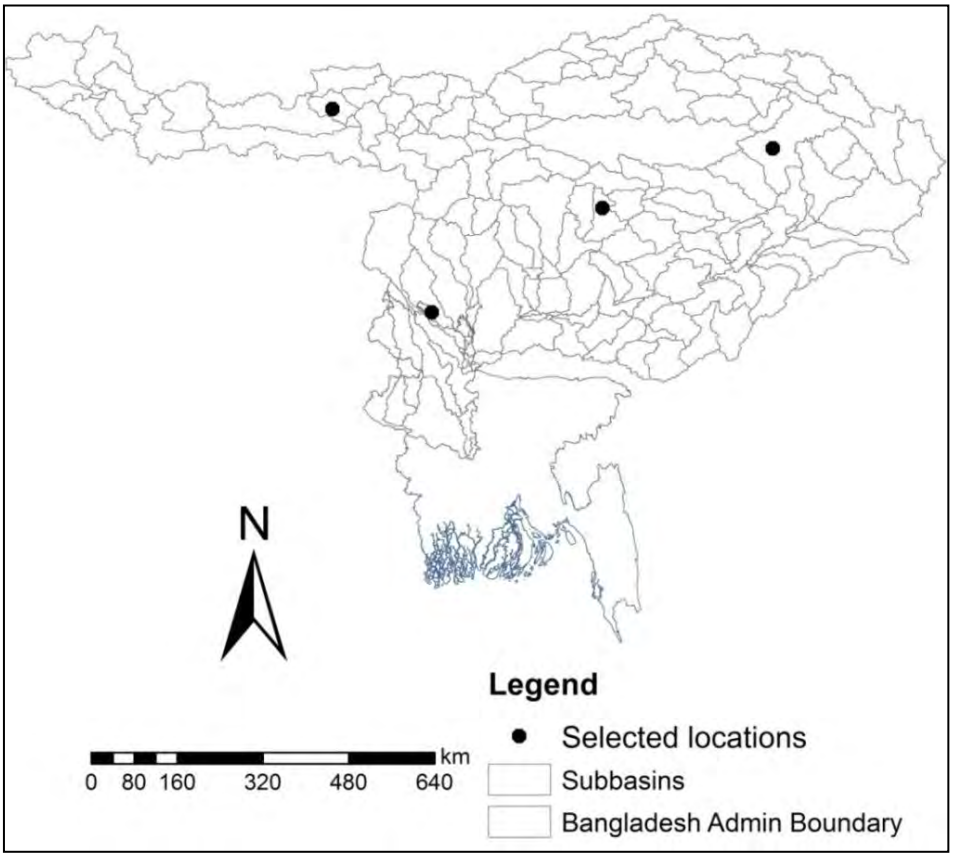

Figure 5.3: Selected locations in Brahmaputra river basin for GCM data extraction and analysis

5.3.1 Selection of Points for Analysis:

Because of their coarse resolution, only a few GCM grids fall upon Brahmaputra River Basin. Estimating the temperature and precipitation of the whole basin for all the models and RCPs using all the grids are quite cumbersome. So an attempt has been made to select a few representative points over the BRB which can provide a better idea of the climate parameters such as temperature and precipitation. In the present study four points are selected over the basin at which GCM projected climatic variables are extracted and used for further analysis. Figure 5.3 shows the location of the points selected for extracting the GCM outputs. Following sections analyzes the temperature and precipitation data obtained from eight GCMs. Appendix A represents all box-plot, bar chart and scatter plots generated from the results of the analysis of climate data obtained from GCM data.

5.3.1.1 RCP 2.6

Temperature and precipitation change for eight GCMs are analyzed for RCP 2.6. The results are separated for three periods; viz. 2010-2039 (2020s), 2040-2069 (2050s) and 2070-2099 (2080s). Monthly precipitation/temperature data for each model was averaged and compared with the base period data (1971-2000). Table 5.3 shows the changes in precipitation (%) for 8 GCMs.

$$\Delta P(\%) = \frac{(Prcp - Pbase)}{Pbase} \times 100 \qquad (5.1)$$

Table 5.3: Precipitation change (%) for RCP 2.6

Model	2020s	2050s	2080s
BCC-CSM1.1	7.36	14.36	16.10
BCC-CSM1.1(m)	5.82	7.68	1.83
GISS-E2-H	3.56	3.86	6.05
GISS-E2-R	2.85	3.38	-0.58
HadGEM2-ES	-5.59	-3.95	2.37
MIROC-ESM	6.33	10.77	11.89
MIROC-ESM-CHEM	5.70	9.31	18.58
MRI-CGCM3	2.68	9.43	3.76

It is found that the precipitation changes (%) varied between -5.589% to 7.36%, -3.95% to 14.36% and -0.58% to 18.58% for 2020s, 2050s and 2080s, respectively. Median values for these three periods are 4.627%, 8.493% and 4.903%. There is a great variation among the trends of precipitation change. MIROC-ESM-CHEM projects the wettest scenario and GISS-E2-R projects the driest scenario for the RCP 2.6.

Changes in temperature were also analyzed for all the models as shown in Figure 5.4. Temperature changes vary from a minimum of 0.58, 0.69 and 0.67 degree Celsius to maximum of 1.52, 2.11 and 2.01 degree Celsius for 2020s, 2050s and 2080s, respectively. Medians of the temperature change are 0.90, 1.43 and 1.43 degree Celsius for the 2020s, 2050s and 2080s, respectively. MRI-CGCM3 was found to be the warmest and BCC-CSM1.1 was found to be the coolest scenario for RCP 2.6. Figure 5.4 shows the relative position of each scenario for 2020s, 2050s and 2080s.

ΔT C T_{rcp}-T_{base} **(5.2)**

Table 5.4: T C RCP

Model	**2020s**	**2050s**	**2080s**
BCC-CSM1.1	0.86	1.16	1.15
BCC-CSM1.1(m)	0.79	1.26	1.20
GISS-E2-H	1.26	1.61	1.66
GISS-E2-R	0.58	0.69	0.67
HadGEM2-ES	1.37	1.75	1.97
MIROC-ESM	0.94	1.63	1.90
MIROC-ESM-CHEM	1.52	2.11	2.01
MRI-CGCM3	0.70	0.88	1.15

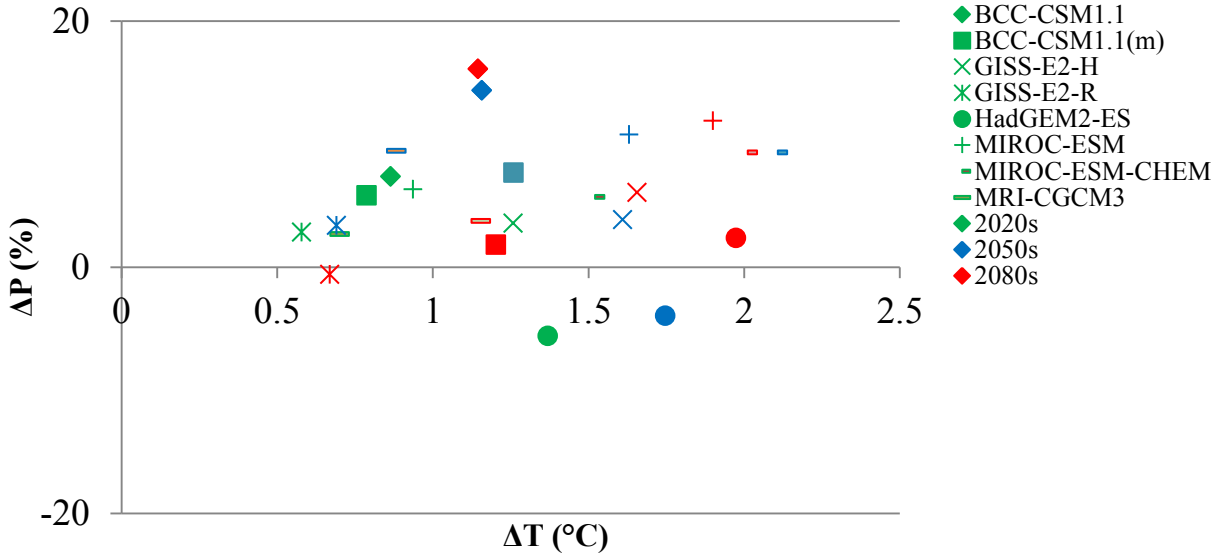

Figure 5.4: ΔT C ΔP(%) plot of all the models for RCP2.6

5.3.1.2 RCP 4.5

Similar to RCP2.6 all other RCP scenarios were also analyzed to determine temperature and precipitation change for eight GCMs. Results obtained for RCP4.5 are separated for three periods; viz. 2010-2039 (2020s), 2040-2069 (2050s) and 2070-2099 (2080s). Monthly precipitation/temperature data for each model was averaged and compared with the base period data (1971-2000). Table 5.5 shows the changes in precipitation (%) and temperature for 8 GCMs.

Table 5.5: Precipitation change (%) for RCP 4.5

Model	2020s	2050s	2080s
BCC-CSM1.1	13.08	17.57	15.91
BCC-CSM1.1(m)	2.46	7.27	8.34
GISS-E2-H	3.75	12.39	19.80
GISS-E2-R	8.00	5.47	9.56
HadGEM2-ES	-0.57	3.02	3.82
MIROC-ESM	-2.50	4.21	10.22
MIROC-ESM-CHEM	1.19	8.51	19.41
MRI-CGCM3	5.17	8.25	7.11

It is found that the precipitation changes (%) varied between -2.50% to 13.08%, 3.03% to 17.57% and 3.82% to 19.80% for 2020s, 2050s and 2080s respectively. Median values for these three periods are 3.11%, 7.76% and 8.89%. There is a great variation among the trends of precipitation change. Based on the % change in 2080s HadGEM2-ES projects the driest and GISS-E2-H projects the wettest scenario for the RCP 4.5.

T T C RCP

Model	2020s	2050s	2080s
BCC-CSM1.1	0.86	1.52	2.11
BCC-CSM1.1(m)	1.06	1.77	2.00
GISS-E2-H	1.51	2.49	2.95
GISS-E2-R	0.86	1.40	1.68
HadGEM2-ES	1.31	2.22	3.14
MIROC-ESM	1.25	2.08	2.97
MIROC-ESM-CHEM	1.11	2.17	3.18
MRI-CGCM3	0.80	1.48	2.08

Changes in temperature were also analyzed for all the models as shown in Table 5.6. Temperature changes vary from a minimum of 0.80, 1.40 and 1.68 degree Celsius to maximum of 1.51, 2.49 and 3.18 degree Celsius for 2020s, 2050s and 2080s respectively. Medians of the temperature changes are 1.08, 1.92 and 2.53degree celsius for 2020s, 2050s and 2080s respectively. Based on the temperature change in 2080s GISS-E2-R is the coolest and HAD-GEM2-ES is the warmest scenario for RCP 4.5.Figure 5.5 shows the relative position of each scenario for 2020s, 2050s and 2080s.

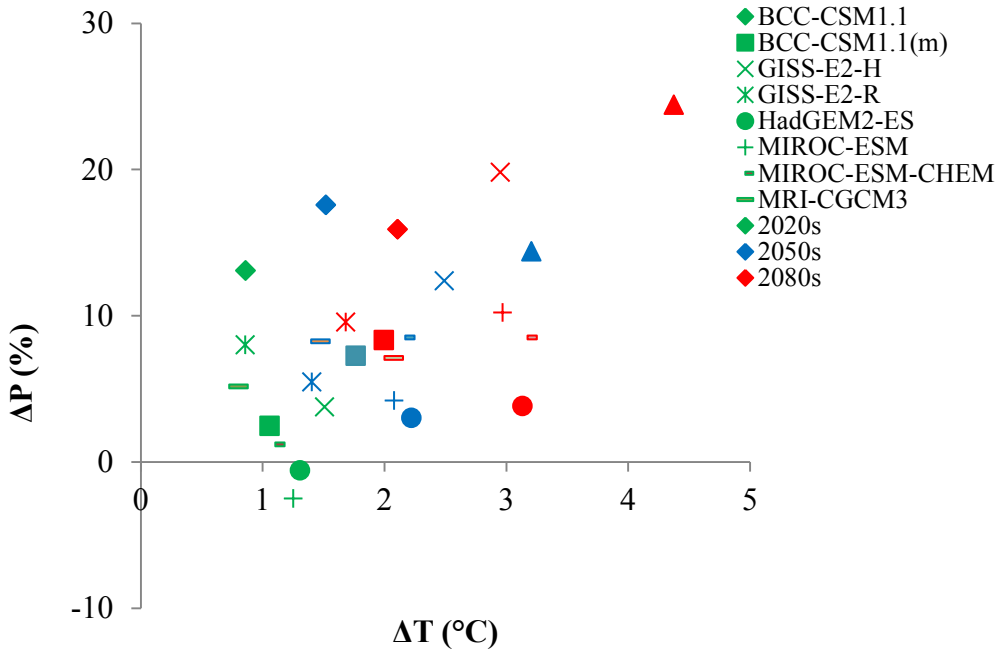

Figure 5.5: ΔT C ΔP(%) plot of all the models for RCP 4.5

5.3.1.3 RCP 6.0

Similar to RCP2.6 all other RCP scenarios were also analyzed to determine temperature and precipitation change for eight GCMs. Results obtained for RCP6.0 are separated for three periods; viz. 2010-2039 (2020s), 2040-2069 (2050s) and 2070-2099 (2080s). Monthly precipitation/temperature data for each model was averaged and compared with the base period data (1971-2000). Table 5.7 shows the changes in precipitation (%) and temperature for 8 GCMs.

Table 5.7: Precipitation change (%) for RCP 6.0

Model	2020s	2050s	2080s
BCC-CSM1.1	12.30	18.61	21.08
BCC-CSM1.1(m)	4.22	0.69	8.77
GISS-E2-H	1.63	4.17	10.00
GISS-E2-R	7.47	4.48	10.12
HadGEM2-ES	-0.56	-9.60	-1.00
MIROC-ESM	6.73	7.45	17.55
MIROC-ESM-CHEM	4.91	12.00	20.01
MRI-CGCM3	4.61	9.23	11.74

It is found that the precipitation changes (%) varied between -0.56% to 12.30%, -9.599% to 18.61% and -1.00% to 21.08% for 2020s, 2050s and 2080s respectively. Median values for these three periods are 4.76%, 5.96% and 10.93%. There is a great variation among the trends of precipitation change. Based on the % change in 2080s HadGEM2-ES projects the driest and BCC-CSM1.1 projects the wettest scenario for RCP 4.5.

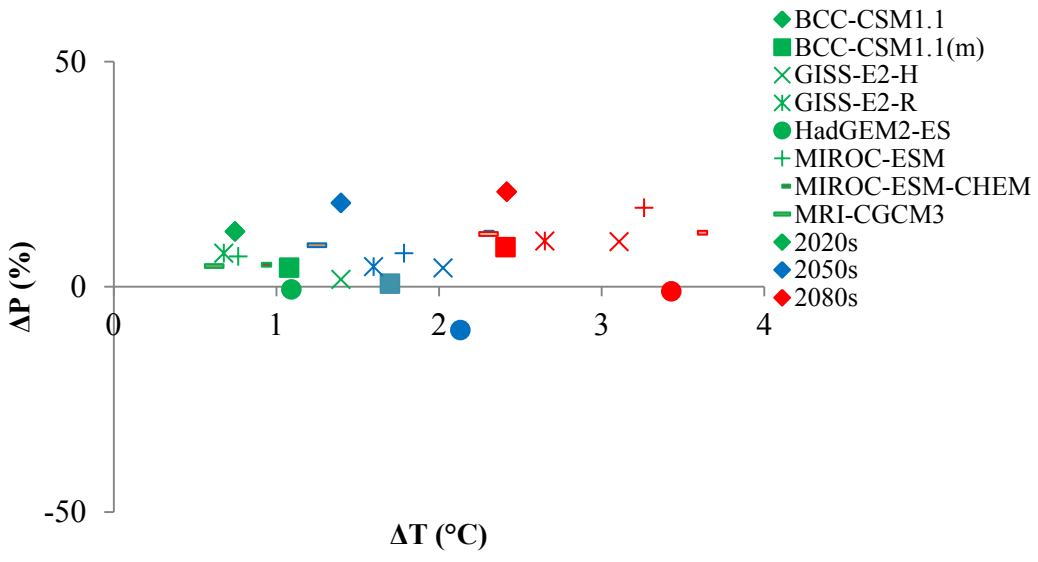

Figure 5.6: ΔT C ΔP(%) plot of all the models for RCP 6.0

Changes in temperature was also analyzed for all the models as shown in Table 5.8. Temperature changes vary from a minimum of 0.620, 1.251 and 2.306 degree Celsius to maximum of 1.40, 2.28 and 3.59 degree Celsius for 2020s, 2050s and 2080s

respectively. Median of the temperature changes are 0.84, 1.74 and 2.88 degree Celsius. Based on the temperature change in 2080s MRI-CGCM3 projects the coolest and MIROC-ESM-CHEM projects the warmest scenario for the RCP 6.0. Figure 5.6 shows the relative position of each scenario for 2020s, 2050s and 2080s.

Table 5.8 T C RCP

Model	2020s	2050s	2080s
BCC-CSM1.1	0.75	1.40	2.42
BCC-CSM1.1(m)	1.08	1.70	2.41
GISS-E2-H	1.40	2.03	3.11
GISS-E2-R	0.68	1.60	2.65
HadGEM2-ES	1.09	2.13	3.43
MIROC-ESM	0.77	1.79	3.26
MIROC-ESM-CHEM	0.91	2.28	3.59
MRI-CGCM3	0.62	1.25	2.31

5.3.1.4 RCP 8.5

RCP scenarios were analyzed to determine temperature and precipitation change for eight GCMs. Results obtained for RCP8.5 are separated for three periods; viz. 2010-2039 (2020s), 2040-2069 (2050s) and 2070-2099 (2080s). Monthly precipitation/temperature data for each model was averaged and compared with the base period data (1971-2000). Table 5.9 shows the changes in precipitation (%) and temperature for 8 GCMs.

Table 5.9: Precipitation change (%) for RCP 8.5

Model	2020s	2050s	2080s
BCC-CSM1.1	10.39	18.90	38.38
BCC-CSM1.1(m)	6.36	6.82	14.29
GISS-E2-H	10.38	10.18	22.96
GISS-E2-R	7.48	14.52	20.92
HadGEM2-ES	-6.67	-6.01	-2.16
MIROC-ESM	6.70	10.45	19.10
MIROC-ESM-CHEM	6.18	17.14	21.70
MRI-CGCM3	8.15	9.34	21.18

It is found that the precipitation changes (%) varied between -6.67% to 10.40%, 6.01% to 18.90% and -2.16% to 38.38% for 2020s, 2050s and 2080s respectively. Medians values for these three periods are 7.10%, 10.31% and 21.05%. There is a great variation among the trends of precipitation change. Based on the % change in 2080s HadGEM2-ES projects the driest and BCC-CSM1.1 projects the wettest scenario for RCP 8.5.

Changes in temperature was also analyzed for all the models. Temperature changes vary from a minimum of 0.76, 2.20 and 3.84 degree Celsius to maximum of 1.33, 3.33 and 5.96 degree Celsius for 2020s, 2050s and 2080s respectively. Medians of the temperature changes are 1.07, 2.44 and 3.92 degree celsius for the 2020s, 2050s and 2080s respectively. Based on the temperature change in 2080s GISS-E2-R is the coolest and MIROC-ESM-CHEM is the warmest model for RCP 8.5.Figure 5.7 shows the relative position of each scenario for 2020s, 2050s and 2080s.

Table 5.10 T C for RCP 8.5

Model	**2020s**	**2050s**	**2080s**
BCC-CSM1.1	1.03	2.21	3.92
BCC-CSM1.1(m)	1.06	2.36	3.88
GISS-E2-H	1.16	2.51	3.92
GISS-E2-R	1.07	2.28	3.84
HadGEM2-ES	1.33	3.02	5.04
MIROC-ESM	1.04	3.00	5.45
MIROC-ESM-CHEM	1.32	3.33	5.96
MRI-CGCM3	0.76	2.19	3.87

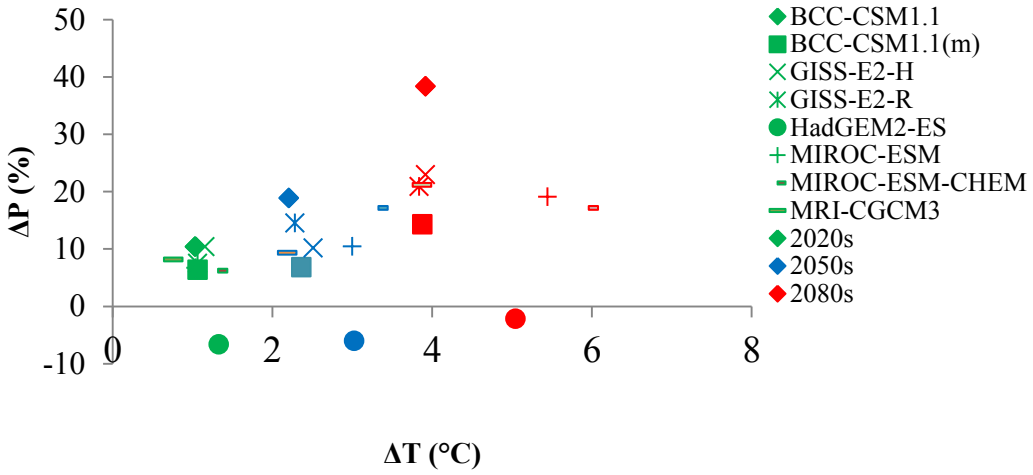

Figure 5.7: ΔT C ΔP(%) plot of all the models for RCP 8.5

5.3.2 Selection of Scenarios:

All the GCM results for 2080s were compared to obtain the warmest, coolest, driest, wettest, moderate warm and moderate wet scenarios for the BRB. Warmest and coolest scenarios are MIROC-ESM-CHEM RCP 8.5 and GISS-E2-R RCP 2.6 which gives the highest and lowest temperature change with respect to base period. On the other hand HadGEM2-ES RCP 8.5 and BCC-CSM1.1 RCP 8.5 are the driest and wettest scenarios based on the change in precipitation with respect to base period. Other two scenarios were selected from the median of changes of precipitation and temperature. GISS-E2-H RCP 4.5 is having a temperature change closest to median value of temperature change whereas MRI-CGCM3 RCP 6 shows precipitation change close to the median value of precipitation change. Fine resolutiontemperature and precipitation projection forthese scenarios will further be generated using pattern scaling which will be used to assess the impact of climate change in BRB.

Table 5.11: Selected scenarios from the analysis of precipitation and temperature change of all the scenarios

ΔP	Max	38.37762	BCC-CSM1.1	RCP 8.5	
ΔP	Min	-2.15689	HadGEM2-ES	RCP 8.5	
ΔP	Median	11.81264	MRI-CGCM3	RCP 6	Close to Median Value
ΔT	Max	5.961434	MIROC-ESM-CHEM	RCP 8.5	
ΔT	Min	0.669602	GISS-E2-R	RCP 2.6	
ΔT	Median	2.802164	GISS-E2-H	RCP 4.5	Close to Median Value

5.4 Sensitivity Analysis

The changes in streamflow under the impact of climate change was investigated by using several hypothetical scenarios (synthetic approach) applied to the climate normal (1981–2010) meteorological data. Incremental climate change scenarios were applied with a hypothetical temperature increase (0, +2 °C , +4 °C and +6 °C) and a

– – 3

examine the change of the SWAT simulated streamflow. Model results (monthly and annual flow) at Bahadurabad station for all these scenarios are given in Appendix B. From the analysis of GCM precipitation it is found that the magnitude at the end of 21st century (2080s) varies between -10% to +40%. So, a detailed analysis of ΔT

C and ΔP -10% to +40% (10% increment) for impact of flow on BRB at Bahadurabad station is presented in this section.

Table 5.12: Mean annual discharge (m^3/s) due to the changes in temperature and precipitation

		ΔP -10%	ΔP	ΔP	ΔP	ΔP 3	ΔP
ΔT	°C	17456	20206	22969	25737	28510	31279
ΔT	°C	16972	19722	22482	25247	28016	30782
ΔT	°C	16413	19157	21911	24673	27439	30205
ΔT	°C	15870	18597	21340	24092	26852	29614

Table 5.13: Changes in mean annual discharge (%) due to the changes in temperature and precipitation

		ΔP -10%	ΔP	ΔP	ΔP	ΔP 3	ΔP
ΔT	°C	-13.61	0.00	13.67	27.37	41.10	54.80
ΔT	°C	-16.01	-2.40	11.26	24.95	38.65	52.34
ΔT	°C	-18.77	-5.19	8.44	22.11	35.80	49.49
ΔT	°C	-21.46	-7.96	5.61	19.23	32.89	46.56

Table 5.14: Mean dry season (Jan-May) discharge (m^3/s) due to the changes in temperature and precipitation

		ΔP -10%	ΔP	ΔP	ΔP	ΔP 3	ΔP
ΔT	°C	7157	8330	9525	10732	11954	13190
ΔT	°C	6908	8079	9269	10474	11694	12926
ΔT	°C	6548	7739	8950	10182	11426	12682
ΔT	°C	6145	7326	8537	9777	11039	12318

Table 5.15: Changes in mean dry season (Jan-May) discharge (%) due to the changes in temperature and precipitation

		ΔP -10%	ΔP	ΔP	ΔP	ΔP 3	ΔP
ΔT	°C	-14.08	0.00	14.35	28.84	43.51	58.34
ΔT	°C	-17.07	-3.01	11.27	25.74	40.38	55.17
ΔT	°C	-21.39	-7.09	7.44	22.23	37.17	52.24
ΔT	°C	-26.23	-12.05	2.48	17.37	32.52	47.88

Table 5.16: Mean wet season (June-December) discharge (m^3/s) due to the changes in temperature and precipitation

	ΔP -10%	ΔP	ΔP	ΔP	ΔP 3	ΔP
24813	28689	32572	36455	40336	44199	24813
24161	28039	31920	35800	39674	43536	24161
23460	27313	31169	35023	38877	42722	23460
22816	26648	30484	34316	38147	41968	22816

Table 5.17: Changes in mean wet season (June-December) discharge (%) due to the changes in temperature and precipitation

		ΔP -10%	ΔP	ΔP	ΔP	ΔP 3	ΔP
ΔT	°C	-13.51	0.00	13.53	27.07	40.60	54.06
ΔT	°C	-15.78	-2.27	11.26	24.79	38.29	51.75
ΔT	°C	-18.23	-4.80	8.64	22.08	35.51	48.91
ΔT	°C	-20.47	-7.11	6.26	19.61	32.97	46.29

5.4.1 Sensitivity to Precipitation Change:

For the BRB changes in average annual streamflow due to the changes in precipitation, while keeping the temperature constant are shown in Figure 5.8. Various precipitation scenarios are analyzed which include -10%, 0%, 10%, 20%, 30% and 40% changes with respect to the base period of 1981-2010. As a first approximation, a linear regression analysis of the streamflow responses for the various scenarios indicated that a 10 % change in precipitation would produce a 13.6 % change in streamflow for Brahmaputra river basin. Table 5.12 and Figure 5.8 shows that the BRB is almost equally sensitive to a reduction and increase in precipitation and the ‘ sensitive to the precipitation

changes.Table 5.14, Table 5.16 and Table 5.18 shows the annual, dry period and wet period discharge (m^3/s) consecutively for various combinations of temperature and precipitation changes. Percentage changes of discharge for annual, dry and wet period is presented in Table 5.15, Table 5.17 and Table 5.19. Mean monthly discharge for variable precipitation while keeping temperature fixed is shown in Figure 5.9. It is observed that the peak discharge is found in July in almost all cases. Changes in monthly mean discharge is shown in Figure 5.10.

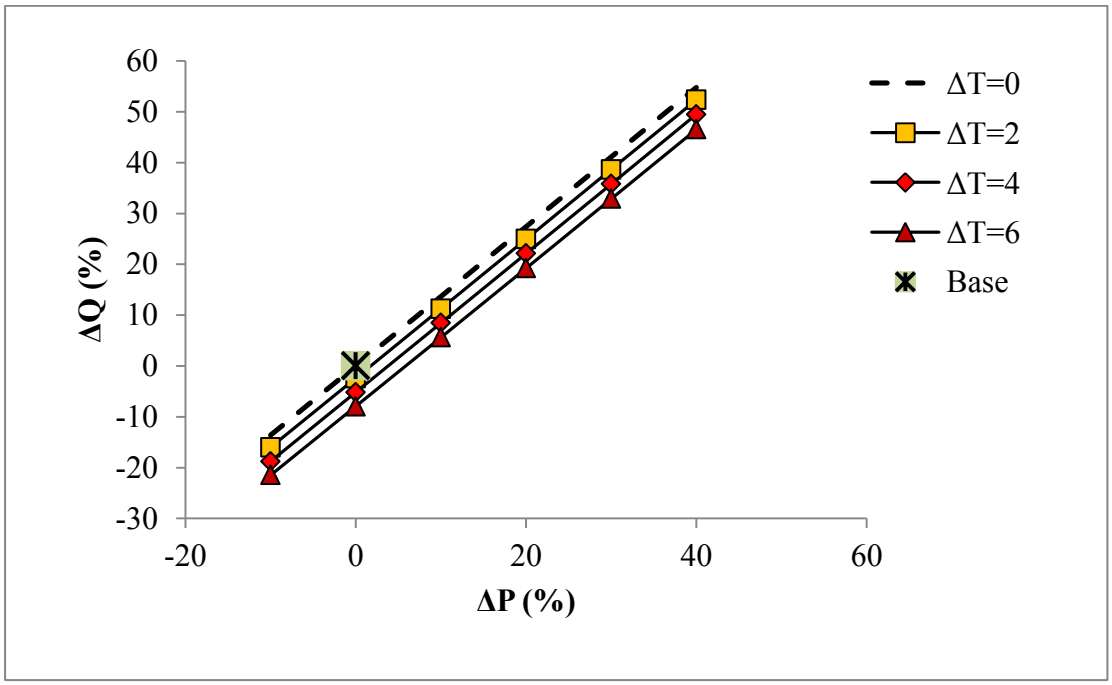

Figure 5.8: Changes in annual mean streamflow (%) at Bahadurabad station dueto changing ΔP (%).

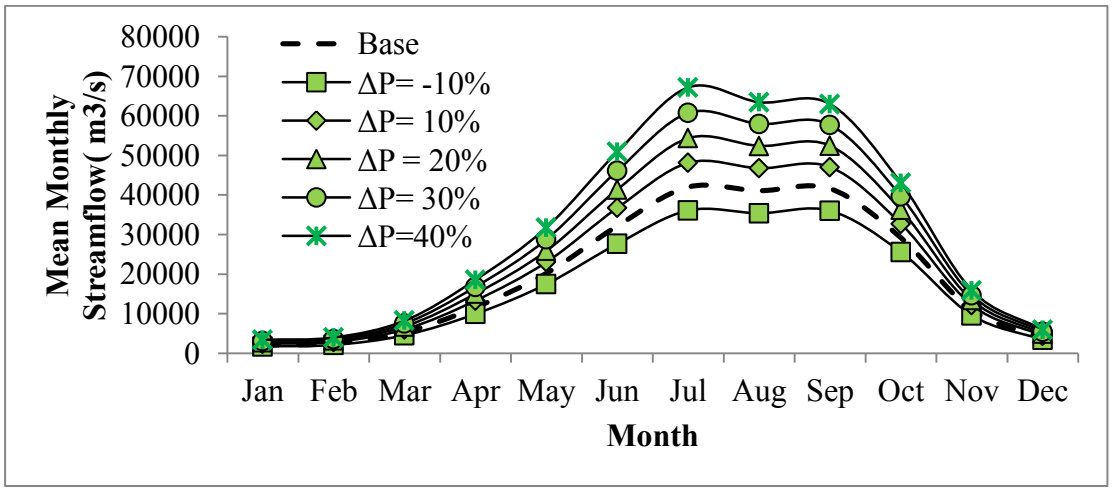

Figure 5.9: Mean monthly streamflow at Bahadurabad station due to ΔT C ΔP=-10% to +40% (10% increment)

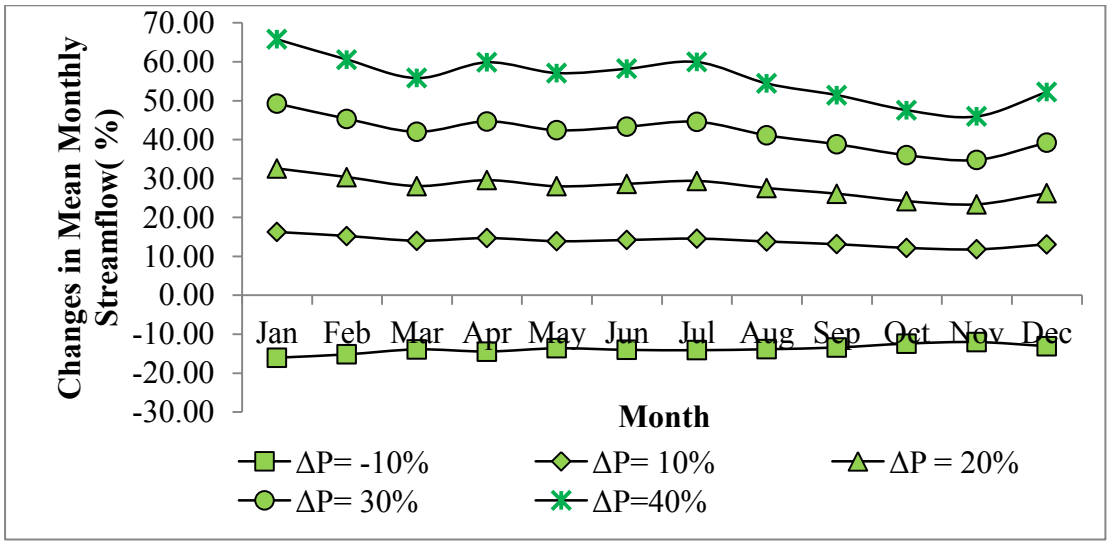

Figure 5.10: Changes in mean monthly streamflow (%) at Bahadurabad station due to ΔT C ΔP=-10% to +40% (10% increment)

5.4.2 Sensitivity to Temperature Change:

The relative sensitivity of streamflow due to the changes in temperature, while keeping the precipitation unchange was assessed for BRB at Bahadurabad station. The relative sensitivity of streamflow to the changes in temperature, while keeping the precipitation unchanged, gives a moderate changes in streamflow as compare to the changes due to precipitation for the basin (Figure 5.11). A linear regression analysis of the streamflow responses for the vario

C 33

for BRB . The sensitivity was found linear. Table 5.14, Table 5.16 and Table 5.18 shows the annual, dry period and wet period discharge (m^3/s) consecutively for various combination of temperature and precipitation change. Percentage change of discharge for annual, dry and wet period is presented in Table 5.15, Table 5.17 and Table 5.19. Mean monthly discharge for variable temperature holding precipitation fixed is shown in Figure 5.12. It is observed that the peak discharge is found in July and September. Changes in monthly mean discharge is shown in Figure 5.13. Discharge is found to decrease in all cases due to evaporation all over the basin.However, monthly discharge in November-March projected to be increased because of enhanced snowmelt due to increase in temperature.

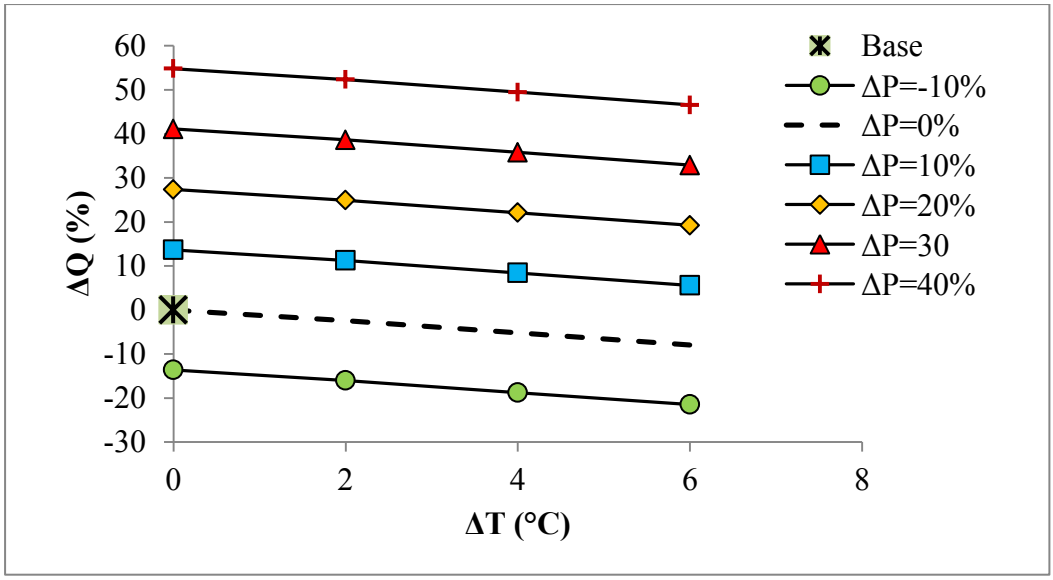

Figure 5.11: Changes in ΔQ (%) at Bahadurabad station due to changing ΔT C

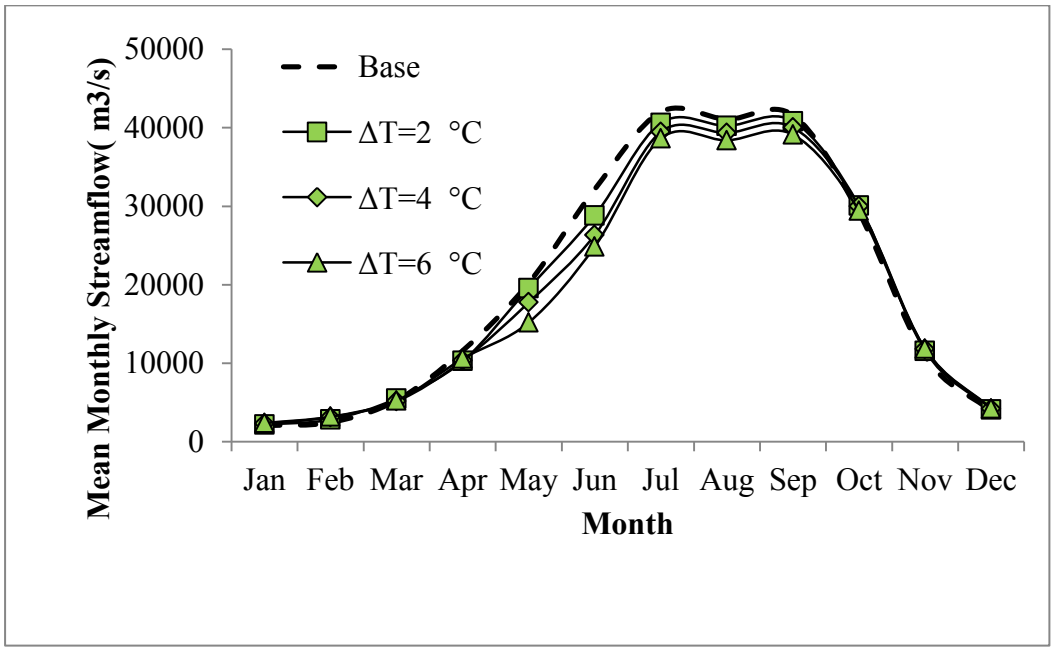

Figure 5.12: Mean monthly streamflow (m^3/s) at Bahadurabad station due to ΔP=0% and ΔT C

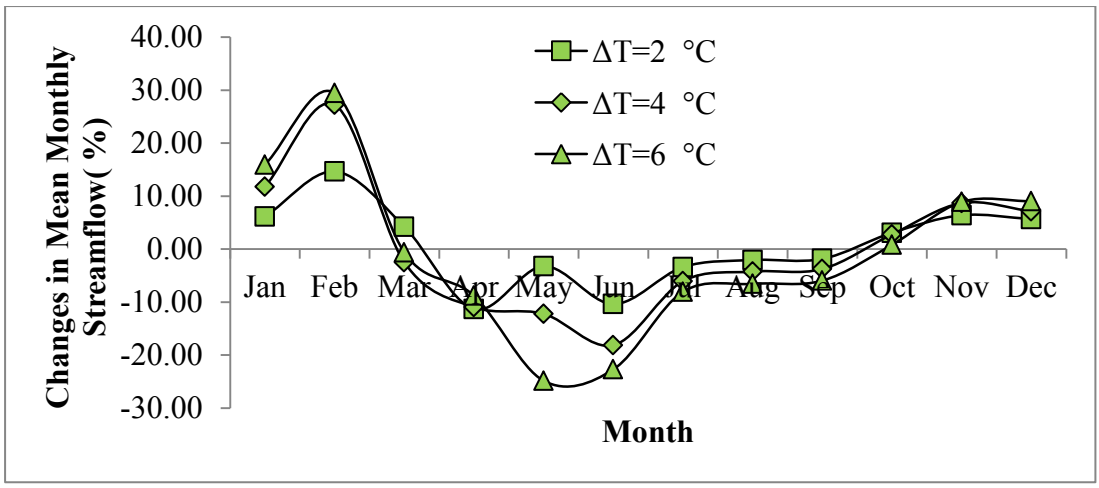

Figure 5.13: Changes in mean monthly streamflow (%) at Bahadurabad station due to ΔP=0% and ΔT C

5.4.3 Sensitivity to the Combined Effect of Temperature and Precipitation

Sensitivity of the flow when both temperature and precipitation changes are taken into account is analyzed. Combination of 0°, 2°, 4° and 6°C temperature change with – 3

the changes in flow. Figure 5.14 shows that the change in slope of ΔQ vs ΔP is very much small and no rapid increase or decrease in the flow has been found for precipitation change holding temperature fixed (holds true vice versa as shown in Figure 5.15). Average ΔQ vs ΔP is around 1.36 and which slightly increases upto 30% ΔP. ΔQ vs ΔP as shown in Figure 5.15 shows a decreasing trend with increasing ΔT upto 4 °C, above which it becomes almost horizontal.

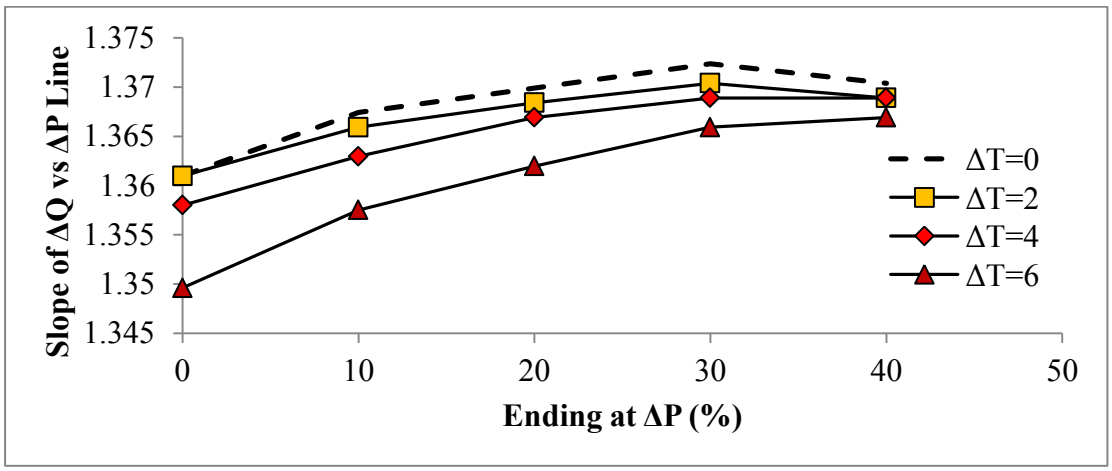

Figure 5.14: Changes in ΔQ vs ΔP at Bahadurabad station due to changing ΔP and ΔT

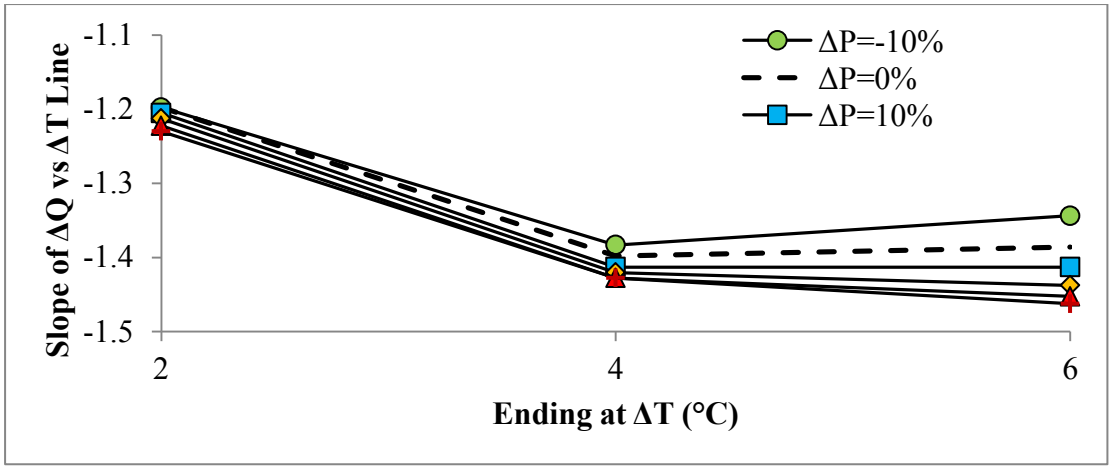

Figure 5.15: Changes in ΔQ vs ΔT at Bahadurabad station due to changing ΔT C

5.5 Spatial Distribution of High Resolution Climate Data

High resolution precipitation and maximum, minimum temperature data obtained through patterns scaling were used as input for assessment of future flow of Brahmaputra river basin. Spatial distribution of temperature and precipitation were plotted for each of the scenarios and time periods (2020s, 2050s and 2080s). Figure 5.16-5.18 shows the spatial distribution of precipitation and maximum, minimum temperature for base period (MarkSim base period: 1961-2005). Spatial distribution of precipitation and temperature for each of the six selected scenarios were also determined for 2020s, 2050s and 2080s. Figure 5.16-5.18 are samples of distribution, all other distributions are shown in Appendix E.

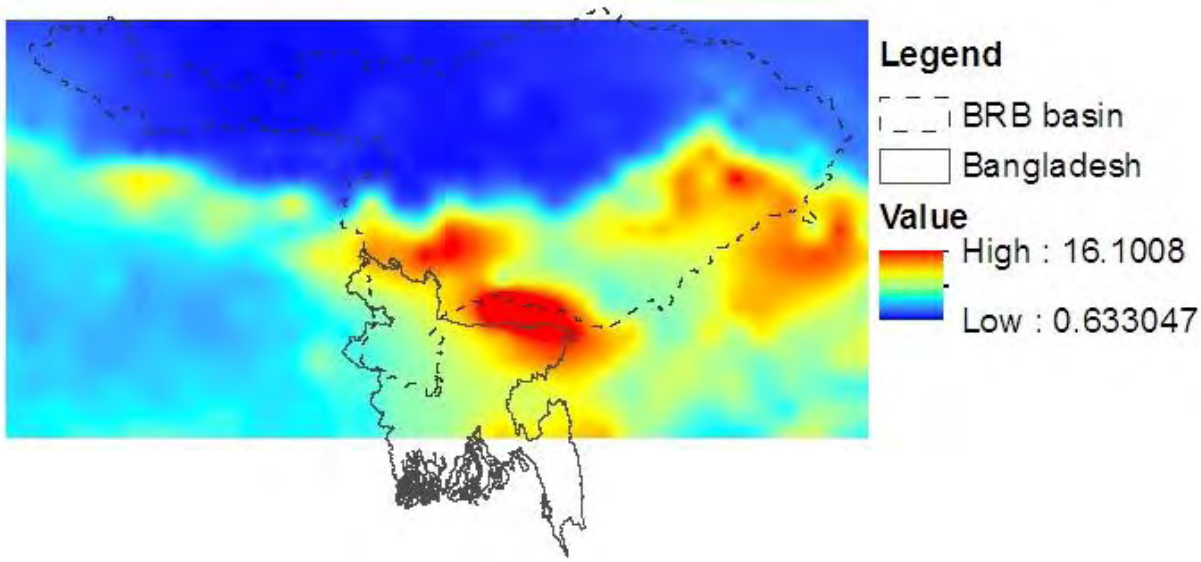

Figure 5.16: Spatial distribution of precipitation for base period

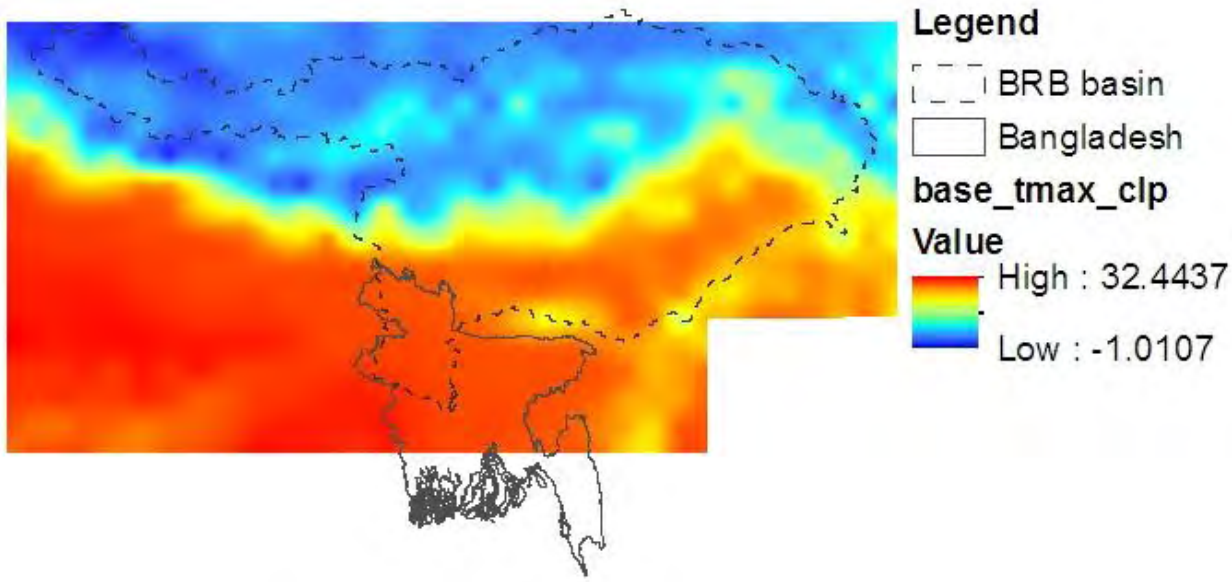

Figure 5.17: Spatial distribution of maximum temperature for base period

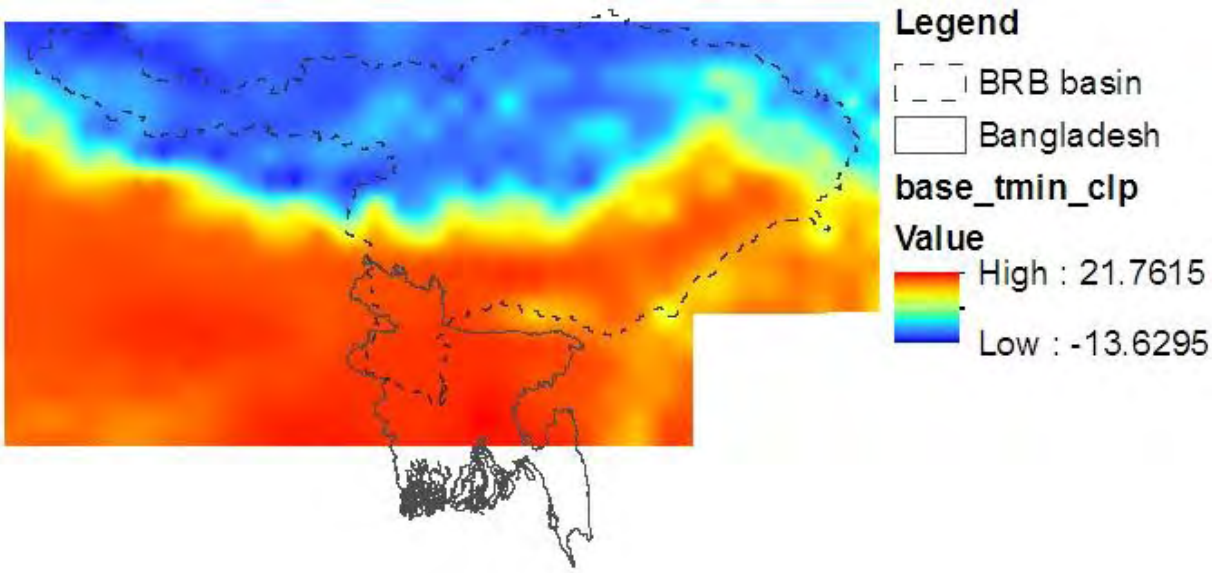

Figure 5.18: Spatial distribution of minimum temperature for base period

5.6 Climate Change Impact on Flow of BRB

Compared to the climate normal, the average annual temperature of the BRB is projected to increase by 0.58-1.51°C, 0.69-3.33°C, and 0.67-5.96°C in 2020s, 2050s, and 2080s, respectively while precipitation is projected to change between -6.67% to 10.39 % by 2020s, -6.01% to 18.90% by 2050s, and -2.6% to 38.38 % by 2080s, respectively. In response to these projected changes to the primary climatic factors, SWAT simulated the mean annual streamflow for six projected

climate change scenarios which are warmest(MIROC-ESM-CHEM RCP 8.5), coolest (GISS-E2-R RCP 2.6), driest (HadGEM2-ES RCP 8.5), wettest (BCC-CSM1.1 RCP 8.5), moderate warm (GISS-E2-H RCP 4.5) and moderate wet (MRI-CGCM3 RCP 6) for 2020s, 2050s, and 2080s, with respect to that of the climate normal were analyzed. It was found that the discharge of BRB is increasing in all of the cases over the 21st century. The enhanced precipitation usually causes an increase in discharge while the enhanced temperature causes decrease in discharge by increasing evaporative losses. It was revealed that for BRB increased discharge due to enhanced precipitation offset the decreased discharge due to enhanced evaporation.

Figure 5.19-5.21 shows monthly mean discharge hydrograph at Bahadurabad station for 2020s, 2050s and 2080s. It is observed that flow hydrographs has a rising trend from 2020s to 2080s, though the flow from December to February decreases for the future scenarios. Monthly range of discharge is lower in 2020s, which increases towards 2080s. From Figure 5.20-21 it is observed that the variability tend to increase between March to May. Flow hydrograph is quite stable during the recession period (Sep-Dec). Almost all the models are seem to give decreased flow during recession for all the periods.

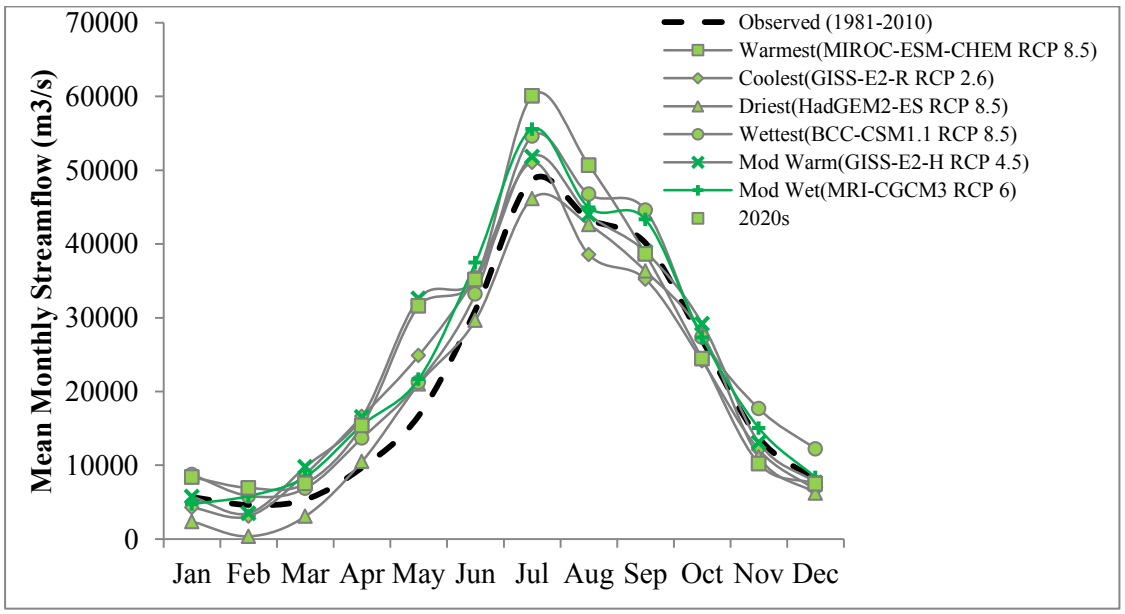

Figure 5.19: Mean monthly discharge (m^3/s) for 2020s at Bahadurabad station for Brahmaputra river basin

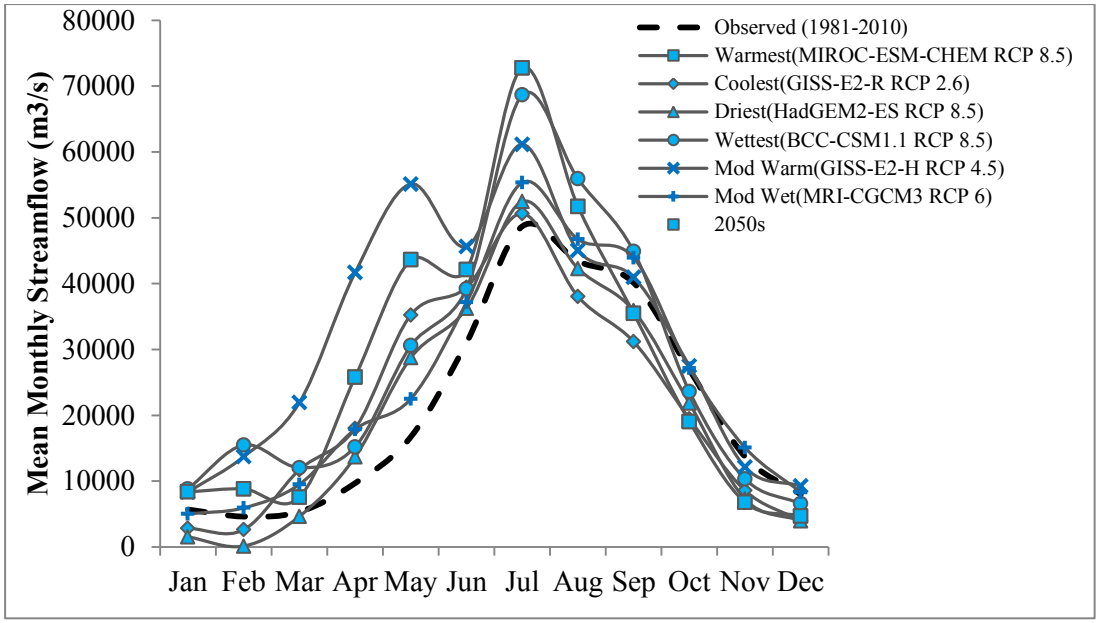

Figure 5.20: Mean monthly discharge (m^3/s) for 2050s at Bahadurabad station for Brahmaputra river basin

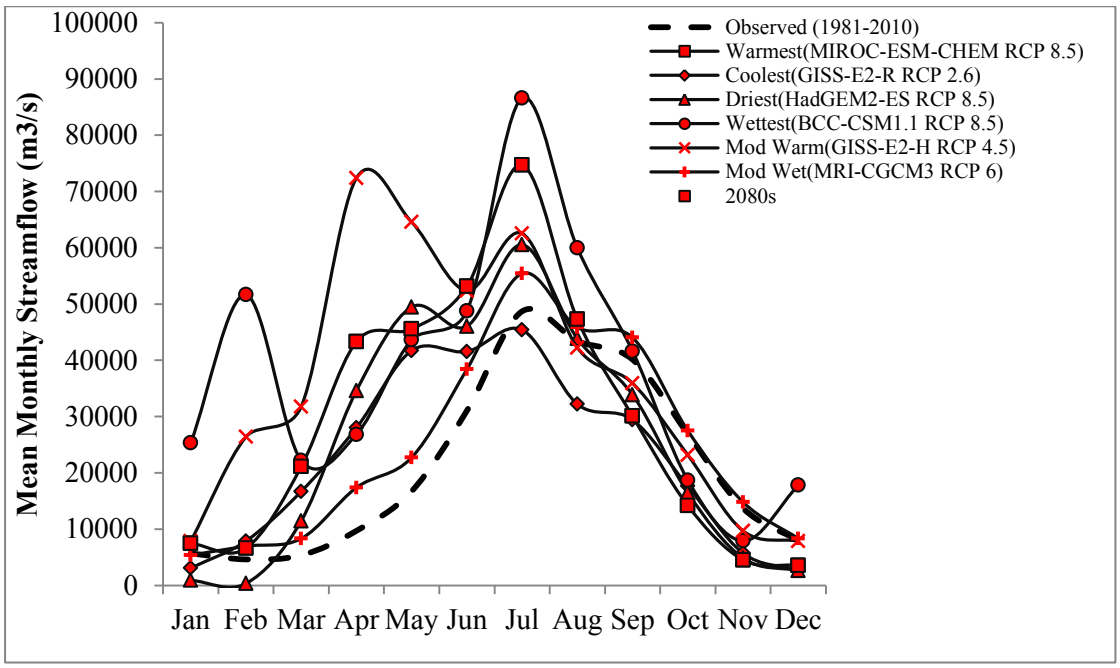

Figure 5.21: Mean monthly discharge (m^3/s) for 2080s at Bahadurabad station for Brahmaputra river basin

5.6.1 Mean Annual Stream Flow Analysis

The model simulated percentage changes in the mean annual streamflow from the climate normal (1981-2010) with respect to climate change scenarios. Figure 5.22-5.24 shows boxplots of differences in the mean annual average streamflow simulated by the model for warmest, coolest, driest, wettest, moderate warm

andmoderate wet with respect to the climate normal. A gradual increase in annual average flow is found from 2020s to 2080s. The range of 75th and 25th percentile is grows from 2020s to 2080s which indicates that uncertainty associated with the projected streamflow of BRB increases as we go distant future.The mean dry season streamflow increase is found to be gradual from 2020s to 2080s, the rate of increase enhanced from 2050s to 2080s. Similar to the mean annual streamflow, the range of variability is higher for the 2080s compared to the early 21st century. Mean wet season flow showed slight increasing pattern in 2020s to 2050s which then decreased from 2050s to 2080s. The range between 75th and 25th percentile is relatively small for 2080s, though the highest and the lowest value is having long range of variation.

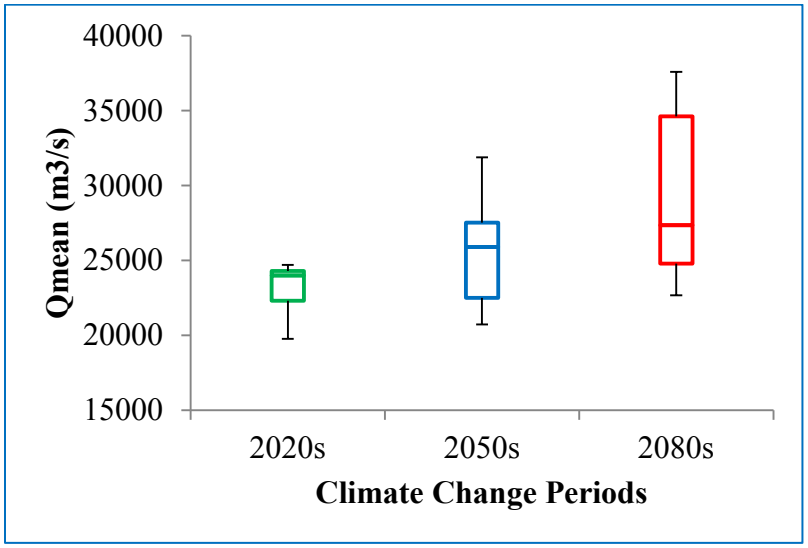

Figure 5.22: Box-plot of mean annual discharge (m^3/s) of all the scenarios for 2020s, 2050s and 2080s

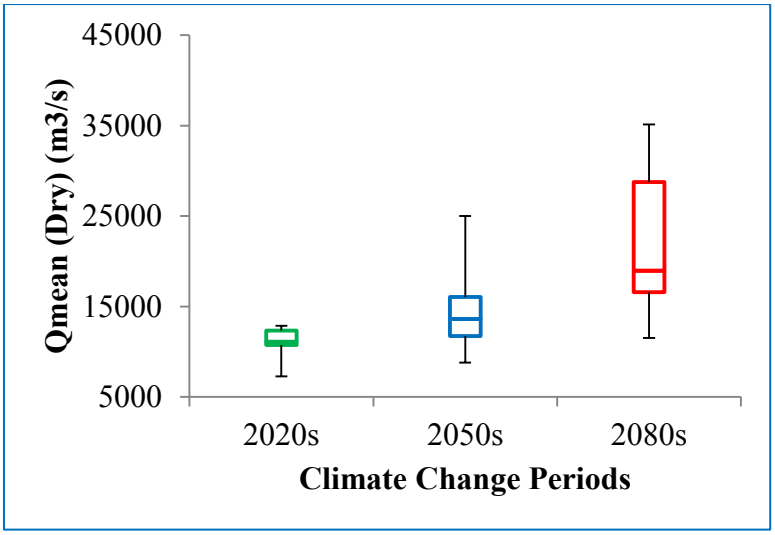

Figure 5.23: Box-plot of mean dry period discharge (m^3/s) of all the scenarios for 2020s, 2050sand 2080s

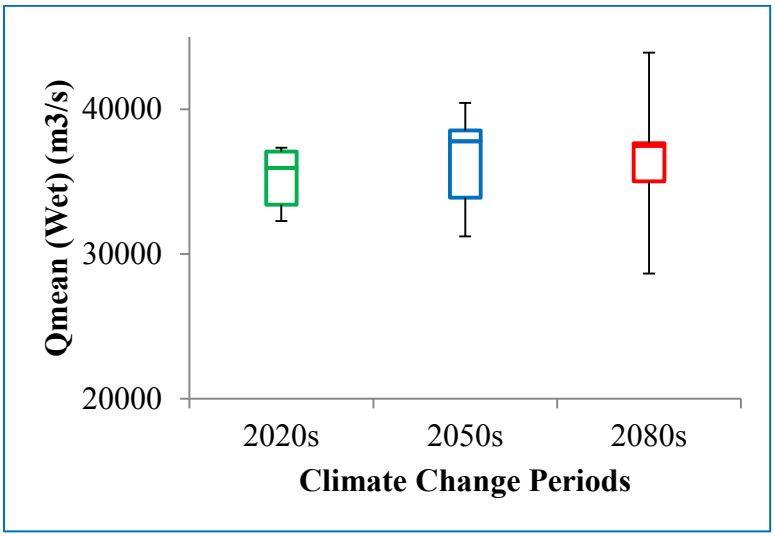

Figure 5.24: Box-plot of mean wet period discharge (m^3/s) of all the six scenarios for 2020s, 2050sand 2080s

5.6.1.1 Changes in Streamflow in 2020s

5.6.1.1.1 Mean Annual flow analysis for 2020s

In 2020s, mean annual streamflow is found to increase in all the scenarios other than the driest one (Had-Gem2-ES) as shown in Table 5.18. The maximum projected increase in discharge of 15.02% was found for MIROC-ESM-CHEM (RCP 8.5), whereas HADGEM2-ES (RCP 8.5) was found to give the maximum projected decrease in discharge with -3.29% changes compared to the base flow. Coolest scenario gave slight increase of 0.80% in mean annual discharge. All the other

scenarios showed increase in projected annual discharges which were very close in percentage change, viz. 11.04%, 10.18% and 11.70% for wettest, moderate warm and moderate wet scenarios.

5.6.1.1.2 Dry Period Flow Analysis for 2020s

Mean dry season (Dec-May) flow was found to increase for all the scenarios in 2020s (Table 5.18). Maximum projected increase in discharge was found for GISS-E2-H (RCP 4.5) with 80.09% change and the minimum projected increase was 12.42% which was given obtained for HADGEM2-ES (RCP 8.5). MIROC-ESM-CHEM (RCP 8.5) gave relatively high increase in discharge with 73.99% change. All other scenarios, viz. GISS-E2-R (RCP 2.6), BCC-CSM1.1 (RCP 8.5) and MRI-CGCM3 (RCP 6.0) gave an increased projected discharge with 46.13%, 31.37% and 33.35% consecutively.

Table 5.18: Change in Discharge (%) for all the six scenarios in 2020s

	Warmest (MIROC-ESM-CHEM RCP 8.5)	**Coolest (GISS-E2-R RCP 2.6)**	**Driest (HadGEM2-ES RCP 8.5)**	**Wettest (BCC-CSM1.1 RCP 8.5)**	**Mod Warm (GISS-E2-H RCP 4.5)**	**Mod Wet (MRI-CGCM3 RCP 6)**
Mean Annual	15.02	0.80	-3.29	11.04	10.18	11.70
Mean Dry Season (Jan-May)	73.99	46.13	12.42	31.37	80.09	33.35
Mean Wet Season (June-December)	10.03	-3.04	-4.62	9.32	4.26	9.87

5.6.1.1.3 Wet Period Flow Analysis for 2020s

In 2020s, mean wet season (Jun-Nov) flow was found to increase for almost all the scenarios (Table 5.18). Highest increase in projected flow was found for MIROC-ESM-CHEM (RCP 8.5) with 10.03% change. BCC-CSM1.1 (RCP 8.5) and MRI-CGCM3 (RCP 6.0) also gave high increase in flow with 9.32% and 9.87% consecutively. Highest decrease in discharge was found for the driest scenario HADGEM2-ES (RCP 8.5) with -4.62% change. GISS-E2-R (RCP 2.6) also projects a decreasing flow with -3.04% changes. The moderate warm scenario GISS-E2-H (RCP 4.5) gave slight increase in flow with 4.26% change compared to the base flow.

5.6.1.2 Changes in Streamflow in 2050s

5.6.1.2.1 Mean annual flow analysis for 2050s

In 2050s, mean annual streamflow is found to increase in all the scenarios (Table 5.19). The maximum projected increase in discharge of 32.46% was found for GISS-E2-H (RCP 4.5), whereas GISS-E2-R (RCP 2.6) was found to give the minimum projected increase in discharge with 1.80% change compared to the base flow. Driest scenario gave slight increase of 2.78% in mean annual discharge. MIROC-ESM-CHEM (RCP 8.5) and BCC-CSM1.1 (RCP 8.5) showed almost same increase in projected annual discharges which are 26.89% and 26.27% consecutively. MRI-CGCM3 (RCP 6.0) gave medium change of 13.38% compared to the base period flow.

5.6.1.2.2 Dry Period Flow Analysis for 2050s

Mean dry season (Dec-May) flow was found to increase for all the scenarios in 2050s(Table 5.19). Maximum projected increase in discharge was found for GISS-E2-H (RCP 4.5) with 232.49% change and the minimum projected increase was 41.93% which was given obtained for MRI-CGCM3 (RCP 6.0). MIROC-ESM-CHEM (RCP 8.5) gave relatively high increase in discharge with 139.26% change. All other scenarios, viz. GISS-E2-R (RCP 2.6), BCC-CSM1.1 (RCP 8.5) and HADGEM2-ES (RCP 8.5) gave an increased projected discharge with 91.17%, 77.16% and 48.82% consecutively.

5.6.1.2.3 Wet Period Flow Analysis for 2050s

In 2050s, mean wet season (Jun-Nov) flow was found to increase for almost all the scenarios (Table 5.19). Highest increase in projected flow was found for BCC-CSM1.1 (RCP 8.5) with 22.63% change. MIROC-ESM-CHEM (RCP 8.5) and GISS-E2-H (RCP 4.5) also gave high increase in flow with 16.71% and 15.52% consecutively. Highest decrease in discharge was found for the GISS-E2-R (RCP 2.6) with -5.76% change. HADGEM2-ES (RCP 8.5) also projects a decreasing flow with -1.12% change. The remaining scenario, viz. moderate wet scenario MRI-CGCM3 (RCP 6.0) gave increase in flow with 10.96% change compared to the base flow.

Table 5.19: Change in Discharge (%) for all the six scenarios in 2050s

	Warmest (MIROC-ESM-CHEM RCP 8.5)	Coolest (GISS-E2-R RCP 2.6)	Driest (HadGEM2-ES RCP 8.5)	Wettest (BCC-CSM1.1 RCP 8.5)	Mod Warm (GISS-E2-H RCP 4.5)	Mod Wet (MRI-CGCM3 RCP 6)
Mean Annual	26.27	1.80	2.78	26.89	32.46	13.38
Mean Dry Season (Jan-May)	139.26	91.17	48.82	77.16	232.49	41.93
Mean Wet Season (June-December)	16.71	-5.76	-1.12	22.63	15.53	10.96

5.6.1.3 Changes in Streamflow in 2080s

5.6.1.3.1 Mean Annual Flow Analysis for 2080s

In 2080s, mean annual streamflow is found to increase compared to the mean base flow in all the scenarios other than the coolest one (GISS-E2-R RCP 2.6)as shown in Table 5.20. The maximum projected increase in discharge of 47.44% was found for BCC-CSM1.1 (RCP 8.5), whereas GISS-E2-R (RCP 2.6) was found to give the maximum projected decrease in discharge with -0.91% change compared to the base flow. Other scenarios gave variable increase indischarge, 29.50%, 18.96%, 38.82% and 13.60% increase in mean annual streamflow were found for MIROC-ESM-CHEM (RCP 8.5), HADGEM2-ES (RCP 8.5), GISS-E2-H (RCP 4.5) and MRI-CGCM3 (RCP 6.0).

5.6.1.3.2 Dry Period Flow Analysis for 2080s

Mean dry season (Dec-May) flow was found to increase for all the scenarios in 2080s (Table 5.20). Maximum projected increase in discharge was found for GISS-E2-H (RCP 4.5) with 335.54% change and the minimum projected increase was 41.35% which was given obtained for MRI-CGCM3 (RCP 6.0). All other scenarios, viz. MIROC-ESM-CHEM (RCP 8.5), GISS-E2-R (RCP 2.6), HADGEM2-ES (RCP 8.5) and BCC-CSM1.1 (RCP 8.5) gave an increased projected discharge with 187.03%, 140.37%, 173.80% and 189.48% consecutively.

5.6.1.3.3 Wet Period Flow Analysis for 2080s

In 2080s, mean wet season (Jun-Nov) flow was found to increase for all the scenarios except GISS-E2-R (RCP 2.6) which gave -12.86% change in mean wet period flow (Table 5.20). Highest increase in projected flow was found for BCC-CSM1.1 (RCP

8.5) with 35.42% change. MIROC-ESM-CHEM (RCP 8.5), GISS-E2-H (RCP 4.5) and MRI-CGCM3 (RCP 6.0) gave high increase in flow with 16.17%, 13.71% and 11.25% consecutively. Highest decrease in discharge was found for the GISS-E2-R (RCP 2.6) with -12.86% change. HADGEM2-ES (RCP 8.5) also projects a small increase in flow with 5.86% change.

Table 5.20: Changes in Discharge (%) for all the six scenarios in 2080s

	Warmest (MIROC-ESM-CHEM RCP 8.5)	**Coolest (GISS-E2-R RCP 2.6)**	**Driest (HadGEM2-ES RCP 8.5)**	**Wettest (BCC-CSM1.1 RCP 8.5)**	**Mod Warm (GISS-E2-H RCP 4.5)**	**Mod Wet (MRI-CGCM3 RCP 6)**
Mean Annual	29.50	-0.91	18.96	47.44	38.82	13.60
Mean Dry Season (Jan-May)	187.03	140.37	173.80	189.48	335.54	41.35
Mean Wet Season (June-December)	16.17	-12.86	5.86	35.42	13.71	11.25

For better understanding of the relative changes in mean annual, mean dry period and mean wet period discharge, scatter plot of changes in discharge (%) for both changes C) and precipitation (%) is shownin Figure 5.25-5.30.

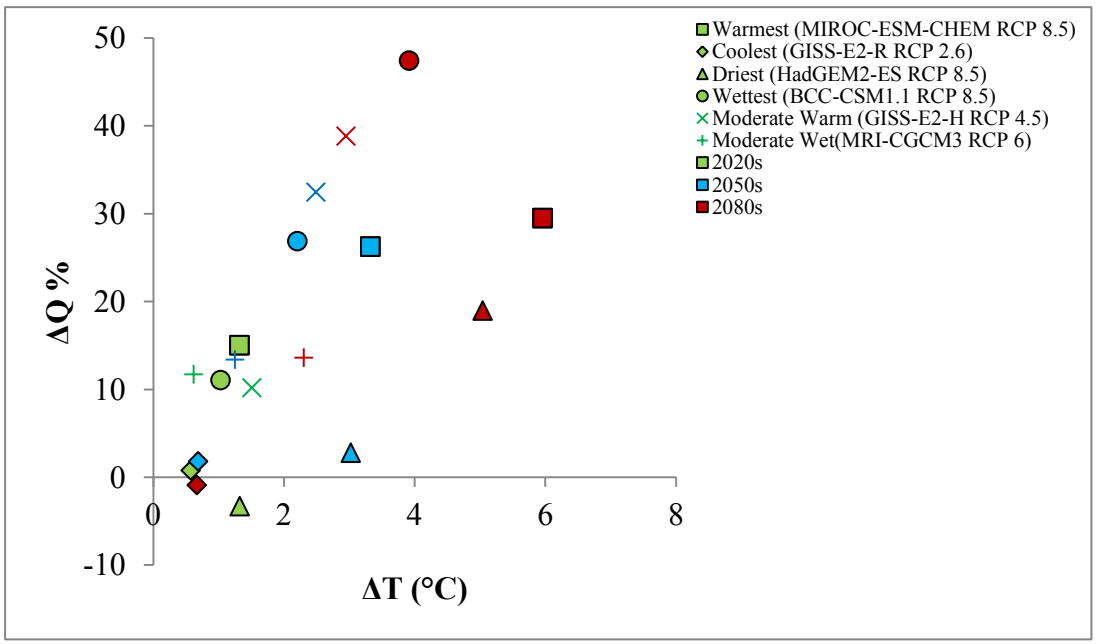

Figure 5.25: ΔT C
2020s, 2050s and 2080s

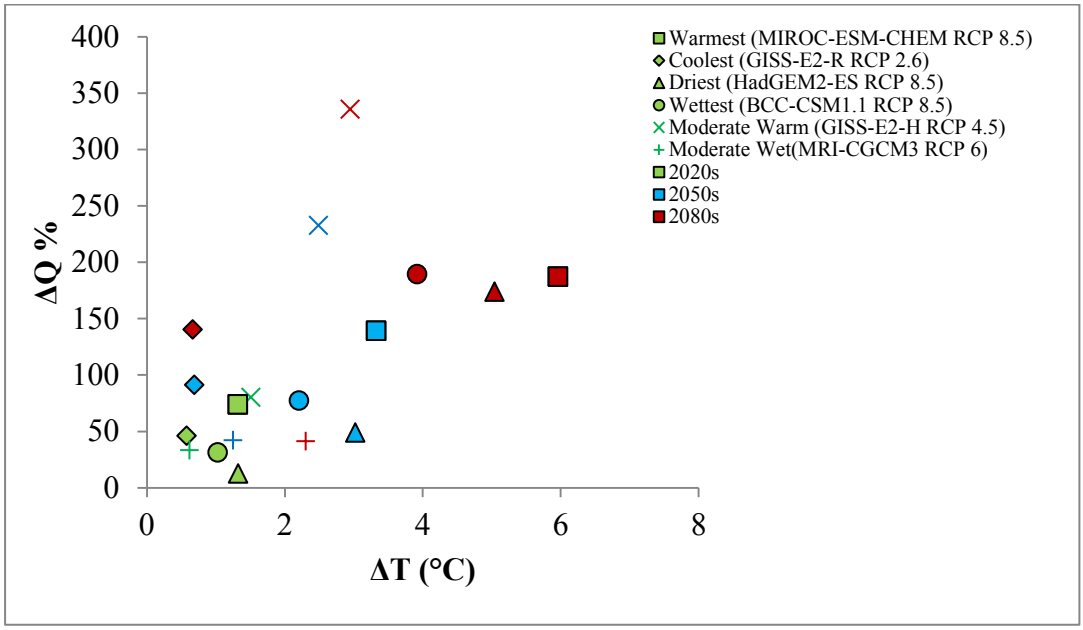

Figure 5.26 ΔT C
scenariosfor 2020s, 2050s and 2080s

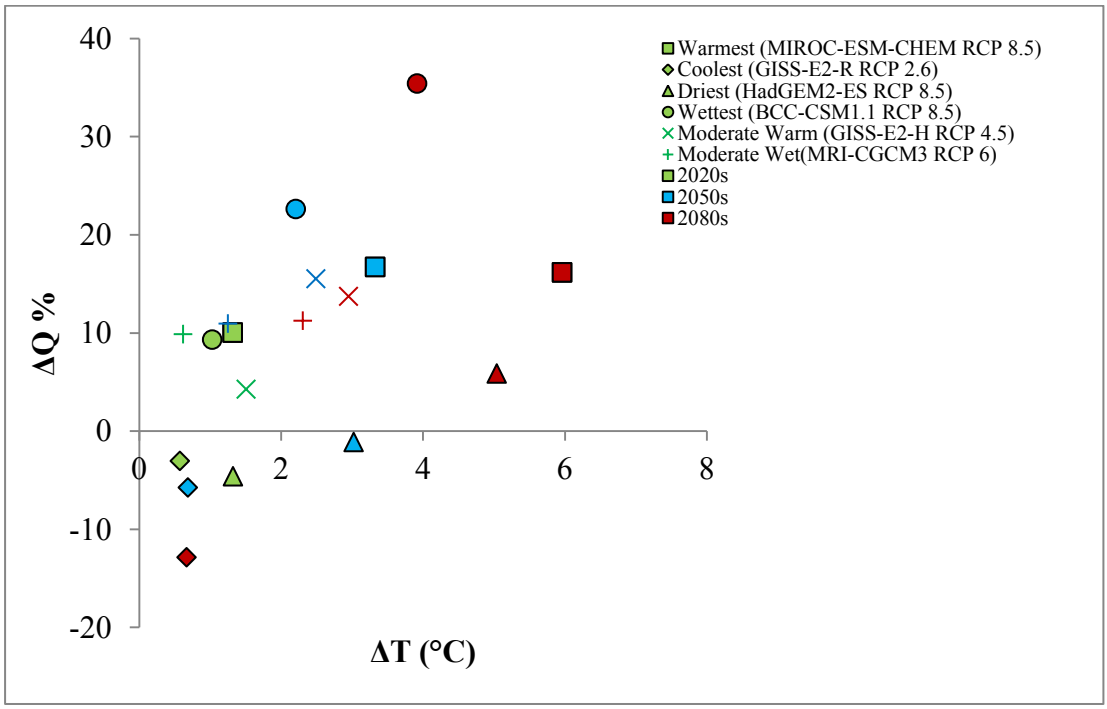

Figure 5.27 ΔT C
for 2020s, 2050s and 2080s

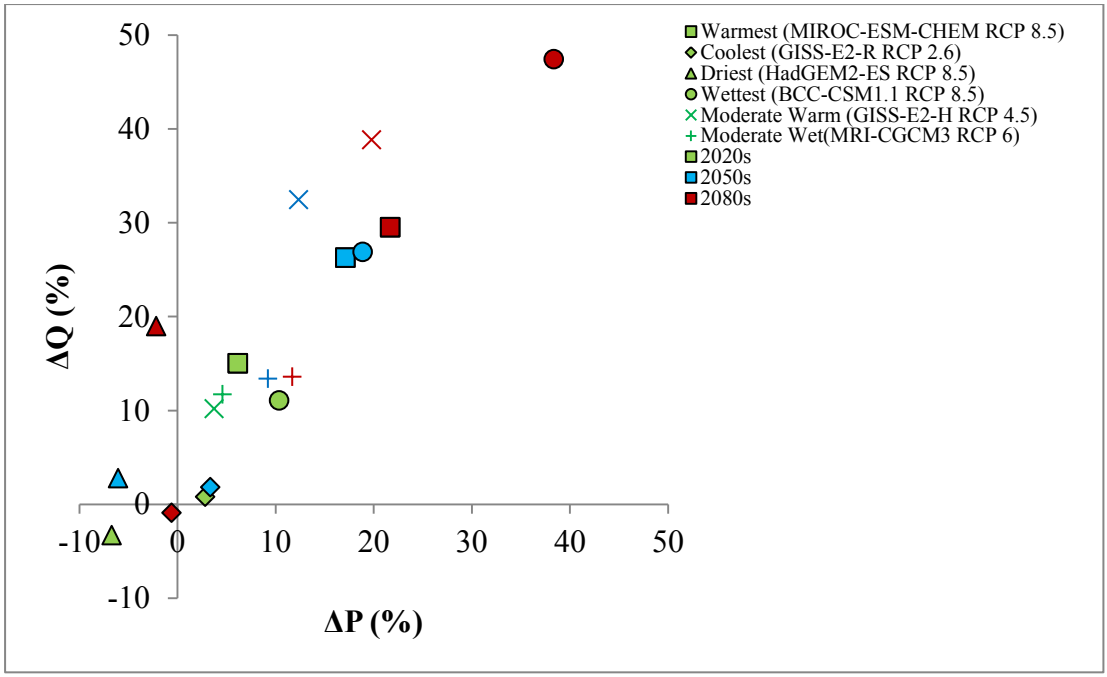

Figure 5.28 ΔP (%) vs changes in mean annual discharge (%) of six scenarios for2020s, 2050s and 2080s

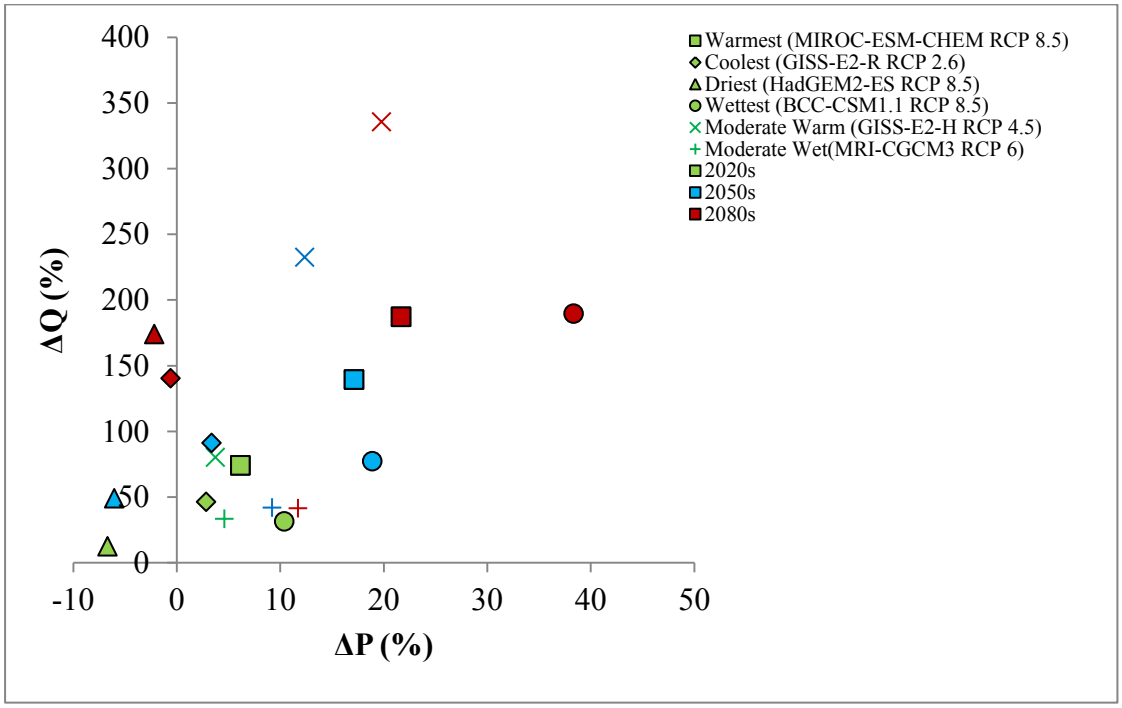

Figure 5.29 ΔP (%) vs changes in mean dry period discharge (%) of six scenarios for2020s, 2050s and 2080s

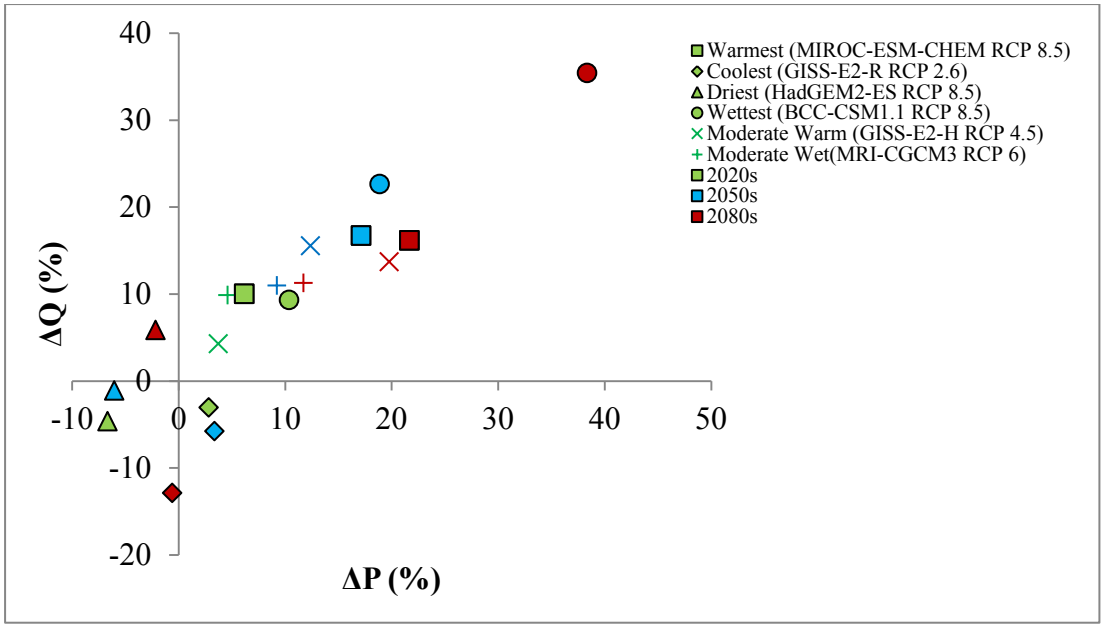

Figure 5.30 ΔP six scenarios for2020s, 2050s and 2080s

5.6.1.4 Multiple Linear Regression Analysis for Mean Annual Streamflow

As discussed in Section 5.4, changes in Brahmaputra River Basin (BRB) streamflow under the impact of climate change is sensitive to the changes in temperature and precipitation in the basin. An attempt has been taken to develop an equation to project the future streamflow of BRB under various changes in temperature and precipitation. Since changes in streamflow is linearly related to temperature change and precipitation changes, a multiple regression model has been setup to study how the changes in streamflow will behave under variable precipitation and temperature changes.

Multiple linear regression attempts to model the relationship between two or more explanatory variables and a response variable by fitting a linear equation to observed data. In this study, precipitation and temperature changes projected by 6 selected climate change scenarios (e.g., Warmest, Coolest, Wettest, Driest, Moderate Warming, and Moderate Wetting) have been used as predictors and SWAT simulated streamflow of BRB under those temperature and precipitation changes have been used as observed data. The model has been presented below:

$$Q_{Mean} = a_1 + a_2 * (\Delta T) + a_2 * (\Delta P) \qquad \textbf{(5.3)}$$

where, Q_{Mean} is the modeled future average annual streamflow of BRB under the impact of climate change; ΔT and ΔP are the projected changes in temperature (°C) and precipitation (%) with respect to the base period (1971-2000), respectively; and a_1, a_2, a_3 are the regression coefficient.

SWAT simulated Q_{Mean} of equation 5.3 has been fitted against the projected ΔT and ΔP of selected climate scenarios to determine the coefficients a_1, a_2, anda_3,

$$Q_{Mean} = 21535 + 575 * (\Delta T) + 349 * (\Delta P) \qquad m^3/s \qquad \textbf{(5.4)}$$

Equation 5.4 has been used to model the average annual streamflow of BRB at Bahadurabad station under changed future climate of 21st century using the projected changes in temperature (°C) and precipitation (%) with respect to the base period (1971-2000) and compared with the SWAT simulated average annual streamflow and good correlation (R^2=0.78) has been achieved. Table C19 and Table C31 (Appendix C) shows the overall statistics and goodness of fit of this multivariate regression model. Figure 5.31 shows the correlation where the SWAT simulated average annual streamflow under 6 selected climate change scenarios for the 2020s, 2050s, and 2080s has been plotted in the X-axis and estimated average annual streamflow of BRB using equation 5.4 has been plotted in Y-axis. In general, the relationship is quite linear over the 21st century. However, as expected the uncertainty increase as we go distant future which can be observed by increasing scattering from 2020s to 2080s. Equation 5.4 may be used to project average annual streamflow of BRB under changing climate where detailed hydrologic modeling is constraint.

The equation 5.4 has been tested for historical data at Bahadurabad station. Due to the lack of observed historical climate data outside Bangladesh, basin averaged precipitation before base period (1981-2010) was collected from literature. Average precipitation in BRB during the period 1961-1990 is 1276.97 mm (Immerzeel, 2008). Though the period used here overlaps with the base period of current model, it was the only reliable option we could take into consideration. Average annual precipitation for the model base period 1981-2010 was found 1479 mm, this is the

averaged precipitation used in the present model which is bias corrected NASA POWER data. Temperature change per 100 year in BRB is 0.6 °C (immerzeel, 2008). So, temperature change per 30 years can be considered about 0.20 °C. The change in temperature and precipitation during 1960-1990 compared to 1981-2010 was found about -0.2°C and 15.82%. Mean annual flow using the equation was found 26941 m^3/s whereas observed discharge of that station for that period was found 20036 m^3/s. A deviation of 6904 m^3/s is found at Bahadurabad which is quite high. So, it is evident that the equation does not represent the historical flow condition, only projected flow in future obtained using this equation can only be used.

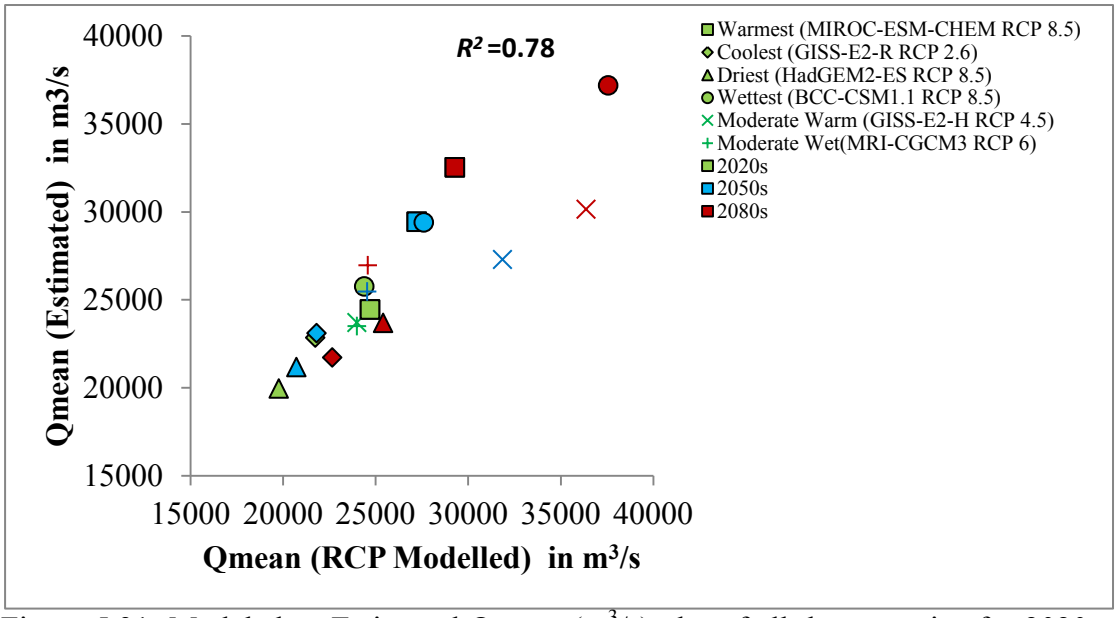

Figure 5.31: Modeled vs Estimated Qmean (m^3/s) plot of all the scenarios for 2020s, 2050s and 2080s

5.6.2 Maximum Annual Stream Flow Analysis

The model simulated percentage changes in the maximum annual streamflow from the climate normal (1981-2010) for different climate change scenarios has been assessed . Figure 5.31-5.33 shows boxplots of differences in the maximum annual average streamflow simulated by the model for warmest, coolest, driest, wettest, moderate warm and moderate wet with respect to the climate normal. The maximum annual average flow is found increasing from 2020s to 2080s. Range of variability also increased which indicates increasing uncertainty. For maximum average dry period flow increased at relatively higher rate. The range of 75th and 25th percentile decreased in 2080s though the range between the highest and lowest flow was found too high. Maximum average wet period flow increased gradually from

2020s to 2050s, the rate of increase slowed from 2050s to 2080s. The range of variability is found high for both 2050s and 2080s in case of maximum annual wet period flow.

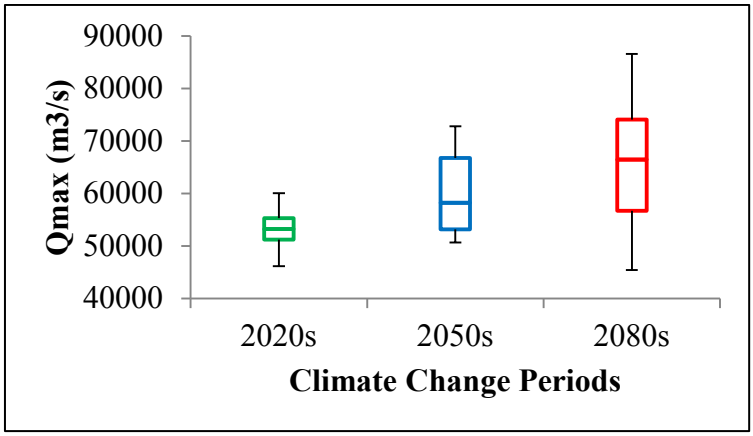

Figure 5.32: Box-plot of max annual discharge (m^3/s) of all the six scenariosfor 2020s, 2050s and 2080s

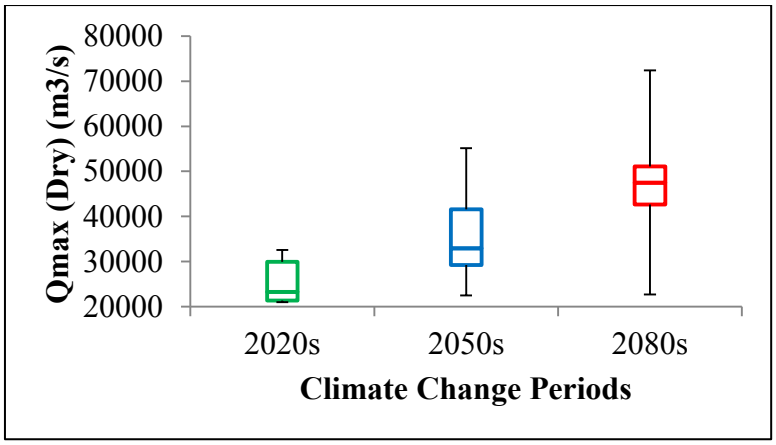

Figure 5.33: Box-plot of max dry period discharge (m^3/s) of all the six scenariosfor 2020s, 2050s and 2080s

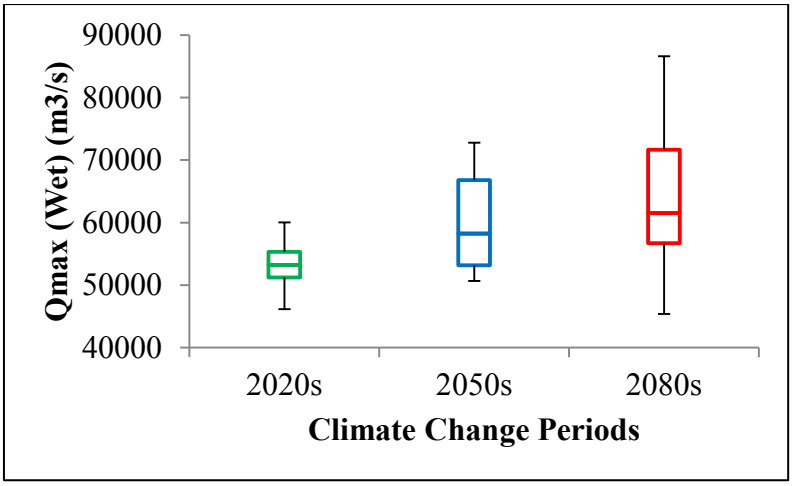

Figure 5.34: Box-plot of max wet period discharge (m^3/s) of all the six scenariosfor 2020s, 2050s and 2080s

5.6.2.1 Changes in streamflow in 2020s

5.6.2.1.1 Maximum Annual Flow Analysis for 2020s

In 2020s, maximum annual streamflow is found to increase in almost all the scenarios. The maximum projected increase in discharge of 16.70% was found for MIROC-ESM-CHEM (RCP 8.5), whereas GISS-E2-R (RCP 2.6) was found to give the maximum projected decrease in discharge with -3.59% change compared to the base flow. HADGEM2-ES (RCP 8.5) gave slight decrease of -1.83% in maximum annual discharge. All the other scenarios showed increase in projected annual discharges which were 7.62%, 1.32% and 4.96% for wettest, moderate warm and moderate wet scenarios.

5.6.2.1.2 Maximum Dry Period Flow Analysis for 2020s

Maximum dry season (Dec-May) flow was found to increase for all the scenarios in 2020s. Maximum projected increase in discharge was found for GISS-E2-H (RCP 4.5) with 94.80% change and the minimum projected increase was 25.58% which was given obtained for HADGEM2-ES (RCP 8.5). MIROC-ESM-CHEM (RCP 8.5) gave relatively high increase in discharge with 88.91% change. All other scenarios, viz. GISS-E2-R (RCP 2.6), BCC-CSM1.1 (RCP 8.5) and MRI-CGCM3 (RCP 6.0) gave an increased projected discharge with 48.69%, 26.89% and 29.62% consecutively.

5.6.2.1.3 Maximum Wet Period Flow Analysis for 2020s

In 2020s, max wet season (Jun-Nov) flow was found to increase for almost all the scenarios. Highest increase in projected flow was found for MIROC-ESM-CHEM (RCP 8.5) with 16.70% change. BCC-CSM1.1 (RCP 8.5) also gave relatively high increase in flow with 7.62%. Highest decrease in discharge was found for the driest scenario GISS-E2-R (RCP 2.6) with -3.59% change. HADGEM2-ES (RCP 8.5) projects a decreasing flow with -1.83% change. The moderate warm GISS-E2-H (RCP 4.5) and moderate wet MRI-CGCM3 (RCP 6.0) scenarios gave slight increase in flow with 1.31% and 4.96% change consecutively.

Table 5.21: Change in Maximum Discharge (%) for all the six scenarios in 2020s

	Warmest (MIROC-ESM-CHEM RCP 8.5)	Coolest (GISS-E2-R RCP 2.6)	Driest (HadGEM2-ES RCP 8.5)	Wettest (BCC-CSM1.1 RCP 8.5)	Mod Warm (GISS-E2-H RCP 4.5)	Mod Wet (MRI-CGCM3 RCP 6)
Max Annual	16.71	-3.59	-1.83	7.62	1.32	4.96
Max Dry Season (Dec-May)	88.91	48.69	25.58	26.89	94.80	29.62
Max Wet Season (June-Nov)	16.71	-3.59	-1.83	7.62	1.32	4.96

5.6.2.2 Changes in streamflow in 2050s

5.6.2.2.1 MaximumAnnual Flow Analysis for 2050s

In 2050s, maximum annual streamflow is found to increase for almost all the scenarios (Table 5.22). The maximum projected increase in discharge of 37.47% was found for MIROC-ESM-CHEM (RCP 8.5), whereas GISS-E2-R (RCP 2.6) was found to give the maximum projected decrease in discharge with
-3.59% change compared to the base flow. BCC-CSM1.1 gave relatively higher change with 29.69% and HAD-GEM2-ES gave small decrease in flow with -0.88% change. Rest of the scenarios, viz. GISS-E2-H (RCP 4.5) and MRI-CGCM3 (RCP 6.0) gave 15.52% and 7.64% increase in flow compared to the base flow.

5.6.2.2.2 MaximumDry Period Flow Analysis for 2050s

Maximum dry season (Dec-May) flow was found to increase for all the scenarios in 2020s(Table 5.22). Maximum projected increase in discharge was found for GISS-E2-

H (RCP 4.5) with 229.60% change and the minimum projected increase was 34.54% which was given obtained for MRI-CGCM3 (RCP 6.0). MIROC-ESM-CHEM (RCP 8.5) gave relatively high increase in discharge with 160.91% change. All other scenarios, viz. GISS-E2-R (RCP 2.6), BCC-CSM1.1 (RCP 8.5) and HADGEM2-ES (RCP 8.5) gave an increased projected discharge with 110.71%, 82.83% and 71.85% consecutively.

5.6.2.2.3 MaximumWet Period Flow Analysis for 2050s

In 2050s, maximum wet season (Jun-Nov) flow was found to increase for almost all the scenarios (Table 5.22). Highest increase in projected flow was found for MIROC-ESM-CHEM (RCP 8.5) with 37.47% change. BCC-CSM1.1 (RCP 8.5) and GISS-E2-H (RCP 4.5) also gave high increase in flow with 29.69% and 15.52% consecutively. Highest decrease in discharge was found for the GISS-E2-R (RCP 2.6) with -4.32% change. HADGEM2-ES (RCP 8.5) also projects a decreasing flow with -0.88% change. The remaining scenario, viz. moderate wet scenario MRI-CGCM3 (RCP 6.0) gave increase in flow with 7.64% change compared to the base flow.

Table 5.22: Change in Maximum Discharge (%) for all the six scenarios in 2050s

	Warmest (MIROC-ESM-CHEM RCP 8.5)	Coolest (GISS-E2-R RCP 2.6)	Driest (HadGEM2-ES RCP 8.5)	Wettest (BCC-CSM1.1 RCP 8.5)	Mod Warm (GISS-E2-H RCP 4.5)	Mod Wet (MRI-CGCM3 RCP 6)
Max Annual	37.47	-4.33	-0.88	29.69	15.52	7.64
Max Dry Season (Dec-May)	160.91	110.72	71.85	82.83	229.60	34.54
Max Wet Season (June-Nov)	37.47	-4.33	-0.88	29.69	15.52	7.64

5.6.2.3 Changes in Streamflow in 2080s

5.6.2.3.1 Maximumannual flow analysis for 2080s

In 2080s, maximum annual streamflow is found to increase in all the scenarios other than the coolest one (GISS-E2-R RCP 2.6) as shown in Table 5.23. The maximum projected increase in discharge of 63.58% was found for the wettest scenario BCC-CSM1.1 (RCP 8.5), whereas GISS-E2-R (RCP 2.6) was found to give the maximum projected decrease in discharge with -13.28% change compared to the base flow. Other scenarios gave variable increase in flow, 41.07%, 14.36%, 18.12% and 5.62%

increase in mean annual streamflow were found for MIROC-ESM-CHEM (RCP 8.5), HADGEM2-ES (RCP 8.5), GISS-E2-H (RCP 4.5) and MRI-CGCM3 (RCP 6.0).

5.6.2.3.2 MaximumDry Period Flow Analysis for 2080s

Mean dry season (Dec-May) flow was found to increase for all the scenarios in 2080s(Table 5.23). Maximum projected increase in discharge was found for GISS-E2-H (RCP 4.5) with 285.87% change and the minimum projected increase was 35.82% which was given obtained for MRI-CGCM3 (RCP 6.0). All other scenarios, viz. MIROC-ESM-CHEM (RCP 8.5), GISS-E2-R (RCP 2.6), HADGEM2-ES (RCP 8.5) and BCC-CSM1.1 (RCP 8.5) gave an increased projected discharge with 172.25%, 149.41%, 195.70% and 169.88% consecutively.

5.6.2.3.3 MaximumWet Period Flow Analysis for 2080s

In 2080s, maximum wet season (Jun-Nov) flow was found to increase for all the scenarios except GISS-E2-R (RCP 2.6) which gave -12.86% change in mean wet period flow(Table 5.23). Highest increase in projected flow was found for BCC-CSM1.1 (RCP 8.5) with 41.07% change. MIROC-ESM-CHEM (RCP 8.5), GISS-E2-H (RCP 4.5), HADGEM2-ES (RCP 8.5) and MRI-CGCM3 (RCP 6.0) gave high increase in flow with 41.07%, 18.13%, 14.36% and 5.63% consecutively. Highest decrease in discharge was found for the GISS-E2-R (RCP 2.6) with -13.28% change.

Table 5.23: Change in Maximum Discharge (%) for all the six scenarios in 2080s

	Warmest (MIROC-ESM-CHEM RCP 8.5)	Coolest (GISS-E2-R RCP 2.6)	Driest (HadGEM2-ES RCP 8.5)	Wettest (BCC-CSM1.1 RCP 8.5)	Mod Warm (GISS-E2-H RCP 4.5)	Mod Wet (MRI-CGCM3 RCP 6)
Max Annual	41.07	-13.28	14.36	63.59	18.13	5.63
Max Dry Season (Dec-May)	172.25	149.41	195.70	160.88	285.87	35.82
Max Wet Season (June-Nov)	41.07	-13.28	14.36	63.59	18.13	5.63

For better understanding of the relative changes in maximum annual, maximum dry period and maximum wet period discharge, scatter plot of changes in discharge (%) for

C) and precipitation (%) is shown in Figure 5.35-5.40.

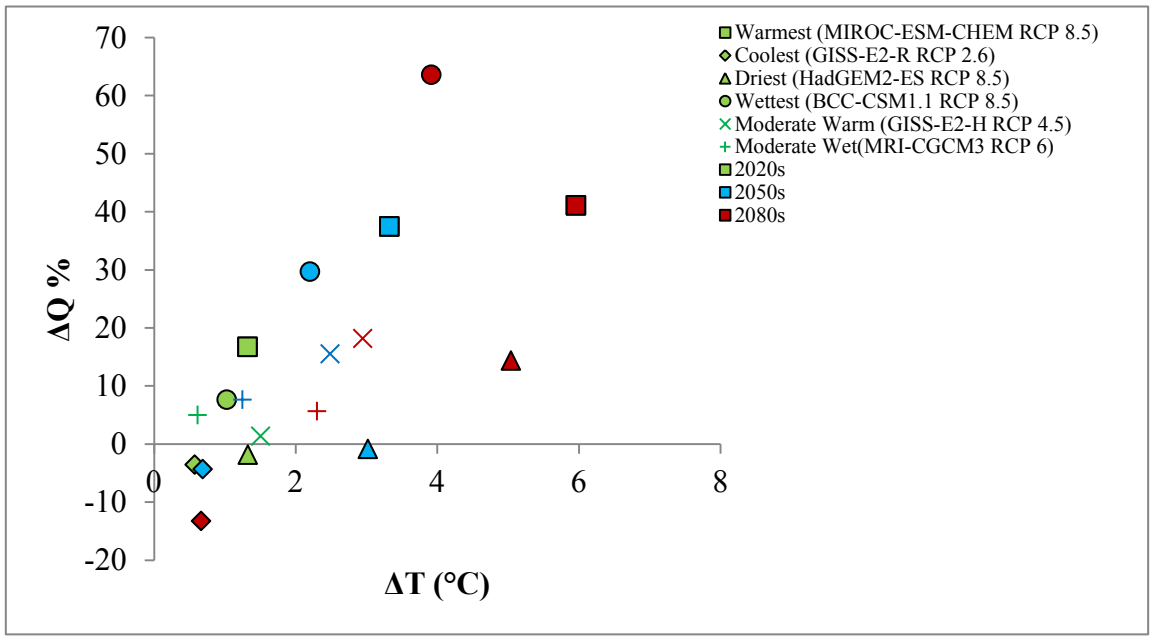

Figure 5.35 ΔT C
for2020s, 2050s and 2080s

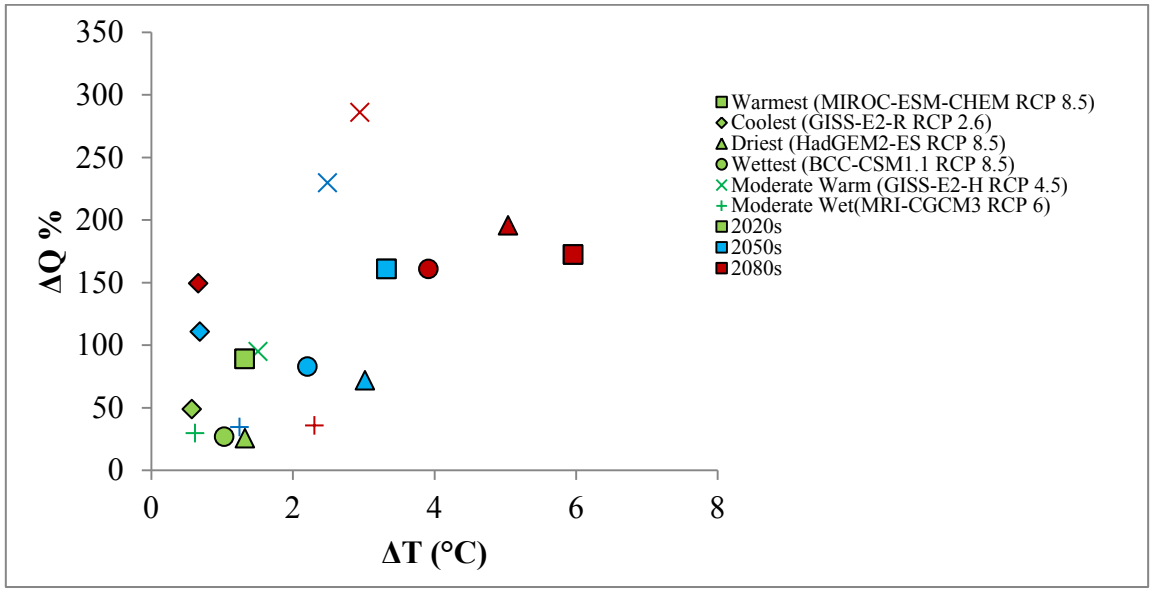

Figure 5.36 ΔT C
for2020s, 2050s and 2080s

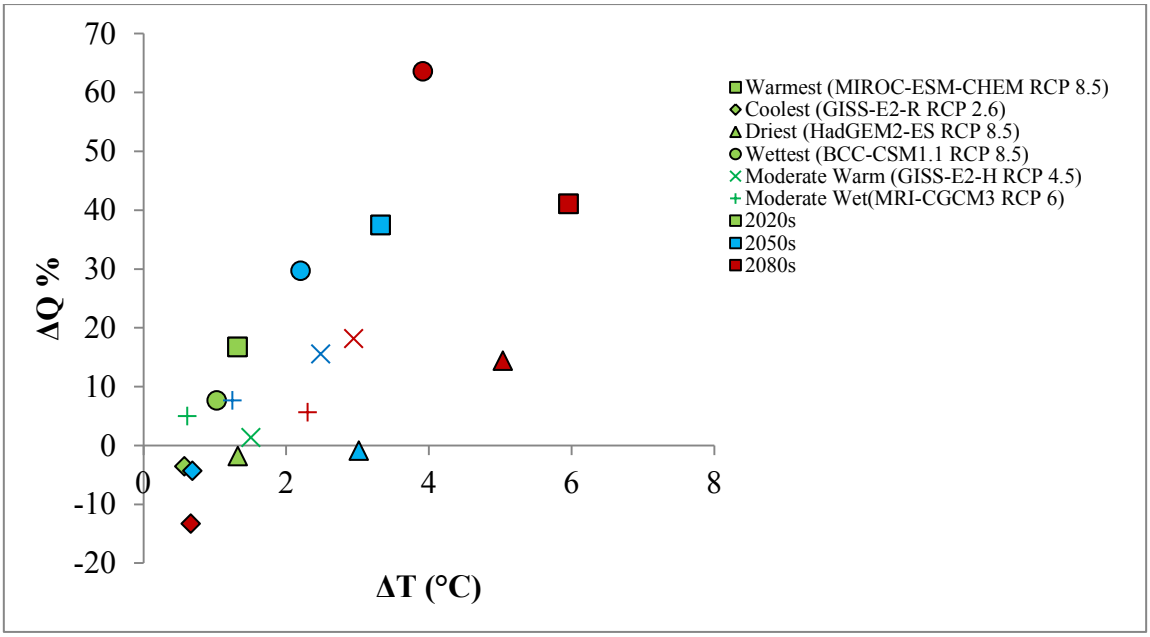

Figure 5.37 ΔT C
scenarios for 2020s, 2050s and 2080s

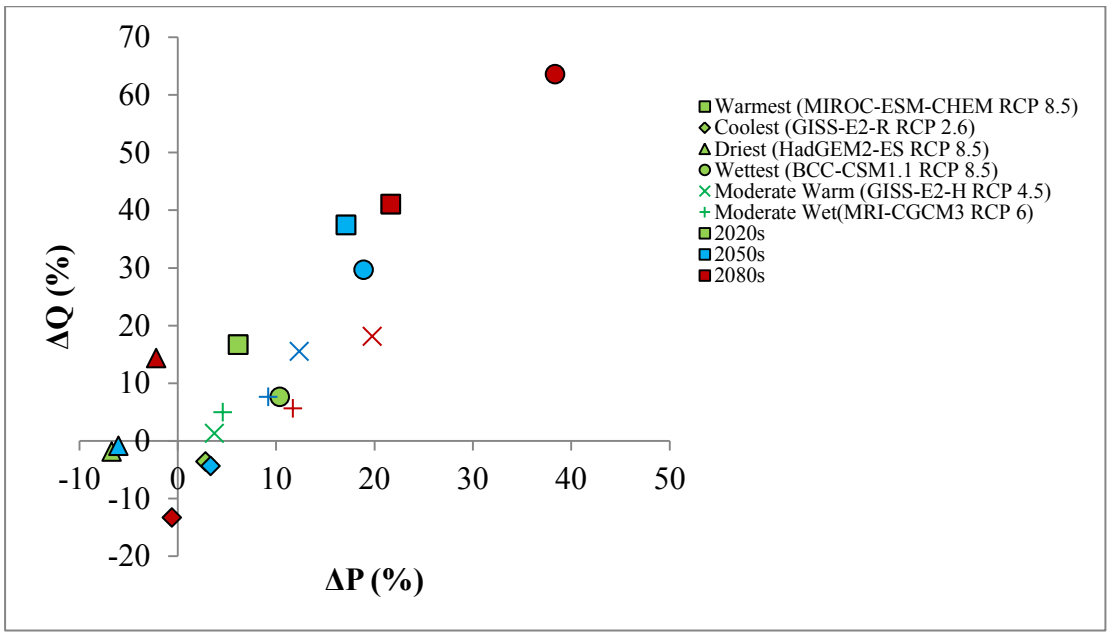

Figure 5.38 ΔP (%) vs changes in maximum annual discharge (%) of six scenarios for2020s, 2050s and 2080s

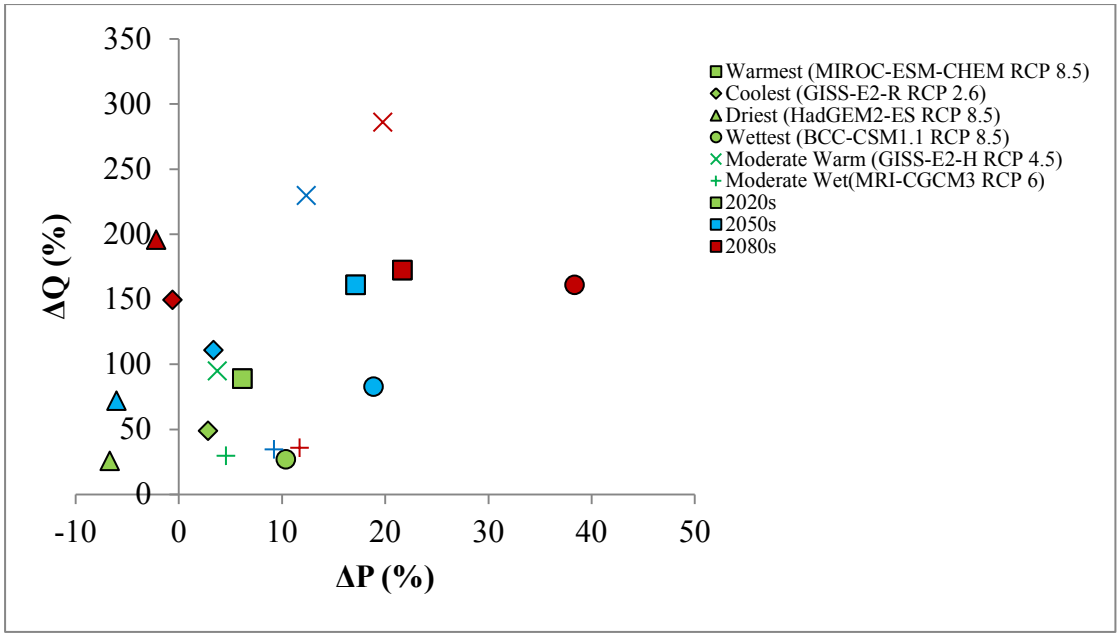

Figure 5.39 ΔP (%) vs changes in maximum dry period discharge (%) of six scenarios for 2020s, 2050s and 2080s

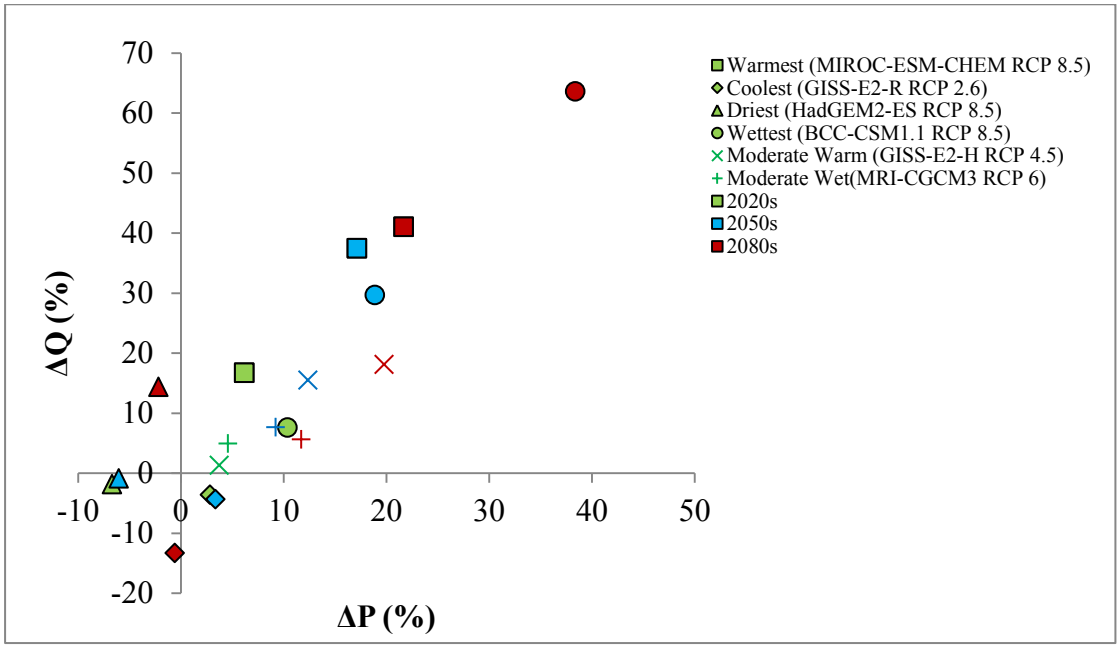

Figure 5.40 ΔP (%) vs changes in maximum wet period discharge (%) of six scenarios for 2020s, 2050s and 2080s

5.6.2.4 Multiple Linear Regression Analysis for Maximum Annual Streamflow

As discussed in Section 5.4, changes in Brahmaputra River Basin (BRB) streamflow under the impact of climate change is sensitive to the changes in temperature and precipitation in the basin. An attempt has been taken to develop an equation to project the maximum future streamflow of BRB under various changes in temperature

and precipitation. Since changes in streamflow is linearly related to temperature change and precipitation changes, a multiple regression model has been setup to study how the changes in streamflow will behave under variable precipitation and temperature changes.

Multiple linear regression attempts to model the relationship between two or more explanatory variables and a response variable by fitting a linear equation to observed data. In this study, precipitation and temperature changes projected by 6 selected climate change scenarios (e.g., Warmest, Coolest, Wettest, Driest, Moderate Warming, and Moderate Wetting) have been used as predictors and SWAT simulated maximum annual streamflow of BRB under those temperature and precipitation changes have been used as observed data. The model has been presented below:

$$Q_{Max} = a_1 + a_2 * (\Delta T) + a_2 * (\Delta P) \quad \textbf{(5.5)}$$

where, $Q_{Max}$is the modeled future maximum annual streamflow of BRB under the impact of climate change; ΔT and ΔP are the projected changes in temperature (°C) and precipitation (%) with respect to the base period (1971-2000), respectively; and a_1, a_2, a_3 are the regression coefficient.

SWAT simulated Q_{Max} of equation 5.5 has been fitted against the projected ΔT and ΔP of selected climate scenarios to determine the coefficients a_1, a_2, anda_3,

$$Q_{Max} = 47110 + 2655 * (\Delta T) + 731 * (\Delta P)\ \mathrm{m^3/s} \quad \textbf{(5.6)}$$

Equation 5.6 has been used to model the annual maximum streamflow of BRB under changed future climate of 21st century using the projected changes in temperature (°C) and precipitation (%) with respect to the base period (1981-2010) and compared with the SWAT simulated annual maximum streamflow and good correlation (R^2=0.92) has been achieved. Table C27 and Table C29 (AppendixC) shows the overall statistics and goodness of fit of this multivariate linear regression model. Figure 5.41 shows the correlation where the SWAT simulated annual maximum streamflow under 6 selected climate change scenarios for the 2020s, 2050s, and 2080s has been plotted in

the X-axis and estimated annual maximum streamflow of BRB using equation 5.6 has been plotted in Y-axis. In general, the relationship is quite linear over the 21st century. However, as expected the uncertainty increase as we go distant future which can be observed by increasing scattering from 2020s to 2080s. Equation 5.6 may be used to project average annual streamflow of BRB under changing climate where detailed hydrologic modeling is constraint.

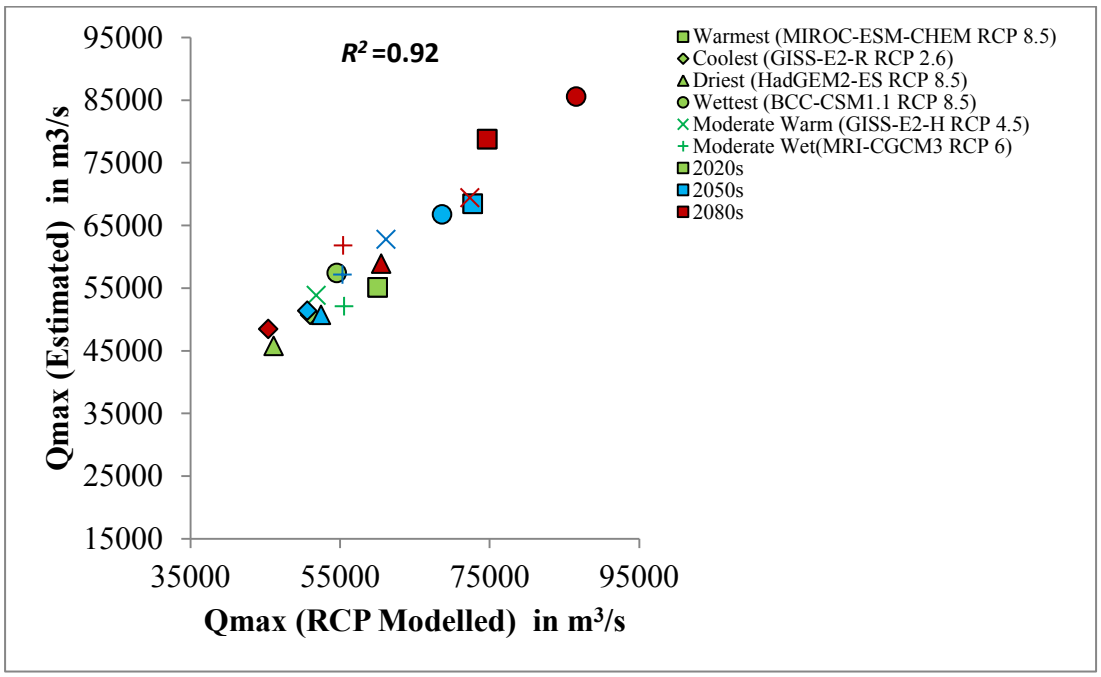

Figure 5.41: Modeled vs Estimated Q_{max} (m^3/s) plot of all the scenarios for 2020s, 2050s and 2080s

5.6.3 Minimum Annual Stream Flow Analysis

The model simulated percentage changes in the minimum annual streamflow from the climate normal (1981-2010) for different climate change scenarios has been assessed .Changes in streamflow in 2020s

5.6.3.1 Changes in Streamflow in 2020s

5.6.3.1.1 Minimum Annual Flow Analysis for 2020s

In 2020s, minimum annual streamflow showed both increasing and decreasing pattern. Highest increase in minimum projected discharge was found for MIROC-ESM-CHEM (RCP 8.5) with +47.37% change whereas highest decrease was found for HADGEM2-ES (RCP 8.5) with -91.08% change.BCC-CSM1.1 (RCP 8.5) gave 46.39% increase in discharge. All other scenarios, viz. GISS-E2-R (RCP 2.6), GISS-

E2-H (RCP 4.5) and MRICGCM3 gave a decrease in flow with -24.86%, -12.49% and -16.68% change.

5.6.3.1.2 Minimum Dry Period Flow Analysis for 2020s

Minimum dry season (Dec-May) flow for 2020s is identical to the minimum annual flow described in the previous section (Minimum Annual Flow Analysis for 2020s). As described earlier other than the wettest and warmest scenarios, all other scenarios gave decrease in minimum dry period flow.

5.6.3.1.3 Minimum Wet Period Flow Analysis for 2020s

Minimum wet period flow was found to decrease in all the scenarios except the wettest and moderate wet scenarios which gave 29.90% and 9.78% increase consecutively.Other scenarios, viz. warmest, coolest, driest and mod.warm scenarios gave -25.36%, -11.67%, -18.91% and -4.61% change. Magnitude of minimum flow for mean annual, dry period and wet period is presented in Appendix C.

Table 5.24: Change in Minimum adjusted discharge (%) for all the six scenarios in 2020s

	Warmest (MIROC-ESM-CHEM RCP 8.5)	Coolest (GISS-E2-R RCP 2.6)	Driest (HadGEM2-ES RCP 8.5)	Wettest (BCC-CSM1.1 RCP 8.5)	Mod Warm (GISS-E2-H RCP 4.5)	Mod Wet (MRI-CGCM3 RCP 6)
Min Annual	47.37	-24.86	-91.08	46.39	-12.49	-16.68
Min Dry Season (Dec-May)	47.37	-24.86	-91.08	46.39	-12.49	-16.68
Min Wet Season (June-Nov)	-25.36	-11.67	-18.91	28.90	-4.61	9.78

5.6.3.2 Changes in streamflow in 2050s

5.6.3.2.1 Minimum Annual Flow Analysis for 2050s

In 2050s, minimum annual streamflow showed both increasing and decreasing pattern. Highest increase in minimum projected discharge was found for BCC-CSM1.1 (RCP 8.5) with +55.19% change whereas highest decrease was found for HADGEM2-ES (RCP 8.5) with -96.42% change. MIROC-ESM-CHEM (RCP 8.5), BCC-CSM1.1 (RCP 8.5) and GISS-E2-H (RCP 4.5) gave 47.04%, 55.19% and

46.72% increase in discharge. All other scenarios, viz. GISS-E2-R (RCP 2.6), and MRICGCM3 gave a decrease in flow with -50.05% and -11.65% change.

5.6.3.2.2 Minimum Dry Period Flow Analysis for 2050s

Minimum dry season (Dec-May) flow for 2050s is identical to the minimum annual flow described in the previous section (Minimum Annual Flow Analysis for 2050s).

5.6.3.2.3 Minimum Wet Period Flow Analysis for 2050s

Minimum wet period (June-November) flow was found to decrease in all the scenarios except the moderate wet scenario which gave 10.15% increase.Other scenarios, viz. warmest, coolest, driest, wettest and mod.warm scenarios gave -50.56%, -37.46%, -46.99% and -24.67% and -11.51% change. Magnitude of minimum flow for mean annual, dry period and wet period is presented in AppendixC.

Table 5.25: Change in Minimum adjusted discharge (%) for all the six scenarios in 2050s

	Warmest (MIROC-ESM-CHEM RCP 8.5)	**Coolest (GISS-E2-R RCP 2.6)**	**Driest (HadGEM2-ES RCP 8.5)**	**Wettest (BCC-CSM1.1 RCP 8.5)**	**Mod Warm (GISS-E2-H RCP 4.5)**	**Mod Wet (MRI-CGCM3 RCP 6)**
Min Annual	47.04	-50.05	-96.42	55.19	46.72	-11.65
Min Dry Season (Dec-May)	47.04	-50.05	-96.42	55.19	46.72	-11.65
Min Wet Season (June-Nov)	-50.56	-37.46	-46.99	-24.67	-11.51	10.15

5.6.3.3 Changes in Streamflow in 2080s

5.6.3.3.1 Minimum annual flow analysis for 2080s

In 2080s, minimum annual streamflow showed decreasing pattern for all the scenarios except the warmest one (MIROC-ESM-CHEM RCP 8.5) which gave an increase of 41.07%. All other scenarios viz. coolest, driest, wettest, mod.warm and mod. wet gave decrease in discharge with -99.07%, -99.95%, -97.53%, -99.24% and -99.48% change.

5.6.3.3.2 Minimum Dry Period Flow Analysis for 2080s

Similar to minimum annual flow in 2080s, only warmest scenario gave increase in discharge during dry period with 172.25% change. All other scenarios viz. coolest, driest, wettest, mod.warm and mod. wet gave decrease in discharge with -98.64%, -99.79%, -88.80%, -96.53% and -97.63 change.

5.6.3.3.3 Minimum Wet Period Flow Analysis for 2080s

Minimum wet period discharge for 2080s also showed increase in discharge for warmest scenario with 41.07% change. All other scenarios viz. coolest, driest, wettest, mod.warm and mod. wet gave decrease in discharge with -95.69%, -96.36%, -94.06%, -92.71% and -88.87% change.

Table 5.26: Change in Minimum adjusted discharge (%) for all the six scenarios in 2080s

	Warmest (MIROC-ESM-CHEM RCP 8.5)	**Coolest (GISS-E2-R RCP 2.6)**	**Driest (HadGEM2-ES RCP 8.5)**	**Wettest (BCC-CSM1.1 RCP 8.5)**	**Mod Warm (GISS-E2-H RCP 4.5)**	**Mod Wet (MRI-CGCM3 RCP 6)**
Min Annual	41.07	-99.70	-99.95	-97.53	-99.24	-99.48
Min Dry Season (Dec-May)	172.25	-98.64	-99.79	-88.80	-96.53	-97.63
Min Wet Season (June-Nov)	41.07	-95.69	-96.36	-94.06	-92.71	-88.87

For better understanding of the relative changes in maximum annual, maximum dry period and maximum wet period discharge, scatter plot of changes in discharge (%) C) and precipitation (%) is shown in Figure 5.42-5.47.

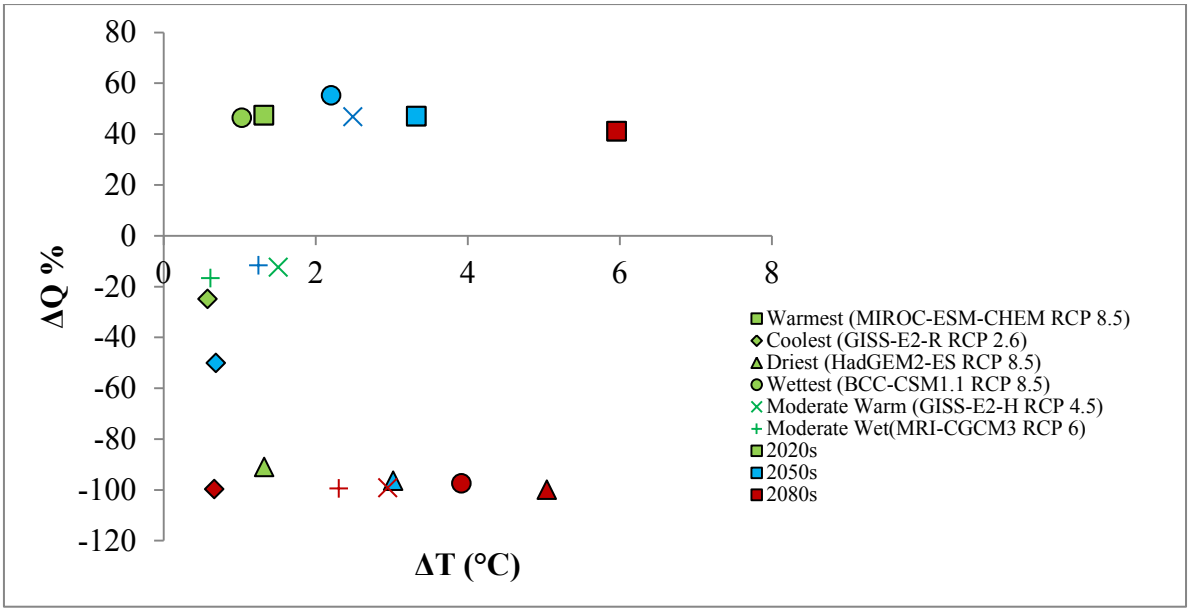

Figure 5.42 ΔT C minimum annual discharge (%) of six scenarios for 2020s, 2050s and 2080s

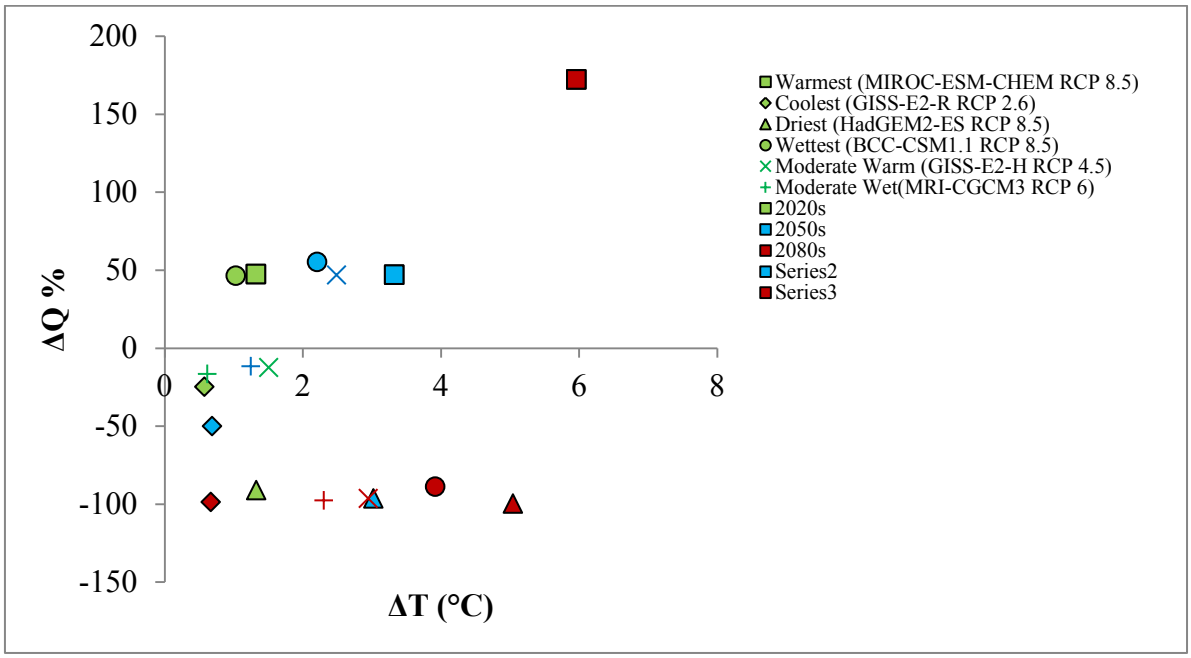

Figure 5.43 ΔT C minimum dry period discharge (%) of six scenarios for 2020s, 2050s and 2080s

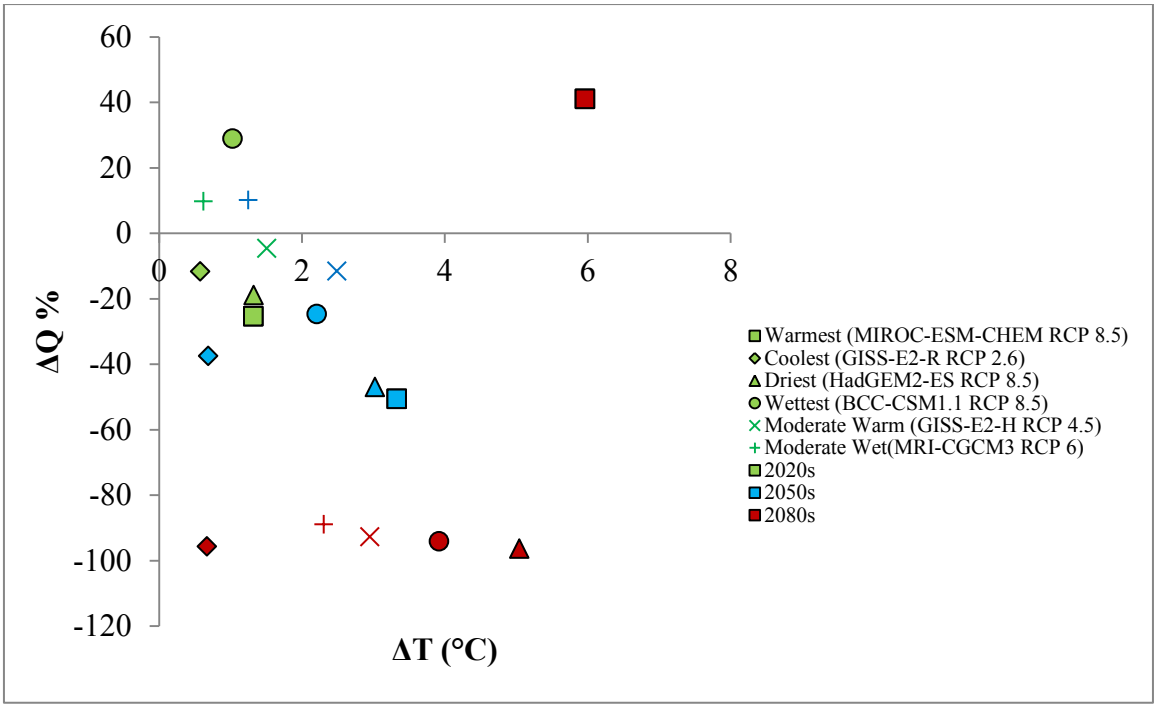

Figure 5.44: ΔT C minimum wet period discharge (%) of six scenarios for 2020s, 2050s and 2080s

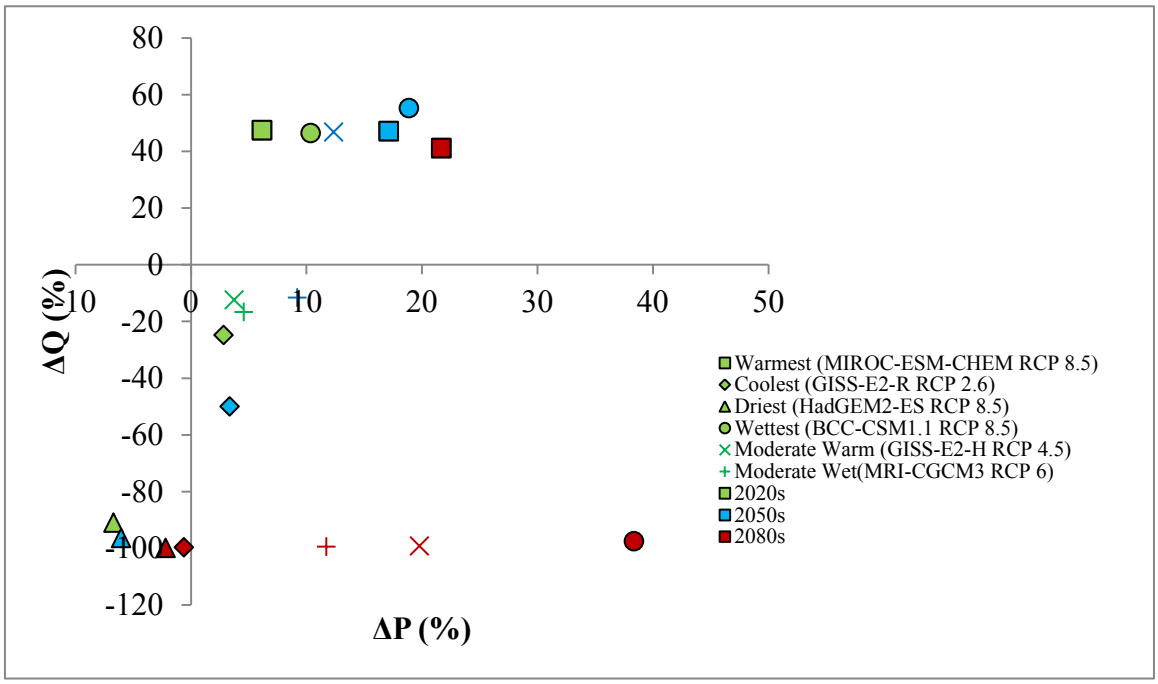

Figure 5.45 ΔP (%) vs changes in minimum annual discharge (%) of six scenarios for 2020s, 2050s and 2080s

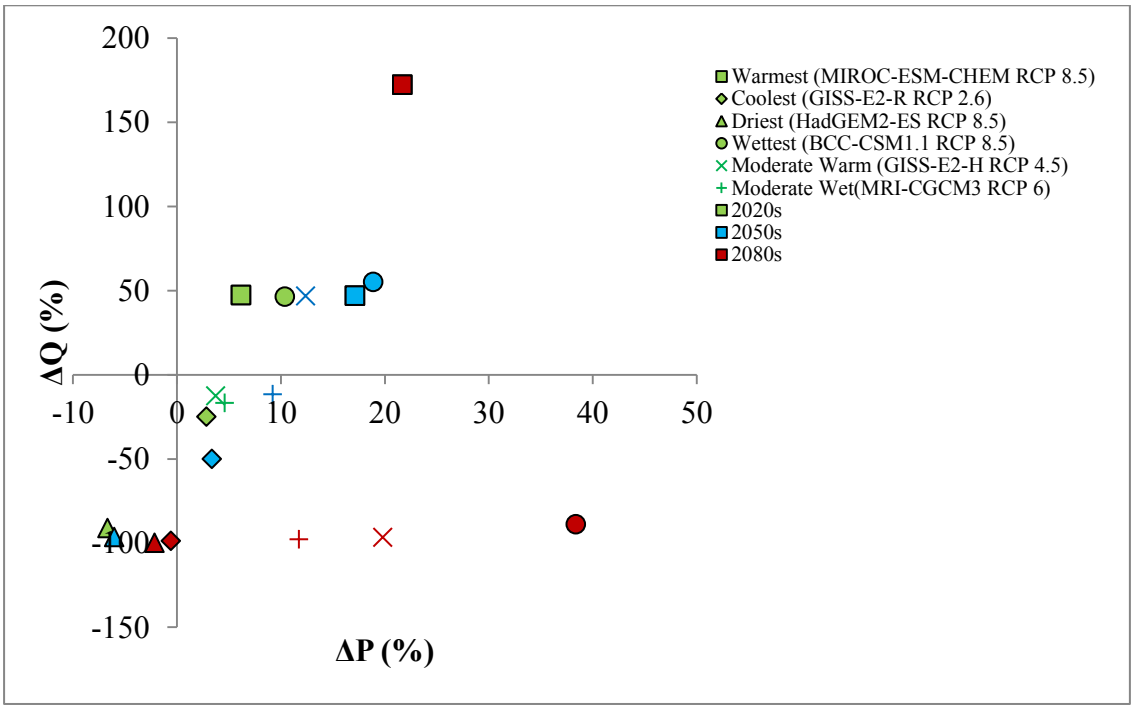

Figure5.46 ΔP (%) vs changes in minimum dry period discharge (%) of six scenarios for 2020s, 2050s and 2080s

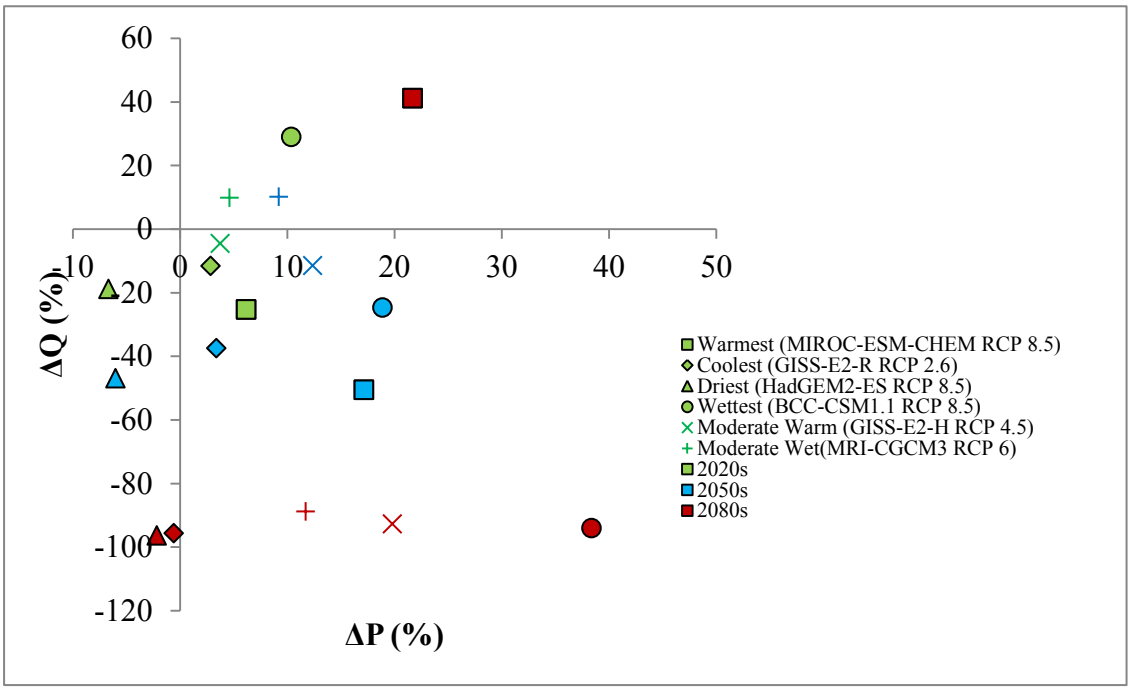

Figure 5.47 ΔP (%) vs changes in minimum wet period discharge (%) of six scenarios for 2020s, 2050s and 2080.

5.6.4 Climate Change Impact at Kurigram Station

Mean monthly discharge hydrograph at Kurigram station for 2020s, 2050s and 2080s is shown in Figure 48-50. It is observed that flow hydrographs has a rising trend from 2020s to 2080s, though the flow from December to February decreases for the future scenarios. Monthly range of discharge is lower in 2020s, which increases towards 2080s. It is observed that the variability tend to increase between March to May. Flow hydrograph is quite stable during the recession period (Sep-Dec). Almost all the models are seem to give decreased flow during recession for all the periods.

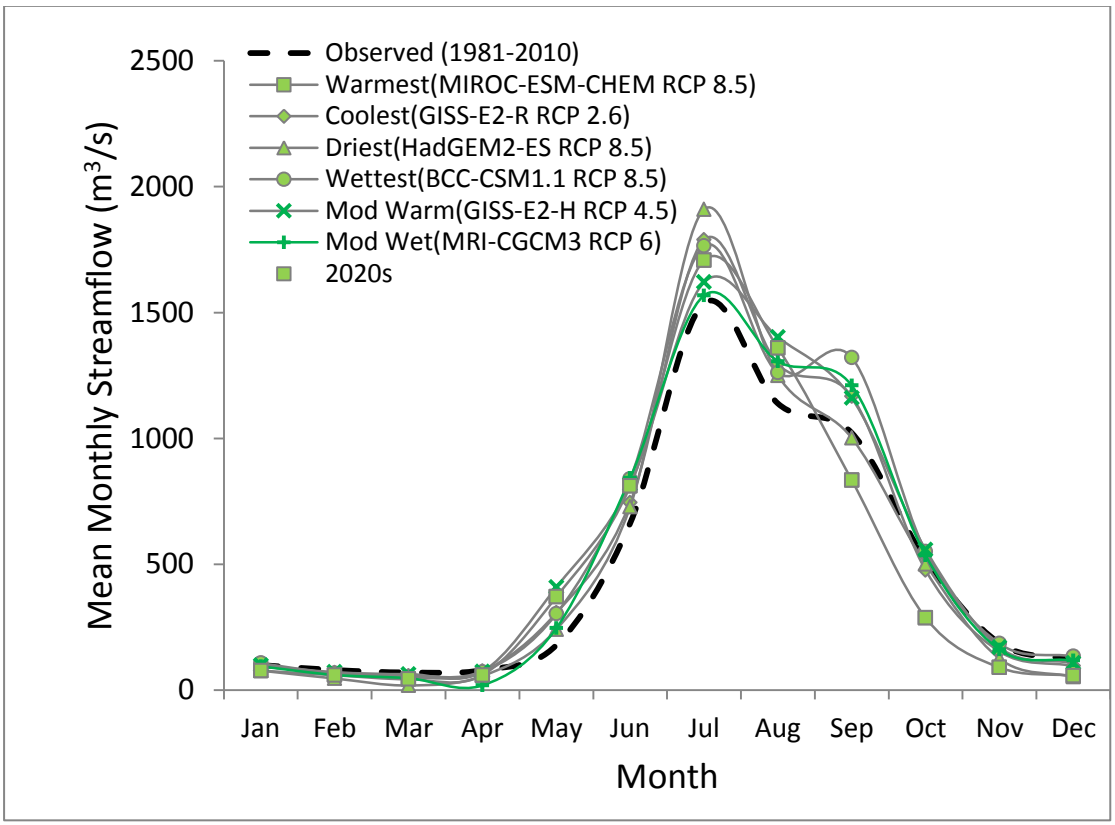

Figure 5.48: Mean monthly streamflow at Kurigram station in 2020s

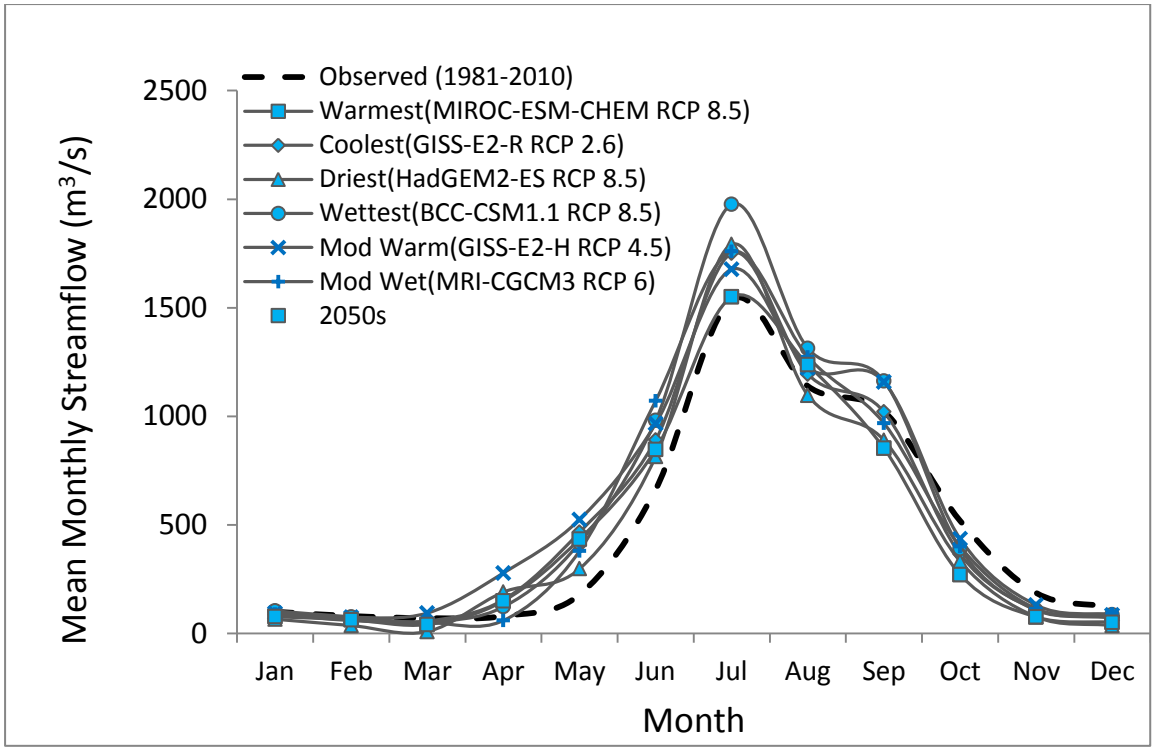

Figure 5.49: Mean monthly streamflow at Kurigram station in 2050s

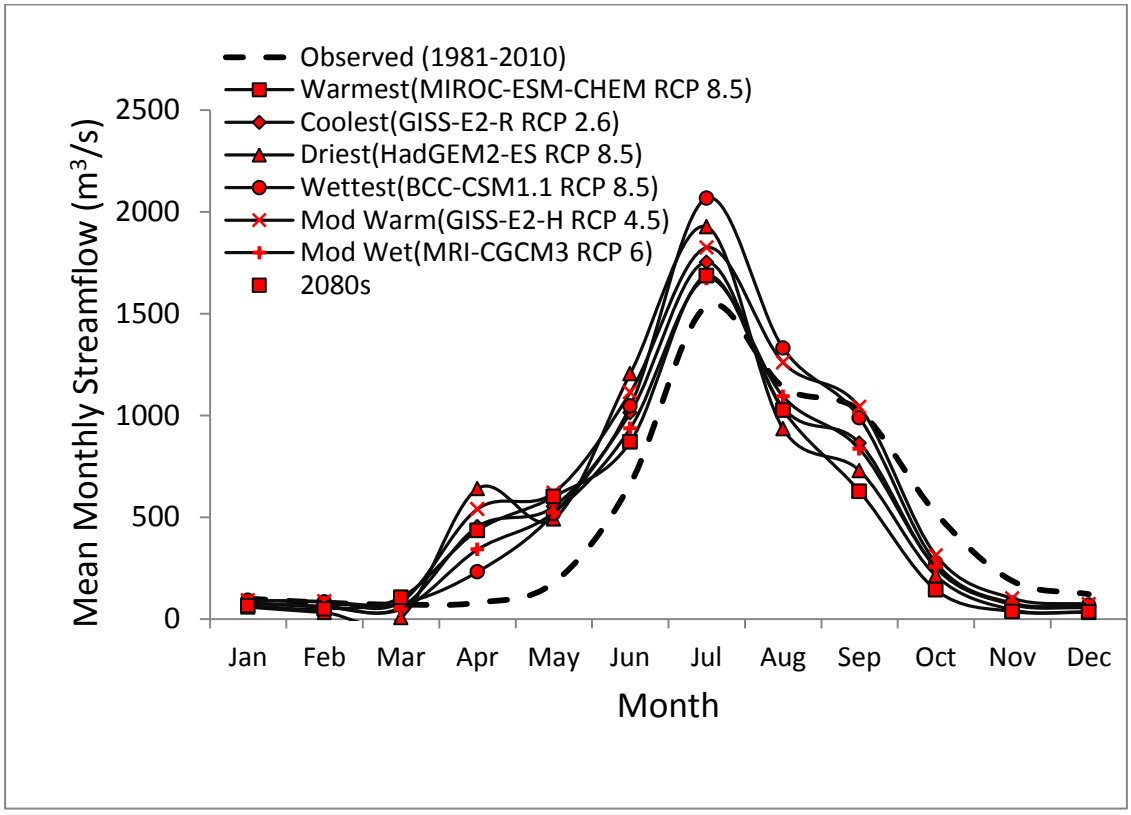

Figure 5.50: Mean monthly streamflow at Kurigram station in 2080s

Chapter 6
Conclusions and Recommendations

6.1 Conclusions

In this study, potential impacts of climate change on the future streamflow of BRB has been assessed by using SWAT hydrological model on the basis of climate change scenarios projected by multiple GCMs forced by several RCP scenarios of IPCC 5th Assessment (AR5) report for 2020s, 2050s, and 2080s of the 21st century.

Initially after calibration and validation of the hydrological model of Brahmaputra River Basin, sensitivity of the flow to temperature and precipitation change at Bahadurabad station was assessed. Changes in discharge (ΔQ due to changes in temperature (ΔT, holding precipitation fixed) and due to changes in precipitation (ΔP, holding temperature fixed) were found almost linear in both cases. Average slope of $\Delta Q/\Delta P$ with precipitation change is around 1.36. Average slope of $\Delta Q/\Delta T$ with Temperature change is around -1.35.

Six climate change scenarios, viz. warmest, coolest, driest, wettest, moderate warm and moderate wet were selected based on the precipitation and temperature data obtained from four RCPs (RCP 2.6, RCP 4.5, RCP 6.0 and RCP 8.5) of eight GCMs (BCC-CSM1.1, BCC-CSM1.1(m), GISS-E2-H, GISS-E2-R, Had-GEM2-ES, MIROC-ESM, MIROC-ESM-CHEM, MRI-CGCM3). From the analysis of temperature and precipitation data BCC-CSM1.1 RCP 8.5, HadGEM2-ES RCP 8.5, MIROC-ESM-CHEM RCP 8.5, GISS-E2-R RCP 2.6, MRI-CGCM3 RCP 6.0 and GISS-E2-H RCP 4.5 were selected as the wettest, driest, warmest, coolest, moderate wet and moderate warm scenario, respectively. In order to obtain high resolution temperature and precipitation data of these scenarios, pattern scaling technique was used. These data was further used to run SWAT model of Brahmaputra River Basin.

In general, Brahmaputra River Basin projected an increase in the mean annual streamflow for the 21st century under the climate change projections for almost all the six scenarios considered in this study. However, GISS-E2-R RCP2.6 (coolest) and HadGem2-ES RCP8.5 (driest) projected decrease in annual average flow at

Bahadurabad station during 2080s and 2020s respectively. The maximum projected increase in mean annual streamflow found are 15.019%, 32.457% and 47.436% for MIROC-ESM-CHEM RCP8.5 (warmest), GISS-E2-H RCP4.5 (mod. warm) and BCC-CSM1.1 RCP8.5 (wettest) in 2020s, 2050s and 2080s respectively. The minimum projected change in streamflow found are -3.290%, 1.800% and -0.908% for HadGEM2-ES RCP8.5 (driest), GISS-E2-R RCP2.6(coolest) and GISS-E2-R RCP2.6 in 2020s, 2050s and 2080s respectively.

On the average, at the end of 21stcentury (2080s), the mean dry and wet period streamflow of BRB is projected to increase by about 177.93% and 11% of their mean dry and wet period discharge, respectively. In 2080s, maximum increase in dry and wet period flow was found for GISS-E2-H RCP 4.5 (mod. warm) and BCC-CSM1.1 RCP8.5 (wettest), respective. Lowest dry and wet period flow were found for MRI-CGCM3 RCP6.0 (mod. wet) and GISS-E2-R RCP2.6 (coolest) consecutively.

Multiple variable linear regression analysis was done to generate q

BRB

C $R^2$for the equations of mean annual discharge (m^3/s) and maximum discharge (m^3/s) were found to be 0.78 and 0.98, respectively.. It is to be noted that, Bangladesh is a flood prone country and very much susceptible to climate change where sophisticated models are not available to local community. So, the equation obtained through multi variable regression, especially the equation for maximum discharge may be used by local authorities and community to get a good idea about flow near Bahaduabad station for planning, agricultural production and other important aspects.

6.2 Recommendations for Future Studies

Recommendations for further extension of the present work and minimize the uncertainties have been discussed in the following section

The model was calibrated and validated at Bhadurabad station as data was available at this station only for Brahmaputra River Basin. As there exists numerous flow regulations in the upstream of Bangladesh, it is recommended to calibrate the model

at more upstream points outside the boundary of Bangladesh if it is possible to collect data either through Indo-Bangladesh Join River Commission, or others sources.

In the present research eight GCMs were taken into consideration based on the availability of GCM output for selecting scenarios. In order to minimize uncertainties associated with streamflow projection for future period, it is recommended to select the scenarios comparing outputs of more GCMs.

In the present study land cover map was taken for one year at the beginning of 21st century. For better approximation of future projected flow land use scenarios can be incorporated in this model.

Pattern scaling method was used to obtain high resolution climate data. In future the model can be tested with statistically and dynamically downscaled climate data which may give better approximation of the flow with reduced uncertainty.

Reference

Abaurrea J, Asín J., 2005. Forecasting local daily precipitation patterns in a climate change scenario. Climate Research, 28, 183–197.

Abbott, M.B., Bathurst, J.C., Cunge, J.A., Connell, P.E., Rasmussen, J., 1986a. An introduction to the European Hydrological System—Systeme Hydrologique E _SHE‘ History and philosophy of a physicallybased distributed modelling system., J. Hydrol., 87, 45–59.

Abbott, M.B., Bathurst, J.C., Cunge, J.A., Connell, P.E., Rasmussen, J., 1986b. An introduction to the European Hydrological System—Systeme Hydrologique E _SHE‘ , Structure of a physically based, distributed modelling system. J. Hydrol., 87, 61–77.

Agrawala, S., Ota, T., Ahmed, A. U., Smith, J., and van Aalst, M., 2005, Development and climate change in Bangladesh: focus on coastal flooding and the Sundarbans, Organisation for Economic Co-operation and Development (OECD), Paris.

Alcamo, J., G.J. van denBorn, A.F. Bouwman, B.J. deHaan, K. Klein Goldewijk, O. Kleer, J. Krabec, R. Leemans, J .G.J. Olivier, A.M.C. Toet, H.J.M. deVries, and H.J. van der Word, 1994. Modeling the global society-biosphere -climate system. Water Air Soil Pollut., 76, 1 -78.

Arnold, J. G. and G. Bernhardt, 1993. A comprehensive surface-groundwater flow model. J. Hydrol., 142, 47-69.

Arnold, J.G and Williams, J.R., 1995. SWRRB- A watershed scale model for soil and water resources management. In V.P. Singh (ed) Computer models of watershed hydrology. Water Resources Publications, 847-908.

Arnold, J. G. and Allen, P. M., 1996. Estimating hydrologic budgets for three Illinois watersheds, J. Hydrol., 176, 57–77.

Arnold, J.G., Srinivasan, R., Muttiah, R.S., Williams, J.R., 1998a. Large area hydrologic modelling and assessment.Part I. Model development. Journal of American Water Resources Association, 34(1), 73–89.

Arnold, J.G., Srinivasan, R., Muttiah, R.S., Williams, J.R., 1998b. Large area hydrologic modelling and assessment.Part I. Model development. Journal of American Water Resources Association, 34(1), 91–101.

Bandaragoda, C., Tarboton, D.G., and Woods, R., 2004. Alication of TOPNET in the distributed model Intercomparison project. Journal of Hydrology, 298(1-4), 178-201

Bárdossy A, Bogardi I, Matyasovszky I. 2005. Fuzzy rule-based downscaling of precipitation. Theoretical and Alied Climatology, 82, 119–129.

Bergant K, Kajfez-Bogataj L. 2005. N-PLS regression as empirical downscaling tool in climate change studies. Theoretical and Alied Climatology 81, 11–23.

Beven, K. J. and Kirkby, M. J., 1976. Towards a simple physically based variable contributing model of catchment hydrology. Working Paper 154, School of Geography, University of Leeds.

Beven, K., 1989. Changing ideas in hydrology –The case of physically based models. J Hydrol., 105, 157-172.

Beven, K., Lamb, R., Quinn, P., Romanowicz, R., Freer, J., 1995.TOPMODEL. In, Singh, V.P., (Ed.), Computer Models of Watershed Hydrology, 18. Water Resources Publications, Highlands Ranch, CO, 18. 627–668.

Biftu, G.F., and Gan, T.Y., 2001. Semi-distributed, physically based, hydrologic modelling of the Paddle River Basin, Alberta, using remotely sensed data. Journal of Hydrology, 244, 137-156.

Biftu, G. F., and T.Y. Gan, 2004.Semi-distributed, Hydrologic Modelling of Dry Catchment with Remotely Sensed and Digital Terrain Elevation Data. International Journal of Remote Sensing 25(20), 4351-4379.

Boe, J., Terray, L., Habetsb, F. and Martinc, E., 2007.Statistical and dynamical downscaling of the Seine basin climate for hydro-meteorological studies. Int. J. Climatol., 27, 1643–1655.

Bouraoui, F., Grizzetti, B., Granlund, K., Rekolainen, S. and Bidoglio, G., 2004. Impact of climate change on the water cycle and nutrient losses in a finnish catchment. Climatic Change 66, 109 –126.

Cabre MF, Solman SA, Nunez MN, 2010. Creating regional climate change scenarios S A ‘ ‘

technique, Validity and limitations. Clim Change 98(3–4),449–469

Calver, A., and Wood, W.L., 1995. The Institute of Hydrology Distributed Model. In, Singh, V.P., (Ed.), Computer Models of Watershed Hydrology, 17. Water Resources Publications, Highlands Ranch, CO. 17, 595–626.

Carpenter, T.M., Georgakakos, K.P., Sperfslage, J.A., 2001. On the parametric and NEXRAD-radar sensitivities of a distributed hydrologic model suitable for operational use. J. Hydrol. 254, 169–193.

Carter, T., M. Posch, and H. Tuomenvirta, 1995. SILMUSCEN CLIGEN ‘ guide. Guidelines for the construction of climatic scenarios and use of a stochastic weather generator in the Finnish Research Programme on Climate Change (SILMU).Publications of the Academy of Finland, 1/95,62.

Carter, T.R., M. Posch, and H. Tuomenvirta, 1996. The SILMU scenarios, specifying F ‘ G 3 3 -260.

Chen, J., François, Brissette, F.P., Leconte, R, 2010. A daily stochastic weather generator for preserving low-frequency of climate variability. Journal of Hydrology, 388, 480-490.

Cheng, C.S., Guilong, L., and Qian, L., 2010. A Synoptic Weather Typing Aroach to Simulate Daily Rainfall and Extremes in Ontario, Canada, Potential for Climate Change Projections. Journal of Alied Meteorology and Climatology, 49, 845-866.

Chiew F.H.S., Whetton P.H., McMahon T.A. and Pittock A.B., 1995.Simulation of the impacts of climate change on runoff and soil moisture in Australian catchments. Journal of Hydrology, 167, 121–147.

Chiew, F.H.S., Kirono, D.G.C., Kent, D.M., Frost, A.J., Charles, S.P., Timbal, B., Nguyen, K.C., and Fub, G., 2010. Comparison of runoff modelled using rainfall from different downscaling methods for historical and future climates. Journal of Hydrology, 387, 10–23.

Chow, V.T., Maidment, D.R., and Mays, L.W., 1988.Alied Hydrology. Tata McGraw-Hill Education (reprint edition).

Clarke LE, Edmonds JA, Jacoby HD, Pitcher H, Reilly JM, Richels R (2007) Scenarios of greenhouse gas emissions and atmospheric concentrations. Sub-report 2.1a of Synthesis and Assessment Product 2.1. Climate Change Science Program and the Subcommittee on Global Change Research, Washington DC.

Clarke L, Edmonds J, Krey V, Richels R, Rose S, Tavoni M (2010) International climate policy architectures, overview of the EMF 22 international scenarios. Energ Econ 31(sul 2),S64–S81.

Climate Variability and Change in Bangladesh Impacts, 2006. Vulnerability and Risks Published by CLIMATE CHANGE CELL, Component 4B of comprehensive disaster management programme CDMP.

Cohen, S.and Kulkarni, T., 2001. Water Management & Climate Change in the Okanagan Basin.Environment Canada & University of British Columbia.

Collier MA et.al., 2011. The CSIROMk3.6.0 Atmosphere-Ocean GCM, participation in CMIP5 and data publication. MODSIM 2011. Perth, 12-16.

Collins WJ et.al., 2011. Development and evaluation of an Earth System model-HadGEM2. GMD 4(4), 1051-1075.

Cunge, J.A., 1969, On the subject of a flood propogation method (Muskingum method), Journal of Hydraulics Research, International Association of Hydraulics Research, 7, no. 2, 205-230.

Davies, a. S., 2004.Urban water management vs. Climate change, impacts on cold region wastewater inflows. Climatic Change, 64, 103–126.

De Roo, A.P.J., Wesseling, C.G. and Van Deursen, W.P.A., 2000. Physically based river basin modelling within a GIS, The LISFLOOD model. Hydrological Processes, 14, 1981–1992

Dessai S, Lu XF, Hulme M., 2005. Limited sensitivity analysis of regional climate change probabilities for the 21st century. J Geophys Res Atmos, 110(D19), D19108.

Donatelli, M.; Campbell, G.S. 1997.A simple model to estimate global solar radiation.PANDA Project, Subproject 1, Series 1, Paper 26, ISCI, Bologna, IT.

Donner LJ et.al., 2011. The dynamical core, physical parameterizations, and basic simulation characteristics of the atmospheric component AM3 of the GFDL Global.

Dufresne JL et.al., 2013. Climate change projections using the IPSL-CM5 Earth System Model, from CMIP3 to CMIP5. Climate Dynamics, 1-43.

Dunne JP et.al. GFDL‘ ESM G l Coupled Climate-Carbon Earth System Models. Part I, Physical Formulation and Baseline Simulation Characteristics. J. Climate, 25, 6646-6665.

Eum, H., Simonovic,S.P.Kim, Y-O, 2010. Climate Change Impact Assessment Using K-Nearest Neighbor Weather Generator, Case Study of the Nakdong River Basin in Korea. Journal of Hydrologic Engineering, October.

Fowler, A., 1999. Potential climate change impacts on water resources in the Auckland Region (New Zealand). Clim. Res., 11, 221-245.

Fowler, H.J. and Ekström, M., 2009. Multi-model ensemble estimates of climate change impacts on UK seasonal precipitation extremes. Int. J. Climatol, 29, 385–416.

Fujino J, Nair R, Kainuma M, Masui T, Matsuoka Y (2006) Multigas mitigation analysis on stabilization scenarios using aim global model. The Energy Journal Special issue, 3,343–354.

Gain, K., Immerzeel W. W., F. C. Sperna Weiland, and M. F. P. Bierkens, 2011. Impact of climate change on the stream flow of the lower Brahmaputra, trends in high and low flows based on discharge-weighted ensemble modeling, Hydrol. Earth Syst. Sci., 1537.

Geng, S.; Auburn, J.; Brandstetter, E.; Li, B., 1988. A program to simulate meteorological variables, Documentation for SIMMETEO. Agronomy Report No. 204, University of California, Crop Extension, Davis, California, US.

Ghosh S. and Dutta, S, 2012. Impact of climate change on flood characteristics in Brahmaputra basin using a macro-scale distributed hydrological model, J. Earth Syst. Sci.121, No. 3, 637–657 ;Indian Academy of Sciences.

Giorgi F, 2008. A simple equation for regional climate change and associated uncertainty. J Clim 21(7),1589–1604.

Githui, F., Gitau, W., Mutua, F., and Bauwens, W., 2009. Climate Change Impact on SWAT Simulated Streamflow in Western Kenya. Int. J. Climatol, 29, 1823-1834.

Gosain, A.K., Mani, A., Dwivedi, C., 2009. Hydrological modelling literature review, Report No.1. Indo-Norwegian Institutional Cooperation Program 2009-2011.

Graham Wayn, 2013. "T B ‘ G R Concentration Pathways" skeptical science.

Grayson, R.B., Bloschl, G., and Moore, I.D., 1995. Distributed Parameter Hydrologic Modelling using vector elevation data, THALES and TAPES-C. In, Singh, V.P., (Ed.), Computer Models of Watershed Hydrology, 18. Water Resources Publications, Highlands Ranch, CO, 19, 669–696.

Grayson, R.B., More, I.D., and McMahon, T.A., 1992. Physically based hydrological modelling 1, A terrain based model for investigative purposes. Water Resour. Res., 28(10), 2639-2658.

Green, W.H. and G.A. Ampt. 1911. Studies on soil physics, 1. The flow of air and water through soils.Journal of Agricultural Sciences. 4, 11-24.

Guo,S. , Wang,J., Xiong,L., Ying,A., and Li, D., 2002. A macro-scale and semi-distributed monthly water balance model to predict climate change impacts in China . Journal of Hydrology, 268, 1–15.

Hargreaves, G.L., G.H. Hargreaves, and J.P. Riley. 1985. Agricultural benefits for Senegal River Basin. J. Irrig. And Drain. Engr. 111(2),113-124

Harris GR, Collins M, Sexton DMH, Murphy JM, Booth BBB, 2010. Probabilistic projections for 21st century European climate. Nat Hazards Earth Syst Sci 10(9),2009–2020. doi,10.5194/nhess-10-2009-2010

Harris GR, Sexton DMH, Booth BBB, Collins M, Murphy JM, Webb MJ, 2006. Frequency distributions of transient regional climate change from perturbed physics ensembles of general circulation model simulations. Clim Dynam, 27(4), 357–375

Hay, L. E., McCabe, Jr., G. J., Wolock, D. M., and Ayers, M. A., 1992, 'Use of Weather Types to Disaggregate General Circulation Model Predictions', J. Geophys. Res. 97, D3, 2781-2790.

Hulme, M. and T.R. Carter, 2000.The changing climate of Europe., Assessment of the Potential Effects of Climate Change in Europe [Parry, M.L. (ed.)]. Report of the ACACIA Concerted Action, UEA, Norwick, UK, 3, 350.

Hulme, M., Wigley, T.M.L., Barrow, E.M., Raper, S.C.B., Centella, A., Smith, S. andChipanshi, A. C., 2000. Using a Climate Scenario Generator for Vulnerability and Adaptation Assessments, MAGICC and SCENGEN Version 2.4 Workbook, Climate Research Unit,Norwich, UK, 52.

Hassell, D., Boorman, P., McDonald, R., and Hill, S., 2002. Climate Change Scenarios for the United Kingdom, The UKCIP02 Scientific Report. Tyndall Centre for Climate Change Research, School of Environmental Sciences, University of East Anglia, Norwich, UK. 120

Hibbard KA, Meehl G, Cox P, Friedlingstein P, 2007. A strategy for climate change stabilizationexperiments. Eos 88, 217–221.

Hulme, M., T. Jiang, and T.M.L. Wigley, 1995a, SCENGEN, A Climate Change SCENario GENerator, Software User Manual, Version 1.0. Climatic Research Unit, University of East Anglia,Norwich,38.

Hulme, M., S.C.B. Raper, and T.M.L. Wigley, 1995b, An integrated framework to address climate change (ESCAPE) and further developments of the global and regional climate modules (MAGICC). Energy Policy, 23, 347-355.

Hulme, M., Wigley, T.M.L., Barrow, E.M., Raper, S.C.B., Centella, A., Smith, S. and Chipanshi, A. C., 2000. Using a Climate Scenario Generator for Vulnerability and Adaptation Assessments, MAGICC and SCENGEN Version 2.4 Workbook, Climate Research Unit, Norwich, UK, 52.

Hulme, M.and Carter, T. R., 1999. Representing uncertainty in climate change scenarios and impact studies. In Carter, T. R., Hulme, M., and Viner, D. (eds.) Representing uncertainty in climate change scenarios and impact studies. ECLAT Report Number 1. CRU, Norwich, UK.

Huth R. 2002. Statistical downscaling of daily temperature in Central Europe. Journal of Climate 15, 1731–1742.

Immerzeel, W., 2008. Historical trends and future predictions of climate variability in the Brahmaputra basin, International, Journal Of Climatology, Int. J. Climatol., 28, 243–254.

IPCC AR4 WG2, 2007. Parry, M.L.; Canziani, O.F.; Palutikof, J.P.; van der Linden, P.J.; and Hanson, C.E., ed., Climate Change 2007. Impacts, Adaptation and Vulnerability, Contribution of Working Group II to the Fourth Assessment Report of the Intergovernmental Panel on Climate Change, Cambridge University Press, ISBN 978-0-521-88010-7 (pb, 978-0-521-70597-4).

IPCC Expert Meeting Report, 2007.Towards New Scenarios for Analysis of Emissions, Climate Change, Impacts, and Response Strategie, 19–21.

IPCC.Climate Change, 2001. The Scientific Basis. Contribution of Working Group I to the IPCC Third Assessment Report. 2001

Ishizaki Y, Shiogama H, Emori S, Yokohata T, Nozawa T, Ogura T, Abe M, Yoshimori M, Takahashi K, 2012. Temperature scaling pattern dependence on representative concentration pathway emission scenarios. Climatic Change, In revision

Islam, Z. and Gan, T., 2015.Hydrologic Modeling of the Blue River Basin Using NEXRAD Precipitation Data with a Semidistributed and a Fully Distributed Model.J. Hydrol. Eng. , 10.1061/(ASCE)HE.1943-5584.0001179 , 04015015.

Islam, Z. 2011a. A Review on Climate Change Modeling for Hydrological Impact Studies, Tech. Report, doi, 10.13140/2.1.1398.8648.

Islam, Z. 2011b. A Review on Physically Based Hydrologic Modeling, Tech. Report, doi, 10.13140/2.1.4544.5924

Ivanov, V.Y., Vivoni, E. R., Bras, R. L., and Entekhabi, D., 2004. Preserving high-resolution surface and rainfall data in operational-scale basin hydrology, a fully distributed aroach. Journal of Hydrology, 298(1-4), 80-111.

Jiang, T., Chen, Y.D., Xu, C.-Y., Chen, X., Chen, X., and Singh, V.P., 2007. Comparison of hydrological impacts of climate change simulated by six hydrological models in the Dongjiang Basin, South China. Journal of Hydrology, 336, 316–333

Jones P G, Thornton P K., 1993, A rainfall generator for agricultural alications in the tropics, Agricultural and Forest Meteorology, 63, 1-19.

Jones P G, Thornton P K., 1997. Spatial and temporal variability of rainfall related to a third-order Markov model, Agricultural and Forest Meteorology, 86, 127-138.

Jones, P.G. 1991. The CIAT Climate Database Version 3.41.Machine readable dataset.Centro Internacional de Agricultura Tropical (CIAT), Cali, Colombia.

Jones, P.G., and P.K. Thornton. 1999. Fitting a third-order Markov rainfall model to interpolated climate surfaces. Agricultural and Forest Meteorology, 97, 213-231.

Jones P. G., 2009. MarkSim_standalone.V2 for DSSAT users, Waen Associates, Gwynedd.

Jones, R.N., K.J. Hennessy, and D.J. Abbs, 1999. Climate Change Analysis Relevant to Jabiluka, ttachment C. Assessment of the Jabiluka Project, Report of the Supervising Scientist to the World Heritage Committee. Environment Australia, Canberra.

Jones, P.G., Thornton P.K., 2013 , Generating downscaled weather data from a suite of climate models for agricultural modelling alications, Agricultural System, 114, 1-5.

Kay, L. and Jones, D.A., 2010. Transient changes in flood frequency and timing in Britain under potential projections of climate change. Int. J. Climatol., (Published online in Wiley Online Library).

Kenny, G.J., R.A. Warrick, B.D. Campbell, G.C. Sims, M. Camilleri, P.D. Jamieson, N.D. Mitchell, H.G. McPherson, and M.J. Salinger, 2000. Investigating climate change impacts and thresholds, an alication of the CLIMPACTS integrated assessment model for New Zealand agriculture. Clim. Change, 46(1/2), 91-113.

Kerkhoven, E. and Gan T.Y., 2011. Unconditional Uncertainties of Historical and Simulated River Flows Subjected to Climate Change. Journal of Hydrology, 396 (1-2), 113-127.

Kerkhoven, E. and Gan, T.Y., 2008. Development of a Hydrologic Scheme for Use in Land Surface Models and its Alication to Climate Change in the Athabasca River Basin.Cold Region Atmospheric and Hydrologic Studies.The Mackenzie GEWEX Experience.

Kerkhoven, E. and Gan, T.Y., 2010. Differences and sensitivities in potential hydrologic impact of climate change to regional-scale Athabasca and Fraser River basins of the leeward and windward sides of the Canadian Rocky Mountains respectively. Climatic Change (published online) .

Kirkevag A, Iversen T, Seland O, debernard JB, Storelvmo T, Kristjansson JE , 2008. Aerosol-cloud-climate interaction in the climate model CAM-Oslo. Tellus A.

Kite, G.W., 1995.The SLURP Model. In, Singh, V.P., (Ed.), Computer Models of Watershed Hydrology, 17. Water Resources Publications, Highlands Ranch, CO, 15, 521-562.

Knox, J.C., 1993. Large increases in flood magnitude in response to modest changes in climate. Nature, 361, 430 - 432.

Knudsen, A., Thomson, A., and Refsgaard, J.C., 1986. WATBAL, A semi-distributed, physically based hydrological modelling system. Nordic Hydrology, 17, 347-362.

Kouwen, N. 2000. WATFLOOD/SPL9, Hydrological Model and Flood Forecasting System. Department of Civil Engineering, University of Waterloo, Waterloo, ON.

Kouwen, N., 1988, WATFLOOD. A micro-computer based flood forecasting system based on real-time weather radar. Canadian Water Resources Journal, 13, 62–77.

Kouwen, N., Mousavi, S. F., 2002. WATFLOOD/SPL9 hydrological model & flood forecasting system. In, Singh, P. and Frevert, D.K., (Ed.), Mathematical models of large watershed hydrology, 649-685.

Krasovskaia, I. and Gottschalk, L., 1992. Stability of River Flow Regimes. Nordic Hydrology, 23, 137-154.

Lettenmaier, D. P. and Gan, T. Y., 1990.Hydrologic sensitivity of the Sacremento-San Joaquin River Basin, California, to global warming. Water Resour. Res. 26, 69–86.

López-Moreno, J. I., Goyettea, S. and Benistona, M., 2008. Climate change prediction over complex areas, spatial variability of uncertainties and predictions over the Pyrenees from a set of regional climate models. Int. J. Climatol. 28, .1535–1550.

Lu, X., and Hulme, M., 2002. A short note on scaling GCM climate response pattern, Tech. Report, Prepared for AIACC regional study team.

Matula, C., 2005. Regional, seasonal and predictor-optimized downscaling to provide groups of local scale scenarios in the complex structured terrain of Austria. Meteorologische Zeitschrift, 14(1), 31-47.

May W, 2008. C — °C- z on" simulated by the ECHAM5/MPI-OM coupled climate model. Clim Dynam 31(2–3), 283–313.

Middelkoop H, Daamen K, Gellens D, Grabs W, Kwadijk JCJ, Lang H, Parmet BWAH, Schädler B, Schulla J, and Wilke K. , 2001. Impact of climate change on hydrological regimes and water resources management in the rhine Basin. Climatic Change, 49,105–128.

Miller N.L., Bashford K.E., Strem E. 2003. Potential impacts of climate change on California hydrology. Journal of the American Water Resources Association, 39(4), 771–784.

Mirza, M. Q. and Dixit A., 1997. Climate Change and Water Management in The Gbm Basins; Journal of water resources development. ISSN, 1027-0345.

Mirza, M. Q., 2002. Global warming and changes in the probability of occurrence of floods in Bangladesh and implications Global Environmental Change, 12, 127–138.

Mirza, M. Q., Warrick R. A. and Ericksen N. J., 2003. The implications of climate change on floods of the Ganges, Brahmaputra and Meghna rivers in Bangladesh, Climatic Change, 57, .287–318.

Mitchell JFB, Johns TC, Eagles M, Ingram WJ, Davis RA, 1999. Towards the construction of climate change scenarios. Clim Chang 41(3–4), 547–581

Mitchell TD ,2003. Pattern scaling - an examination of the accuracy of the technique for describing future climates. Clim Chang 60(3), .217–242

Mitchell, J.F.B., S. Manabe, Meleshko, and T. Tokioka, 1990, Equilibrium climate change - and its implications for the future. In, Climate Change, The IPCC Scientific Assessment. Report prepared by Working Group I [Houghton, J.T.,

G.J. Jenkins, and J.J. Ephraums(eds.)]. Cambridge University Press, Cambridge, United Kingdom, and New York, NY, USA, 131-164.

Mitchell, J.F.B., T.C. Johns, M. Eagles, W.J. Ingram, and R.A. Davis, 1999. Towards the construction of climate change scenarios. Clim. Change, 41, 547-581.

Monteith, J.L. 1977.Climate and the efficiency of crop production in Britain. Phil. Trans. Res. Soc. London Ser. B 281, 277-329.

Moriasi, D. N., Arnold, J. G., Van Liew, M. W., Bingner, R. L., Harmel, R. D., and Veith, T. L, 2007. Model Evaluation Guidelines for Systematic Quantification of Accuracy in Watershed Simulations.

Moss RH, Edmonds JA, Hibbard KA, Manning MR, Rose SK, van Vuuren DP, Carter TR, Emori S, Kainuma M, Kram T et al, 2010. The next generation of scenarios for climate change research and assessment. Nature 463,747–756

Murphy JM, Booth BBB, Collins M, Harris GR, Sexton DMH, Webb MJ, 2007. A methodology for probabilistic predictions of regional climate change from perturbed physics ensembles. Philos Trans R Soc A Math Phys Eng Sci 365(1857), 1993–2028.

Murphy, J.M., Hassell, D., Boorman, P., McDonald, R., and Hill, S., 2002. Climate Change Scenarios for the United Kingdom, The UKCIP02 Scientific Report. Tyndall Centre for Climate Change Research, School of Environmental Sciences, University of East Anglia, Norwich,UK. . 120.

Nash, L. and Gleick, P., 1991. Sensitivity of streamflow in the colorado basin to climatic changes. Journal of Hydrology, 125, 221-241.

Neitsch, S.L., Arnold, J.G., Kiniry, J.R., and Williams, J.R., 2005. Soil and Water Assessment Tool (SWAT), Theoretical Documentation.

Nemec, J. and Schaake, J., 1982. Sensitivity of water resources system to climate variation.Hydrol. Sci. J. 27, 327–343.

Nolihan, J, and Mahfouf, J., 1996. ISBA land surface parameterization scheme. Global and Planetary Change, 13, 145-159.

Nolihan, J, and Planton, S., 1989. A simple parameterization of land surface processes for meteorological models. Monthly Weather Review, 17.

Oglesby, R. J., and Saltzman, B., 1992, Equilibrium climate statistics of a GCM as a function of atmospheric carbon dioxide. Part I, geographic distributions of primary variables. Journal of Climate5, 66-92.

Oki T, Kanae S, 2006, Global Hydrological Cycles and World Water Resources. Science 313:1068–1072.

Orlowsky, B., Bothe, O., Fraedrich, K., Gerstengarbe, F.-W., and Zhu, X., 2010. Future Climates From Bias-Bootstraed Weather Analogs, An Alication to The Yangtze River Basin. Journal of Climate, 23, 3509-3524.

Palutikof, J.P., 1987. The Influence of Climate Change and Climatic Variability on the Hydrologic Regime and Water Resources in England and Wales.Proceedings of the Vancouver Symposium.IAHSPubl.no. 168.

Parry, M.L., T.R. Carter, and M. Hulme, 1996. What is a dangerous climate change? Global Environ. Change, 6, 1 -6.

Penlap EK, Matulla C, von Storch H, Kamga FM. 2004. Downscaling of GCM scenarios to assess precipitation changes in the little rainy season (March-June) in Cameroon. Climate Research 26, 85–96.

Pittock, A.B., 1993, Climate scenario development. I n, Modelling Change in Environmental Systems [Jakeman, A.J., M.B. Beck, and M.J. McAleer (eds.)]. John Wiley, Chichester, New York, 481-503.

Priestley, C.H.B. and R.J. Taylor. 1972. On the assessment of surface heat flux and evaporation using large-scale parameters. Mon. Weather Re100, 81-92.

Qian, Y., Ghan, S.J. and Leung, L.B., 2010. Downscaling hydroclimatic changes over the Western US based on CAM subgrid scheme and WRF regional climate simulations. Int. J. Climatol., 30, 675–693.

Qian, B., Gameda, S., Jong, R.D., Falloon, P. and Gornall, J., 2010. Comparing scenarios of Canadian daily climate extremes derived using a weather generator. Climatic Research, 41, 131–149.

Raisanen J, Ruokolainen L, 2006. Probabilistic forecasts of near-term climate change based on a resampling ensemble technique. Tellus Ser A Dyn Meteorol Oceanogr 58(4), .461–472

Ramaswamy, and T.C. Chen, 1997. Linear additivity of climate response for combined albedo and greenhouse perturbations.Geophys. Res. Lett., 24, 567-570.

Refsgaard, J.C., and Abbott, M.B., 1996. The role of distributed hydrological modelling in eater resources management, 1-16.

Riahi K, Grübler A, Nakicenovic N (2007) Scenarios of long-term socio-economic and environmental development under climate stabilization. Technol Forecast Soc Chang 74,887–935.

Ritchie, J.T. 1972. A model for predicting evaporation from a row crop with incomplete cover. Water Resour. Res. 8, 1204-1213.

Risbey, J.S., 1998. Sensitivities of water suly planning decisions to streamflow and climate scenario uncertainties. Water Policy, 1, 321-340.

Rossi, C. G., Dybala, T. J., Moriasi, D. N., Arnold, J. G., Amonett, C., and Marek, T., 2008. Hydrologic calibration and validation of the soil and water assessment tool for the Leon River watershed, Soil Water Conserv., 6, 533–541.

Rotmans, J., Hulme, M., and Downing, T. E., 1994, Climate-change implications for Europe – an alication of the ESCAPE model. Global Environmental Change4, 97-124.

Ruosteenoja K, Tuomenvirta H, Jylha K, 2007. GCM-based regional temperature and precipitation change estimates for Europe under four SRES scenarios alying a super-ensemble pattern-scaling method. Clim Chang 81(1), 193–208.

Sanderson BM, Knutti R, 2012. On the interpretation of constrained climate model ensembles. Geophys Res Lett 39.

Santer, B.D., T.M.L. Wigley, M.E. Schlesinger, and J.F.B.Mitchell, 1990, Developing Climate Scenarios from Equilibrium GCM results.Report No. 47, Max -Planck-Institut-für -Meteorologie, Hamburg, 29.

Schaake, J. C. and Liu, C., 1989. Development and alications of simple water balance models to understand the relationship between climate and water resources. New Directions for Surface Water Modelling (Proceedings of the Baltimore Symposium, May 1989) IAHS Publ. No. 181, 343–352.

Schlesinger, M.E., N. Andronova, A. Ghanem, S. Malyshev, T. Reichler, E. Rozanov, W. Wang, and F. Yang, 1997. Geographical Scenarios of Greenhouse Gas and AnthropogenicSulfate-Aerosol Induced Climate Changes. CRG manuscript, July 1997. University of Illinois, Department of Atmospheric Sciences, Urbana, IL, 85.

Schlesinger, M.E., S. Malyshev, E.Rozanov, F. Yang, N.G. Andronova, B. de Vries, A. Grübler, K. Jiang, T. Masui, T. Morita, J. Penner, W. Peer, A. Sankovski and Y. Zhang, 2000. Geographical distributions of temperature change for scenarios of greenhouse gas and sulfur dioxide emissions. Tech. Forecast. Soc. Change, 65, 167-193.

Schmidt GA et.al., 2006. Present day atmospheric simulations using GISS Model E, Comparison to in-situ, satellite and reanalysis data. J. Climate 19, 153-192.

Seidel, K. and Jaroslav Martinec and Michael F., 2000. Baumgartner; modelling runoff and impact of climate change in large himalayan basins, ICIWRM-2000. Roorkee, India.

Shackley, S., Young, P., Parkinson, S. and Wynne, B., 1998. Uncertainty, Complexity and Concepts of Good Science in Climate Change Modelling, Are GCMs the Best Tools? Climatic Change, 38 (2), 159-205.

Shen,C., and Phanikumar, M.S., 2010. A process-based, distributed hydrologic model based on a large-scale method for surface–subsurface coupling. Advances in Water Resources, 33, 1524–1541.

Sloan, P.G. and I.D. Moore. 1984. Modeling subsurface streamflow on steeply sloping forested watersheds. Water Resources Research. 20(12), 1815-1822.

Sloan, P.G., I.D. Moore, G.B. Coltharp, and J.D. Eigel. 1983. Modeling surface and subsurface stormflow on steeply-sloping forested watersheds. Water Resources Inst. Report 142. UniKentucky, Lexington.

Smith J.B, Pitts G., 1997. Regional climate change scenarios for vulnerability and adaptation assessments. Climatic Change, 36, 3–21.

Song Z, Qiao F, Song Y, 2012. Response of the equatorial basin-wide SST to wave mixing in a climate model, An amendment to tropical bias, J. Geophys. Res., 117.

Sorooshian, S. and Gupta, K., 1995. Model calibration, in, Computer Models of Watershed Hydrology, edited by, Singh, P., Water Resources Publications, Colorado, USA.

Souvignet, M., Gaese, H., Ribbe, L., Kretschmer, N. and Oyarzún, R., 2010.Statistical downscaling of precipitation and temperature in north-central Chile, an assessment of possible climate change impacts in an arid Andean watershed Statistical downscaling of precipitation and temperature in north-central Chile. Hydrological Sciences Journal, 55(1), 41-57.

Sushama, L., Laprise, R., Caya, D., Frigon, A., Slivitzky, M., 2006. Canadian RCM projected climate -change signal and its sensitivity to model errors. Int. J. Climatol., 26, 2141–2159

SWAT-CUP, 2012. SWAT Calibration and Uncertainty Programs, User Manual.

The representative concentration pathways, an overview, van Vuuren et. al, 2011. Climatic Change 109, 5–31.

Therrien, R., McLaren, R.G., Sudicky, E.A. and Panday, S.M. 2005. HydroGeoSphere, a three-dimensional numerical model describing fully-integrated subsurface and surface flow and solute transport, Groundwater Simulations Group, University of Waterloo, Waterloo, Ontario, Canada, 322.

Therrien, R., McLaren, R.G., Sudicky, E.A. and Panday, S.M. 2010. HydroGeoSphere, A Three-dimensional Numerical Model Describing Fully-integrated Subsurface and Surface Flow and Solute Transport. Groundwater Simulations Group, Waterloo, Canada.

Tolika,K., Maheras, P., Vafiadis, M., Flocasc, H.A., and Arseni-Papadimitrioua, A., 2007. Simulation of seasonal precipitation and raindays over Greece, a statistical downscaling technique based on artificial neural networks (ANNs). Int. J. Climatol., 27, 861–881.

USDA-SCS, Hydrology,1972. National Engineering Hand Book Sect. 4, Washington, DC, USDA-SCS.

USDA Soil Conservatopm service. 1972. National Engineering Handbook Section 4 Hydrology, 4-10.

Van der Knijff, J.M., Younis, J. and De Roo, A.P.J., 2010. LISFLOOD, a GIS-based distributed model for river basin scale water balance and flood simulation. International Journal of Geographical Information Science, 24(2), 189–212.

Van Vuuren DP, Den Elzen MGJ, Lucas PL, Eickhout B, Strengers BJ, Van Ruijven B, Wonink S, Van Houdt R, 2007. Stabilizing greenhouse gas concentrations at low levels, an assessment of reduction strategies and costs. Clim Chang 81,119–159.

Van Vuuren ,Jae Edmonds, Mikiko Kainuma, Keywan Riahi, Allison Thomson, Kathy Hibbard, George C. Hurtt, Tom Kram, Volker Krey, Jean-Francois Lamarque, Toshihiko Masui, Malte Meinshausen, Nebojsa Nakicenovic, Steven J. Smith, Steven K. Rose, 2011a,The representative concentration pathways, an overview, Climatic Change, 109, 5–31.

Van Vuuren DP, Riahi K, 2011b, The relationship between short-term emissions and long-term concentration targets—a letter. Climatic Change 104, Issue 3–4, 793–801.

Vieux, B.E., Gauer, N., 1994. Finite element modeling of storm water runoff using GRASS GIS. Microcomput. Civil Eng. 9(4), 263–270.

Vrac, M., Stein, M., and Hayhoe, K., 2007.Statistical downscaling of precipitation through nonhomogeneous stochastic weather typing. Climate research, 34, 169–184.

Wang, J., Yang, H., Li, L., Gourley, J. J., Sadiq, I. K., Yilmaz, K. K., Adler, R. F., Policelli, F. S., Habib, S., Irwn, D., Limaye, A. S., Korme, T. & Okello, L., 2011. The coupled routing and excess storage (CREST) distributed hydrological model. Hydrol.Sci. J. 56(1), .84–98.

Warrick, R. A., Bhuiya, A. H., and Mirza, M. Q., 1996, The greenhouse effect and climate change, in: The Implications of Climate and Sea-Level Change for Bangladesh, Kluwer Academic Publishers, Dordrecht, Briefing Document.

Watanabe et.al., 2010. Improved Climate Simulation by MIROC5, Mean States, Variability, and Climate Sensitivity. J. Climate., 23, 6312-6335.

Watanabe S et.al., 2011. MIROC-ESM2010. model description and basic results of CMIP5-20c3m experiments, Geoscientific Model Development, 4 (4), 845-872.

Watterson IG, 2008. Calculation of probability density functions for temperature and precipitation change under global warming. J Geophys Res Atmos, 113(D12), D12106

Watterson IG, Whetton PH, 2011. Joint PDFs for Australian climate in future decades and an idealized alication to wheat crop yield. Aust Meteorol Oceanogr J, 61, 221–230.

Whetton, P.H., A.M. Fowler, M.R. Haylock, and A.B. Pittock, 1993, Implications of climate change due to the enhanced greenhouse effect on floods and droughts in Australia. Climatic Change, 25(3-4), 289-317.

Whetton, P. H., Z. Long, and I.N. Smith, 1998. Comparison of simulated climate change under transient and stabilised increased CO2 conditions. In, Coupled Climate Modelling, Abstracts of Presentations at the Tenth Annual BMRC Modelling Workshop, BMRC, Melbourne [P. J. Meighen (ed.)]. BMRC Research Report, 69, Melbourne, Bureau of Meteorology Research Centre, 93-96.

Widmann M, Bretherton CS, Salath´e EP.,2003. Statistical precipitation downscaling over the Northwestern United States using numerically simulated precipitation as a predictor. Journal of Climate 16, 799–816.

Wilby RL, Dawson CW, Barrow EM., 2002. SDSM – a decision suort tool for the assessment of regional climate change impacts. Environmental and Modelling Software, 17, 145–157.

Wilby RL, Whitehead PG,Wade AJ, Butterfield D, Davis RJ,Watts G. 2006. Integrated modelling of climate change impacts on water resources and quality in a lowland catchment, River Kennet, UK. Journal of Hydrology, 330, 204–220.

Wilby, R. L., Troni, J., Biot, Y., Tedd, L., Hewitson, B. C., Smithe, D. M. and Suttonf, R. T., 2009.A review of climate risk information for adaptation and development planning. Int. J. Climatol., 29, 1193–1215.

Williams, J.R., 1969. Flood routing with variable travel time or variable storage coefficients. Trans. ASAE 12(1),100-103.

Williams, J.R. and R.W. Hann. 1973. HYMO, a problem-oriented computer language for building hydrologic models. Water Resour. Res., 8(1),79-85.

Wilks DS, Wilby RL. 1999. The weather generation game, A review of stochastic weather models. Progress in Physical Geography, 23,329–357.

Wu T, 2012. A Mass-Flux Cumulus Parameterization scheme for Largescale Models, Descriptions and Test with Observations. Clim. Dynam., 38, 725-744.

Xu, C., 2000. Modelling the Effects of Climate Change on Water Resources in Central Sweden. Water Resources Management, 14, 177-189.

Xu, C-Y.and Halldin, S., 1997. The Effect of Climate Change on River Flow and Snow Cover in the NOPEX Area Simulated by a Simple Water Balance Model. Nordic Hydrology, 28 (4/5), 273-282.

Yao, H., Scott, L., Guay, C. and Dillon, P., 2009. Hydrological impacts of climate change predicted for an inland lake catchment in Ontario by using monthly water balance analyses. Hydrol.Process. 23, 2368–2382.

Yukimoto S , 2012. A new global climate model of Metrological Research Institute, MRI-CGCM3- model description and basic performance. J. Meteorol. Soc. Jpn. 90a, .23-64.

Zhang, H., Huang, G.H., Wang, D. and Zhang, X., 2011. Uncertainty assessment of climate change impacts on the hydrology of small prairie wetlands. Journal of Hydrology, 396, .94–103.

Zorita, E. and von Storch, H.,1999. The Analog Method as a Simple Statistical Downscaling Technique, Comparison with more Complicated Methods. J. Climate 12, 2474–2489.

Appendix A

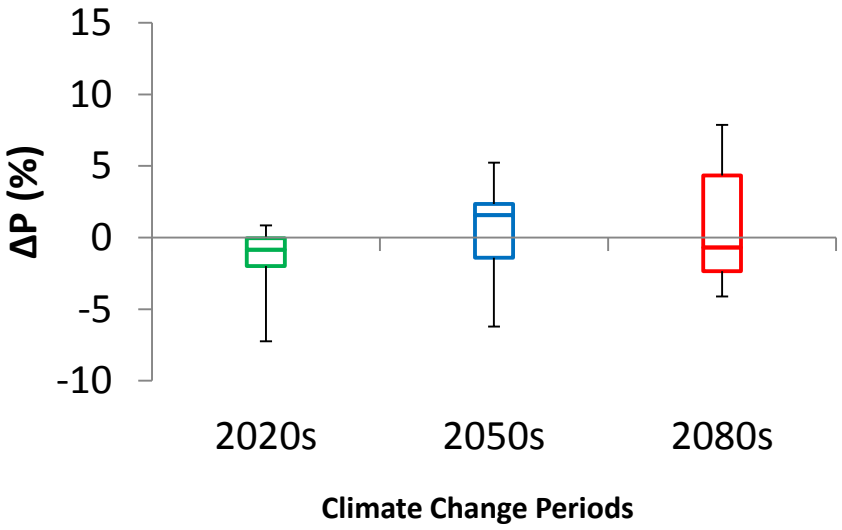

Figure A1: Box plot of change in precipitation for RCP 2.6

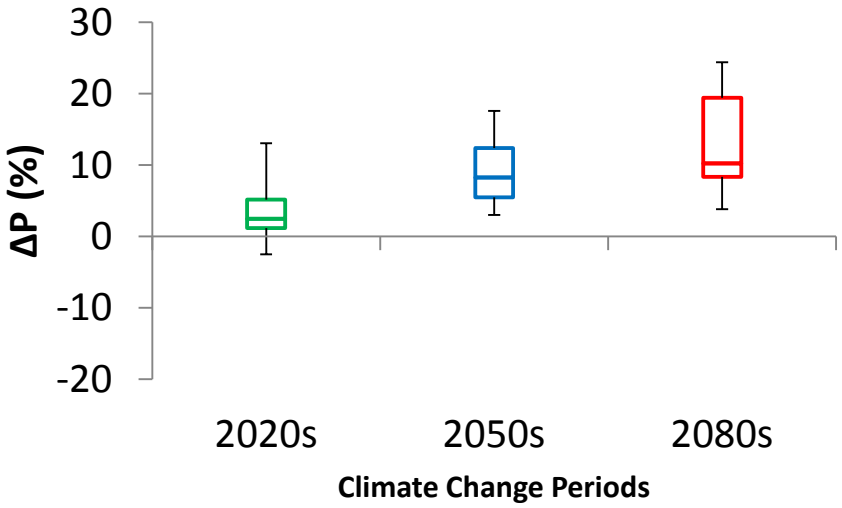

Figure A2: Box plot of change in precipitation for RCP 4.5

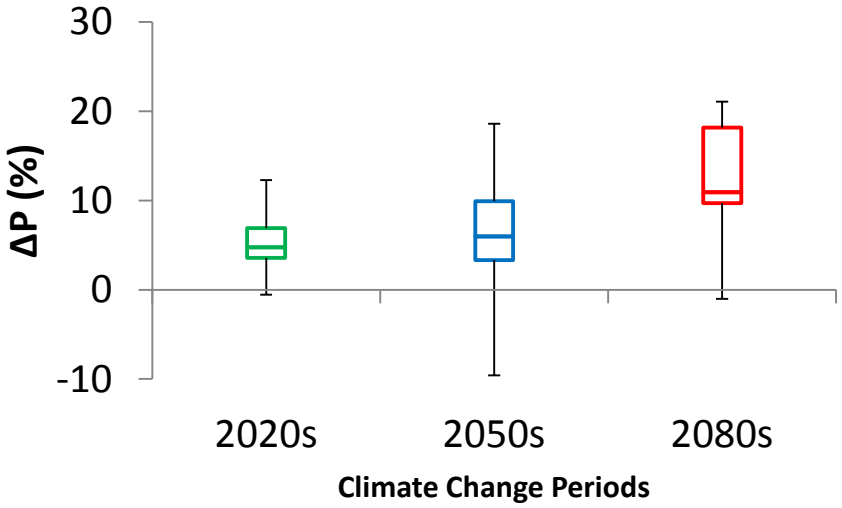

Figure A3: Box plot of change in precipitation for RCP 6.0

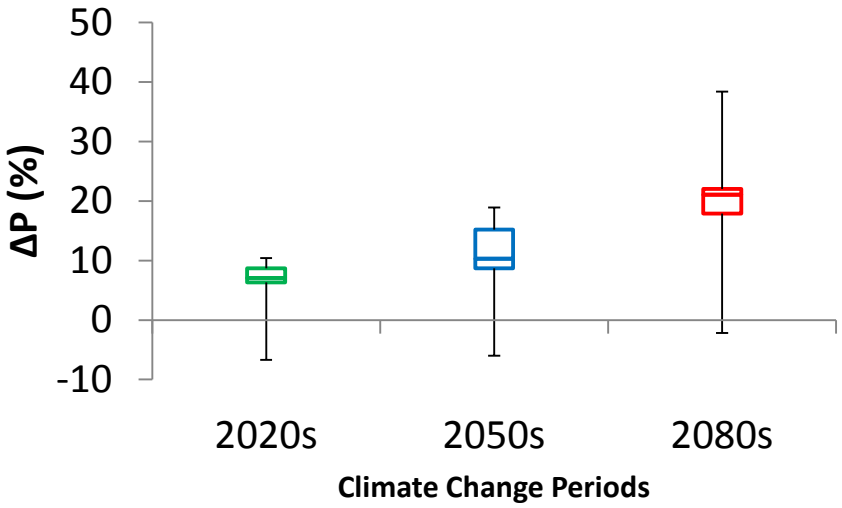

Figure A4: Box plot of change in precipitation for RCP 8.5

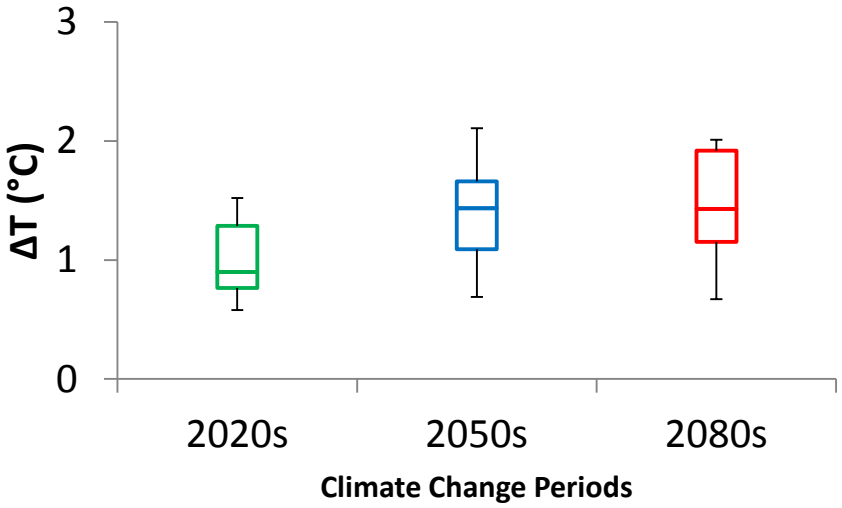

Figure A5: Box plot of change in temperature for RCP 2.6

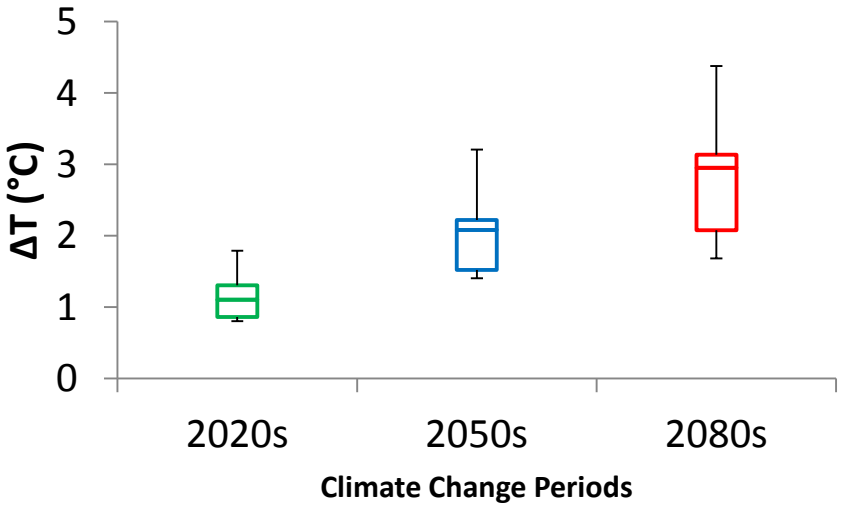

Figure A6: Box plot of change in temperature for RCP 4.5

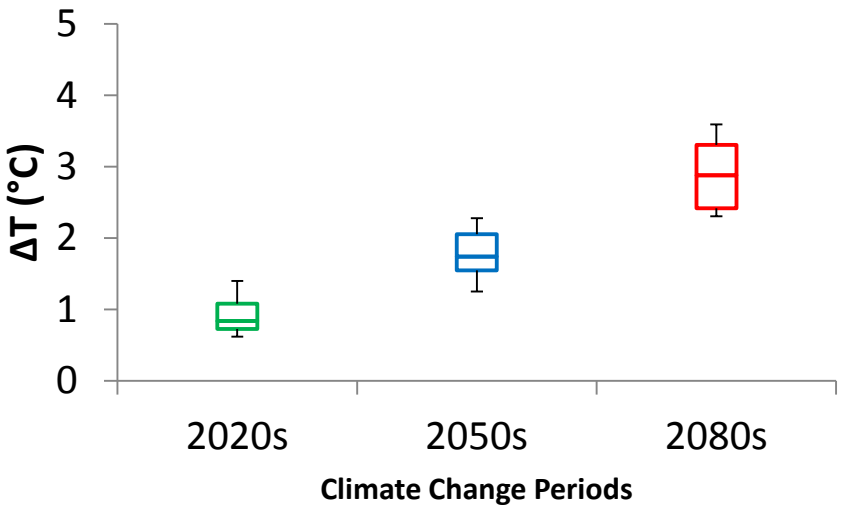

Figure A7: Box plot of change in temperature for RCP 6.0

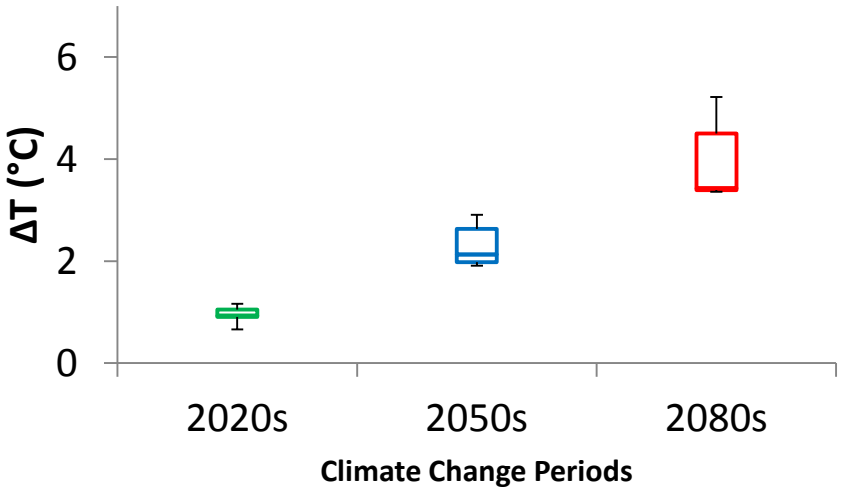

Figure A8: Box plot of change in temperature for RCP 8.5

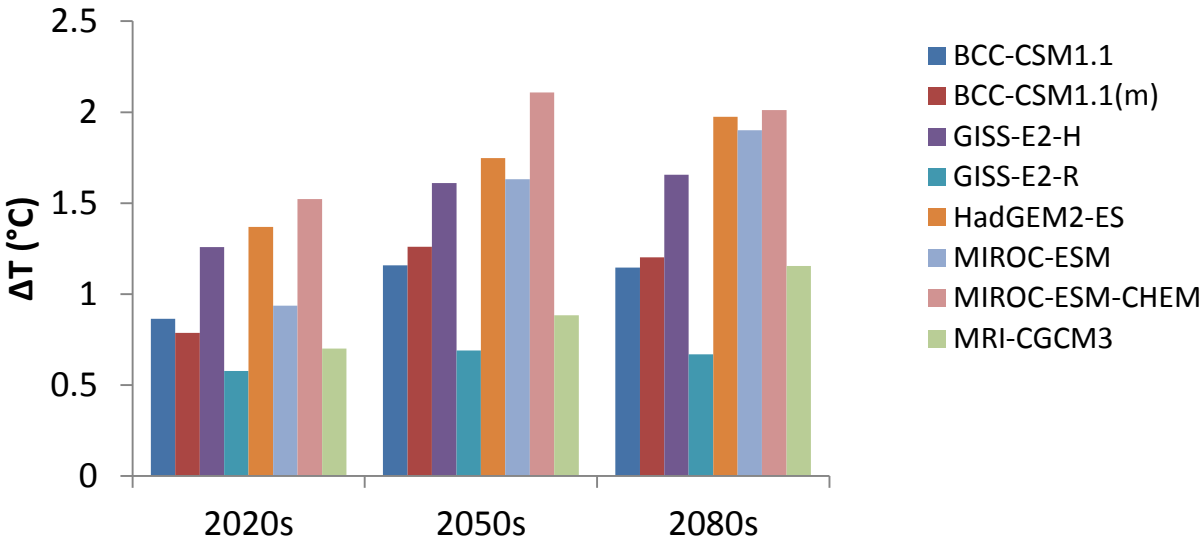

Figure A9: ΔT C G CM RCP 2080s

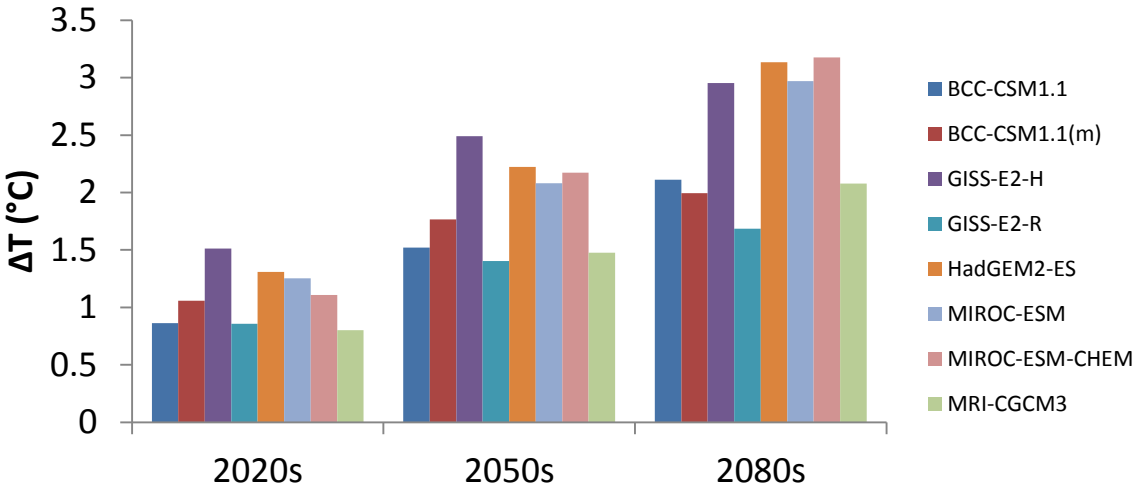

Figure A10: ΔT C G CM RCP 2080s

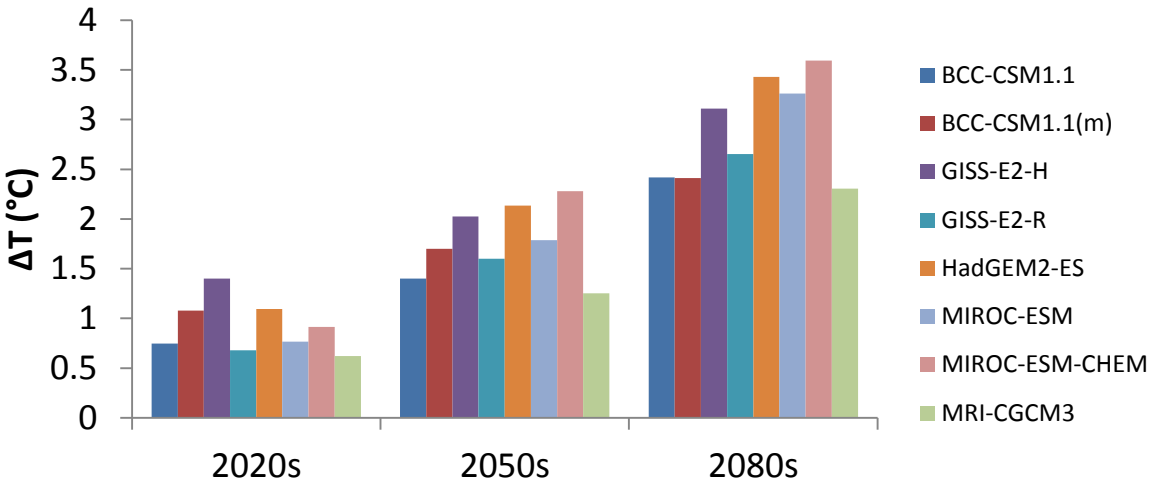

Figure A11: ΔT C G CM RCP 2080s

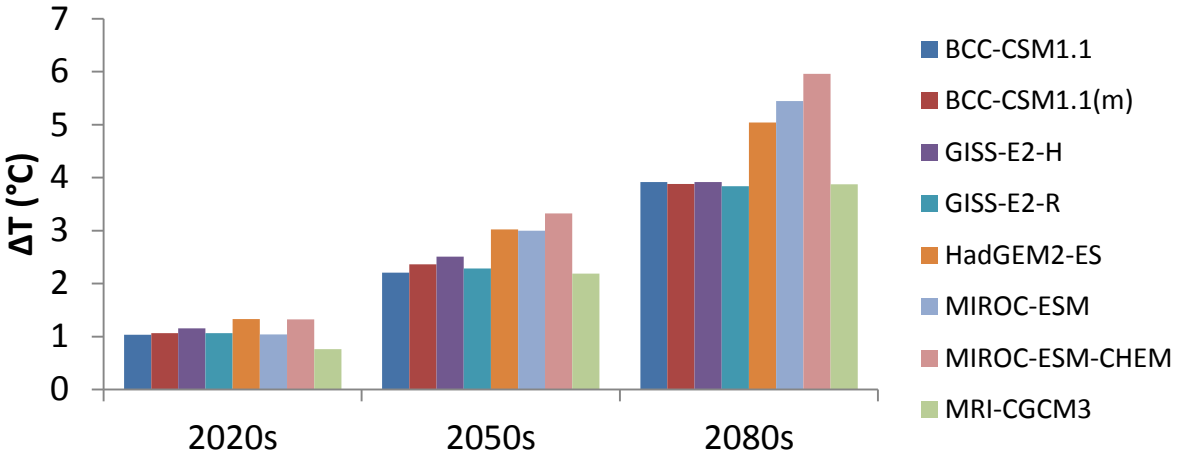

Figure A12: ΔT C G CM RCP 2080s

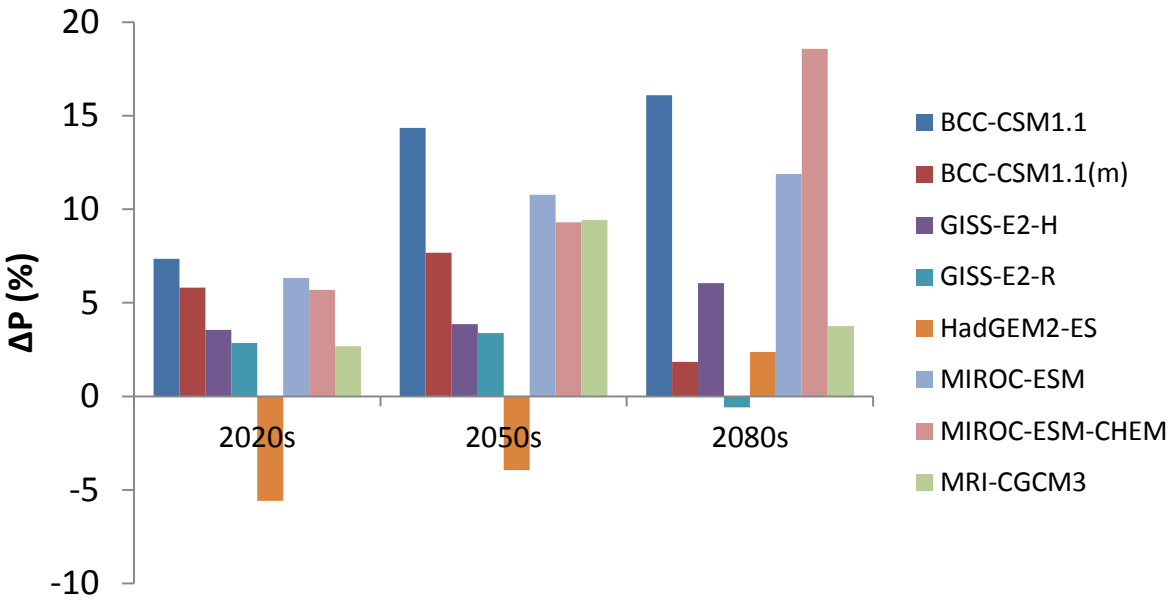

Figure A13: ΔP (%) bar chart of all the GCMs for RCP 2.6 in 2020s, 2050s and 2080s

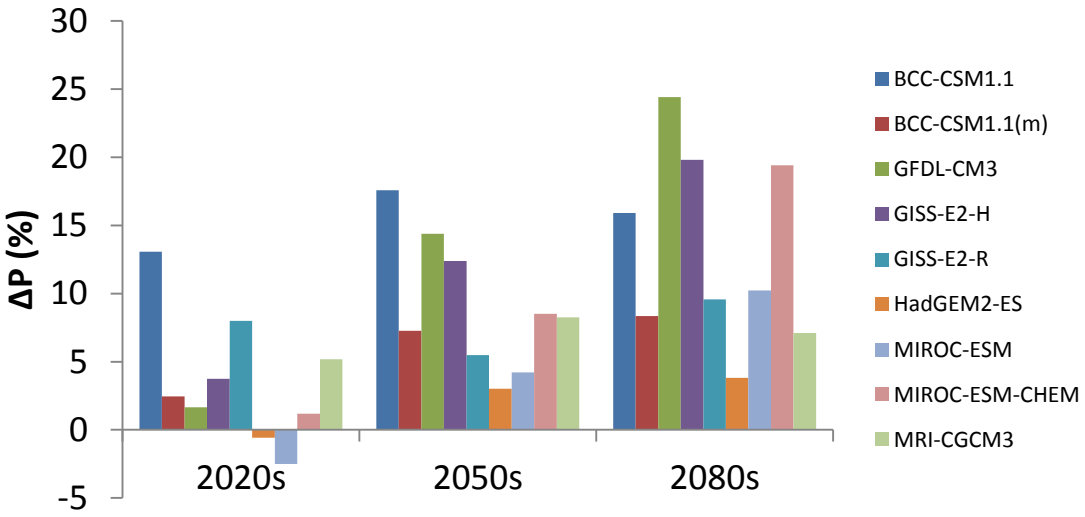

Figure A14: ΔP (%) bar chart of all the GCMs for RCP 4.5 in 2020s, 2050s and 2080s

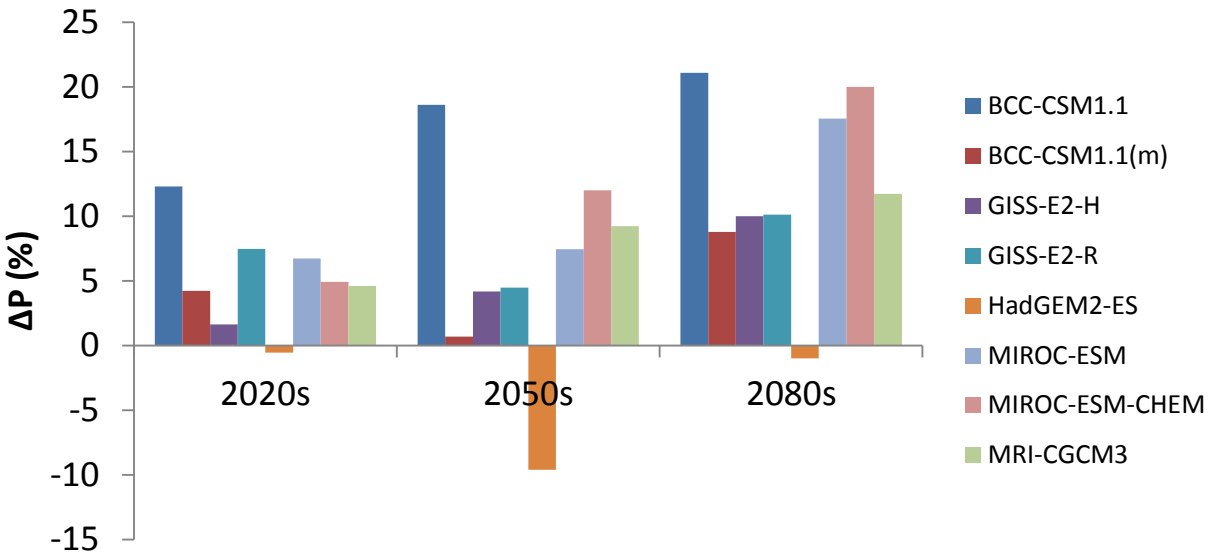

Figure A15: ΔP (%) bar chart of all the GCMs for RCP 6.0 in 2020s, 2050s and 2080s

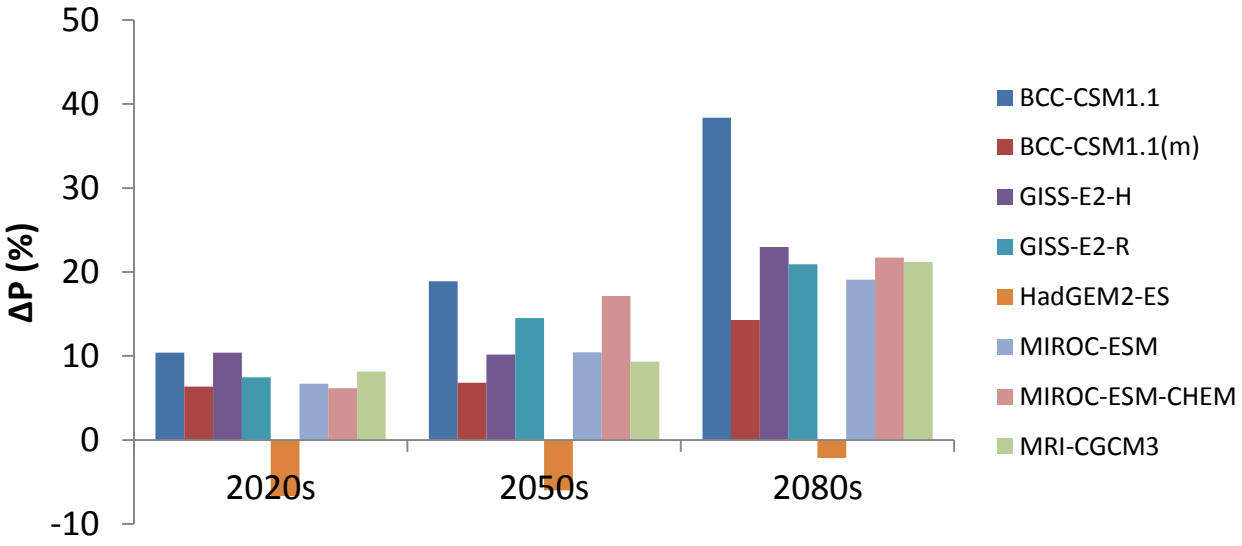

Figure A16: ΔP (%) bar chart of all the GCMs for RCP 8.5 in 2020s, 2050s and 2080s

Appendix B

Sensitivity analysis of mean discharge

Table B1: Flow at Bahadurabad station due to ΔT C ΔP=-20% to +40% (10% increment)

Month	**Average of ΔP% = -20**	**Average of ΔP% = -10**	**Average of ΔP% = 0**	**Average of ΔP% = 10**	**Average of ΔP% = 20**	**Average of ΔP% = 30**	**Average of ΔP% =40**
1	1408	1729	2059	2394	2730	3073	3413
2	1723	2097	2472	2849	3223	3593	3969
3	3818	4552	5286	6027	6770	7507	8236
4	8302	9933	11609	13316	15044	16798	18558
5	14773	17473	20225	23037	25891	28801	31774
6	23242	27663	32173	36745	41386	46118	50897
7	30363	36089	42014	48134	54357	60746	67195
8	29681	35396	41087	46765	52407	57978	63446
9	30383	36014	41588	47046	52444	57725	62977
10	21806	25558	29177	32734	36236	39678	43055
11	8249	9582	10890	12176	13437	14680	15895
12	2878	3387	3896	4407	4919	5425	5931
Annual Average	14719	17456	20206	22969	25737	28510	31279

Table B2: Flow at Bahadurabad station due to ΔT C ΔP=-20% to +40% (10% increment)

Month	Average of ΔP -20	Average of ΔP -10	Average of ΔP	Average of ΔP	Average of ΔP	Average of ΔP 3	Average of ΔP
1	1471	1823	2185	2558	2936	3315	3695
2	1930	2374	2834	3289	3750	4208	4662
3	3838	4668	5509	6363	7213	8060	8913
4	7304	8781	10295	11856	13468	15127	16818
5	14247	16895	19570	22280	25005	27759	30544
6	20234	24473	28837	33327	37915	42613	47398
7	29189	34807	40589	46494	52498	58587	64741
8	28849	34550	40243	45919	51545	57128	62609
9	29692	35305	40823	46236	51556	56804	61964
10	22345	26271	30077	33793	37460	41041	44592
11	8708	10161	11586	12996	14385	15750	17092
12	3012	3561	4117	4676	5238	5798	6358
Annual Average	14235	16972	19722	22482	25247	28016	30782

Table B3: Flow at Bahadurabad station due to ΔT C ΔP=-20% to +40% (10% increment)

Month	Average of ΔP -20	Average of ΔP -10	Average of ΔP	Average of ΔP	Average of ΔP	Average of ΔP 3	Average of ΔP
1	1527	1906	2301	2703	3110	3522	3939
2	2109	2622	3145	3674	4209	4748	5288
3	3545	4337	5155	5997	6863	7741	8629
4	7272	8781	10338	11925	13532	15166	16814
5	12482	15092	17754	20453	23194	25955	28738
6	18267	22239	26344	30579	34914	39384	43927
7	28226	33759	39470	45295	51232	57218	63294
8	28014	33639	39348	45035	50676	56254	61804
9	28892	34525	40030	45450	50760	56030	61174
10	22146	26130	29986	33751	37455	41091	44673
11	8821	10332	11836	13320	14789	16239	17677
12	3030	3598	4174	4753	5337	5923	6506
Annual Average	13694	16413	19157	21911	24672	27439	30205

Table B4: Flow at Bahadurabad station due to ΔT C ΔP=-20% to +40% (10% increment)

Month	Average of ΔP -20	Average of ΔP -10	Average of ΔP	Average of ΔP	Average of ΔP	Average of ΔP 3	Average of ΔP
1	1565	1967	2387	2818	3259	3703	4153
2	2116	2650	3200	3769	4350	4942	5541
3	3637	4435	5253	6097	6954	7834	8733
4	7395	8966	10589	12248	13950	15663	17383
5	10302	12709	15200	17755	20374	23052	25781
6	17059	20902	24870	28928	33075	37318	41633
7	27496	32997	38635	44399	50280	56232	62249
8	27139	32720	38394	44068	49706	55292	60879
9	27991	33591	39114	44583	49943	55217	60400
10	21543	25515	29414	33189	36893	40557	44125
11	8792	10332	11859	13371	14864	16349	17821
12	3064	3653	4248	4849	5452	6062	6670
Annual Average	13175	15870	18597	21340	24092	26852	29614

AppendixC

Analysis of Mean Discharge- 2020s (2010-2030)

Table C1: Discharge (m^3/s) for all the six scenarios in 2020s

	Observed (1981-2010)	Swat (Nasa power)1981-2010	Swat (Worldclim) 1961-2005	Warmest(MIROC-ESM-CHEM RCP 8.5)	Coolest(GISS-E2-R RCP 2.6)	Driest(HadGEM2-ES RCP 8.5)	Wettest(BCC-CSM1.1 RCP 8.5)	Mod Warm (GISS-E2-H RCP 4.5)	Mod Wet (MRI-CGCM3 RCP 6)
Jan	5692.74	2058.95	227.23	334.87	170.75	94.67	348.91	228.72	189.32
Feb	4620.01	2472.41	262.72	394.10	175.91	20.26	332.64	198.85	331.78
Mar	5348.66	5285.60	697.23	979.51	1149.86	401.35	895.56	1276.26	1097.87
Apr	9697.71	11609.37	2091.67	3315.93	3584.63	2268.37	2954.48	3572.07	3329.37
May	16728.98	20225.33	9022.37	17044.07	13415.37	11330.11	11448.78	17575.93	11694.93
Jun	31039.59	32173.00	26545.67	30070.74	30422.96	25357.78	28421.11	30078.15	32032.33
Jul	48707.46	42014.00	37704.00	46491.11	39510.00	35725.56	42264.81	40131.48	43015.00
Aug	43420.81	41087.33	40981.33	47827.41	36402.59	40230.37	44104.81	41522.22	42404.00
Sep	40124.35	41588.33	31076.67	29910.37	27264.81	28132.96	34541.11	30149.63	33544.67
Oct	26920.65	29177.33	14670.67	13315.56	13151.85	15162.22	14896.67	15908.15	14886.33
Nov	13699.61	10889.97	4224.77	3153.41	3731.67	3425.89	5445.81	4029.96	4638.03
Dec	7979.98	3895.97	832.16	781.99	694.64	649.21	1272.64	799.93	869.79

Table C2: Discharge (m^3/s) for all the six scenarios in 2020s

	Observed (1981-2010)	Swat (Nasa power)1981-2010	Swat (Worldclim) 1961-2005	Warmest(MIROC-ESM-CHEM RCP 8.5)	Coolest(GISS-E2-R RCP 2.6)	Driest(HadGEM2-ES RCP 8.5)	Wettest(BCC-CSM1.1 RCP 8.5)	Mod Warm (GISS-E2-H RCP 4.5)	Mod Wet (MRI-CGCM3 RCP 6)
Mean Annual	21165.05	20206.47	14028.04	16134.92	14139.59	13566.56	15577.28	15455.95	15669.45
Mean Dry Season (Dec-May)	8344.68	7591.27	2188.89	3808.41	3198.53	2460.66	2875.50	3941.96	2918.84
Mean Wet Season (June-Nov)	33985.41	32821.66	25867.18	28461.43	25080.65	24672.46	28279.06	26969.93	28420.06

Table C3: Change in Discharge (%) for all the six scenarios in 2020s

	Warmest (MIROC-ESM-CHEM RCP 8.5)	**Coolest (GISS-E2-R RCP 2.6)**	**Driest (HadGEM2-ES RCP 8.5)**	**Wettest (BCC-CSM1.1 RCP 8.5)**	**Mod Warm (GISS-E2-H RCP 4.5)**	**Mod Wet (MRI-CGCM3 RCP 6)**
Jan	47.37	-24.86	-58.34	53.55	0.66	-16.68
Feb	50.01	-33.04	-92.29	26.62	-24.31	26.29
Mar	40.49	64.92	-42.44	28.45	83.05	57.46
Apr	58.53	71.38	8.45	41.25	70.78	59.17
May	88.91	48.69	25.58	26.89	94.80	29.62
Jun	13.28	14.61	-4.47	7.06	13.31	20.67
Jul	23.31	4.79	-5.25	12.10	6.44	14.09
Aug	16.71	-11.17	-1.83	7.62	1.32	3.47
Sep	-3.75	-12.27	-9.47	11.15	-2.98	7.94
Oct	-9.24	-10.35	3.35	1.54	8.44	1.47
Nov	-25.36	-11.67	-18.91	28.90	-4.61	9.78
Dec	-6.03	-16.53	-21.98	52.93	-3.87	4.52

Table C4: Ratios (Projected flow for different scenarios/Base flow (Worldclim))of Discharge for all the six scenarios in 2020s.

	Warmest (MIROC-ESM-CHEM RCP 8.5)	Coolest (GISS-E2-R RCP 2.6)	Driest (HadGEM2-ES RCP 8.5)	Wettest (BCC-CSM1.1 RCP 8.5)	Mod Warm (GISS-E2-H RCP 4.5)	Mod Wet (MRI-CGCM3 RCP 6)
Jan	1.4737	0.7514	0.4166	1.5355	1.0066	0.8332
Feb	1.5001	0.6696	0.0771	1.2662	0.7569	1.2629
Mar	1.4049	1.6492	0.5756	1.2845	1.8305	1.5746
Apr	1.5853	1.7138	1.0845	1.4125	1.7078	1.5917
May	1.8891	1.4869	1.2558	1.2689	1.9480	1.2962
Jun	1.1328	1.1461	0.9553	1.0706	1.1331	1.2067
Jul	1.2331	1.0479	0.9475	1.1210	1.0644	1.1409
Aug	1.1671	0.8883	0.9817	1.0762	1.0132	1.0347
Sep	0.9625	0.8773	0.9053	1.1115	0.9702	1.0794
Oct	0.9076	0.8965	1.0335	1.0154	1.0844	1.0147
Nov	0.7464	0.8833	0.8109	1.2890	0.9539	1.0978
Dec	0.9397	0.8347	0.7802	1.5293	0.9613	1.0452

Table C5: Adjusted discharge (m^3/s) for all the six scenarios in 2020s

	Observed	Warmest (MIROC-ESM-CHEM RCP 8.5)	Coolest (GISS-E2-R RCP 2.6)	Driest (HadGEM2-ES RCP 8.5)	Wettest (BCC-CSM1.1 RCP 8.5)	Mod Warm (GISS-E2-H RCP 4.5)	Mod Wet (MRI-CGCM3 RCP 6)
Jan	5692.74	8389.21	4277.65	2371.71	8741.05	5730.04	4743.03
Feb	4620.01	6930.54	3093.47	356.34	5849.75	3496.81	5834.54
Mar	5348.66	7514.19	8820.96	3078.88	6870.16	9790.58	8422.13
Apr	9697.71	15373.81	16619.61	10516.97	13698.02	16561.40	15436.12
May	16728.98	31602.56	24874.34	21007.92	21227.95	32588.71	21684.36
Jun	31039.59	35161.42	35573.27	29650.60	33232.52	35170.08	37455.09
Jul	48707.46	60058.99	51040.52	46151.63	54599.30	51843.38	55568.42
Aug	43420.81	50674.41	38569.51	42625.14	46730.22	43993.90	44928.16
Sep	40124.35	38618.50	35202.71	36323.62	44597.44	38927.42	43310.89
Oct	26920.65	24434.02	24133.63	27822.65	27335.36	29191.43	27316.40
Nov	13699.61	10225.52	12100.64	11109.10	17659.09	13067.92	15039.71
Dec	7979.98	7498.86	6661.20	6225.63	12203.96	7670.91	8340.80

Table C6: Adjusted discharge (m^3/s) for all the six scenarios in 2020s

	Observed	Warmest (MIROC-ESM-CHEM RCP 8.5)	Coolest (GISS-E2-R RCP 2.6)	Driest (HadGEM2-ES RCP 8.5)	Wettest (BCC-CSM1.1 RCP 8.5)	Mod Warm (GISS-E2-H RCP 4.5)	Mod Wet (MRI-CGCM3 RCP 6)
Mean Annual	21165.05	24706.84	21747.29	19770.02	24395.40	24002.71	24006.64
Mean Dry Season (Dec-May)	8344.68	12884.86	10724.54	7259.57	11431.82	12639.74	10743.50
Mean Wet Season (June-Nov)	33985.41	36528.81	32770.05	32280.46	37358.99	35365.69	37269.78

Analysis of Mean Discharge- 2050s (2040-2069)

Table C7: Discharge (m^3/s) for all the six scenarios in 2050s

	Observed (1981-2010)	Swat (Nasa power) 1981-2010	Swat (Worldclim) 1961-2005	Warmest(MIROC-ESM-CHEM RCP 8.5)	Coolest(GISS-E2-R RCP 2.6)	Driest(HadGEM2-ES RCP 8.5)	Wettest(BCC-CSM1.1 RCP 8.5)	Mod Warm (GISS-E2-H RCP 4.5)	Mod Wet (MRI-CGCM3 RCP 6)
Jan	5692.74	2058.95	227.23	334.13	113.51	61.40	352.64	333.39	200.75
Feb	4620.01	2472.41	262.72	501.41	149.46	8.13	880.45	779.98	337.42
Mar	5348.66	5285.60	697.23	987.03	1529.46	606.34	1571.17	2860.80	1239.53
Apr	9697.71	11609.37	2091.67	5567.63	3885.87	2950.53	3281.90	8990.13	3856.87
May	16728.98	20225.33	9022.37	23540.67	19011.67	15505.00	16496.00	29737.67	12138.57
Jun	31039.59	32173.00	26545.67	36016.33	33729.33	30995.00	33558.00	39009.67	31778.00
Jul	48707.46	42014.00	37704.00	56336.67	39207.00	40622.00	53149.00	47342.67	42851.67
Aug	43420.81	41087.33	40981.33	48829.33	35912.00	39922.67	52784.67	42513.00	44113.67
Sep	40124.35	41588.33	31076.67	27484.33	24143.33	27793.67	34782.33	31717.00	34035.33
Oct	26920.65	29177.33	14670.67	10382.00	10624.53	11898.67	12872.67	14985.33	14787.33
Nov	13699.61	10889.97	4224.77	2088.90	2642.37	2239.37	3182.63	3738.67	4653.50
Dec	7979.98	3895.97	832.16	491.50	417.59	413.38	684.50	965.22	866.65

Table C8: Discharge (m^3/s) for all the six scenarios in 2050s

	Observed (1981-2010)	Swat (Nasa power) 1981-2010	Swat (Worldclim) 1961-2005	Warmest(MIROC-ESM-CHEM RCP 8.5)	Coolest(GISS-E2-R RCP 2.6)	Driest(HadGEM2-ES RCP 8.5)	Wettest(BCC-CSM1.1 RCP 8.5)	Mod Warm (GISS-E2-H RCP 4.5)	Mod Wet (MRI-CGCM3 RCP 6)
Mean Annual	21165.05	20206.47	14028.04	17713.33	14280.51	14418.01	17799.66	18581.13	15904.94
Mean Dry Season (Dec-May)	8344.68	7591.27	2188.89	5237.06	4184.59	3257.46	3877.78	7277.87	3106.63
Mean Wet Season (June-Nov)	33985.41	32821.66	25867.18	30189.59	24376.43	25578.56	31721.55	29884.39	28703.25

Table C9: Ratios (Projected flow for different scenarios/Base flow (Worldclim))of Discharge for all the six scenarios in 2050s.

	Warmest (MIROC-ESM-CHEM RCP 8.5)	Coolest (GISS-E2-R RCP 2.6)	Driest (HadGEM2-ES RCP 8.5)	Wettest (BCC-CSM1.1 RCP 8.5)	Mod Warm (GISS-E2-H RCP 4.5)	Mod Wet (MRI-CGCM3 RCP 6)
Jan	1.4704	0.4995	0.2702	1.5519	1.4672	0.8835
Feb	1.9086	0.5689	0.0310	3.3514	2.9689	1.2844
Mar	1.4157	2.1936	0.8696	2.2535	4.1031	1.7778
Apr	2.6618	1.8578	1.4106	1.5690	4.2981	1.8439
May	2.6091	2.1072	1.7185	1.8283	3.2960	1.3454
Jun	1.3568	1.2706	1.1676	1.2642	1.4695	1.1971
Jul	1.4942	1.0399	1.0774	1.4096	1.2556	1.1365
Aug	1.1915	0.8763	0.9742	1.2880	1.0374	1.0764
Sep	0.8844	0.7769	0.8944	1.1192	1.0206	1.0952
Oct	0.7077	0.7242	0.8111	0.8774	1.0214	1.0080
Nov	0.4944	0.6254	0.5301	0.7533	0.8849	1.1015
Dec	0.5906	0.5018	0.4968	0.8226	1.1599	1.0415

Table C10: Adjusted discharge (m^3/s) for all the six scenarios in 2050s

	Observed	Warmest (MIROC-ESM-CHEM RCP 8.5)	Coolest (GISS-E2-R RCP 2.6)	Driest (HadGEM2-ES RCP 8.5)	Wettest (BCC-CSM1.1 RCP 8.5)	Mod Warm (GISS-E2-H RCP 4.5)	Mod Wet (MRI-CGCM3 RCP 6)
Jan	5692.736	8370.668	2843.721	1538.149	8834.472	8352.13	5029.265
Feb	4620.013	8817.585	2628.399	142.9936	15483.28	13716.46	5933.785
Mar	5348.659	7571.863	11733.03	4651.412	12052.95	21946.16	9508.824
Apr	9697.707	25813.52	18016.25	13679.72	15216.05	41681.44	17881.8
May	16728.98	43648.33	35250.81	28748.86	30586.34	55138.61	22506.93
Jun	31039.59	42113.54	39439.38	36242.15	39239.04	45613.62	37157.7
Jul	48707.46	72777.85	50649.1	52477.05	68659.9	61159.06	55357.42
Aug	43420.81	51735.97	38049.72	42299.12	55926.75	45043.65	46739.6
Sep	40124.35	35486.14	31172.44	35885.54	44908.89	40951.11	43944.41
Oct	26920.65	19050.95	19496	21834.03	23621.32	27498.06	27134.73
Nov	13699.61	6773.656	8568.377	7261.573	10320.3	12123.34	15089.86
Dec	7979.978	4713.227	4004.437	3964.097	6564.028	9255.985	8310.751

Table C11: Adjusted discharge (m^3/s) for all the six scenarios in 2050s

	Observed	Warmest (MIROC-ESM-CHEM RCP 8.5)	Coolest (GISS-E2-R RCP 2.6)	Driest (HadGEM2-ES RCP 8.5)	Wettest (BCC-CSM1.1 RCP 8.5)	Mod Warm (GISS-E2-H RCP 4.5)	Mod Wet (MRI-CGCM3 RCP 6)
Mean Annual	21165.05	27239.44	21820.97	20727.06	27617.78	31873.30	24549.59
Mean Dry Season (Dec-May)	8344.68	16489.20	12412.77	8787.54	14789.52	25015.13	11528.56
Mean Wet Season (June-Nov)	33985.41	37989.69	31229.17	32666.58	40446.03	38731.47	37570.62

Analysis of Mean Discharge- 2080s (2070-2099)

Table C12: Discharge (m^3/s) for all the six scenarios in 2080s

	Observed (1981-2010)	Swat (Nasa power) 1981-2010	Swat (Worldclim) 1961-2005	Warmest(MIROC-ESM-CHEM RCP 8.5)	Coolest(GISS-E2-R RCP 2.6)	Driest(HadGEM2-ES RCP 8.5)	Wettest(BCC-CSM1.1 RCP 8.5)	Mod Warm (GISS-E2-H RCP 4.5)	Mod Wet (MRI-CGCM3 RCP 6)
Jan	5692.74	2058.95	227.23	297.77	122.71	35.87	1010.44	312.86	213.89
Feb	4620.01	2472.41	262.72	375.25	447.95	18.94	2936.40	1500.75	396.43
Mar	5348.66	5285.60	697.23	2748.67	2175.00	1491.56	2894.50	4139.87	1083.29
Apr	9697.71	11609.37	2091.67	9340.57	6038.70	7462.17	5783.90	15613.33	3748.13
May	16728.98	20225.33	9022.37	24563.67	22503.00	26679.00	23537.67	34814.67	12254.10
Jun	31039.59	32173.00	26545.67	45449.00	35537.67	39377.00	41685.00	44785.00	32833.67
Jul	48707.46	42014.00	37704.00	57813.33	35144.33	46866.67	67040.00	48410.00	42907.33
Aug	43420.81	41087.33	40981.33	44627.33	30405.33	41380.00	56594.67	39865.67	43288.00
Sep	40124.35	41588.33	31076.67	23292.00	22786.00	26225.00	32229.67	27812.00	34093.67
Oct	26920.65	29177.33	14670.67	7722.63	9599.90	8958.47	10185.00	12621.67	14978.33
Nov	13699.61	10889.97	4224.77	1395.10	1765.27	1490.87	2436.10	2986.67	4562.63
Dec	7979.98	3895.97	832.16	370.91	281.48	271.58	1855.30	820.13	868.18

Table C13: Discharge (m^3/s) for all the six scenarios in 2080s

	Observed (1981-2010)	Swat (Nasa power) 1981-2010	Swat (Worldclim) 1961-2005	Warmest(MIROC-ESM-CHEM RCP 8.5)	Coolest(GISS-E2-R RCP 2.6)	Driest(HadGEM2-ES RCP 8.5)	Wettest(BCC-CSM1.1 RCP 8.5)	Mod Warm (GISS-E2-H RCP 4.5)	Mod Wet (MRI-CGCM3 RCP 6)
Mean Annual	21165.05	20206.47	14028.04	18166.35	13900.61	16688.09	20682.39	19473.55	15935.64
Mean Dry Season (Dec-May)	8344.68	7591.27	2188.89	6282.81	5261.47	5993.19	6336.37	9533.60	3094.00
Mean Wet Season (June-Nov)	33985.41	32821.66	25867.18	30049.90	22539.75	27383.00	35028.41	29413.50	28777.27

Table C14: Change in Discharge (%) for all the six scenarios in 2080s

	Warmest (MIROC-ESM-CHEM RCP 8.5)	Coolest (GISS-E2-R RCP 2.6)	Driest (HadGEM2-ES RCP 8.5)	Wettest (BCC-CSM1.1 RCP 8.5)	Mod Warm (GISS-E2-H RCP 4.5)	Mod Wet (MRI-CGCM3 RCP 6)
Jan	31.04	-46.00	-84.21	344.67	37.68	-5.87
Feb	42.84	70.51	-92.79	1017.71	471.25	50.90
Mar	294.23	211.95	113.93	315.14	493.76	55.37
Apr	346.56	188.70	256.76	176.52	646.45	79.19
May	172.25	149.41	195.70	160.88	285.87	35.82
Jun	71.21	33.87	48.34	57.03	68.71	23.69
Jul	53.33	-6.79	24.30	77.81	28.39	13.80
Aug	8.90	-25.81	0.97	38.10	-2.72	5.63
Sep	-25.05	-26.68	-15.61	3.71	-10.51	9.71
Oct	-47.36	-34.56	-38.94	-30.58	-13.97	2.10
Nov	-66.98	-58.22	-64.71	-42.34	-29.31	8.00
Dec	-55.43	-66.18	-67.36	122.95	-1.45	4.33

Table C15: Ratios (Projected flow for different scenarios/Base flow (Worldclim))of Discharge for all the six scenarios in 2080s.

	Warmest (MIROC-ESM-CHEM RCP 8.5)	Coolest (GISS-E2-R RCP 2.6)	Driest (HadGEM2-ES RCP 8.5)	Wettest (BCC-CSM1.1 RCP 8.5)	Mod Warm (GISS-E2-H RCP 4.5)	Mod Wet (MRI-CGCM3 RCP 6)
Jan	1.3104	0.5400	0.1579	4.4467	1.3768	0.9413
Feb	1.4284	1.7051	0.0721	11.1771	5.7125	1.5090
Mar	3.9423	3.1195	2.1393	4.1514	5.9376	1.5537
Apr	4.4656	2.8870	3.5676	2.7652	7.4645	1.7919
May	2.7225	2.4941	2.9570	2.6088	3.8587	1.3582
Jun	1.7121	1.3387	1.4834	1.5703	1.6871	1.2369
Jul	1.5333	0.9321	1.2430	1.7781	1.2839	1.1380
Aug	1.0890	0.7419	1.0097	1.3810	0.9728	1.0563
Sep	0.7495	0.7332	0.8439	1.0371	0.8949	1.0971
Oct	0.5264	0.6544	0.6106	0.6942	0.8603	1.0210
Nov	0.3302	0.4178	0.3529	0.5766	0.7069	1.0800
Dec	0.4457	0.3382	0.3264	2.2295	0.9855	1.0433

Table C16: Adjusted discharge (m^3/s) for all the six scenarios in 2080s

	Observed	Warmest (MIROC-ESM-CHEM RCP 8.5)	Coolest (GISS-E2-R RCP 2.6)	Driest (HadGEM2-ES RCP 8.5)	Wettest (BCC-CSM1.1 RCP 8.5)	Mod Warm (GISS-E2-H RCP 4.5)	Mod Wet (MRI-CGCM3 RCP 6)
Jan	5692.74	7459.94	3074.29	898.74	25313.93	7837.89	5358.45
Feb	4620.01	6599.05	7877.48	333.04	51638.29	26391.62	6971.45
Mar	5348.66	21085.94	16685.15	11442.26	22204.68	31758.30	8310.31
Apr	9697.71	43306.17	27997.55	34597.25	26816.21	72388.94	17377.67
May	16728.98	45545.15	41724.33	49467.33	43642.77	64552.21	22721.15
Jun	31039.59	53143.07	41553.84	46043.14	48741.86	52366.66	38392.08
Jul	48707.46	74685.47	45400.79	60544.15	86604.83	62537.88	55429.33
Aug	43420.81	47283.84	32215.26	43843.21	59963.55	42238.73	45864.78
Sep	40124.35	30073.25	29419.93	33860.17	41613.04	35909.21	44019.72
Oct	26920.65	14171.02	17615.80	16438.77	18689.46	23160.74	27485.22
Nov	13699.61	4523.88	5724.21	4834.42	7899.52	9684.84	14795.21
Dec	7979.98	3556.83	2699.21	2604.34	17791.39	7864.62	8325.39

Table C17: Adjusted discharge (m^3/s) for all the six scenarios in 2080s

	Observed	Warmest (MIROC-ESM-CHEM RCP 8.5)	Coolest (GISS-E2-R RCP 2.6)	Driest (HadGEM2-ES RCP 8.5)	Wettest (BCC-CSM1.1 RCP 8.5)	Mod Warm (GISS-E2-H RCP 4.5)	Mod Wet (MRI-CGCM3 RCP 6)
Mean Annual	21165.05	29286.13	22665.65	25408.90	37576.63	36390.97	24587.56
Mean Dry Season (Dec-May)	8344.68	21258.85	16676.33	16557.16	31234.54	35132.26	11510.74
Mean Wet Season (June-Nov)	33985.41	37313.42	28654.97	34260.64	43918.71	37649.68	37664.39

Table C18: Multi-variable regression of simulated (RCP) and estimated ΔQ (%) at Bahadurabad station of Brahmaputra river basin

Criteria	Model and Scenario	Period	ΔT	ΔP%	ΔQ% (RCPs)	ΔQ% (Estimated)
Warmest	Warmest (MIROC-ESM-CHEM RCP 8.5)	2020s	1.322	6.176	15.019	11.003
Coolest	Coolest (GISS-E2-R RCP 2.6)	2020s	0.578	2.847	0.795	5.692
Driest	Driest (HadGEM2-ES RCP 8.5)	2020s	1.327	-6.672	-3.290	-1.357
Wettest	Wettest (BCC-CSM1.1 RCP 8.5)	2020s	1.032	10.395	11.044	14.244
Moderate Warming	Moderate Warm (GISS-E2-H RCP 4.5)	2020s	1.511	3.755	10.179	9.205
Moderate Wetting	Moderate Wet(MRI-CGCM3 RCP 6)	2020s	0.620	4.607	11.701	7.506
Warmest	Warmest (MIROC-ESM-CHEM RCP 8.5)	2050s	3.327	17.144	26.271	27.241
Coolest	Coolest (GISS-E2-R RCP 2.6)	2050s	0.691	3.382	1.800	6.525
Driest	Driest (HadGEM2-ES RCP 8.5)	2050s	3.025	-6.011	2.780	4.082
Wettest	Wettest (BCC-CSM1.1 RCP 8.5)	2050s	2.207	18.903	26.886	25.766
Moderate Warming	Moderate Warm (GISS-E2-H RCP 4.5)	2050s	2.492	12.385	32.457	20.293
Moderate Wetting	Moderate Wet(MRI-CGCM3 RCP 6)	2050s	1.251	9.232	13.380	13.746
Warmest	Warmest (MIROC-ESM-CHEM RCP 8.5)	2080s	5.961	21.698	29.500	39.080
Coolest	Coolest (GISS-E2-R RCP 2.6)	2080s	0.670	-0.584	-0.908	2.645
Driest	Driest (HadGEM2-ES RCP 8.5)	2080s	5.044	-2.157	18.962	13.508
Wettest	Wettest (BCC-CSM1.1 RCP 8.5)	2080s	3.919	38.378	47.436	49.367
Moderate Warming	Moderate Warm (GISS-E2-H RCP 4.5)	2080s	2.952	19.802	38.819	28.739
Moderate Wetting	Moderate Wet(MRI-CGCM3 RCP 6)	2080s	2.307	11.738	13.598	19.145

Table C19: Calculation of multi-variable regression for simulated (RCP) and estimated ΔQ (%).

SUMMARY OUTPUT

$$\Delta Q_{mean} = 1.3134 + 2.8296 * \Delta T + 0.96314 * \Delta P\%$$

Regression Statistics	
Multiple R	0.924219062
R Square	0.854180875
Adjusted R Square	0.834738325
Standard Error	5.872048887
Observations	18

	Coefficients	*Standard Error*	*t Stat*	*P-value*	*Lower 95%*	*Upper 95%*	*Lower 95.0%*	*Upper 95.0%*
Intercept	1.313380446	2.476347987	0.530369905	0.603619184	-3.96483032	6.591591213	-3.96483032	6.591591213
X Variable 1	2.82959906	1.009931015	2.801774594	0.013411619	0.676982067	4.982216053	0.676982067	4.982216053
X Variable 2	0.963140472	0.141235356	6.819400608	5.79887E-06	0.662104438	1.264176506	0.662104438	1.264176506

Table C20: Multi-variable regression of simulated (RCP) and estimated Q (m^3/s) at Bahadurabad station of Brahmaputra river basin

Criteria	Model and Scenario	Period	ΔT	ΔP%	Q (RCPs)	Q (Estimated)
Warmest	Warmest (MIROC-ESM-CHEM RCP 8.5)	2020s	1.322	6.176	24706.836	*24451.366*
Coolest	Coolest (GISS-E2-R RCP 2.6)	2020s	0.578	2.847	21747.293	*22861.329*
Driest	Driest (HadGEM2-ES RCP 8.5)	2020s	1.327	-6.672	19770.016	*19967.840*
Wettest	Wettest (BCC-CSM1.1 RCP 8.5)	2020s	1.032	10.395	24395.402	*25757.316*
Moderate Warming	Moderate Warm (GISS-E2-H RCP 4.5)	2020s	1.511	3.755	24002.714	*23714.249*
Moderate Wetting	Moderate Wet(MRI-CGCM3 RCP 6)	2020s	0.620	4.607	24006.638	*23499.875*
Warmest	Warmest (MIROC-ESM-CHEM RCP 8.5)	2050s	3.327	17.144	27239.443	*29433.711*
Coolest	Coolest (GISS-E2-R RCP 2.6)	2050s	0.691	3.382	21820.971	*23112.780*
Driest	Driest (HadGEM2-ES RCP 8.5)	2050s	3.025	-6.011	20727.058	*21174.247*
Wettest	Wettest (BCC-CSM1.1 RCP 8.5)	2050s	2.207	18.903	27617.777	*29403.995*
Moderate Warming	Moderate Warm (GISS-E2-H RCP 4.5)	2050s	2.492	12.385	31873.302	*27291.614*
Moderate Wetting	Moderate Wet(MRI-CGCM3 RCP 6)	2050s	1.251	9.232	24549.590	*25477.533*
Warmest	Warmest (MIROC-ESM-CHEM RCP 8.5)	2080s	5.961	21.698	29286.134	*32537.687*
Coolest	Coolest (GISS-E2-R RCP 2.6)	2080s	0.670	-0.584	22665.654	*21715.561*
Driest	Driest (HadGEM2-ES RCP 8.5)	2080s	5.044	-2.157	25408.900	*23680.618*
Wettest	Wettest (BCC-CSM1.1 RCP 8.5)	2080s	3.919	38.378	37576.626	*37188.216*
Moderate Warming	Moderate Warm (GISS-E2-H RCP 4.5)	2080s	2.952	19.802	36390.970	*30145.913*
Moderate Wetting	Moderate Wet(MRI-CGCM3 RCP 6)	2080s	2.307	11.738	24587.564	*26959.037*

Table C21: Calculation of multi-variable regression for simulated (RCP) and estimated Q (m^3/s).

SUMMARY

OUTPUT

$$Q_{mean} = 21535 + 575 * \Delta T + 349 * \Delta P\%$$

Regression Statistics	
Multiple R	0.880750148
R Square	0.775720823
Adjusted R Square	0.745816933
Standard Error	2510.047702
Observations	18

	Coefficients	*Standard Error*	*t Stat*	*P-value*	*Lower 95%*	*Upper 95%*	*Lower 95.0%*	*Upper 95.0%*
Intercept	21534.73652	1058.531987	20.3439639	2.46411E-12	19278.529	23790.94405	19278.529	23790.94405
X Variable 1	574.7788625	431.7019617	1.331425181	0.202930513	-345.3720875	1494.929813	-345.3720875	1494.929813
X Variable 2	349.1789346	60.37202474	5.783787045	3.60649E-05	220.4990099	477.8588592	220.4990099	477.8588592

Table C22: Calculation of minimum, maximum, median, 2nd and 3rd quartile of mean discharge (Annual, Dry and wet) for all the scenarios.

	Q_{mean}			Q_{mean} (Dry)			Q_{mean} (Wet)		
Model	**2020s**	**2050s**	**2080s**	**2020s**	**2050s**	**2080s**	**2020s**	**2050s**	**2080s**
Warmest (MIROC-ESM-CHEM RCP 8.5)	24706.84	27239.44	29286.13	12884.86	16489.2	21258.85	36528.81	37989.69	37313.42
Coolest (GISS-E2-R RCP 2.6)	21747.29	21820.97	22665.65	10724.54	12412.77	16676.33	32770.05	31229.17	28654.97
Driest (HadGEM2-ES RCP 8.5)	19770.02	20727.06	25408.90	7259.574	8787.539	16557.16	32280.46	32666.58	34260.64
Wettest (BCC-CSM1.1 RCP 8.5)	24395.40	27617.78	37576.63	11431.82	14789.52	31234.54	37358.99	40446.03	43918.71
Moderate Warm (GISS-E2-H RCP 4.5)	24002.71	31873.30	36390.97	12639.74	25015.13	35132.26	35365.69	38731.47	37649.68
Moderate Wet(MRI-CGCM3 RCP 6)	24006.64	24549.59	24587.56	10743.5	11528.56	11510.74	37269.78	37570.62	37664.39
Min	19770.02	20727.06	22665.65	7259.574	8787.539	11510.74	32280.46	31229.17	28654.97
Quartile 1	22311.15	22503.13	24792.90	10729.28	11749.61	16586.95	33418.96	33892.59	35023.84
Median	24004.68	25894.52	27347.52	11087.66	13601.15	18967.59	35947.25	37780.15	37481.55
Quartile 3	24298.21	27523.19	34614.76	12337.76	16064.28	28740.62	37084.54	38546.03	37660.71
Max	24706.84	31873.30	37576.63	12884.86	25015.13	35132.26	37358.99	40446.03	43918.71

Analysis of Max discharge-2020s

Table C23: Maximum adjusted discharge for all the six scenarios in 2020s

	Observed	Warmest (MIROC-ESM-CHEM RCP 8.5)	Coolest (GISS-E2-R RCP 2.6)	Driest (HadGEM2-ES RCP 8.5)	Wettest (BCC-CSM1.1 RCP 8.5)	Mod Warm (GISS-E2-H RCP 4.5)	Mod Wet (MRI-CGCM3 RCP 6)
Max Annual	48707.46	60058.99	51040.52	46151.63	54599.30	51843.38	55568.42
Max Dry Season (Dec-May)	16728.98	31602.56	24874.34	21007.92	21227.95	32588.71	21684.36
Max Wet Season (June-Nov)	48707.46	60058.99	51040.52	46151.63	54599.30	51843.38	55568.42

Analysis of Max discharge-2050s (2040-2069)

Table C24: Maximum adjusted discharge (m^3/s) for all the six scenarios in 2050s

	Observed	Warmest (MIROC-ESM-CHEM RCP 8.5)	Coolest (GISS-E2-R RCP 2.6)	Driest (HadGEM2-ES RCP 8.5)	Wettest (BCC-CSM1.1 RCP 8.5)	Mod Warm (GISS-E2-H RCP 4.5)	Mod Wet (MRI-CGCM3 RCP 6)
Max Annual	48707.46	72777.85	50649.10	52477.05	68659.90	61159.06	55357.42
Max Dry Season (Dec-May)	16728.98	43648.33	35250.81	28748.86	30586.34	55138.61	22506.93
Max Wet Season (June-Nov)	48707.46	72777.85	50649.10	52477.05	68659.90	61159.06	55357.42

Analysis of Max discharge-2080s (2070-2099)

Table C25: Maximum adjusted discharge (m^3/s) for all the six scenarios in 2080s

	Observed	Warmest (MIROC-ESM-CHEM RCP 8.5)	Coolest (GISS-E2-R RCP 2.6)	Driest (HadGEM2-ES RCP 8.5)	Wettest (BCC-CSM1.1 RCP 8.5)	Mod Warm (GISS-E2-H RCP 4.5)	Mod Wet (MRI-CGCM3 RCP 6)
Max Annual	48707.46	74685.47	45400.79	60544.15	86604.83	72388.94	55429.33
Max Dry Season (Dec-May)	16728.98	45545.15	41724.33	49467.33	51638.29	72388.94	22721.15
Max Wet Season (June-Nov)	48707.46	74685.47	45400.79	60544.15	86604.83	62537.88	55429.33

Table C26: Multi-variable regression of simulated (RCP) and estimated maximumΔQ (%) at Bahadurabad station of Brahmaputra river basin

Criteria	Model and Scenario	Period	ΔT	ΔP%	ΔQ% (RCPs)	ΔQ% (Estimated)
Warmest	Warmest (MIROC-ESM-CHEM RCP 8.5)	2020s	1.322	6.176	16.705	5.480
Coolest	Coolest (GISS-E2-R RCP 2.6)	2020s	0.578	2.847	-3.590	-1.995
Driest	Driest (HadGEM2-ES RCP 8.5)	2020s	1.327	-6.672	-1.832	-10.146
Wettest	Wettest (BCC-CSM1.1 RCP 8.5)	2020s	1.032	10.395	7.622	9.282
Moderate Warming	Moderate Warm (GISS-E2-H RCP 4.5)	2020s	1.511	3.755	1.320	3.398
Moderate Wetting	Moderate Wet(MRI-CGCM3 RCP 6)	2020s	0.620	4.607	4.962	0.341
Warmest	Warmest (MIROC-ESM-CHEM RCP 8.5)	2050s	3.327	17.144	37.469	28.059
Coolest	Coolest (GISS-E2-R RCP 2.6)	2050s	0.691	3.382	-4.330	-0.827
Driest	Driest (HadGEM2-ES RCP 8.5)	2050s	3.025	-6.011	-0.877	-1.536
Wettest	Wettest (BCC-CSM1.1 RCP 8.5)	2050s	2.207	18.903	29.691	25.051
Moderate Warming	Moderate Warm (GISS-E2-H RCP 4.5)	2050s	2.492	12.385	15.523	18.420
Moderate Wetting	Moderate Wet(MRI-CGCM3 RCP 6)	2050s	1.251	9.232	7.643	8.875
Warmest	Warmest (MIROC-ESM-CHEM RCP 8.5)	2080s	5.961	21.698	41.072	45.717
Coolest	Coolest (GISS-E2-R RCP 2.6)	2080s	0.670	-0.584	-13.283	-5.755
Driest	Driest (HadGEM2-ES RCP 8.5)	2080s	5.044	-2.157	14.361	12.442
Wettest	Wettest (BCC-CSM1.1 RCP 8.5)	2080s	3.919	38.378	63.587	56.643
Moderate Warming	Moderate Warm (GISS-E2-H RCP 4.5)	2080s	2.952	19.802	18.127	29.570
Moderate Wetting	Moderate Wet(MRI-CGCM3 RCP 6)	2080s	2.307	11.738	5.629	16.780

Table C27: Calculation of multi-variable regression for simulated (RCP) and estimated max Δ Q (%).

SUMMARY OUTPUT

Regression Statistics	
Multiple R	0.938704463
R Square	0.881166069
Adjusted R Square	0.865321545
Standard Error	7.043755246
Observations	18

$$\Delta Q_{max} = -8.1225 + 4.5982 * \Delta T + 1.218 * \Delta P\%$$

	Coefficients	*Standard Error*	*t Stat*	*P-value*	*Lower 95%*	*Upper 95%*
Intercept	-8.12252839	2.970477505	-2.73441841	0.015359976	-14.45395131	-1.79110546
X Variable 1	4.598154167	1.211452258	3.795571914	0.001759083	2.016004802	7.180303533
X Variable 2	1.217983805	0.169417404	7.189248421	3.12822E-06	0.856879156	1.579088454

Table C28: Multi-variable regression of simulated (RCP) and estimated maximum Q (m^3/s) at Bahadurabad station of Brahmaputra river basin

Criteria	Model and Scenario	Period	ΔT	ΔP%	Q(RCPs)	Q(Estimated)
Warmest	Warmest (MIROC-ESM-CHEM RCP 8.5)	2020s	1.322	6.176	60058.990	*55134.180*
Coolest	Coolest (GISS-E2-R RCP 2.6)	2020s	0.578	2.847	51040.524	*50726.393*
Driest	Driest (HadGEM2-ES RCP 8.5)	2020s	1.327	-6.672	46151.635	*45758.537*
Wettest	Wettest (BCC-CSM1.1 RCP 8.5)	2020s	1.032	10.395	54599.299	*57445.347*
Moderate Warming	Moderate Warm (GISS-E2-H RCP 4.5)	2020s	1.511	3.755	51843.378	*53865.520*
Moderate Wetting	Moderate Wet(MRI-CGCM3 RCP 6)	2020s	0.620	4.607	55568.417	*52123.674*
Warmest	Warmest (MIROC-ESM-CHEM RCP 8.5)	2050s	3.327	17.144	72777.854	*68472.351*
Coolest	Coolest (GISS-E2-R RCP 2.6)	2050s	0.691	3.382	50649.097	*51415.792*
Driest	Driest (HadGEM2-ES RCP 8.5)	2050s	3.025	-6.011	52477.048	*50747.567*
Wettest	Wettest (BCC-CSM1.1 RCP 8.5)	2050s	2.207	18.903	68659.904	*66784.166*
Moderate Warming	Moderate Warm (GISS-E2-H RCP 4.5)	2050s	2.492	12.385	61159.062	*62776.164*
Moderate Wetting	Moderate Wet(MRI-CGCM3 RCP 6)	2050s	1.251	9.232	55357.417	*57178.663*
Warmest	Warmest (MIROC-ESM-CHEM RCP 8.5)	2080s	5.961	21.698	74685.468	*78792.670*
Coolest	Coolest (GISS-E2-R RCP 2.6)	2080s	0.670	-0.584	45400.790	*48461.090*
Driest	Driest (HadGEM2-ES RCP 8.5)	2080s	5.044	-2.157	60544.147	*58924.294*
Wettest	Wettest (BCC-CSM1.1 RCP 8.5)	2080s	3.919	38.378	86604.828	*85560.501*
Moderate Warming	Moderate Warm (GISS-E2-H RCP 4.5)	2080s	2.952	19.802	72388.941	*69417.954*
Moderate Wetting	Moderate Wet(MRI-CGCM3 RCP 6)	2080s	2.307	11.738	55429.329	*61811.265*

Table C29: Calculation of multi-variable regression for simulated (RCP) and estimated maximum Q (m^3/s).

SUMMARY
OUTPUT

Regression Statistics	
Multiple R	0.961291587
R Square	0.924081515
Adjusted R Square	0.913959051
Standard Error	3262.247272
Observations	18

$$Q_{max} = 47110 + 2655 * \Delta T + 731 * \Delta P\%$$

	Coefficients	*Standard Error*	*t Stat*	*P-value*	*Lower 95%*	*Upper 95%*	*Lower 95.0%*	*Upper 95.0%*
Intercept	47110.46948	1375.747992	34.24353135	1.17409E-15	44178.13205	50042.80691	44178.13205	50042.80691
X Variable 1	2654.785418	561.0724233	4.731626984	0.000267519	1458.887856	3850.682979	1458.887856	3850.682979
X Variable 2	730.7566528	78.4640359	9.31326874	1.26348E-07	563.5145191	897.9987864	563.5145191	897.9987864

Table C30: Calculation of minimum, maximum, median, 2nd and 3rd quartile of max discharge (Annual, Dry and wet) for all the scenarios.

	Q_{max}			Q_{max} (Dry)			Q_{max} (Dry)		
Model	**2020s**	**2050s**	**2080s**	**2020s**	**2050s**	**2080s**	**2020s**	**2050s**	**2080s**
Warmest (MIROC-ESM-CHEM RCP 8.5)	60058.99	72777.85	74685.47	31602.56	43648.33	45545.15	60058.99	72777.85	74685.47
Coolest (GISS-E2-R RCP 2.6)	51040.52	50649.10	45400.79	24874.34	35250.81	41724.33	51040.52	50649.1	45400.79
Driest (HadGEM2-ES RCP 8.5)	46151.63	52477.05	60544.15	21007.92	28748.86	49467.33	46151.63	52477.05	60544.15
Wettest (BCC-CSM1.1 RCP 8.5)	54599.30	68659.90	86604.83	21227.95	30586.34	51638.29	54599.3	68659.9	86604.83
Moderate Warm (GISS-E2-H RCP 4.5)	51843.38	61159.06	72388.94	32588.71	55138.61	72388.94	51843.38	61159.06	62537.88
Moderate Wet(MRI-CGCM3 RCP 6)	55568.42	55357.42	55429.33	21684.36	22506.93	22721.15	55568.42	55357.42	55429.33
Min	46151.63	50649.10	45400.79	21007.92	22506.93	22721.15	46151.63	50649.1	45400.79
Quartile 1	51241.24	53197.14	56708.03	21342.05	29208.23	42679.53	51241.24	53197.14	56708.03
Median	53221.34	58258.24	66466.54	23279.35	32918.58	47506.24	53221.34	58258.24	61541.02
Quartile 3	55326.14	66784.69	74111.34	29920.51	41548.95	51095.55	55326.14	66784.69	71648.57
Max	60058.99	72777.85	86604.83	32588.71	55138.61	72388.94	60058.99	72777.85	86604.83

Analysis of Min discharge-2020s

Table C31: Minimum adjusted discharge for all the six scenarios in 2020s

	Observed	Warmest (MIROC-ESM-CHEM RCP 8.5)	Coolest (GISS-E2-R RCP 2.6)	Driest (HadGEM2-ES RCP 8.5)	Wettest (BCC-CSM1.1 RCP 8.5)	Mod Warm (GISS-E2-H RCP 4.5)	Mod Wet (MRI-CGCM3 RCP 6)
Min Annual	4620.01	6930.54	3093.47	356.34	5849.75	3496.81	4743.03
Min Dry Season (Dec-May)	4620.01	6930.54	3093.47	356.34	5849.75	3496.81	4743.03
Min Wet Season (June-Nov)	13699.61	10225.52	12100.64	11109.10	17659.09	13067.92	15039.71

Analysis of Min discharge-2050s (2040-2069)

Table C32: Minimum adjusted discharge (m^3/s) for all the six scenarios in 2050s

	Observed	Warmest (MIROC-ESM-CHEM RCP 8.5)	Coolest (GISS-E2-R RCP 2.6)	Driest (HadGEM2-ES RCP 8.5)	Wettest (BCC-CSM1.1 RCP 8.5)	Mod Warm (GISS-E2-H RCP 4.5)	Mod Wet (MRI-CGCM3 RCP 6)
Min Annual	4620.01	4713.23	2628.40	142.99	6564.03	8352.13	5029.27
Min Dry Season (Dec-May)	4620.01	4713.23	2628.40	142.99	6564.03	8352.13	5029.27
Min Wet Season (June-Nov)	13699.61	6773.66	8568.38	7261.57	10320.30	12123.34	15089.86

Analysis of Min discharge-2080s (2070-2099)

Table C33: Minimum adjusted discharge (m^3/s) for all the six scenarios in 2080s

	Observed	Warmest (MIROC-ESM-CHEM RCP 8.5)	Coolest (GISS-E2-R RCP 2.6)	Driest (HadGEM2-ES RCP 8.5)	Wettest (BCC-CSM1.1 RCP 8.5)	Mod Warm (GISS-E2-H RCP 4.5)	Mod Wet (MRI-CGCM3 RCP 6)
Min Annual	4620.01	3556.83	2699.21	333.04	7899.52	7837.89	5358.45
Min Dry Season (Dec-May)	4620.01	3556.83	2699.21	333.04	17791.39	7837.89	5358.45
Min Wet Season (June-Nov)	13699.61	4523.88	5724.21	4834.42	7899.52	9684.84	14795.21

AppendixD

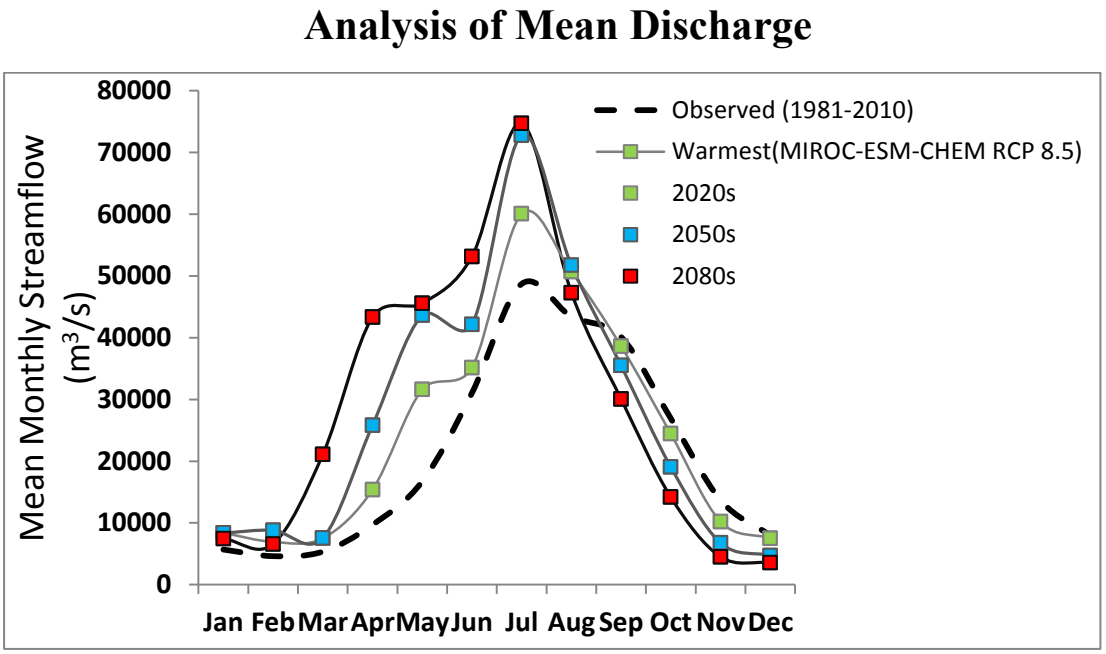

Figure D1: Mean monthly discharge (m^3/s) for the warmest scenario for Brahmaputra river basin

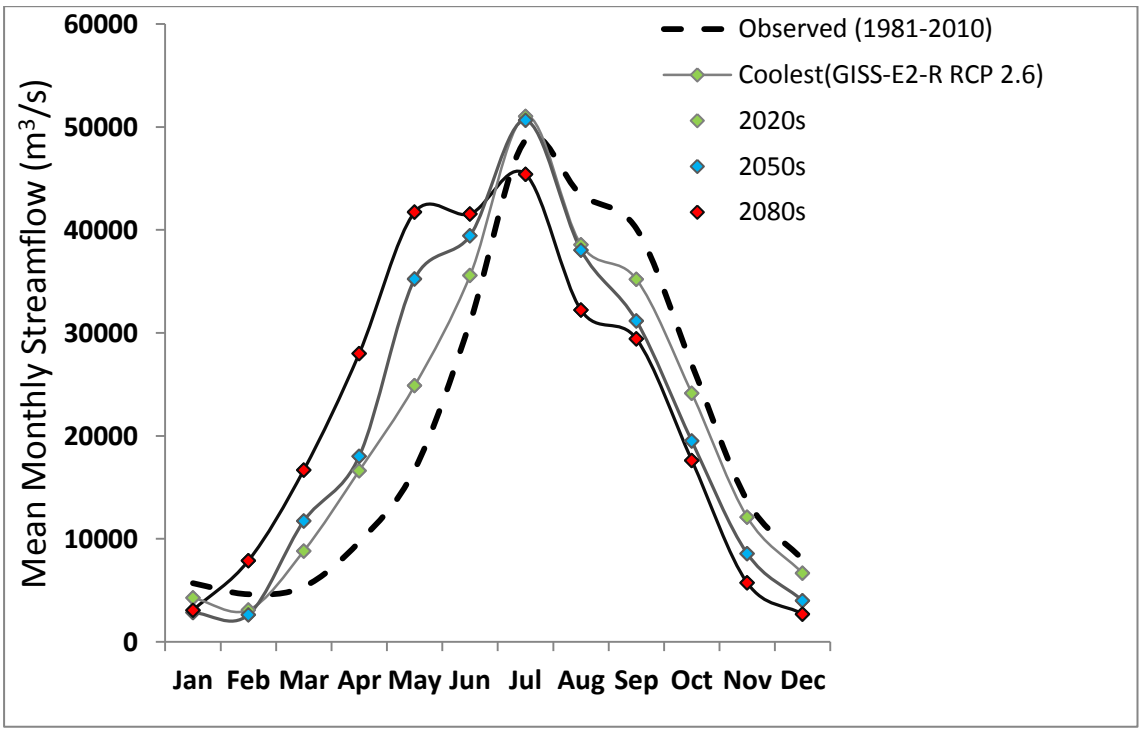

Figure D2: Mean monthly discharge (m^3/s) for the coolest scenario for Brahmaputra river basin

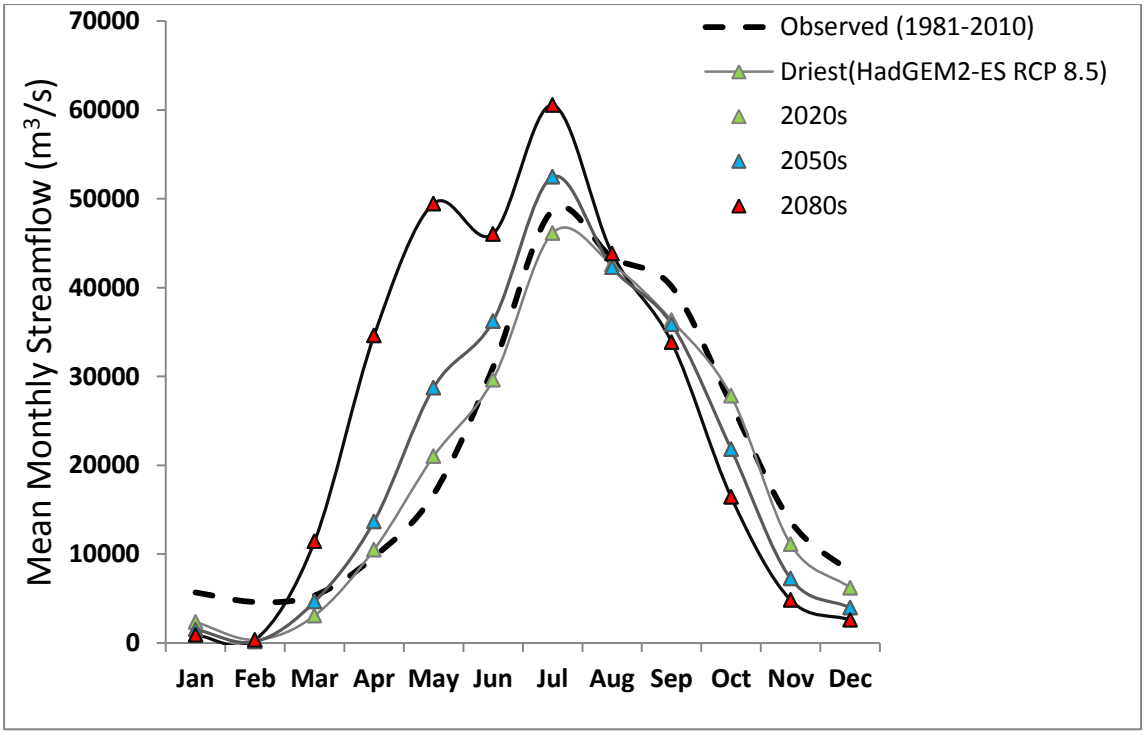

Figure D3: Mean monthly discharge (m^3/s) for the driest scenario for Brahmaputra river basin

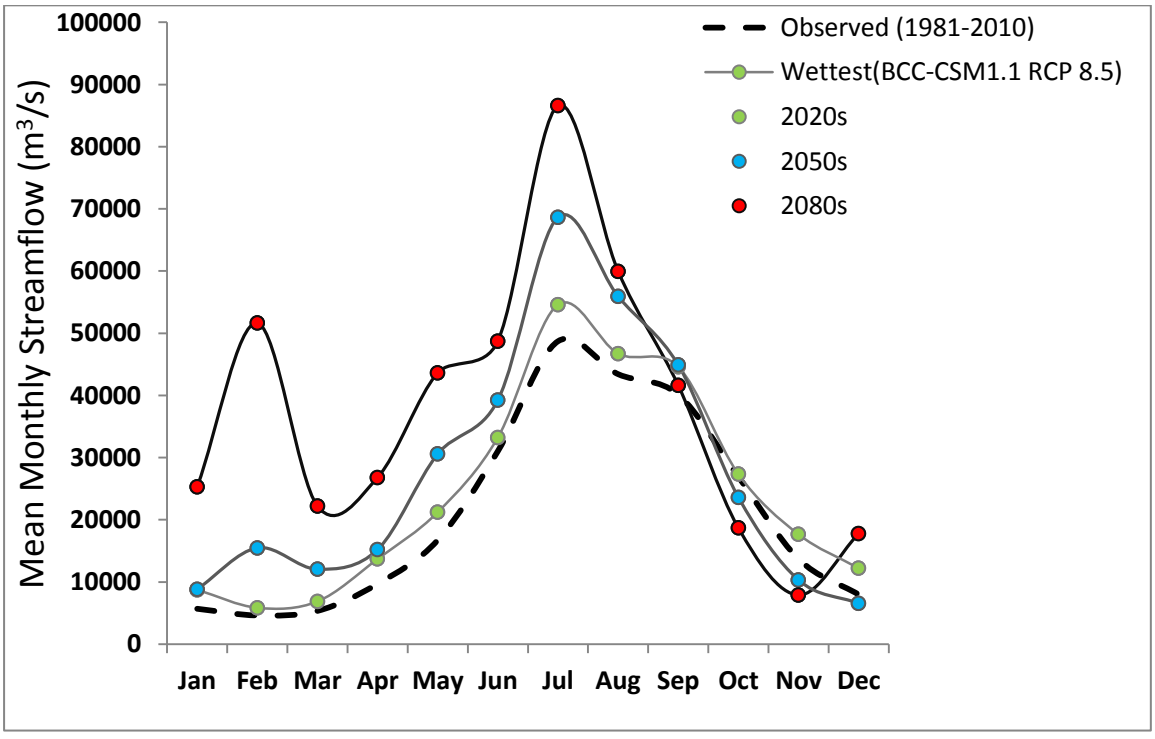

Figure D4: Mean monthly discharge (m^3/s) for the wettest scenario for Brahmaputra river basin

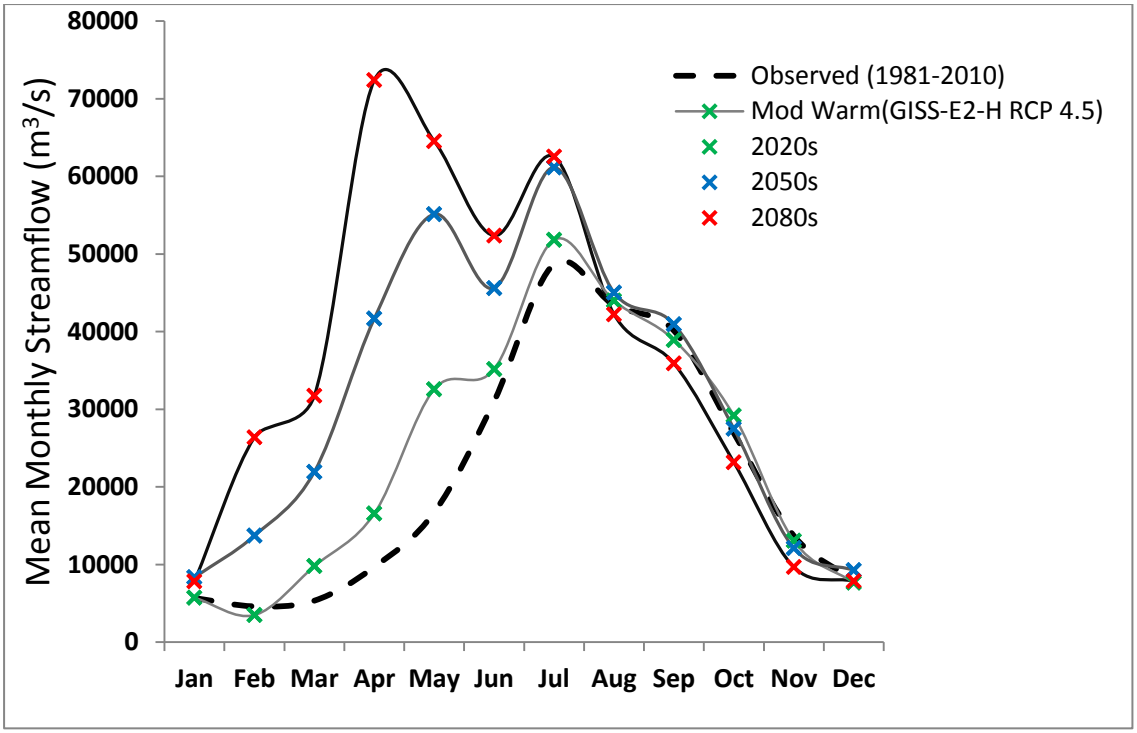

Figure D5: Mean monthly discharge (m^3/s) for the moderate warm scenario for Brahmaputra river basin

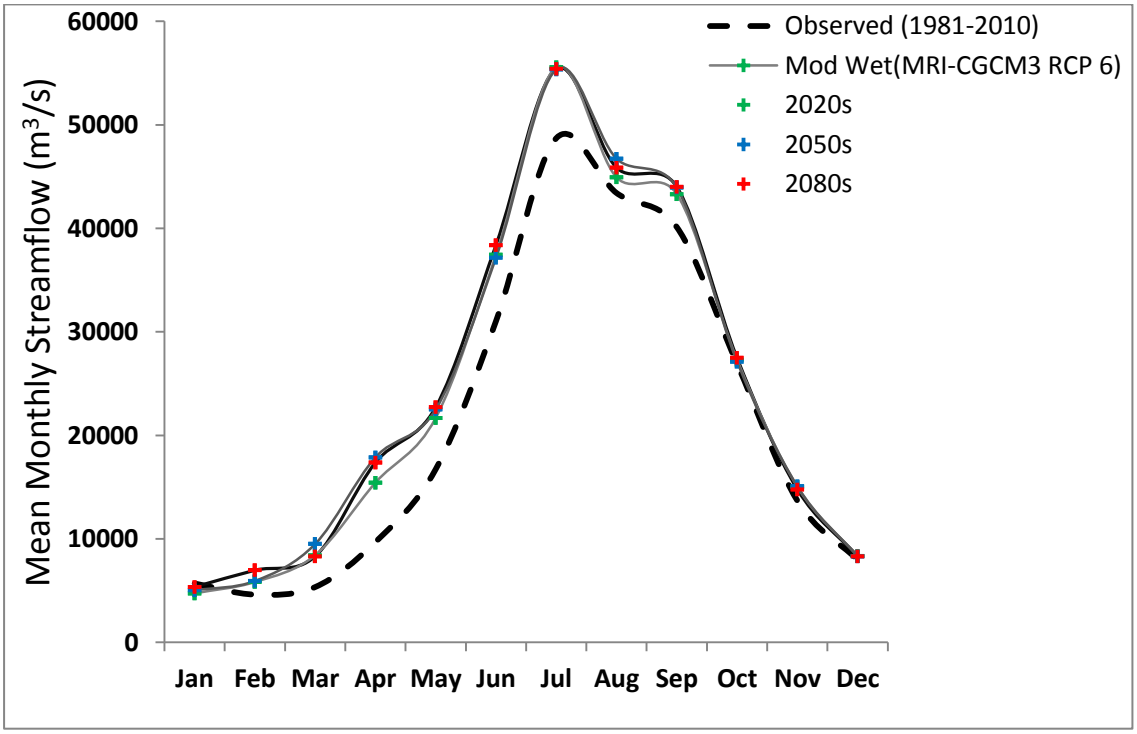

Figure D6: Mean monthly discharge (m^3/s) for the moderate wet scenario for Brahmaputra river basin

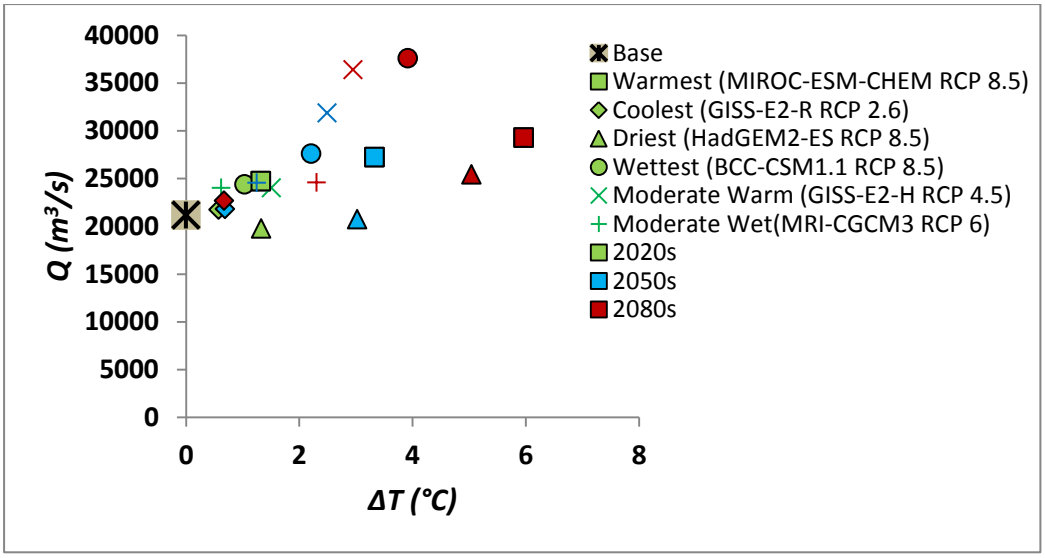

Figure D7: ΔT C) vs mean annual discharge (m^3/s) of six scenarios for 2020s, 2050s and 2080s

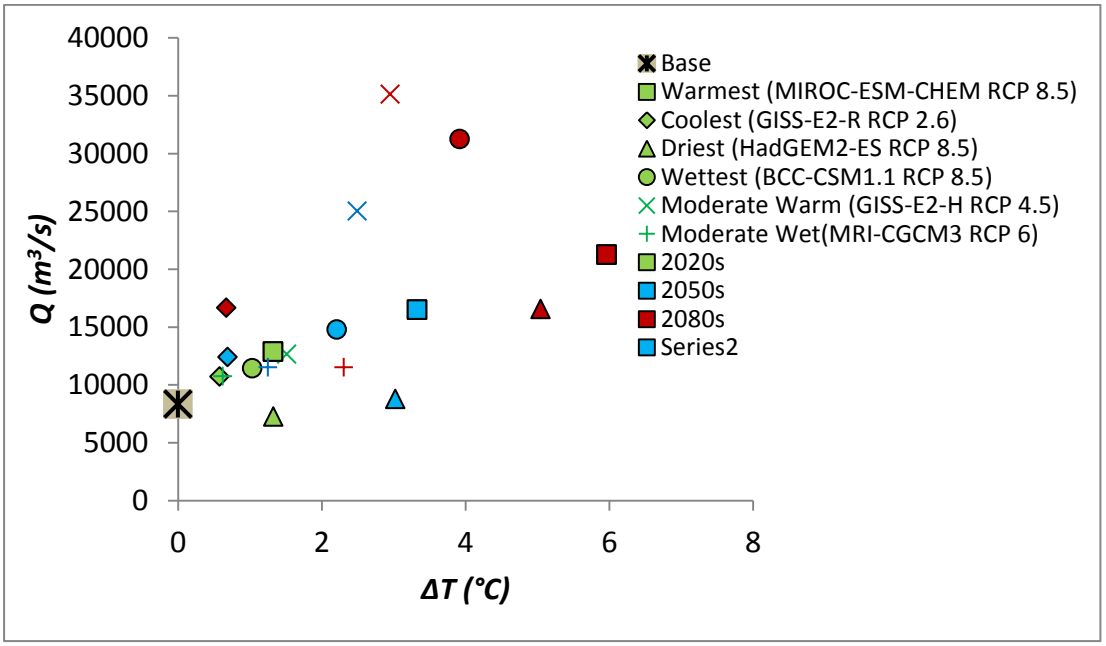

Figure D8: ΔT C) vs mean dry period discharge (m^3/s) of six scenarios for 2020s, 2050s and 2080s

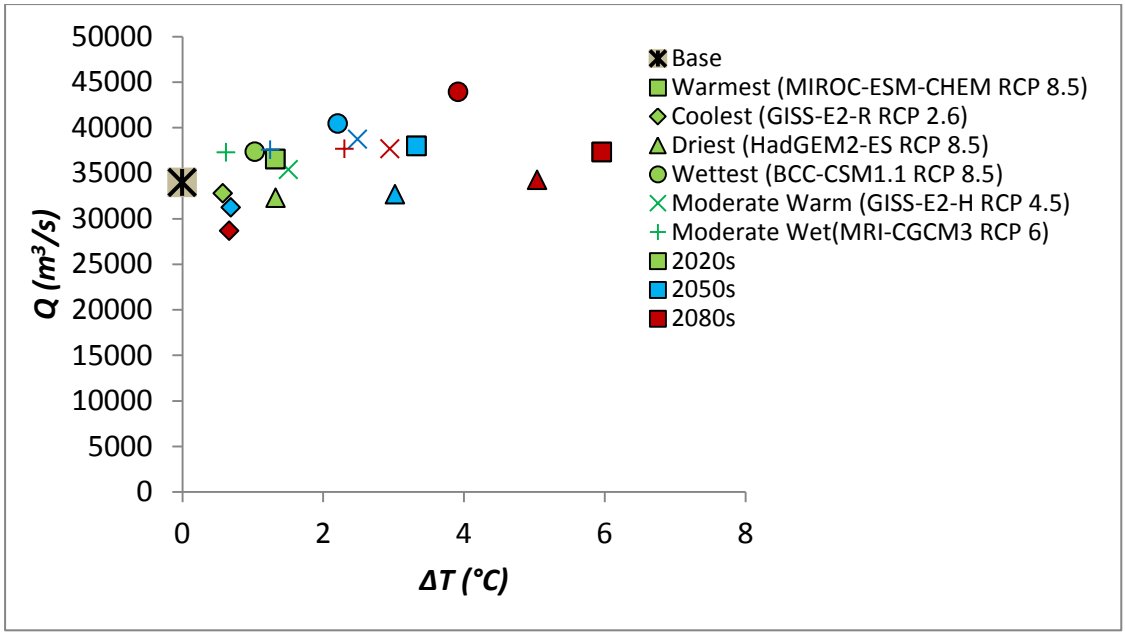

Figure D9: ΔT C) vs mean wet period discharge (m^3/s) of six scenarios for 2020s, 2050s and 2080s

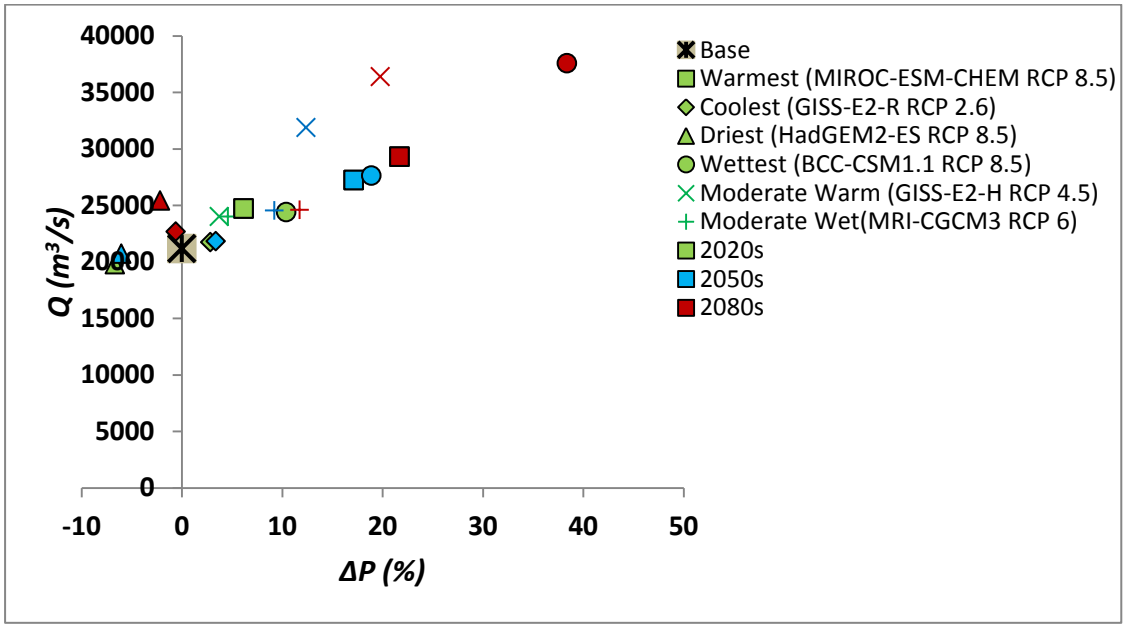

Figure D10: ΔP (%) vs mean annual discharge (m^3/s) of six scenarios for 2020s, 2050s and 2080s

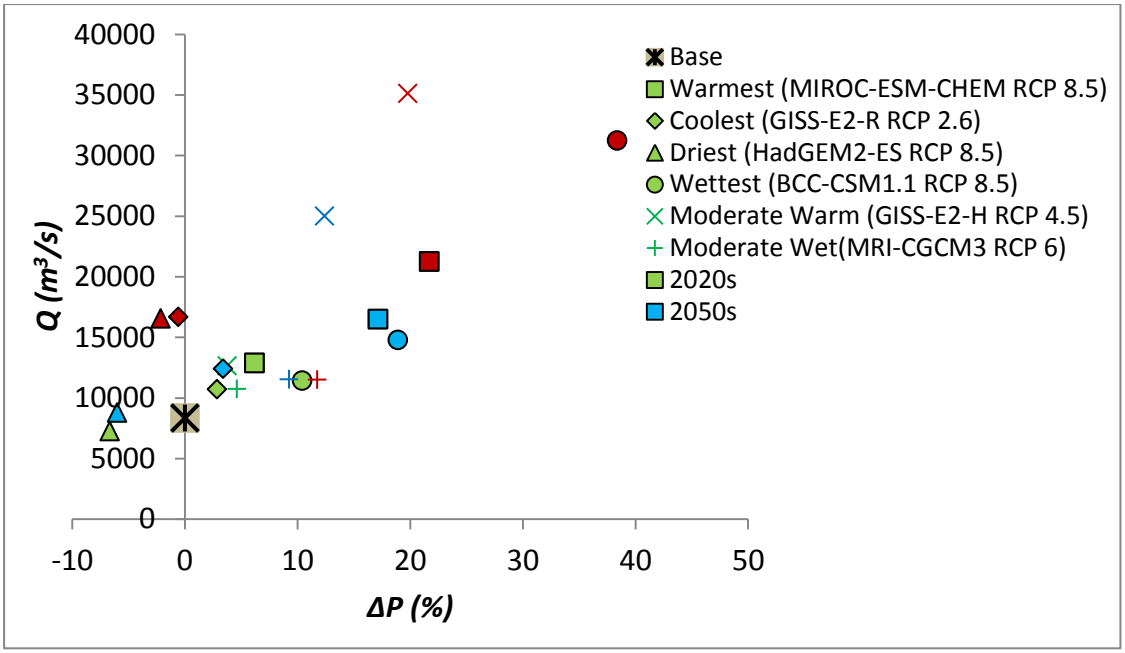

Figure D11: ΔP (%) vs mean dry period discharge (m^3/s) of six scenarios for 2020s, 2050s and 2080s

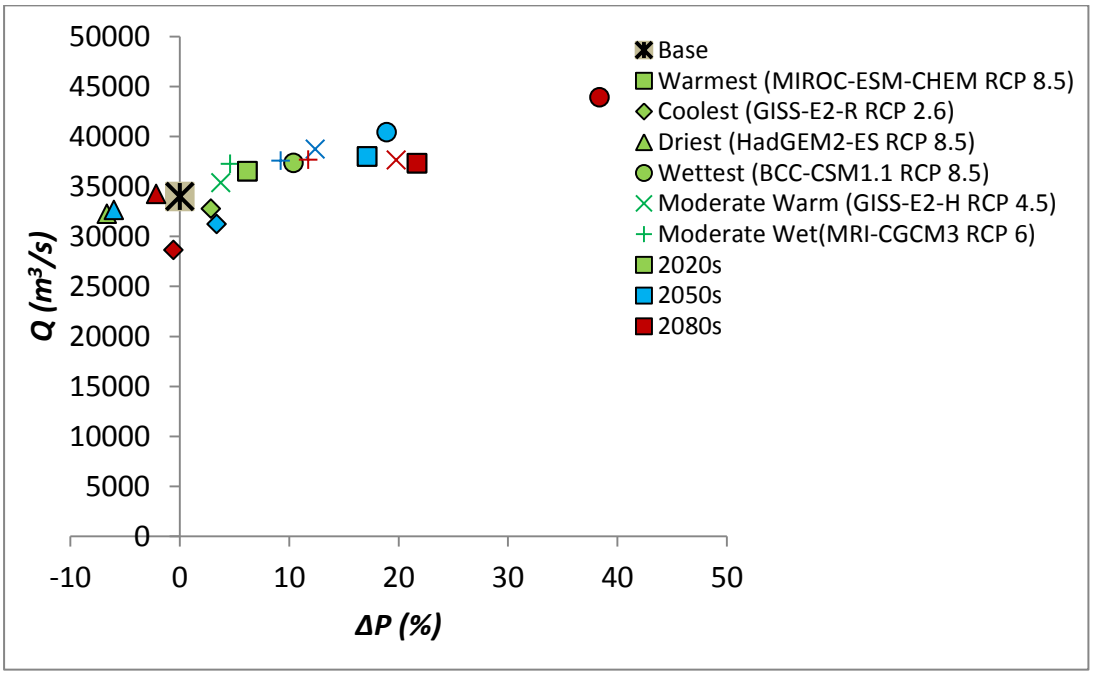

Figure D12: ΔP (%) vs mean wet period discharge (m^3/s) of six scenarios for 2020s, 2050s and 2080s

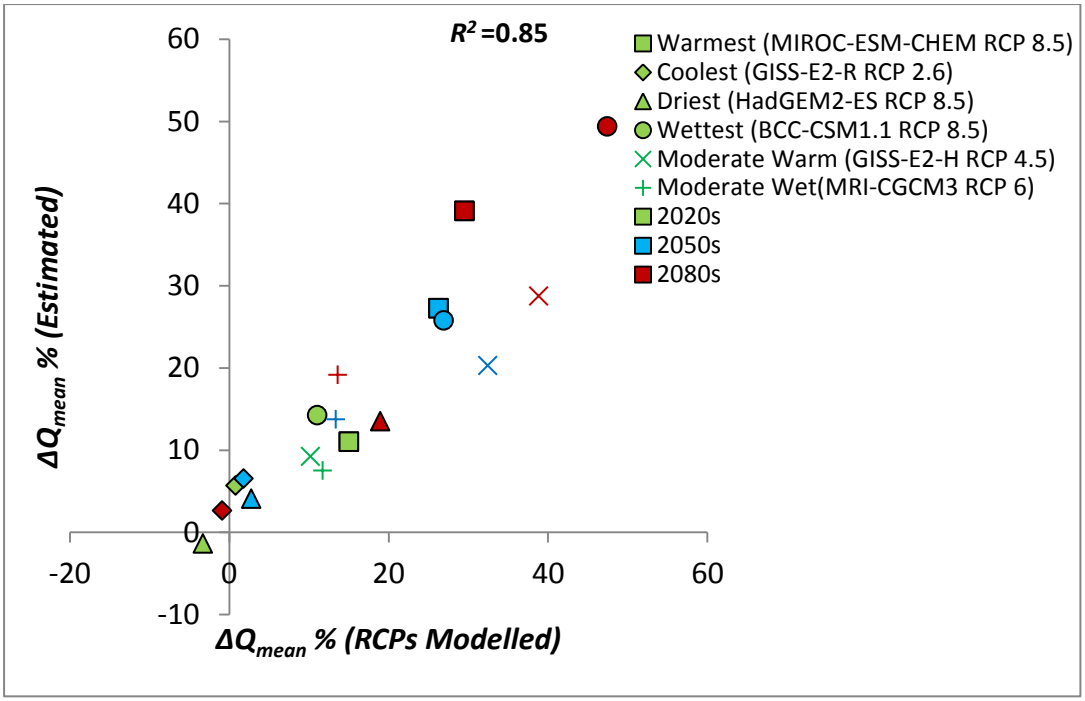

Figure D13: Modeled vs Estimated ΔQ_{mean} (%) plot of all the scenarios for 2020s, 2050s and 2080s

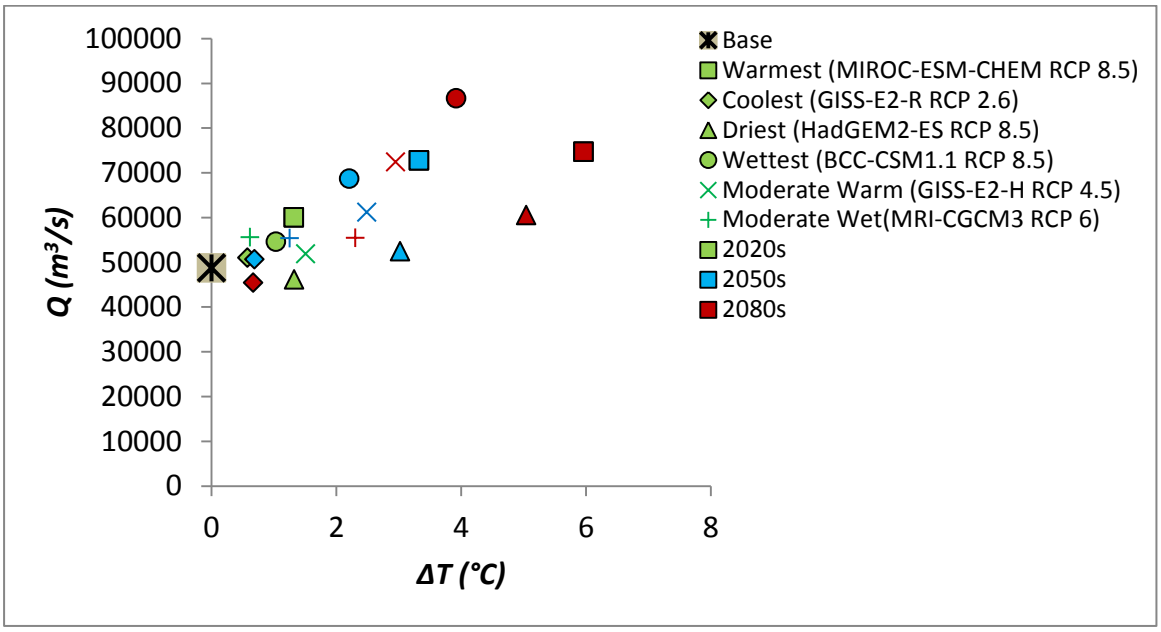

Figure D14 ΔT C) vs maximum annual discharge (m^3/s) of six scenarios for 2020s, 2050s and 2080s

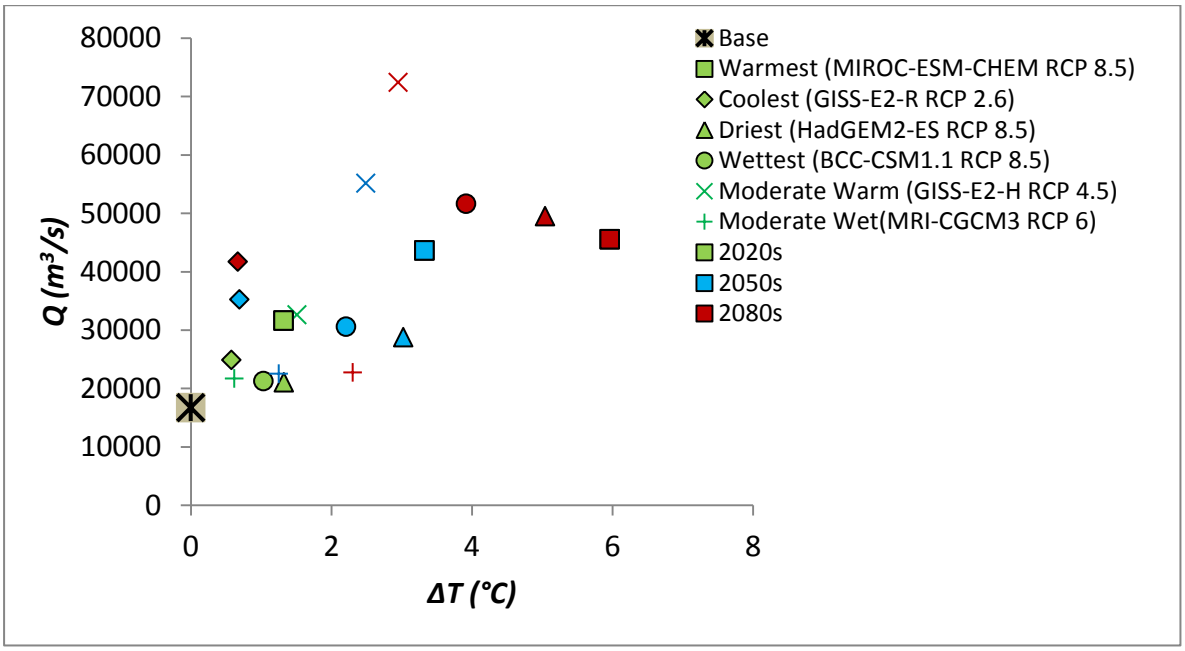

Figure D15 ΔT C) vs maximum dry period discharge (m^3/s) of scenarios for 2020s, 2050s and 2080s

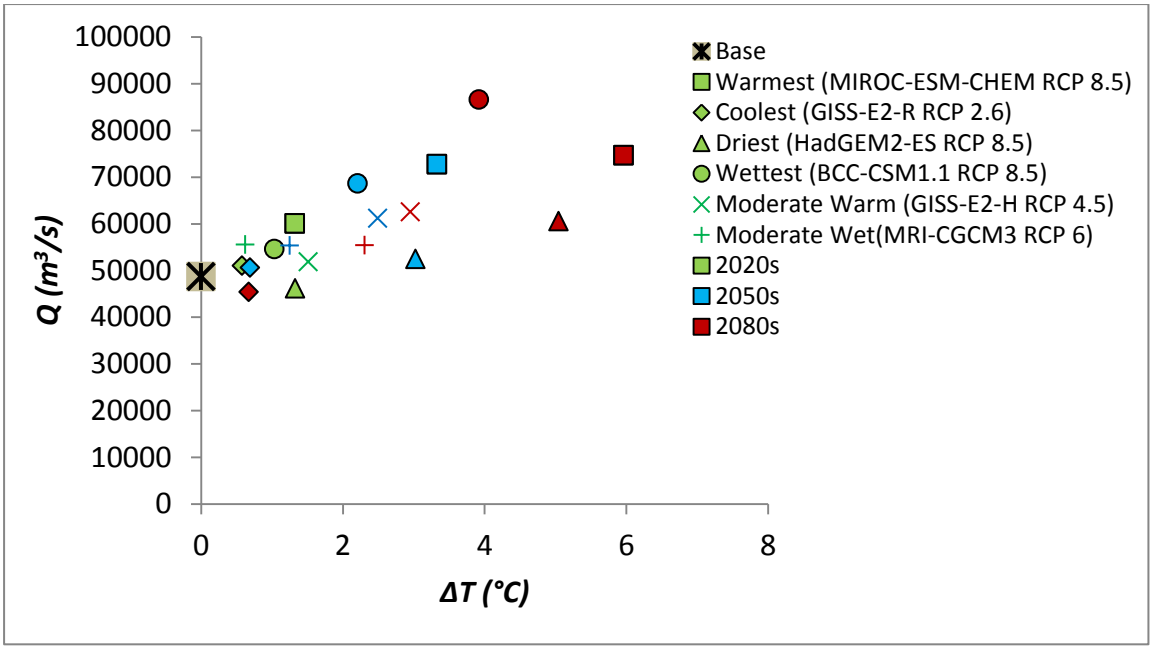

Figure D16 ΔT C) vs changes in maximum wet period discharge (m^3/s) of six scenarios for 2020s, 2050s and 2080s

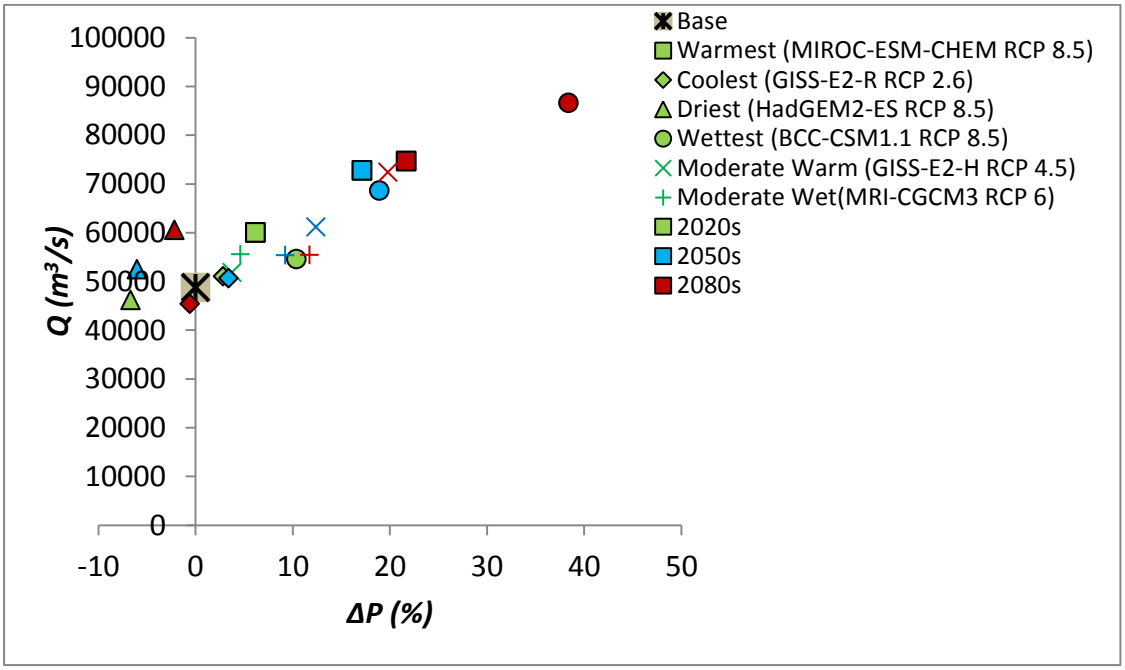

Figure D17 ΔP (%) vs maximum annual discharge (m^3/s) of six scenarios for 2020s, 2050s and 2080s

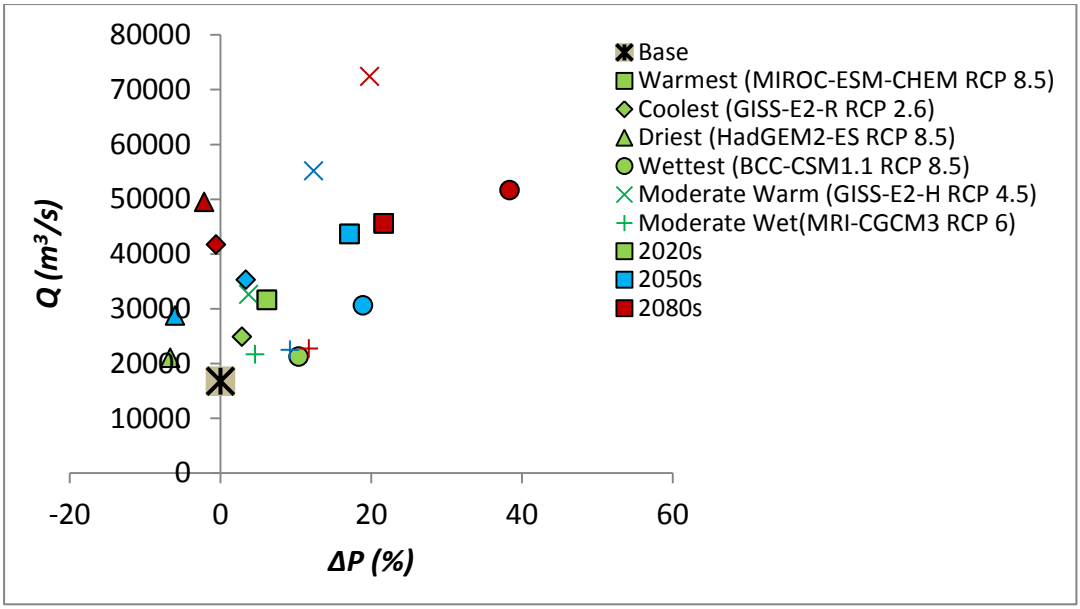

Figure D18 ΔP (%) vs maximum dry period discharge (m^3/s) of six scenarios for 2020s, 2050s and 2080s

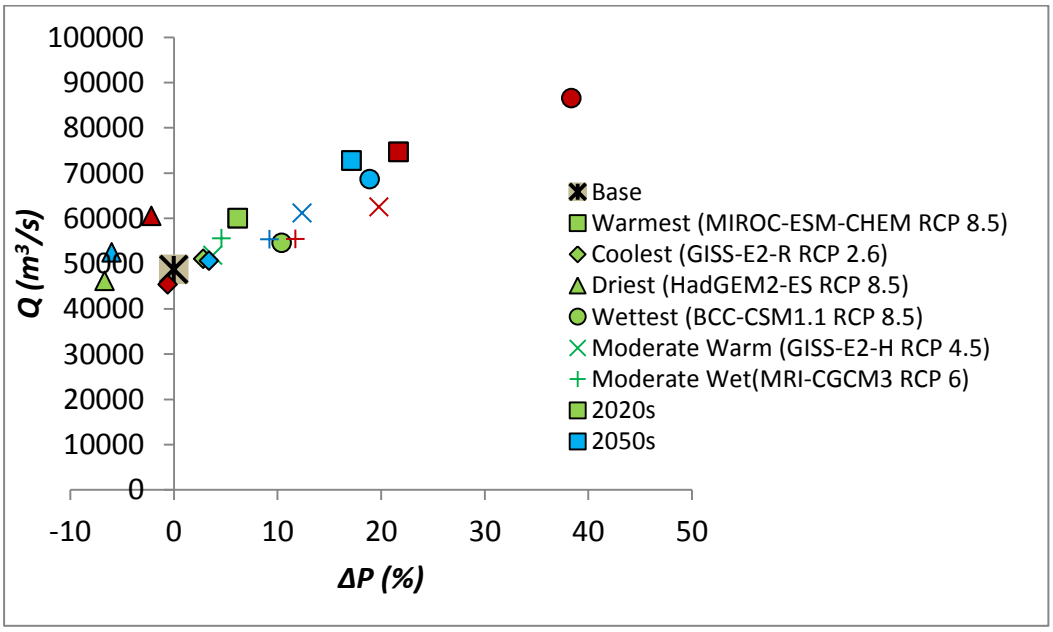

Figure D19 ΔP (%) vs maximum wet period discharge (m^3/s) of six scenarios for 2020s, 2050s and 2080s

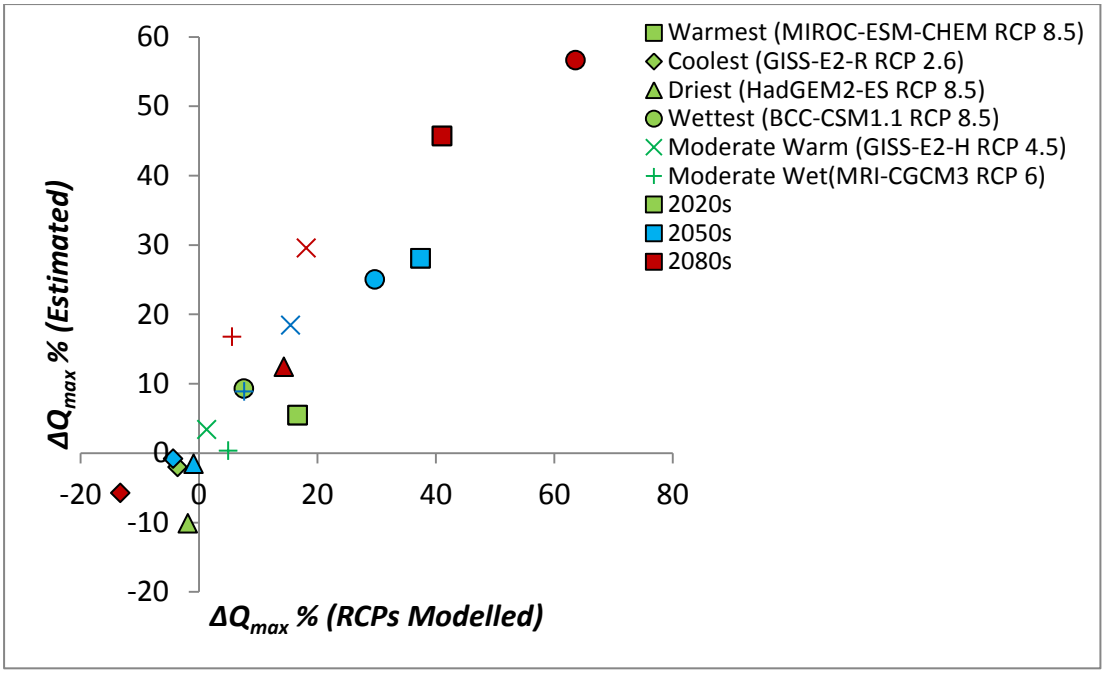

Figure D20: Modeled vs Estimated ΔQ_{max} (%) plot of all the scenarios for 2020s, 2050s and 2080s

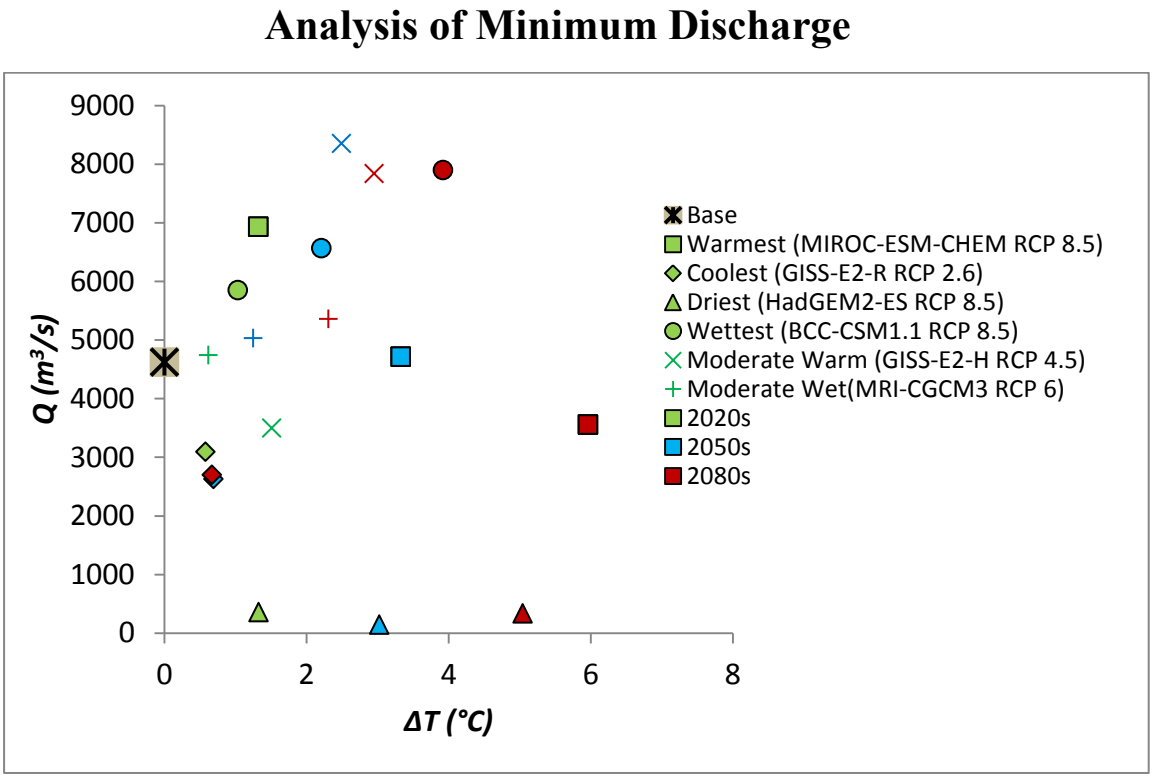

Figure D21 ΔT C) vs minimum annual discharge (m^3/s) of six scenarios for 2020s, 2050s and 2080s

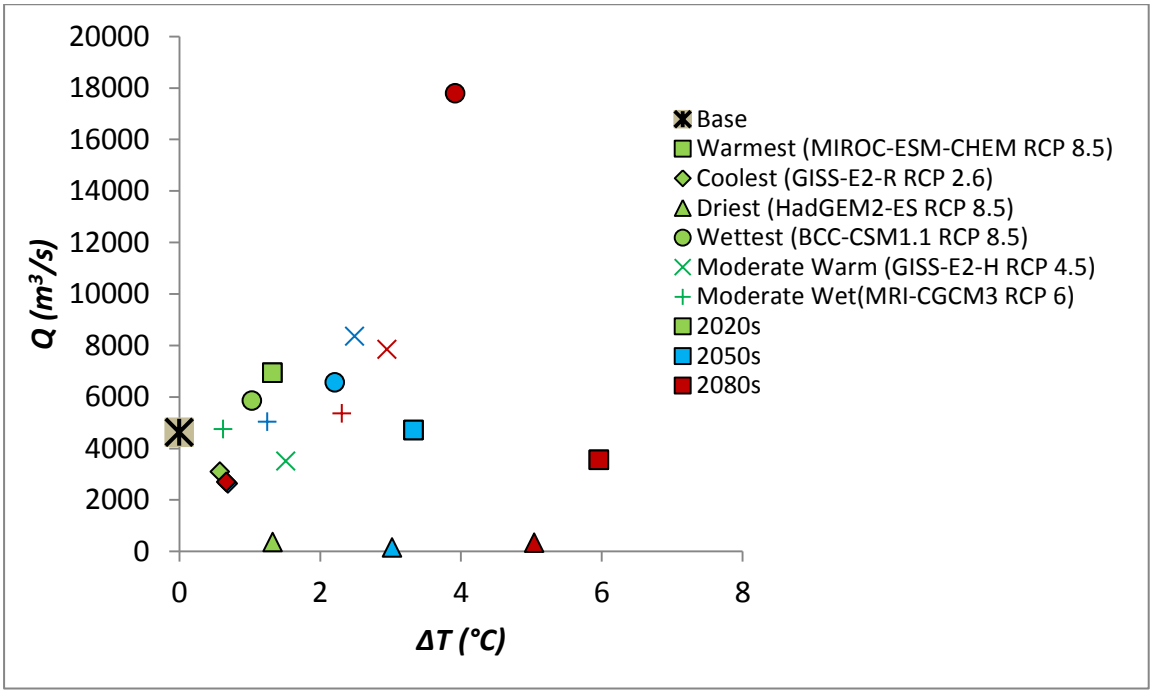

Figure D22 ΔT C) vs minimum dry period discharge (m^3/s) of scenarios for 2020s, 2050s and 2080s

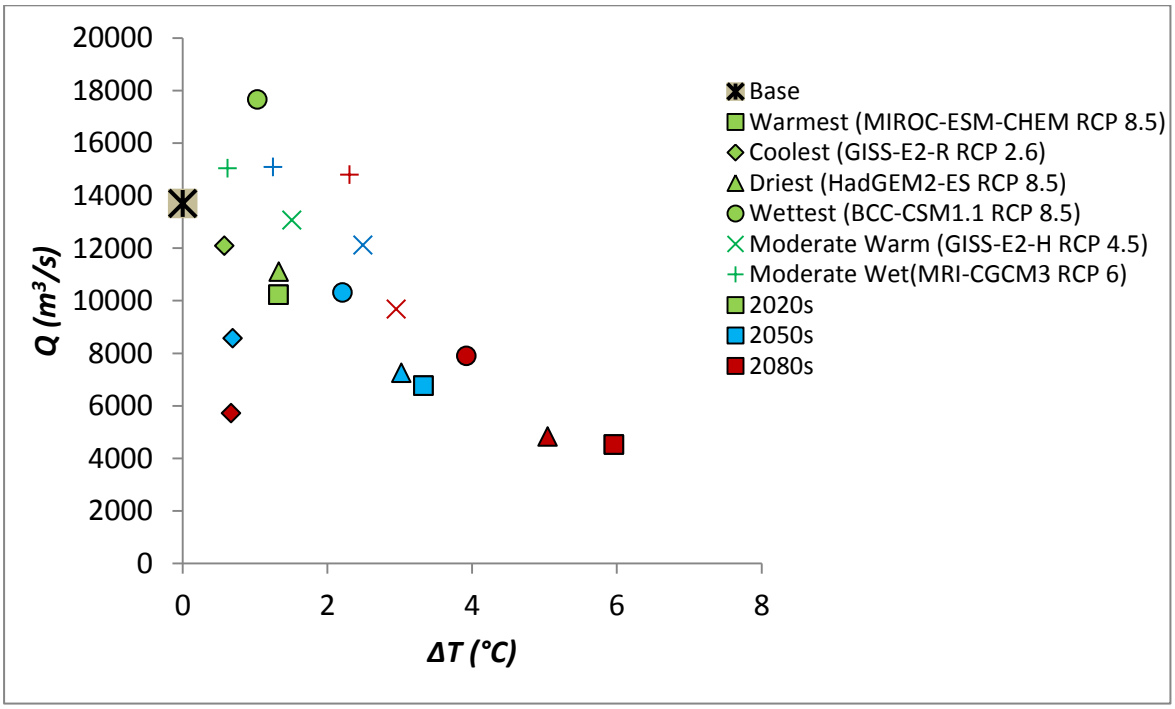

Figure D23 ΔT C) vs changes in minimum wet period discharge (m^3/s) of six scenarios for 2020s, 2050s and 2080s

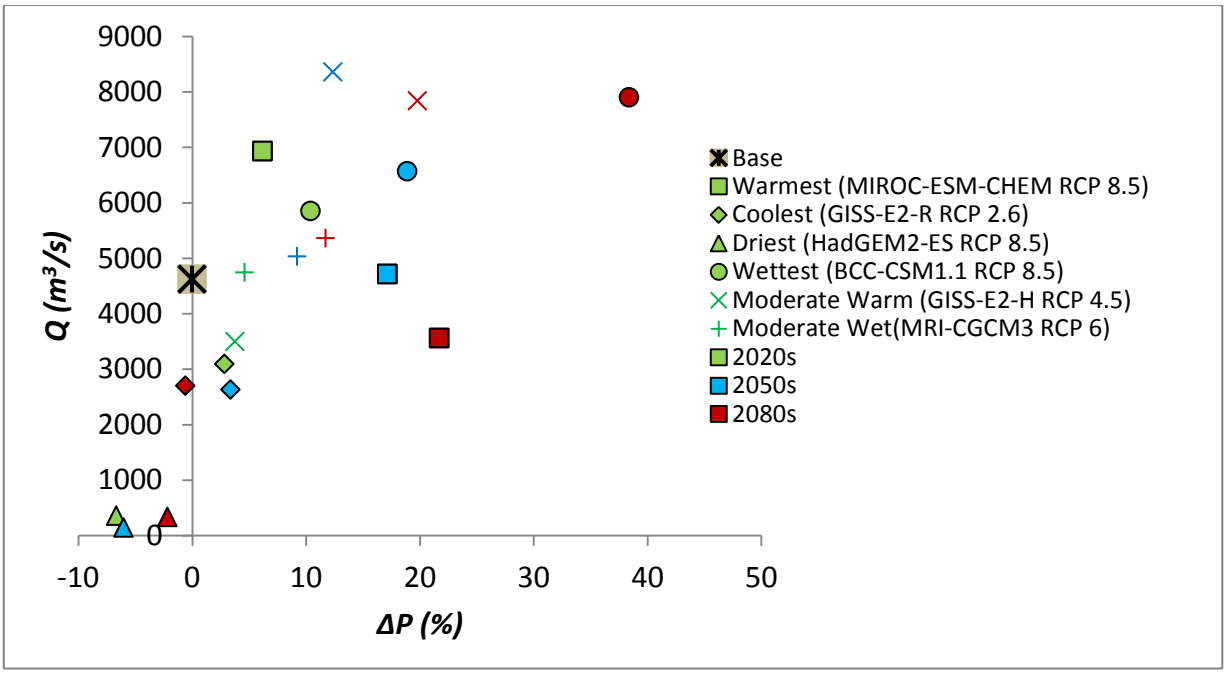

Figure D24 ΔP (%) vs minimum annual discharge (m^3/s) of six scenarios for 2020s, 2050s and 2080s

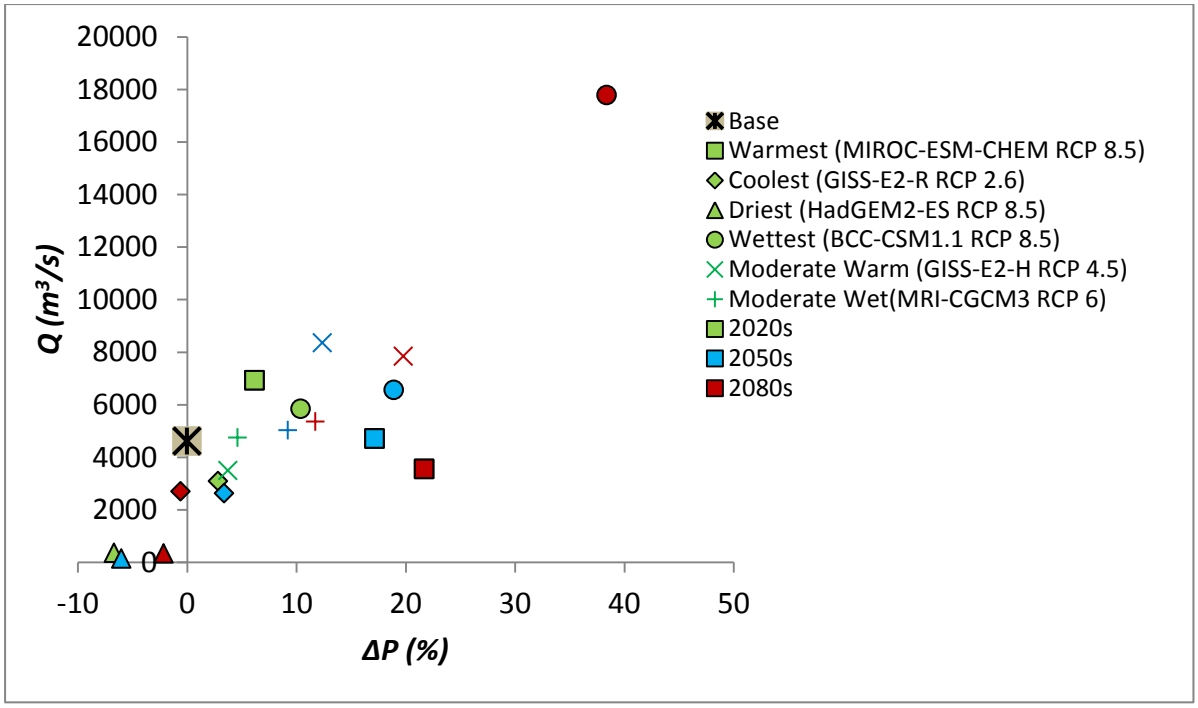

Figure D25 ΔP (%) vs minimum dry period discharge (m^3/s) of six scenarios for 2020s, 2050s and 2080s

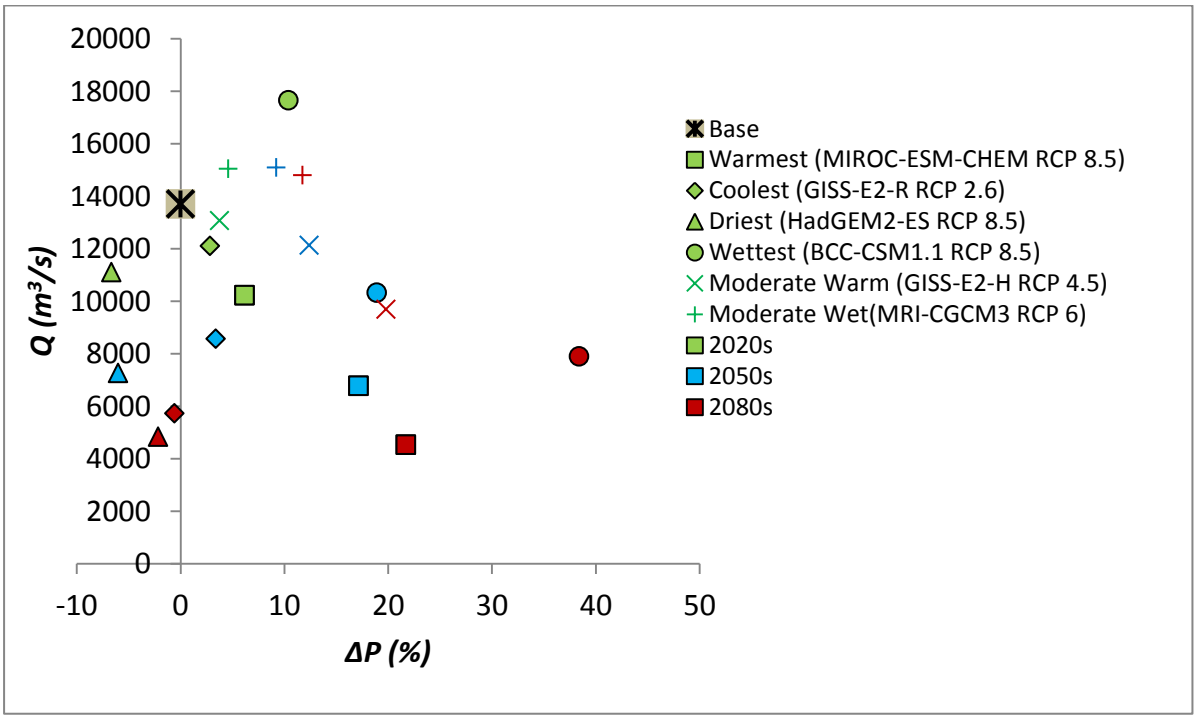

Figure D26 ΔP (%) vs minimum wet period discharge (m^3/s) of six scenarios for 2020s, 2050s and 2080s

AppendixE

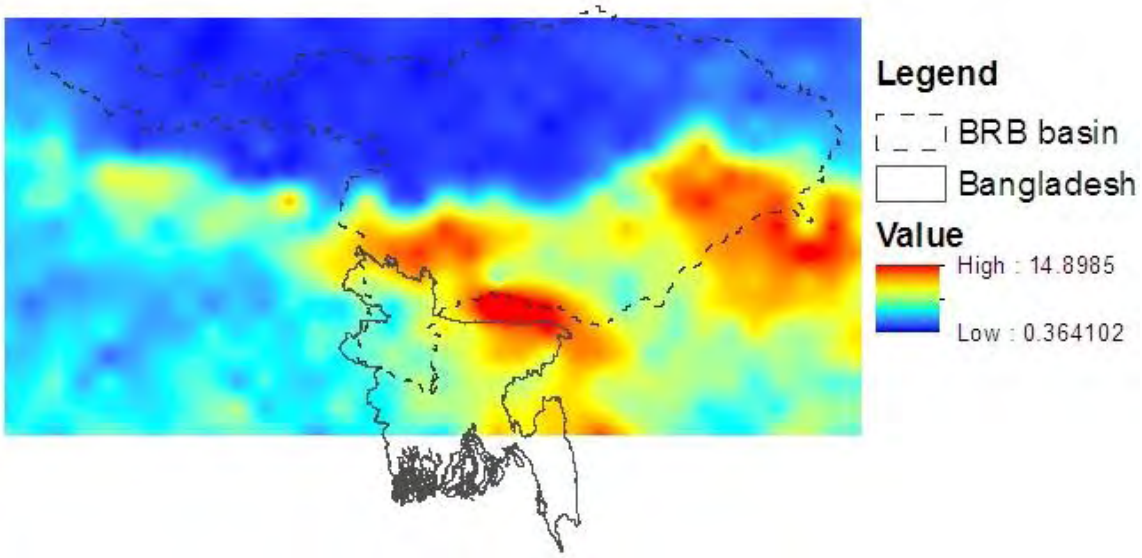

Figure E1: Spatial variation of precipitation (mm) for GISS-E2-H (RCP 4.5) in 2020s

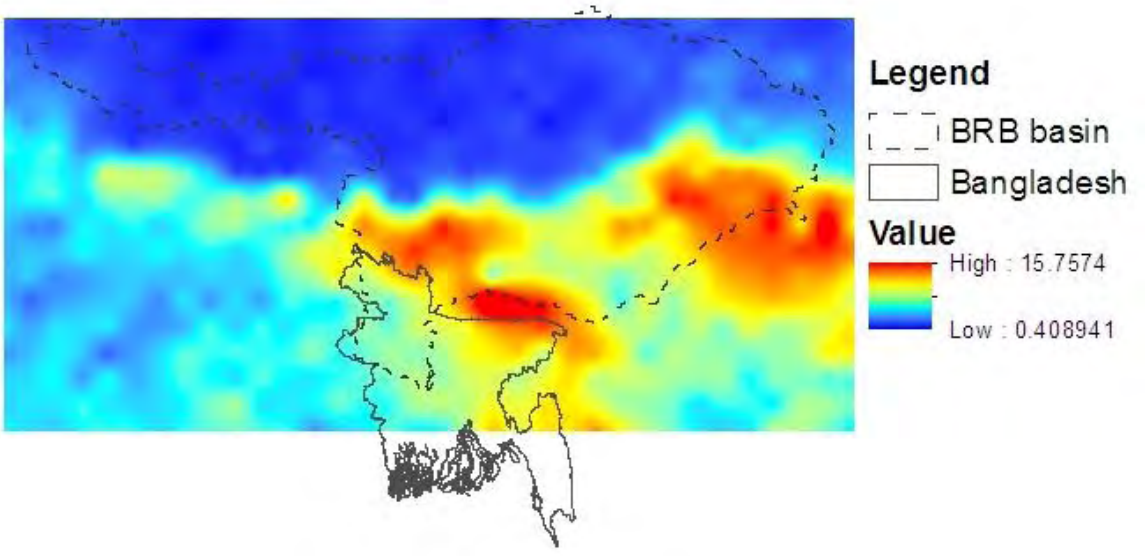

Figure E2: Spatial variation of precipitation (mm) for GISS-E2-H (RCP 4.5) in 2050s

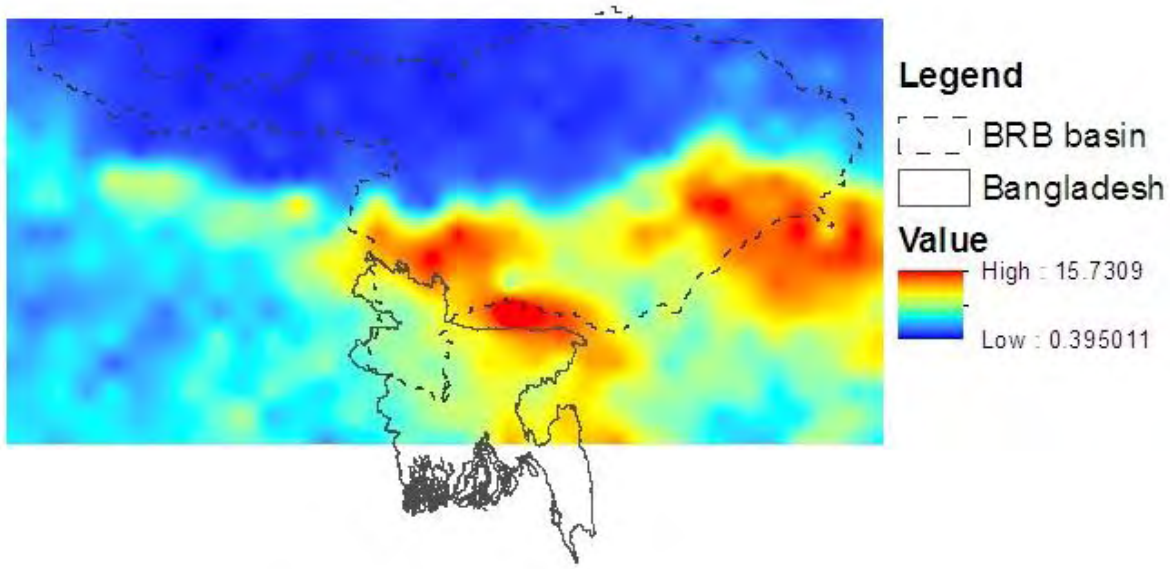

Figure E3: Spatial variation of precipitation (mm) for GISS-E2-H (RCP 4.5) in 2080s

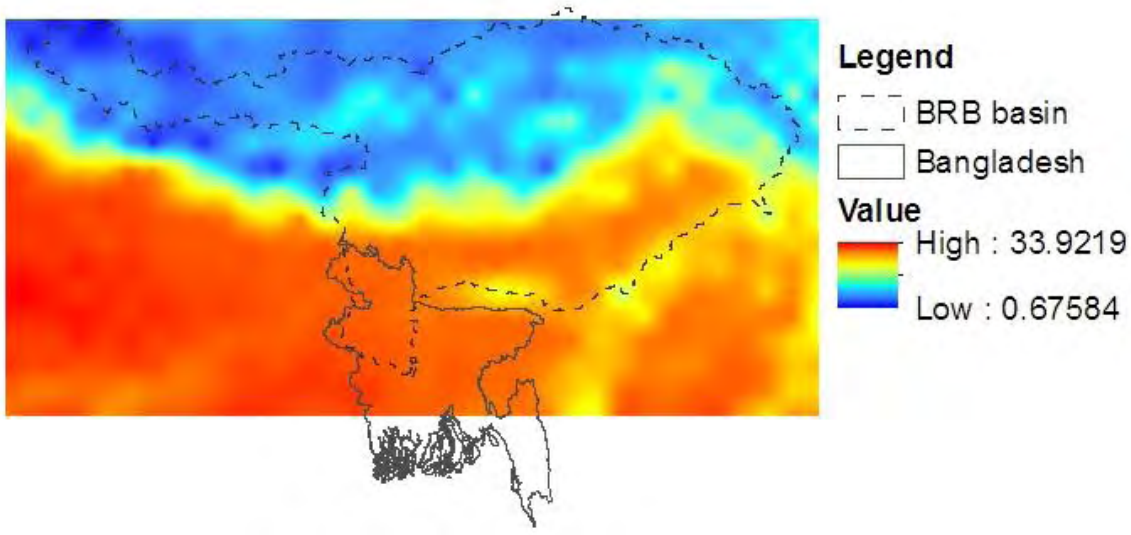

Figure E4 S C GISS-E2-H (RCP 4.5) in 2020s

\

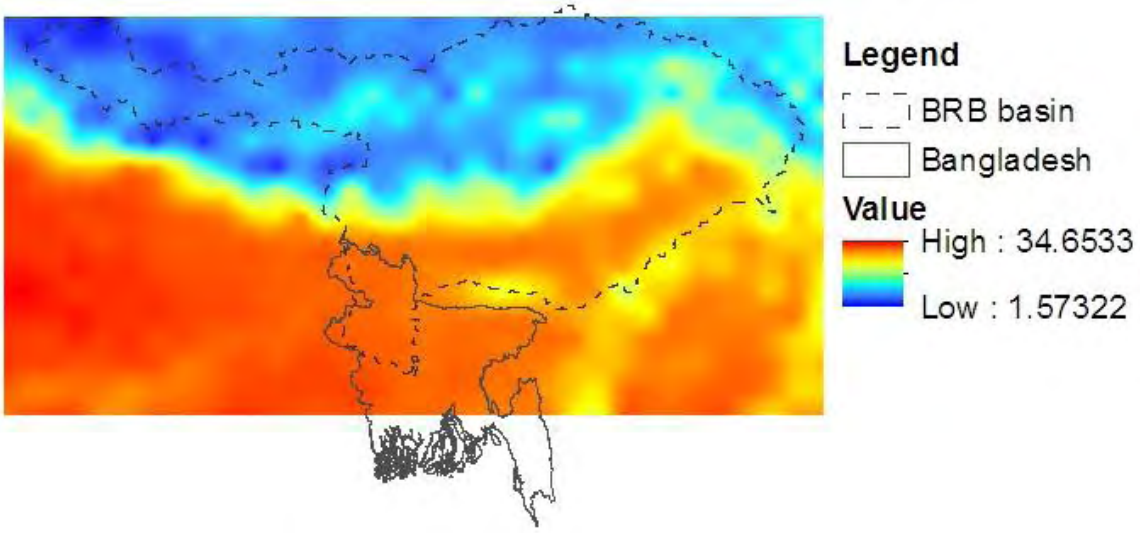

Figure E5 S C GISS-E2-H (RCP 4.5) in 2050s

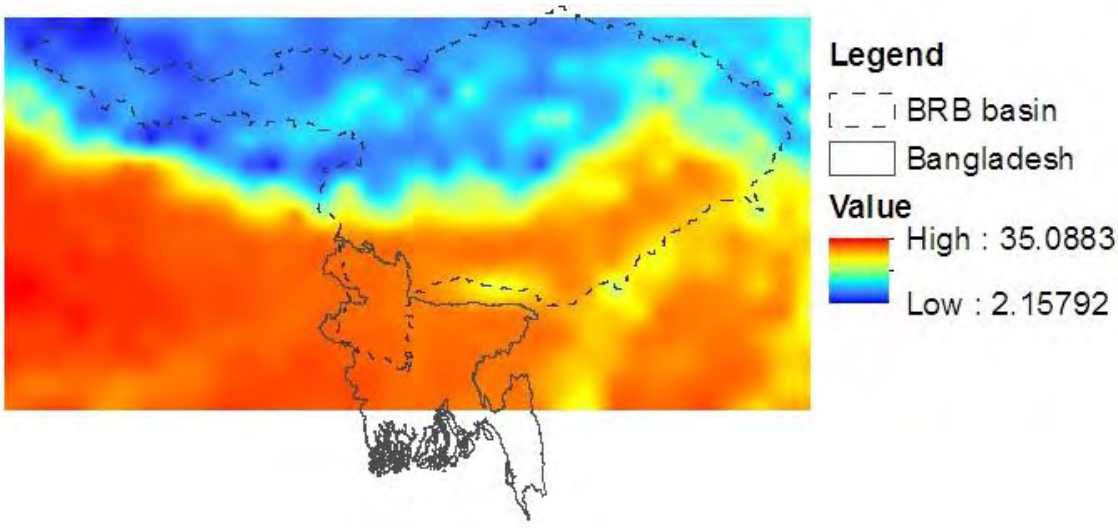

Figure E6: Spatial C GISS-E2-H (RCP 4.5) in 2080s

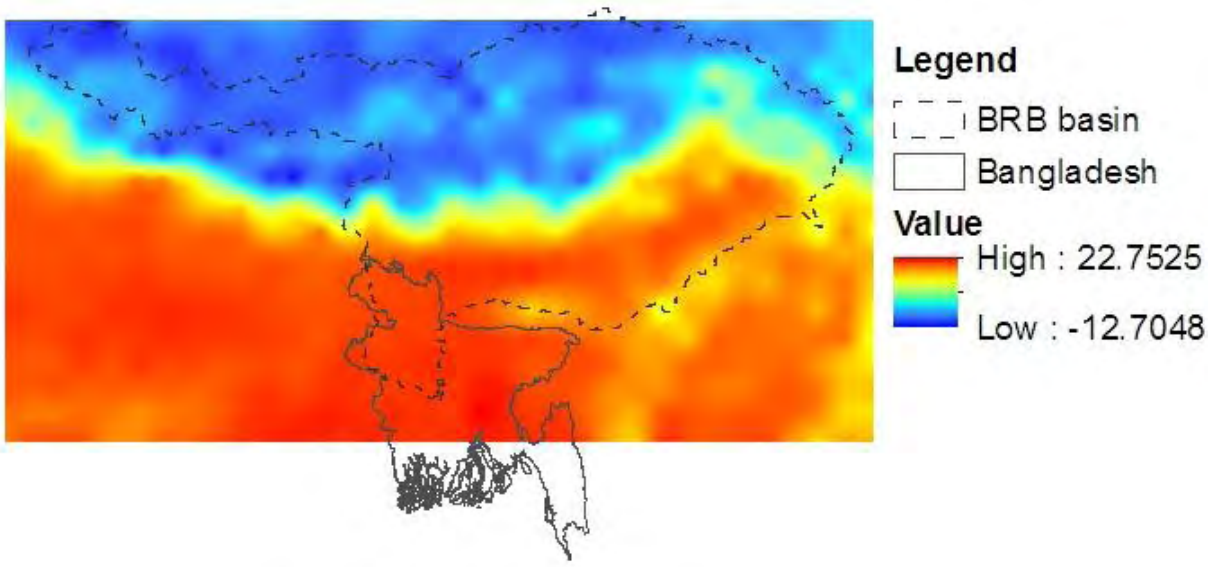

Figure E7 S C GISS-E2-H (RCP 4.5) in 2020s

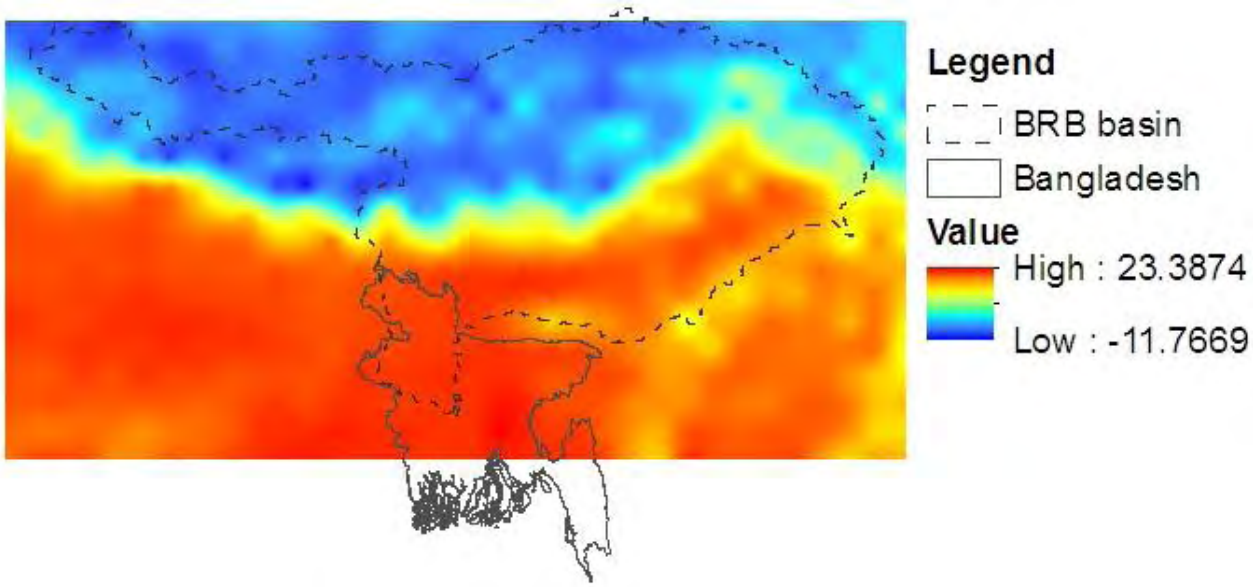

Figure E8 S C GISS-E2-H (RCP 4.5) in 2050s

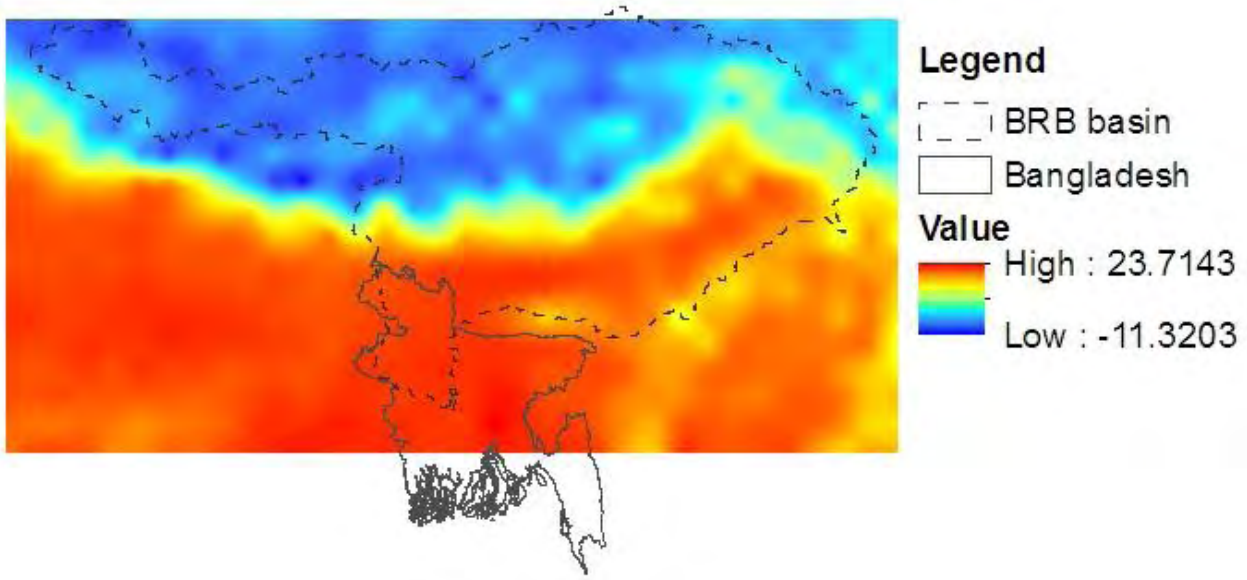

Figure E9 S C GISS-E2-H (RCP 4.5) in 2080s

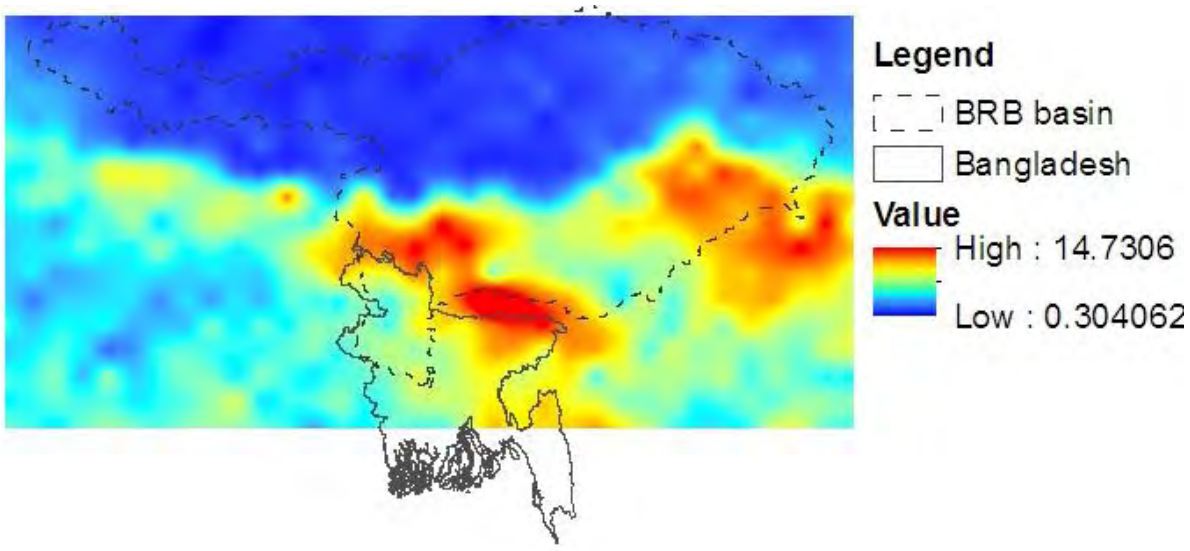

Figure E10: Spatial variation of precipitation (mm) for GISS-E2-R (RCP 2.6) in 2020s

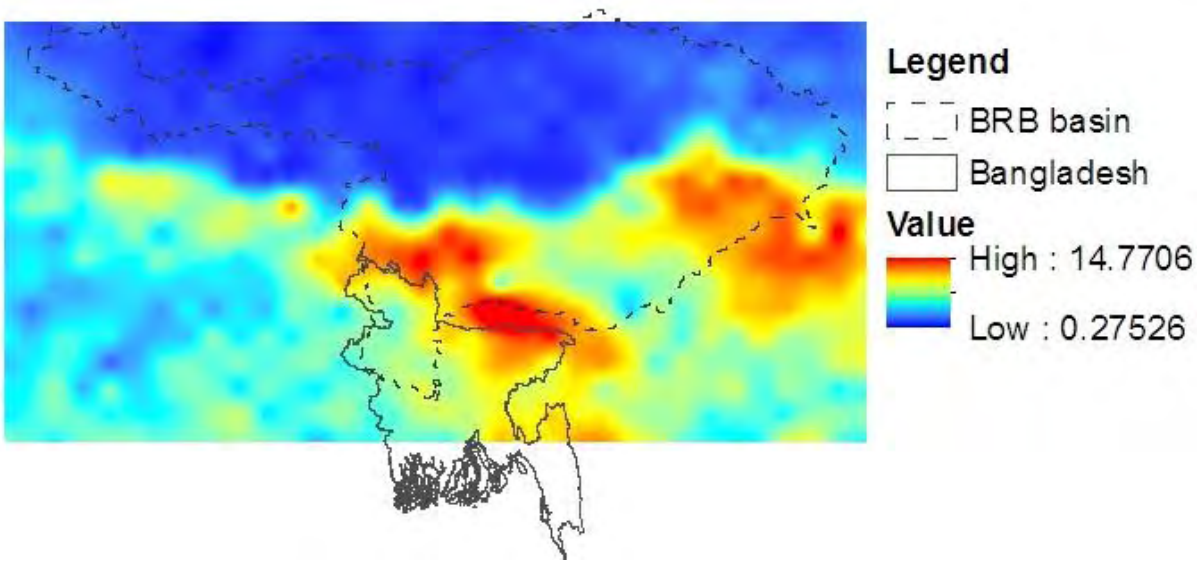

Figure E11: Spatial variation of precipitation (mm) for GISS-E2-R (RCP 2.6) in 2050s

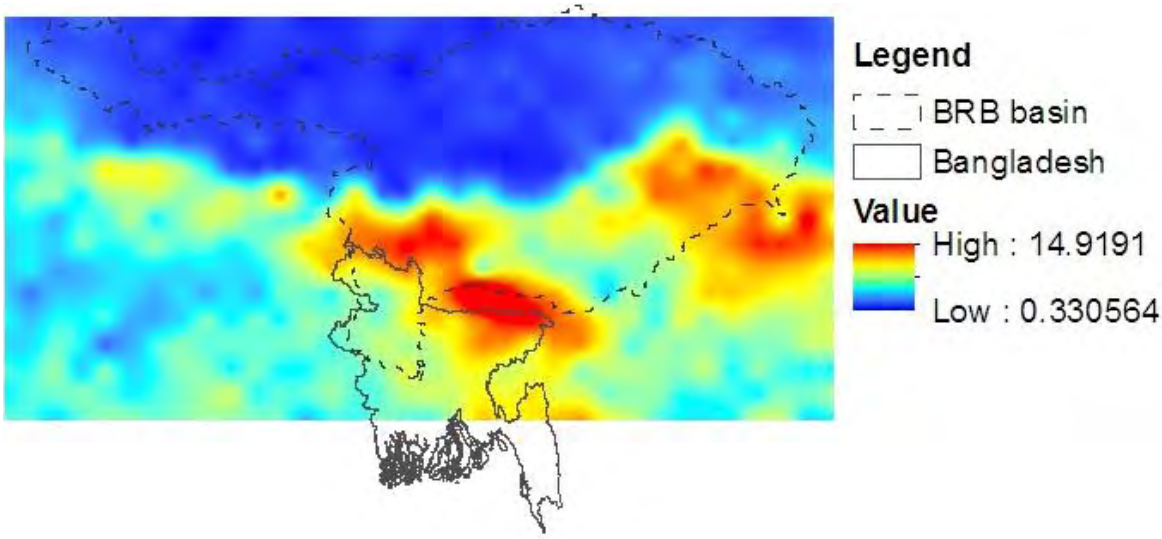

Figure E12: Spatial variation of precipitation (mm) for GISS-E2-R (RCP 2.6) in 2080s

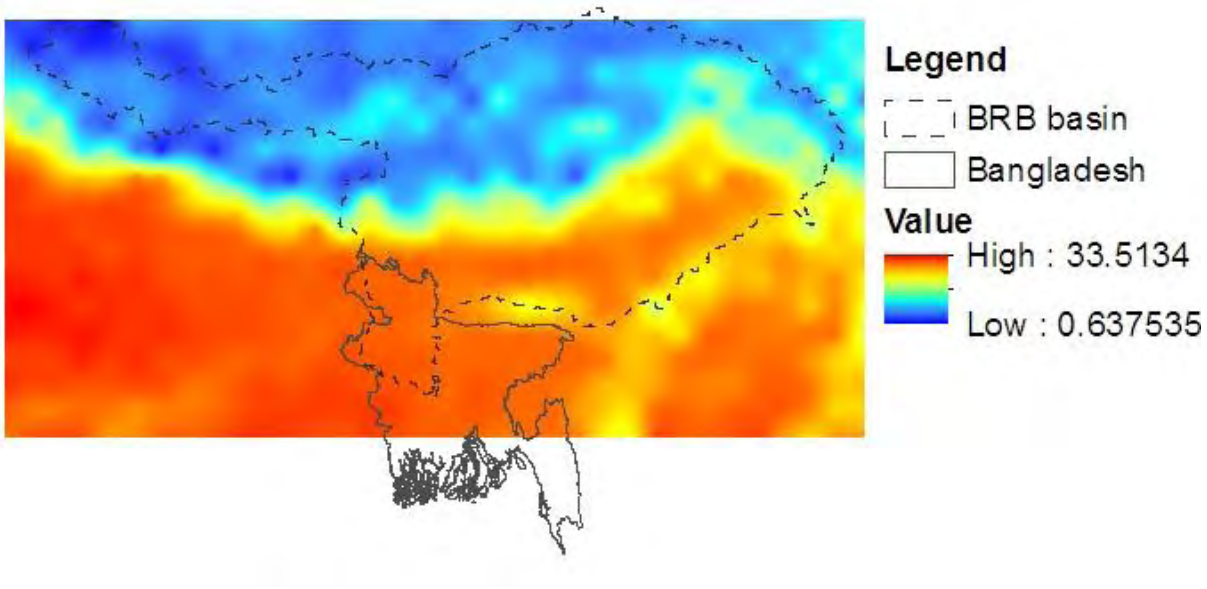

Figure E13 S C GISS-E2-R (RCP 2.6) in 2020s

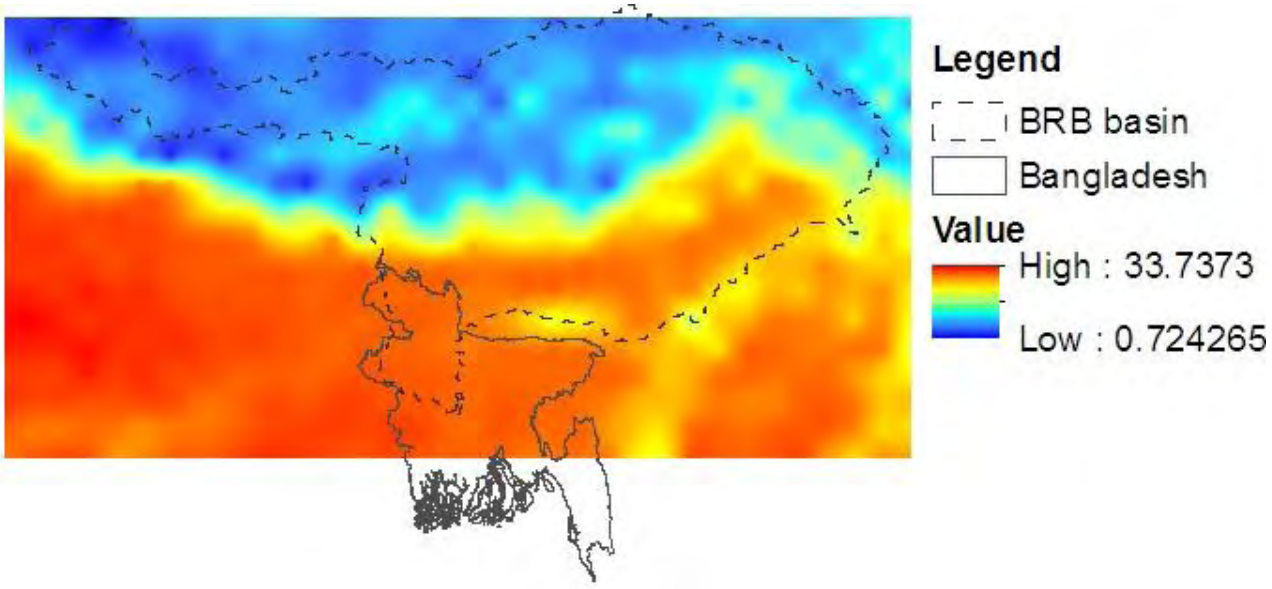

Figure E14: Spatial variation of maximu C GISS-E2-R (RCP 2.6) in 2050s

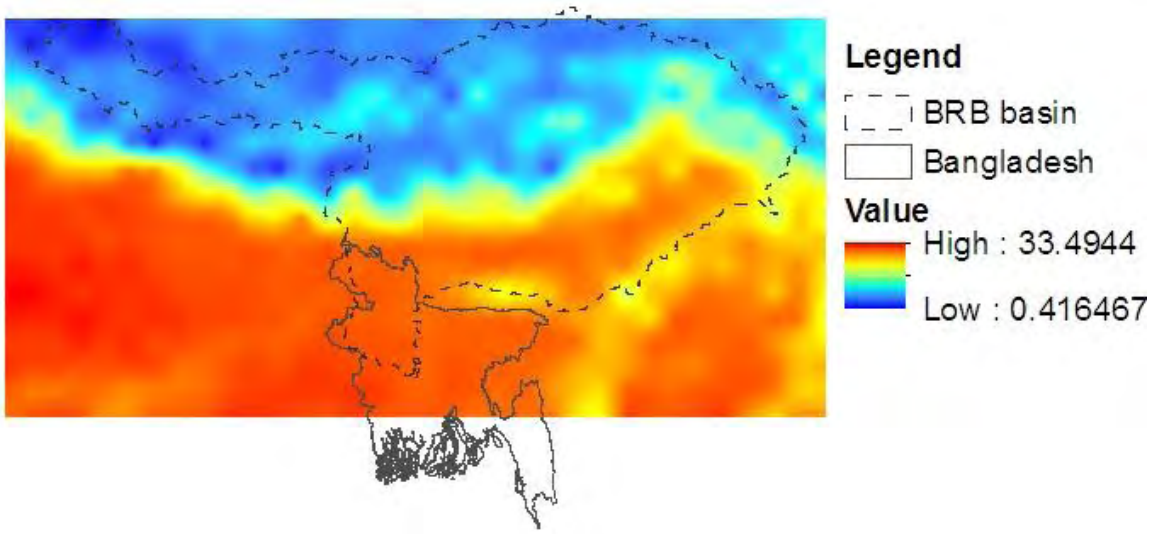

Figure E15 S C GISS-E2-R (RCP 2.6) in 2080s

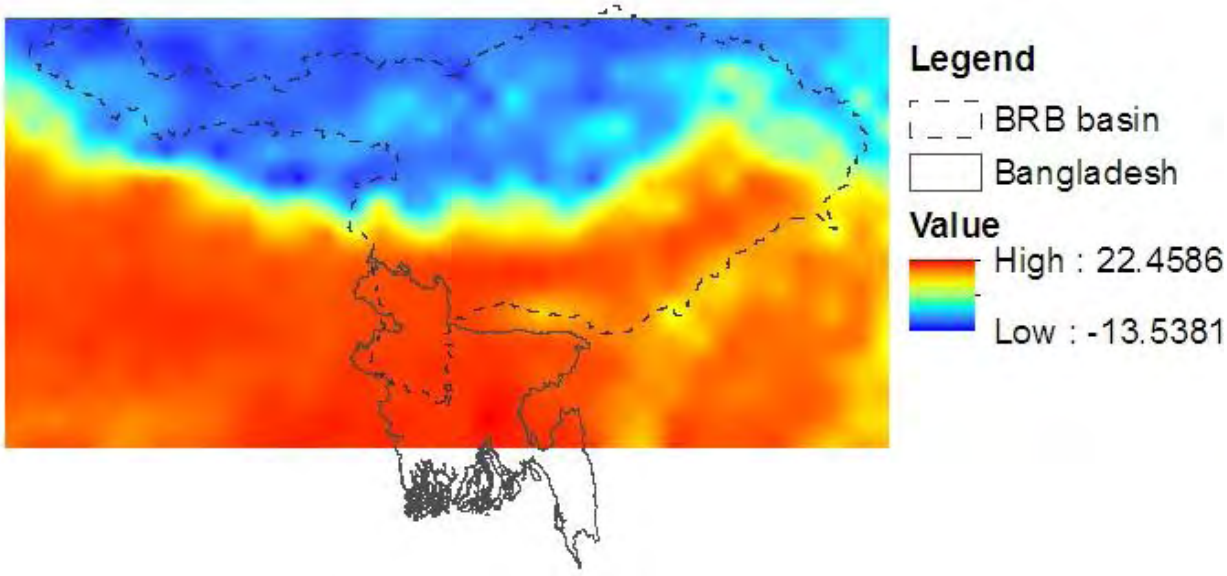

Figure E16 S C GISS-E2-R (RCP 2.6) in 2020s

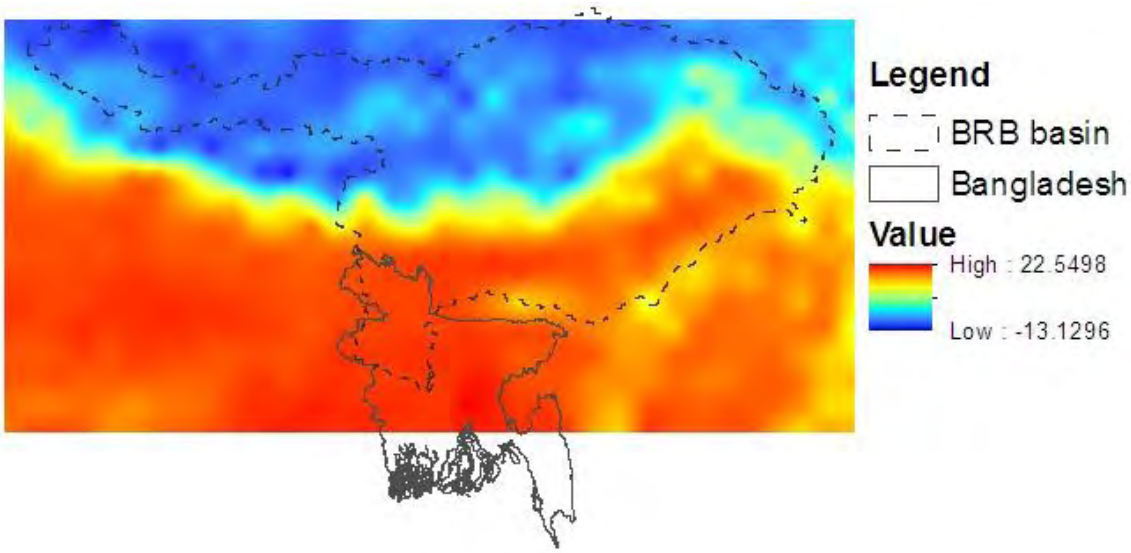

Figure E17 S C GISS-E2-R (RCP 2.6) in 2050s

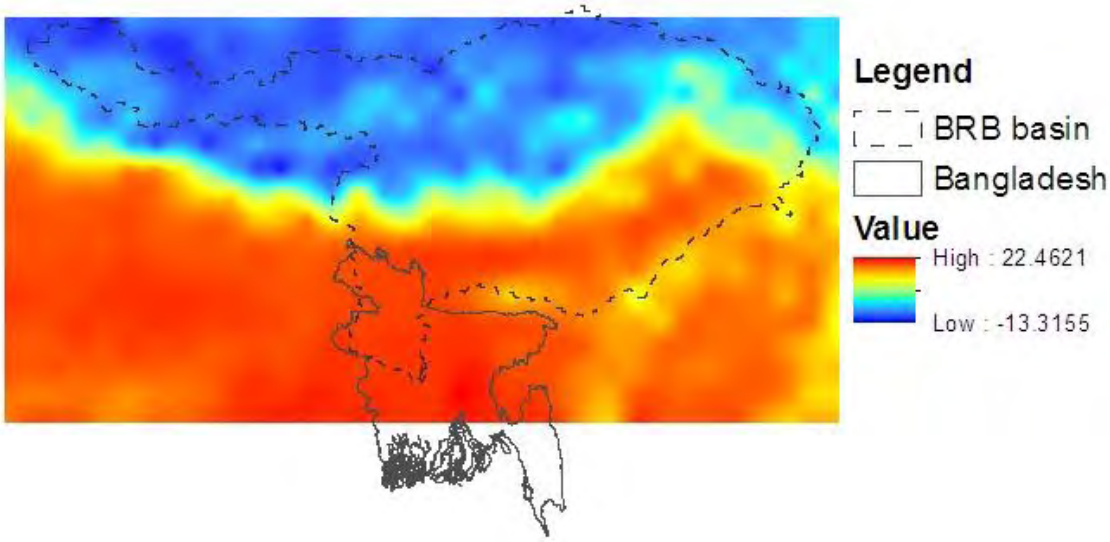

Figure E18 S C GISS-E2-R (RCP 2.6) in 2050s

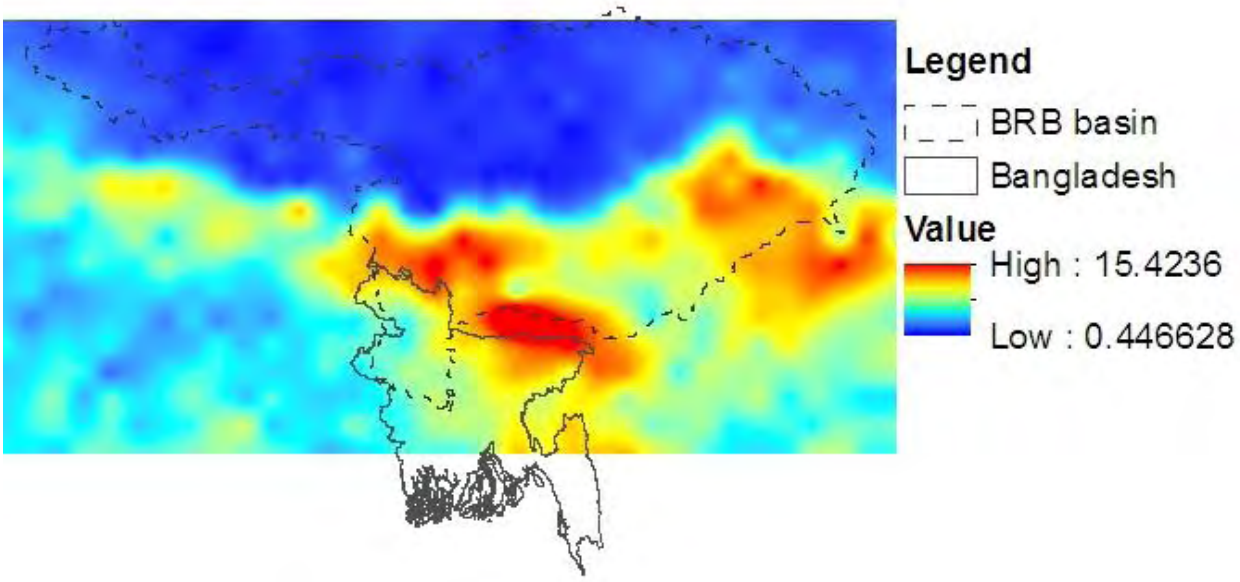

Figure E19: Spatial variation of precipitation (mm) for MRI-CGCM3 (RCP 6.0) in 2020s

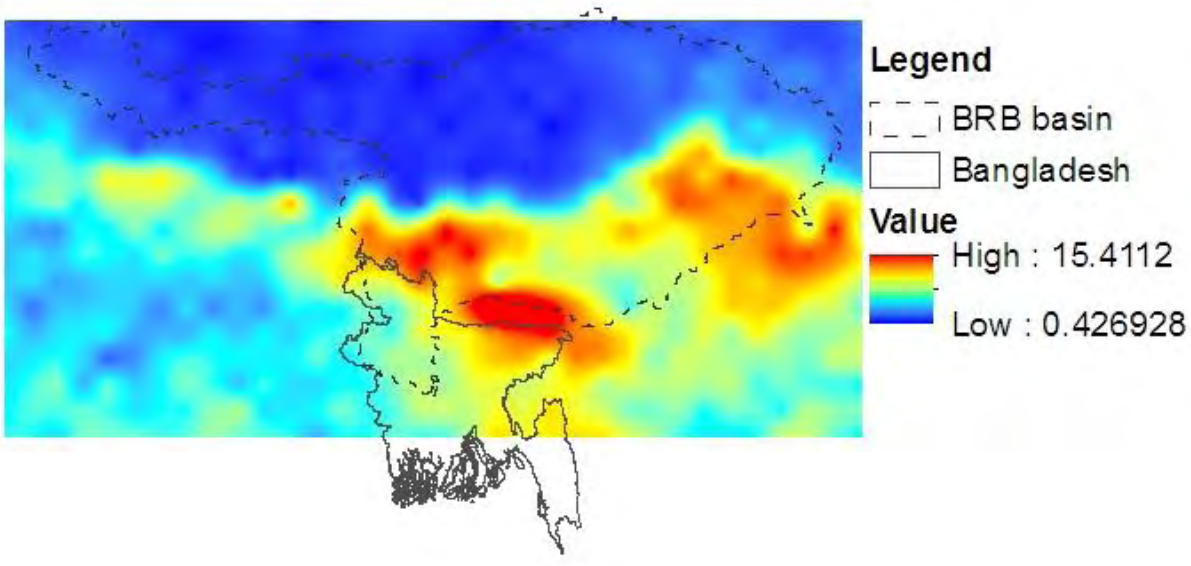

Figure E20: Spatial variation of precipitation (mm) for MRI-CGCM3 (RCP 6.0) in 2050s

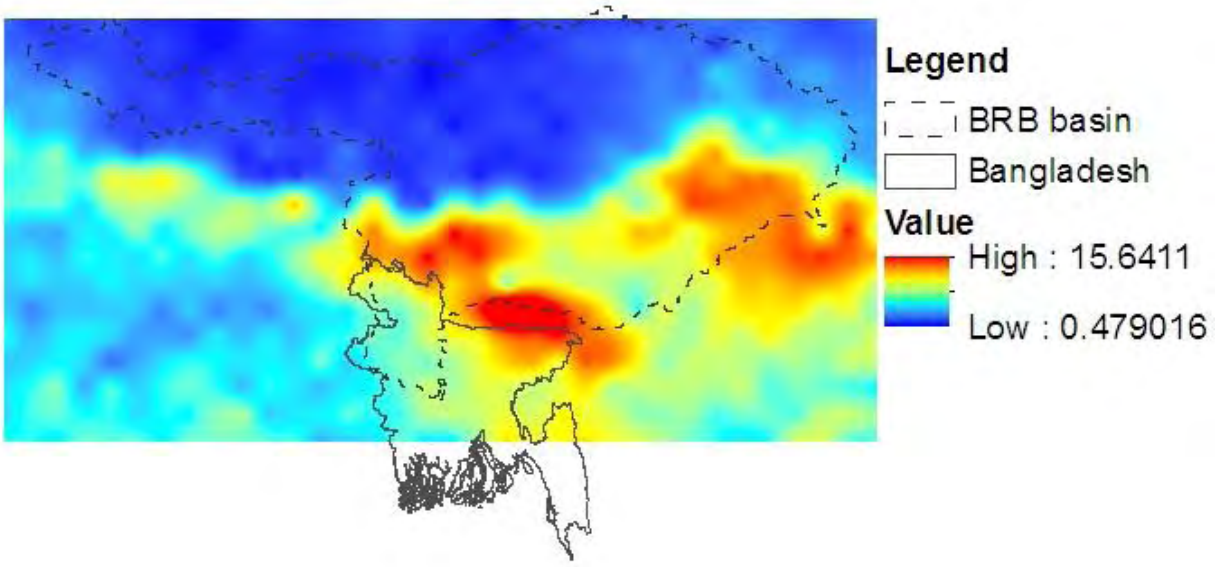

Figure E21: Spatial variation of precipitation (mm) for MRI-CGCM3 (RCP 6.0) in 2080s

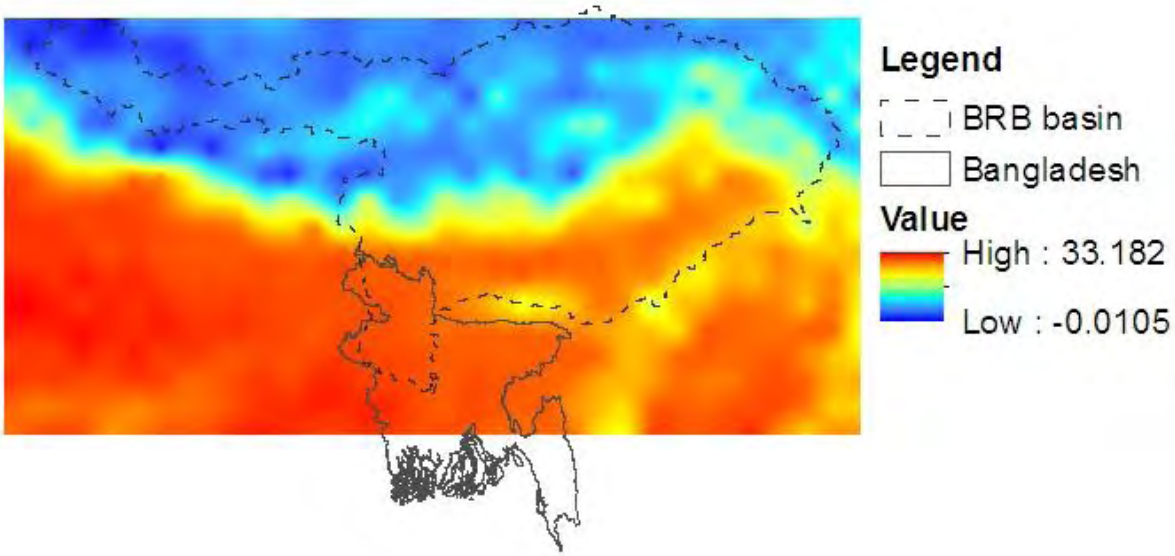

Figure E22 S C MRI-CGCM3 (RCP 6.0) in 2020s

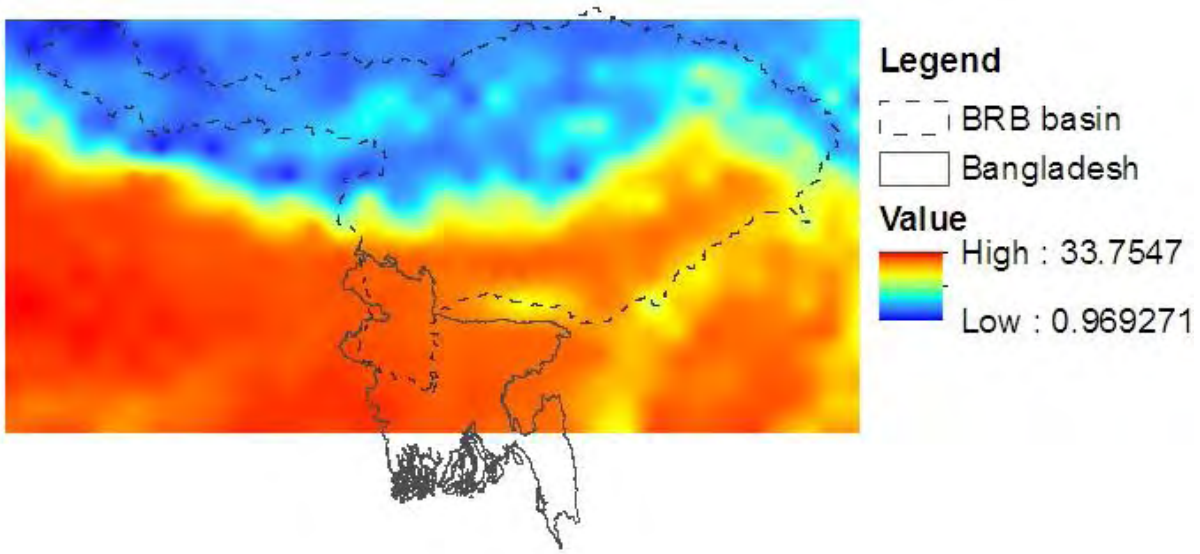

Figure E23 S C MRI-CGCM3 (RCP 6.0) in 2050s

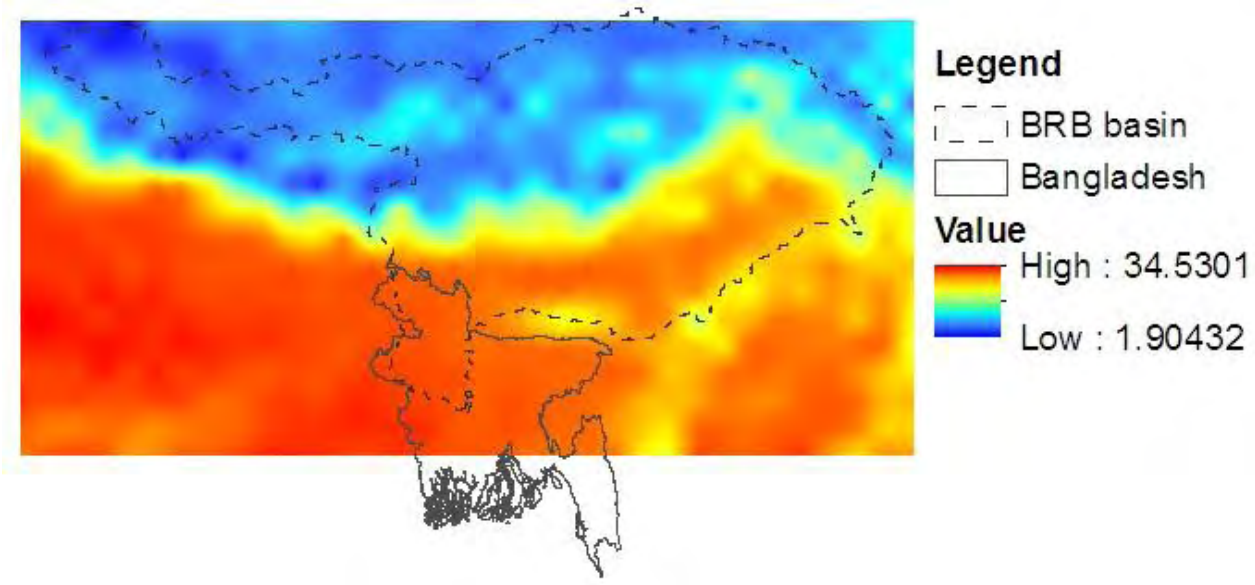

Figure E24 S C MRI-CGCM3 (RCP 6.0) in 2080s

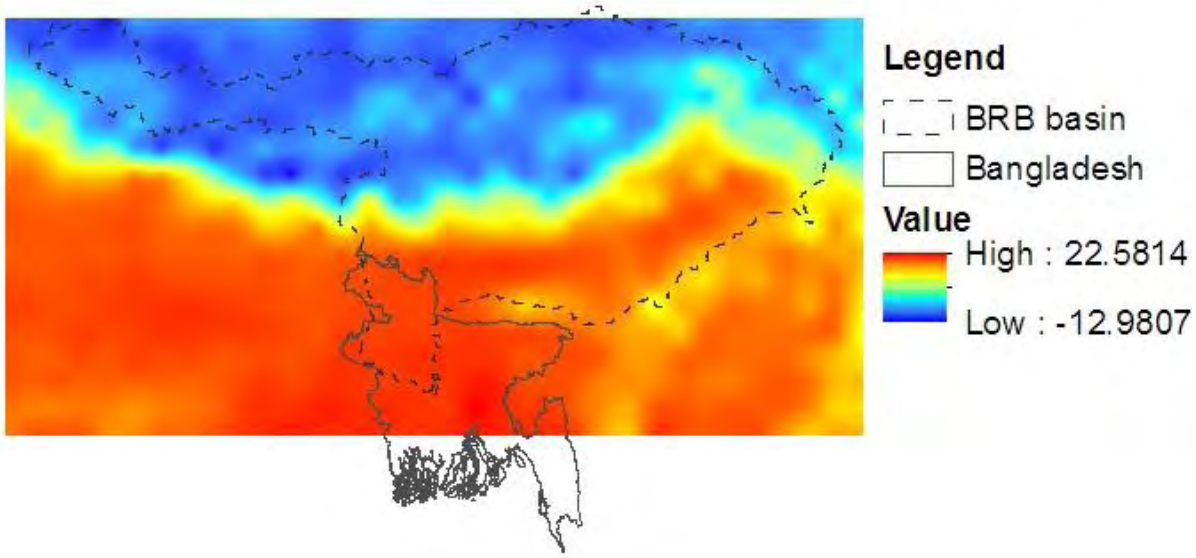

Figure E25: Spatial variation of C MRI-CGCM3 (RCP 6.0) in 2020s

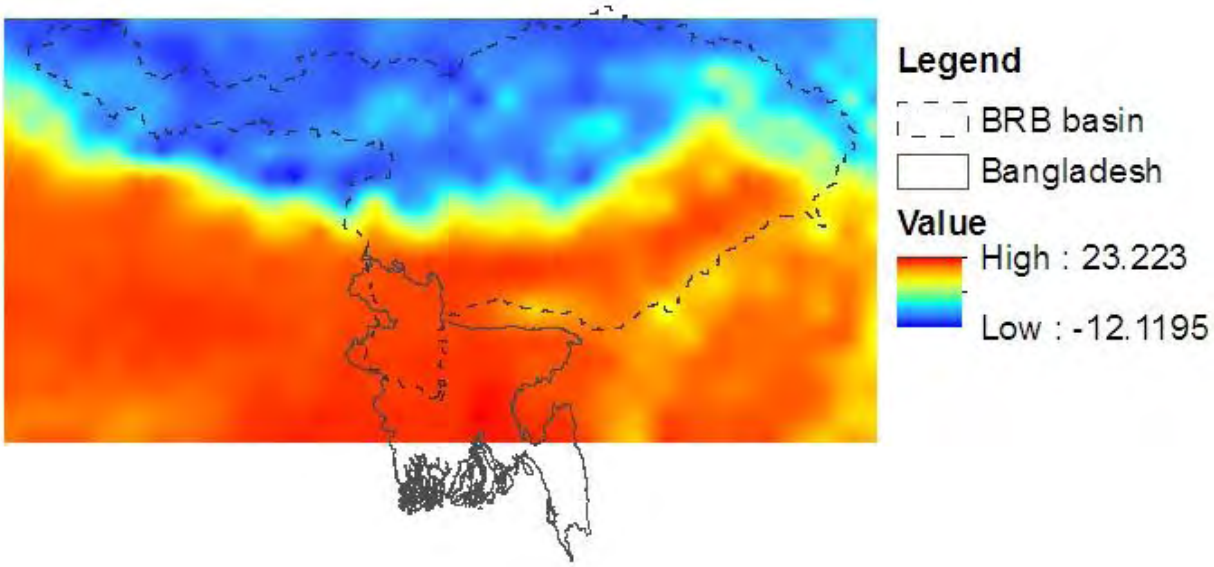

Figure E26 S C MRI-CGCM3 (RCP 6.0) in 2050s

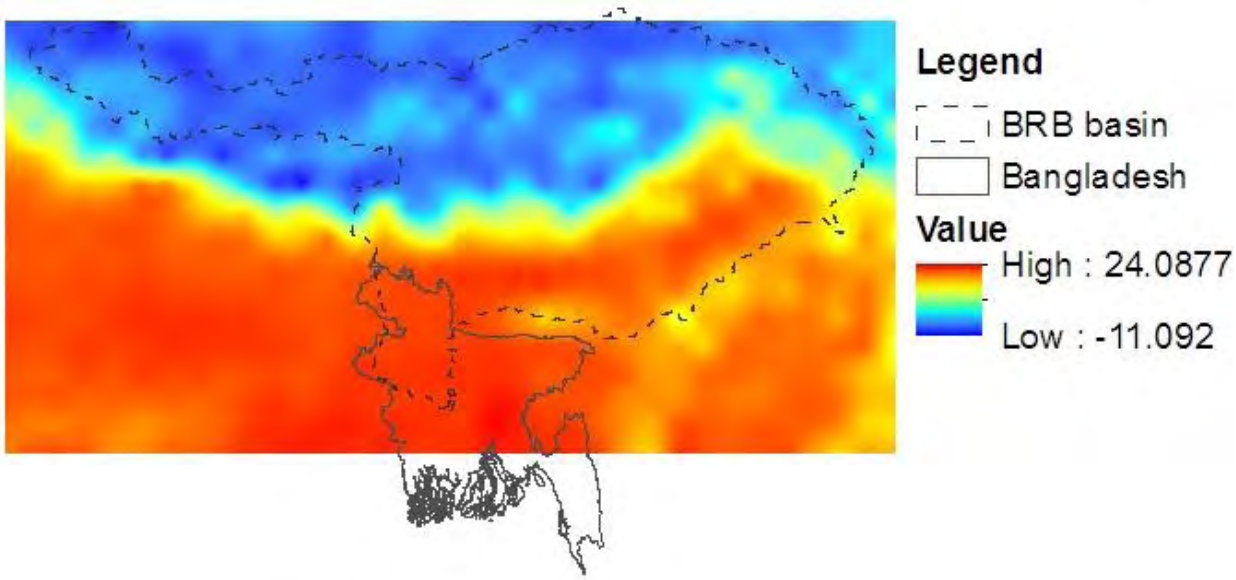

Figure E27 S C MRI-CGCM3 (RCP 6.0) in 2080s

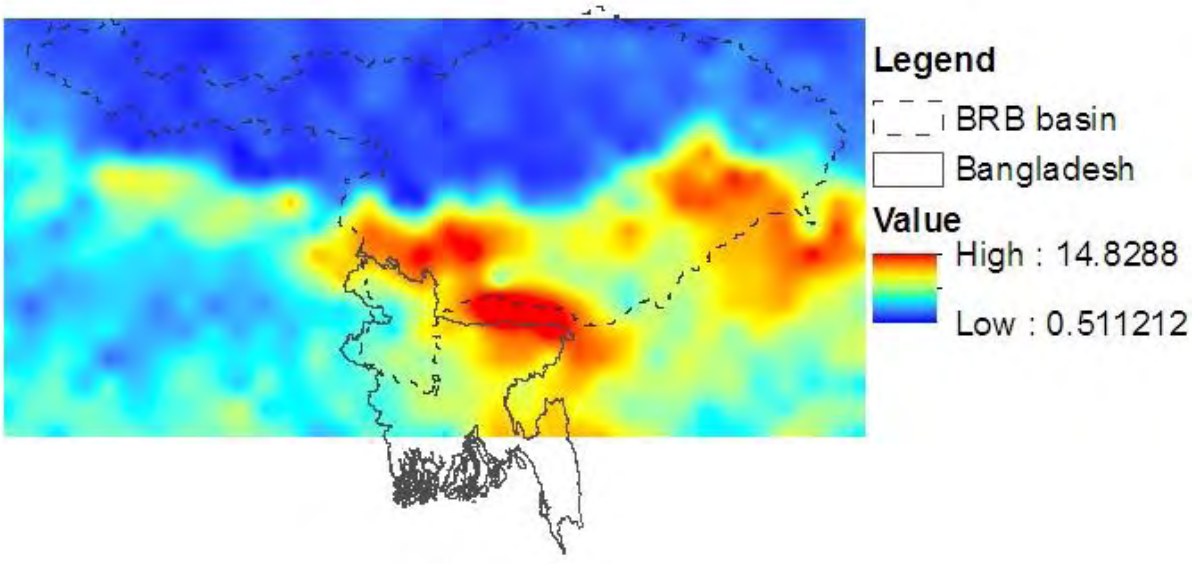

Figure E28: Spatial variation of precipitation (mm) for MIROC-ESM-CHEM(RCP 8.5) in 2020s

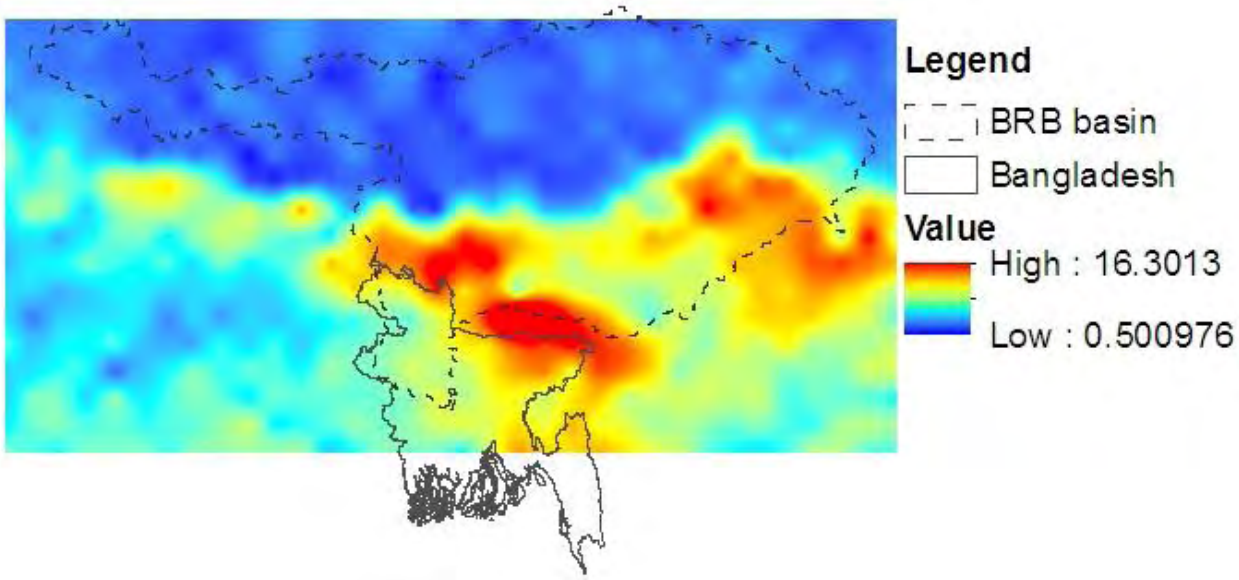

Figure E29: Spatial variation of precipitation (mm) for MIROC-ESM-CHEM(RCP 8.5) in 2080s

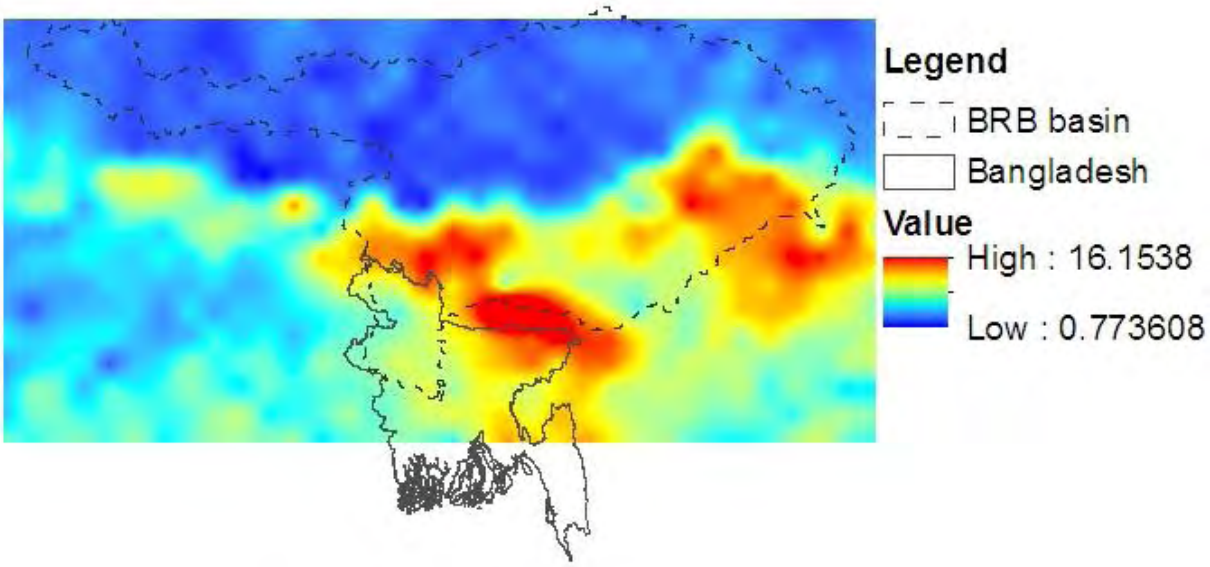

Figure E30: Spatial variation of precipitation (mm) for MIROC-ESM-CHEM(RCP 8.5) in 2080s

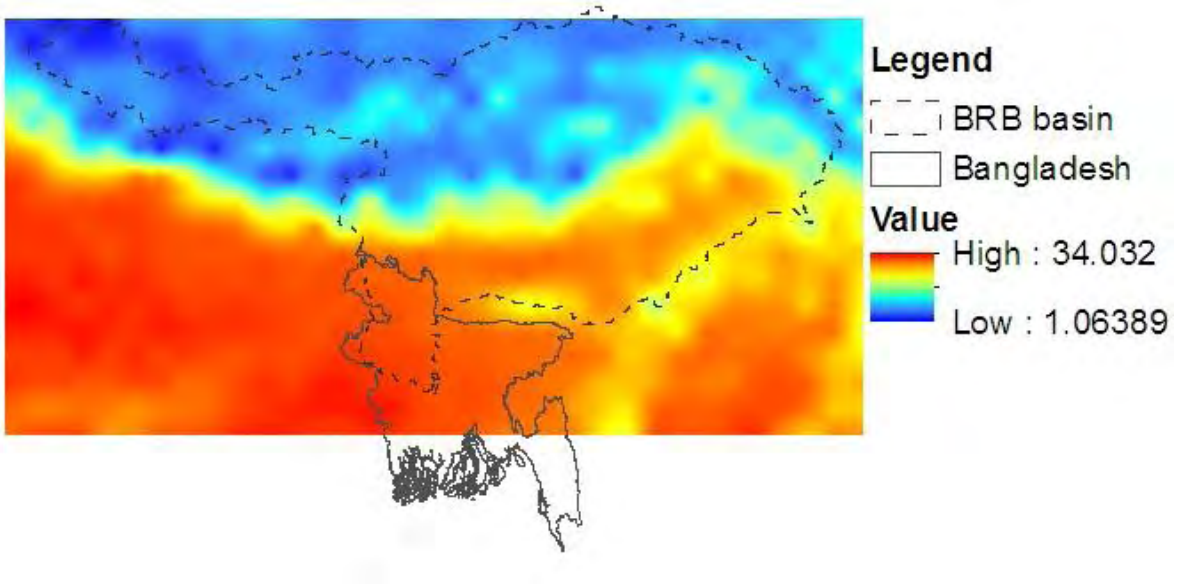

Figure E31 S C MIROC-ESM-CHEM(RCP 8.5) in 2020s

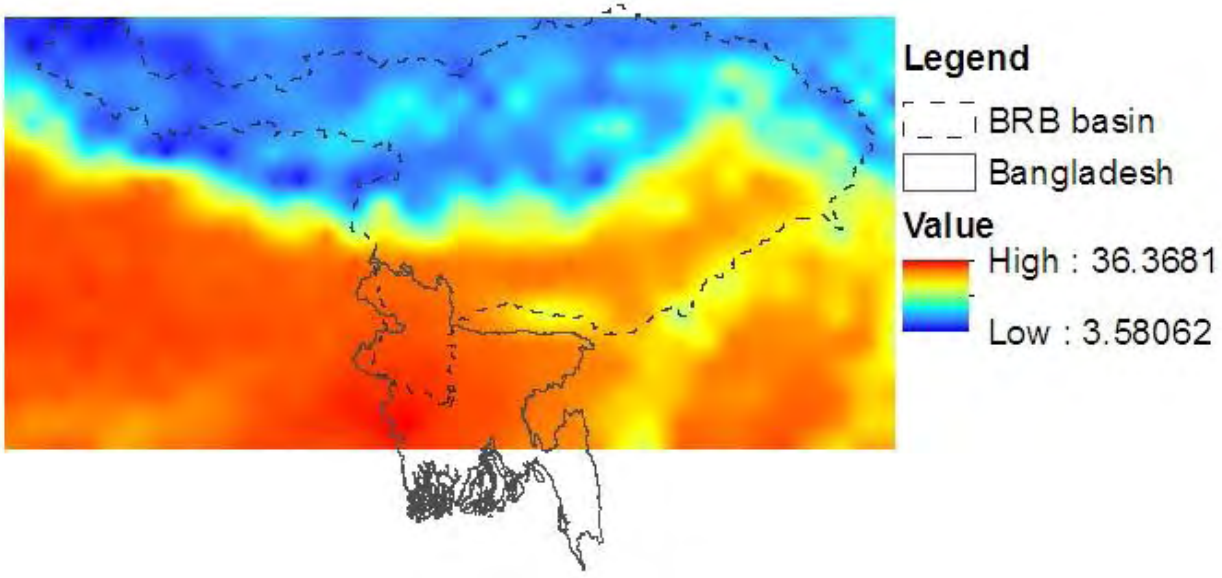

Figure E32 S C MIROC-ESM-CHEM(RCP 8.5) in 2050s

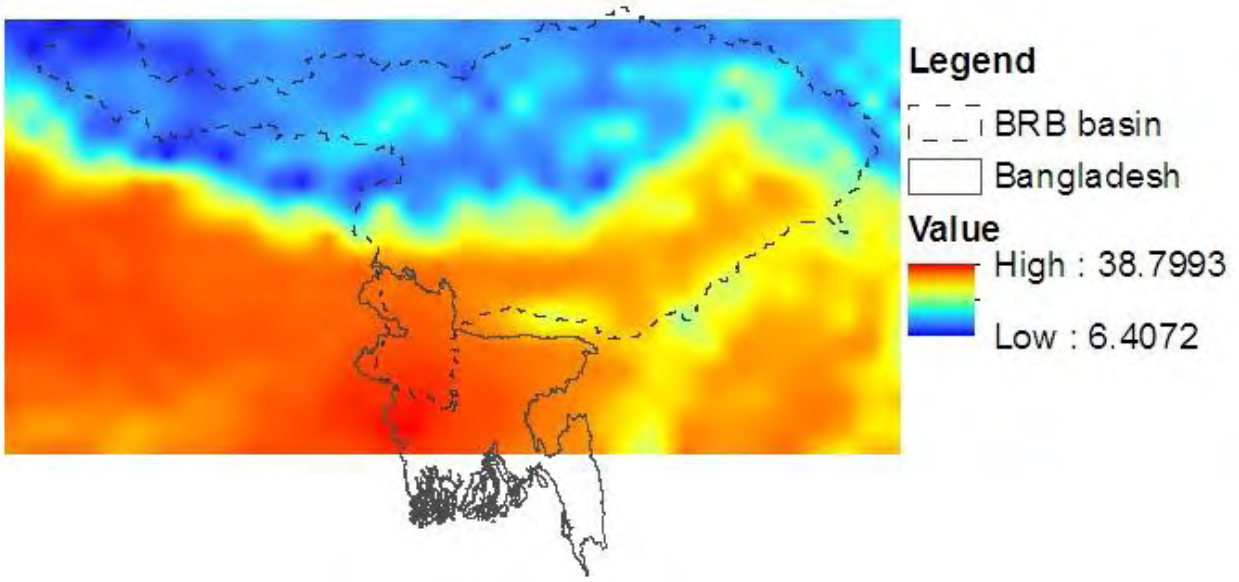

Figure E33: Spatial variation of maximum C MIROC-ESM-CHEM(RCP 8.5) in 2080s

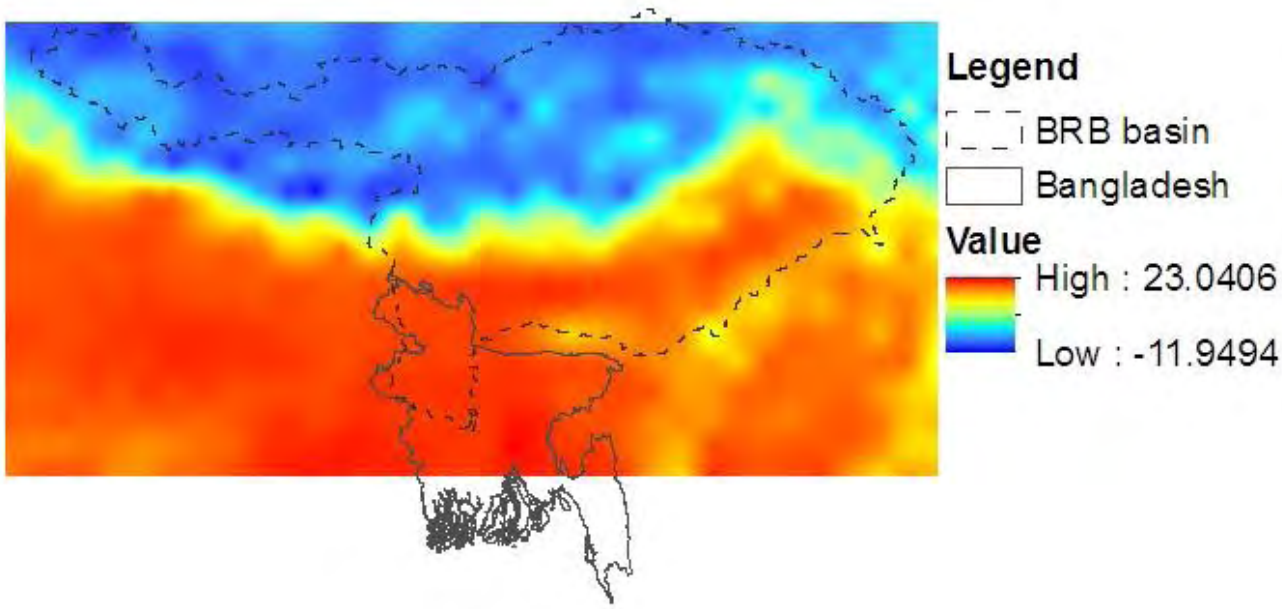

Figure E34 S C MIROC-ESM-CHEM(RCP 8.5) in 2020s

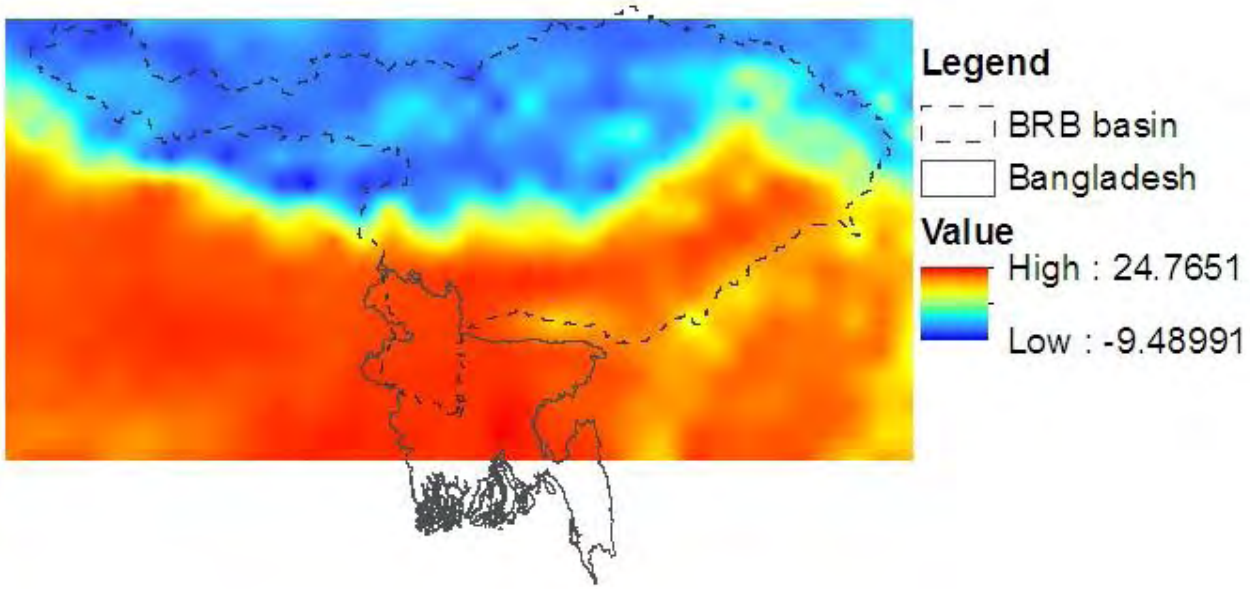

Figure E35 S C MIROC-ESM-CHEM(RCP 8.5) in 2050s

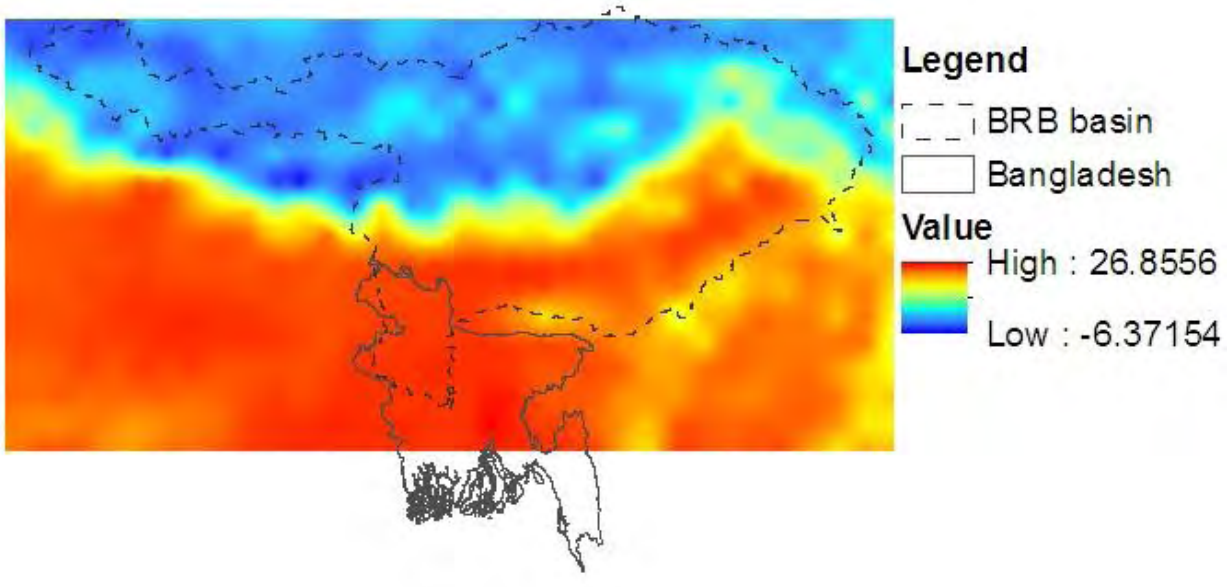

Figure E36 S C MIROC-ESM-CHEM(RCP 8.5) in 2080s

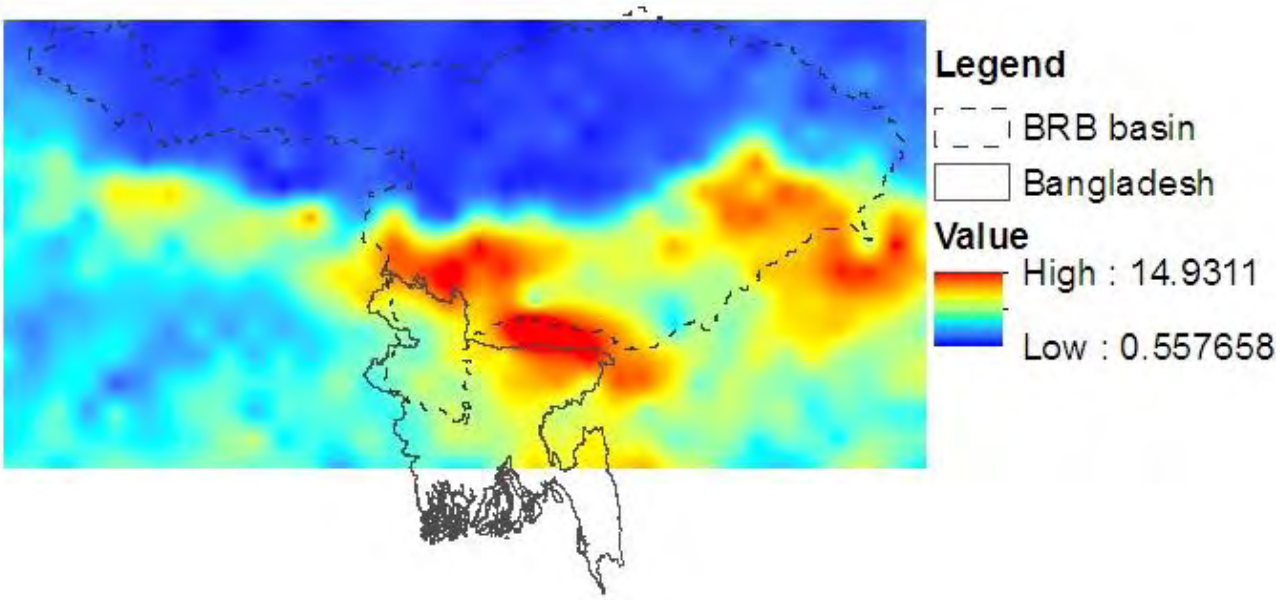

Figure E37: Spatial variation of precipitation (mm) for BCC-CSM1.1(RCP 8.5) in 2020s

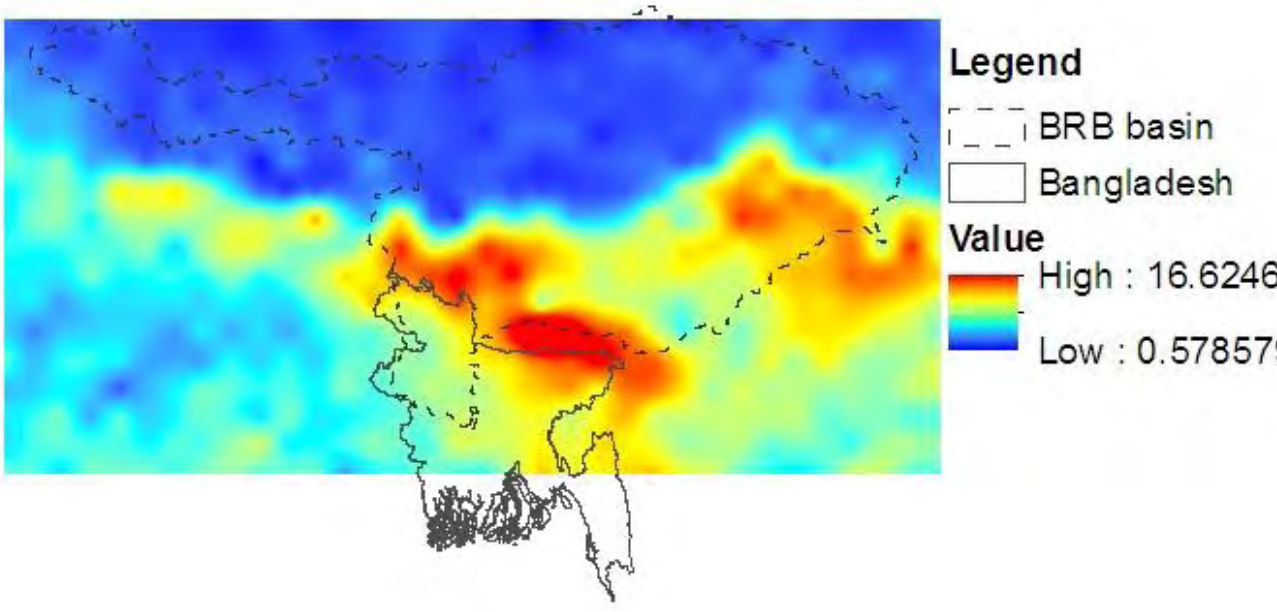

Figure E38: Spatial variation of precipitation (mm) for BCC-CSM1.1(RCP 8.5) in 2050s

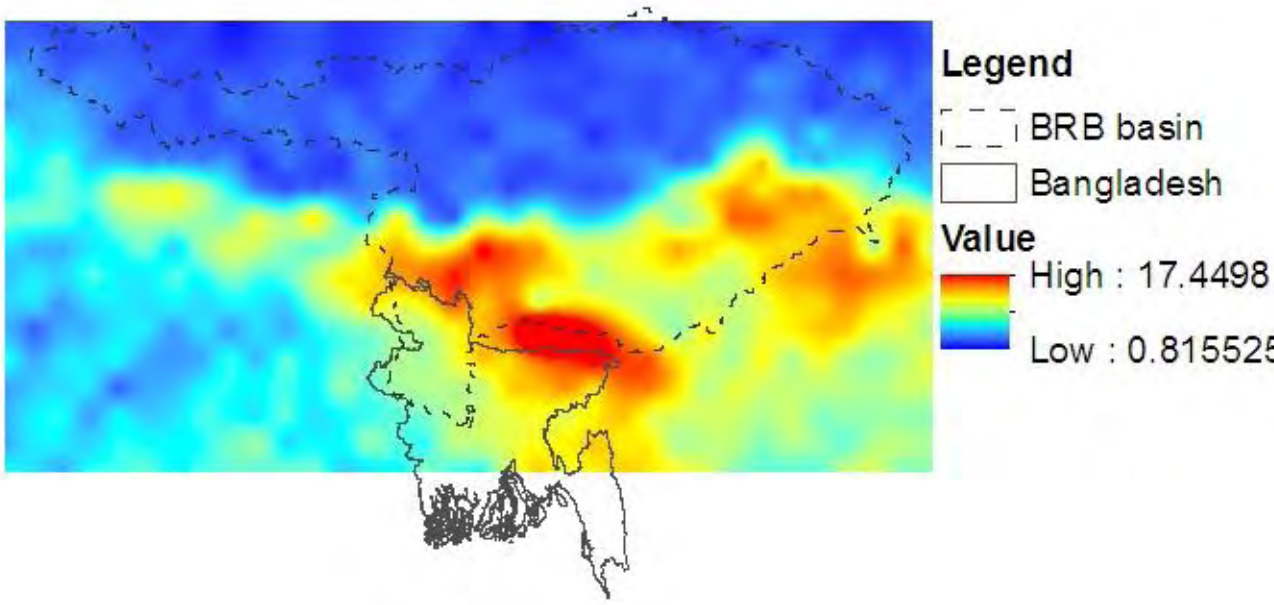

Figure E39: Spatial variation of precipitation (mm) for BCC-CSM1.1(RCP 8.5) in 2080s

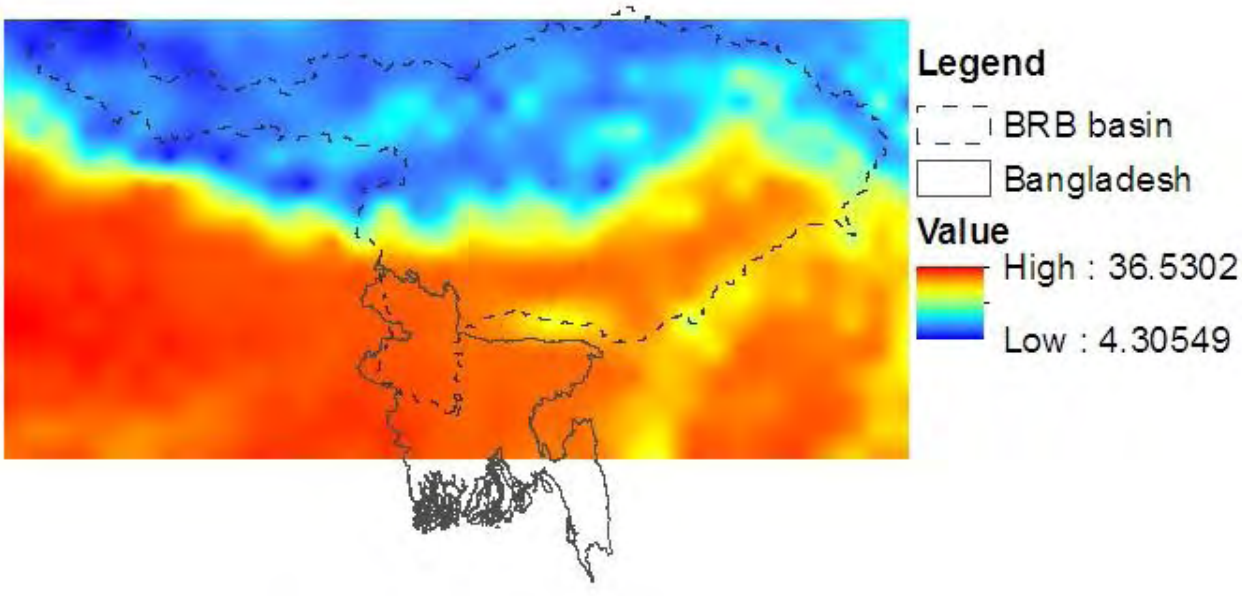

Figure E40 S C BCC-CSM1.1(RCP 8.5) in 2080s

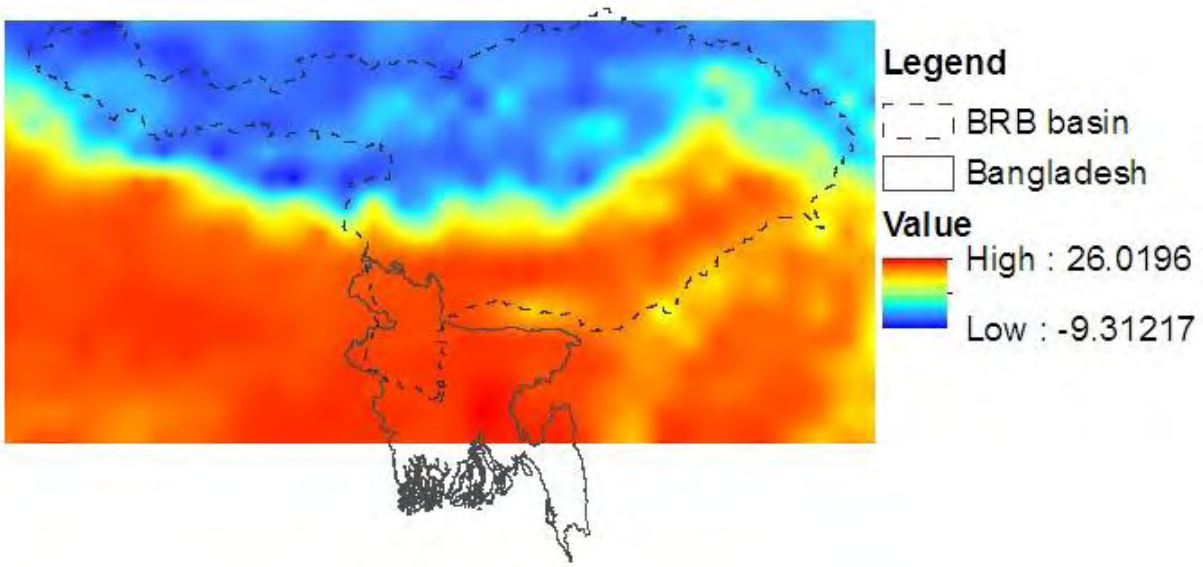

Figure E41: Spatial variation of minimum C BCC-CSM1.1(RCP 8.5) in 2080s

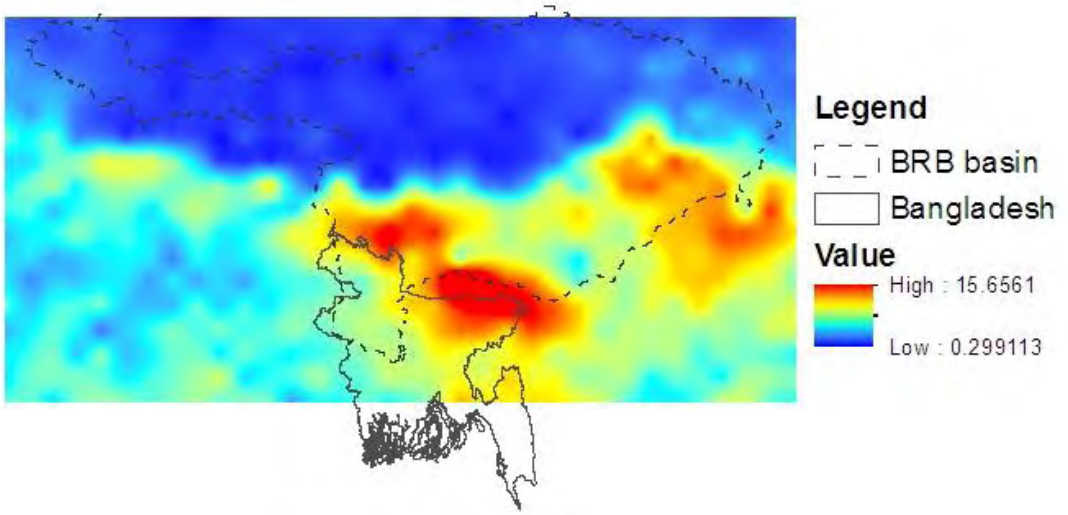

Figure E42: Spatial variation of precipitation (mm) for BCC-CSM1.1(RCP 8.5) in 2020s

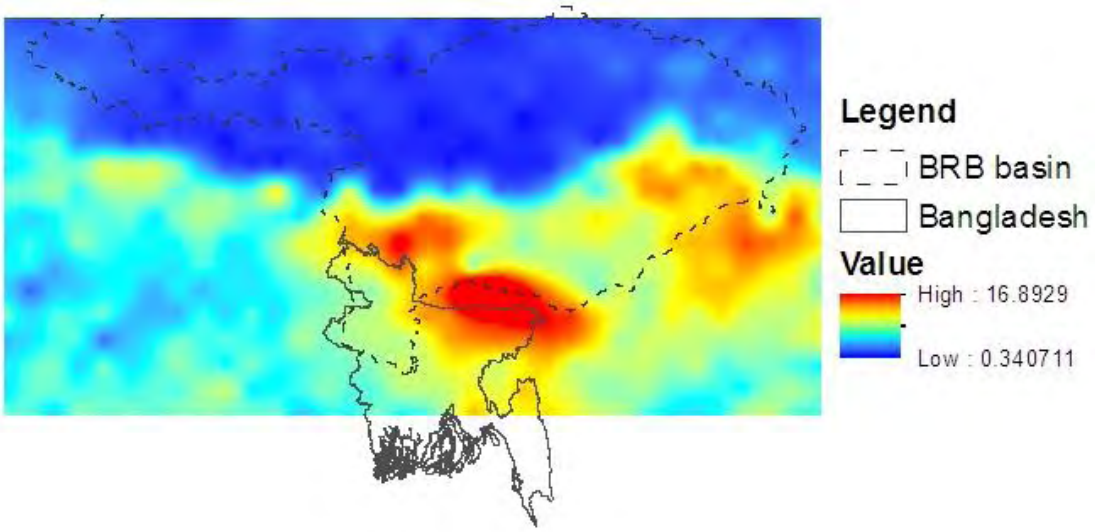

Figure E43: Spatial variation of precipitation (mm) for BCC-CSM1.1(RCP 8.5) in 2050s

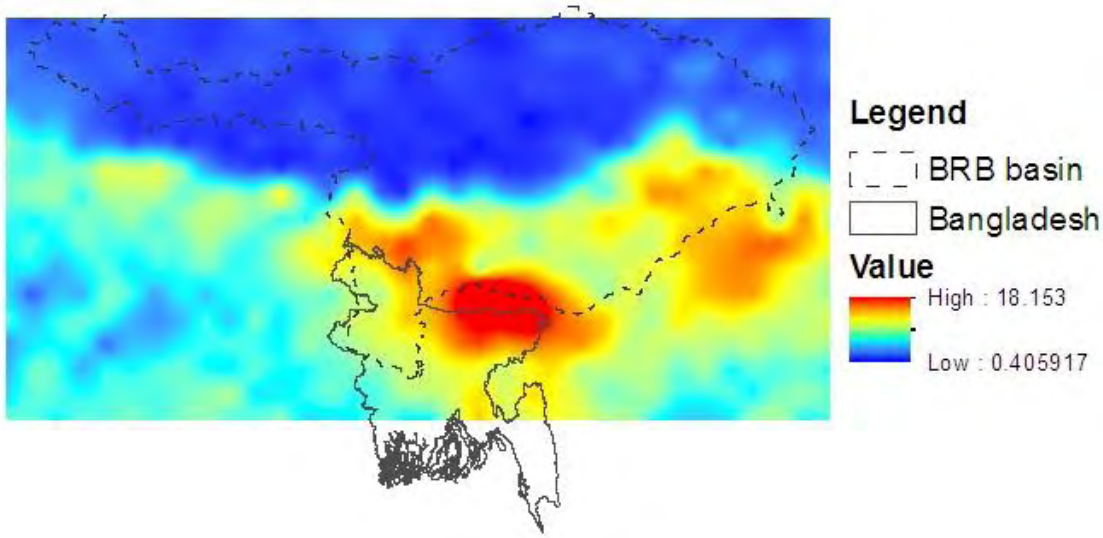

Figure E44: Spatial variation of precipitation (mm) for BCC-CSM1.1(RCP 8.5) in 2080s

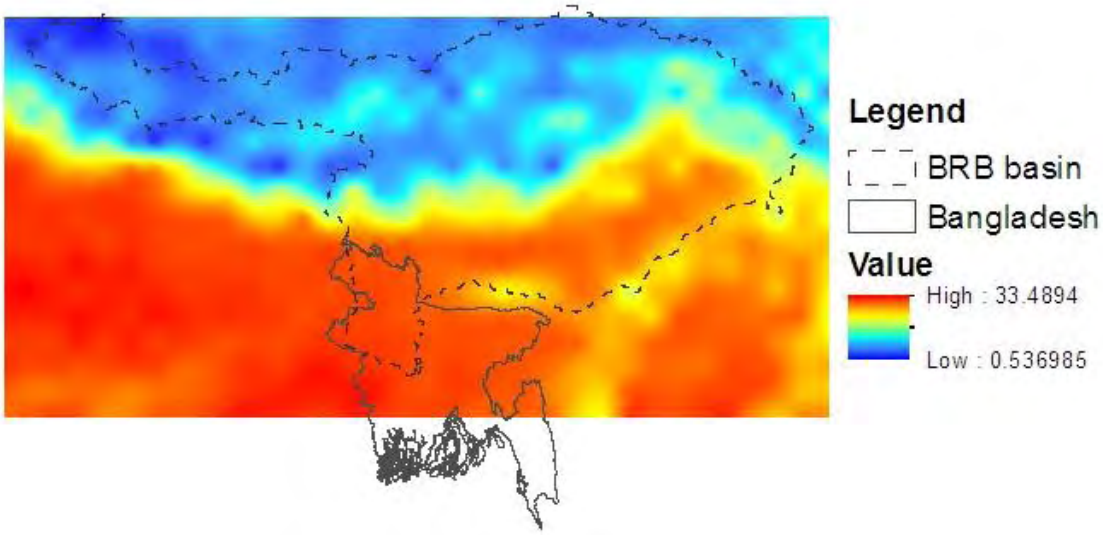

Figure E45 S C BCC-CSM1.1(RCP 8.5) in 2020s

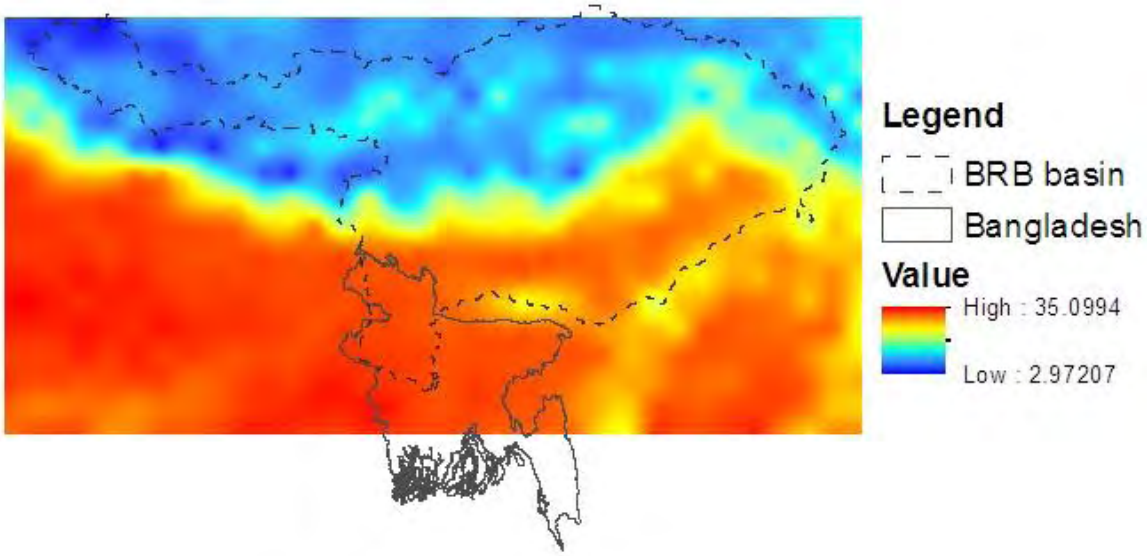

Figure E46 S C BCC-CSM1.1(RCP 8.5) in 2050s

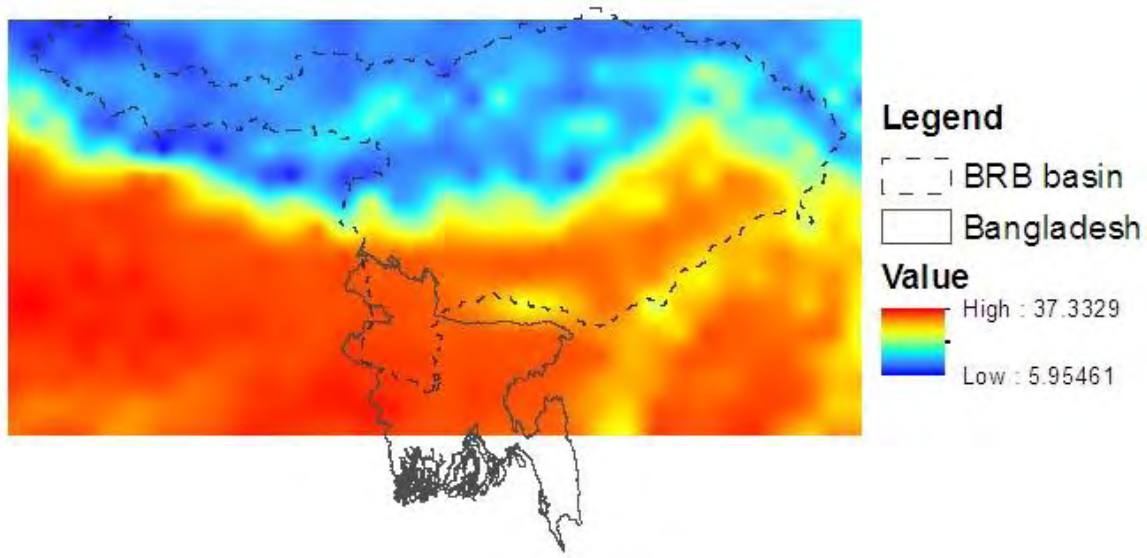

Figure E47 S C for BCC-CSM1.1(RCP 8.5) in 2080s

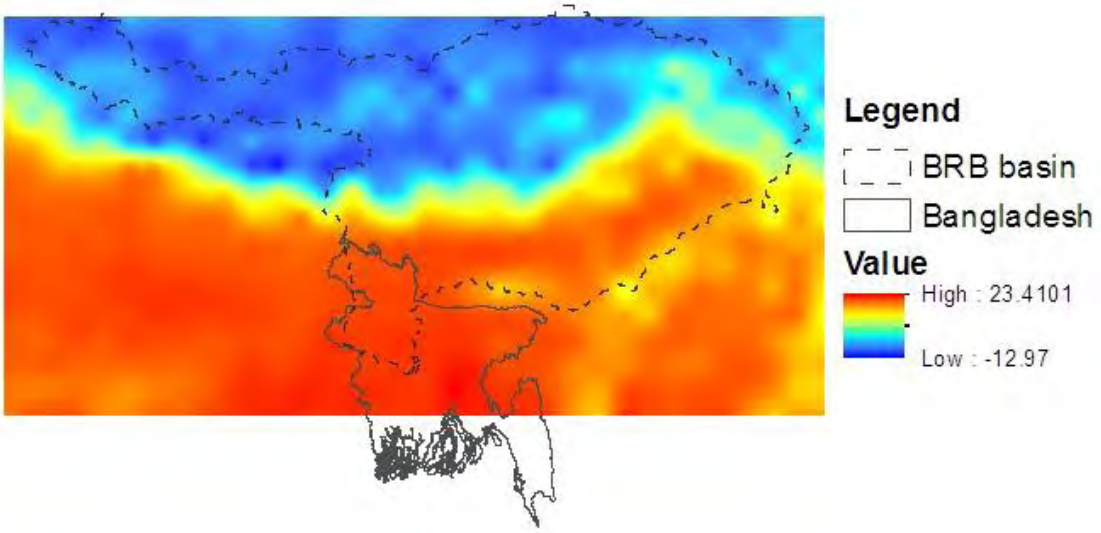

Figure E48 S C) for BCC-CSM1.1(RCP 8.5) in 2020s

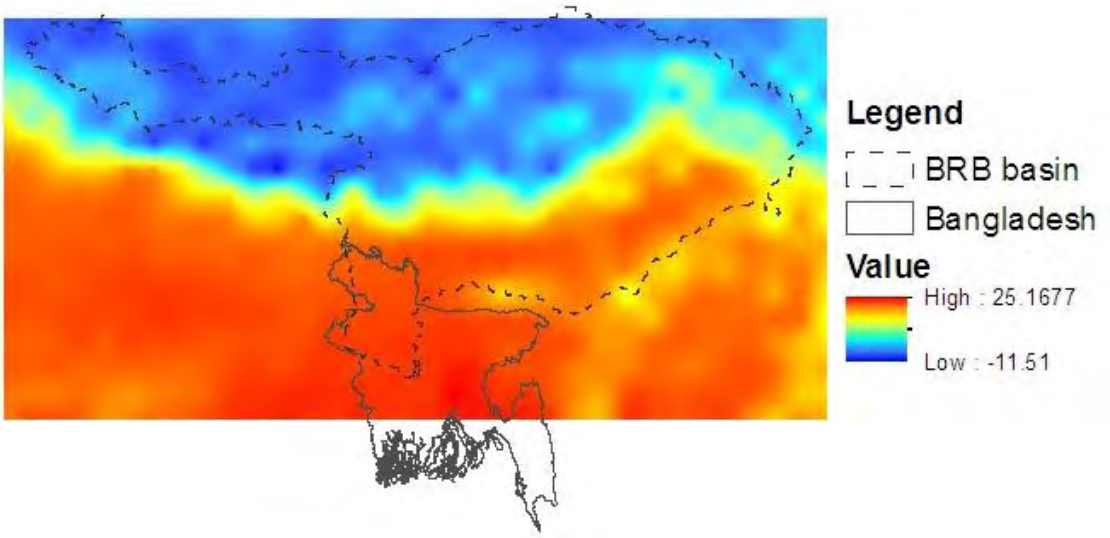

Figure E49 S C) for BCC-CSM1.1(RCP 8.5) in 2050s

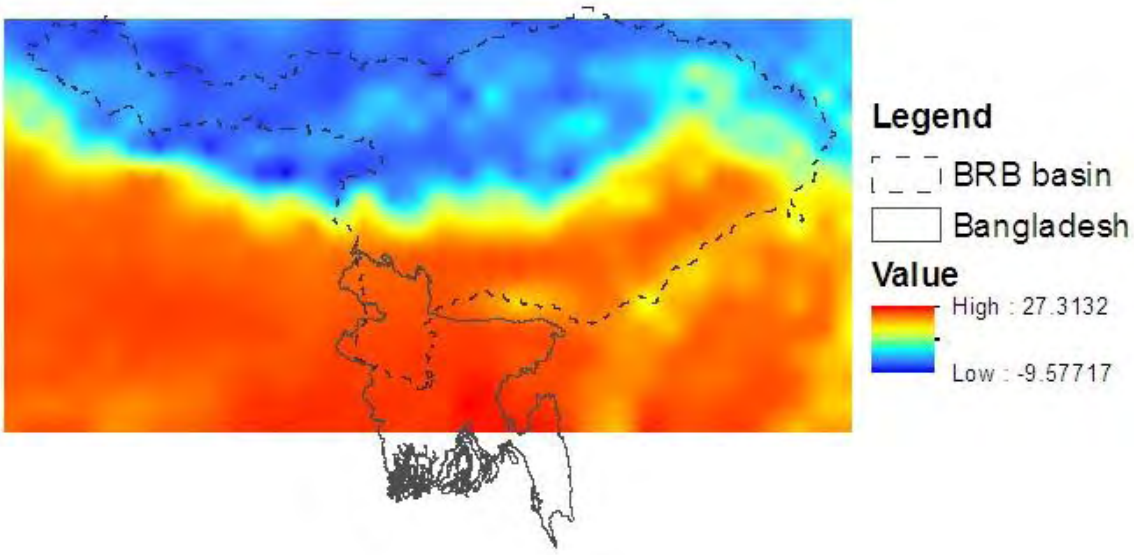

Figure E50 S C) for BCC-CSM1.1(RCP 8.5) in 2080s